JSCSEN 76(4)479–646(2011)

International Year of CHEMISTRY 2011

Journal of the Serbian Chemical Society

Electronic version

VOLUME 76

No 4

BELGRADE 2011

Available on line at

www.shd.org.rs/JSCS/

Journal of the Serbian Chemical Society
JSCS-info@shd.org.rs • www.shd.org.rs/JSCS

J. Serb. Chem. Soc. Vol. 76, No. 4 (2011)

CONTENTS

Published by the Serbian Chemical Society
Karnegijeva 4/III, 11000 Belgrade, Serbia
Printed by the Faculty of Technology and Metallurgy
Karnegijeva 4, P.O. Box 35-03, 11120 Belgrade, Serbia

Journal of the Serbian Chemical Society
JSCS-info@shd.org.rs • www.shd.org.rs/JSCS
J. Serb. Chem. Soc. 76 (4) 479–490 (2011)
JSCS–4134
UDC 547.466.23+547.416:616.8+620.266.1:628.513
Review

REVIEW

Excitatory amino acid β-*N*-methylamino-L-alanine is a putative environmental neurotoxin

SRDJAN LOPIČIĆ[1]*, MARIJA BRATIĆ-STANOJEVIĆ[1], PATHAK DHRUBA[1], DRAGAN PAVLOVIĆ[2], MILICA PROSTRAN[3] and VLADIMIR NEDELJKOV[1]

[1]*Institute for Pathological Physiology, School of Medicine, University of Belgrade, 11000 Belgrade, Serbia,* [2]*Ernst Moritz Arndt University, Greifswald, Germany and* [3]*Institute of Pharmacology, Clinical Pharmacology and Toxicology, School of Medicine, University of Belgrade, 11000 Belgrade, Serbia*

(Received 29 July, revised 4 October 2010)

Abstract: The amino acid β-*N*-methylamino-L-alanine (L-BMAA) has been associated with the amyotrophic lateral sclerosis/parkinsonism-dementia complex in three distinct western Pacific populations. The putative neurotoxin is produced by cyanobacteria, which live symbiotically in the roots of cycad trees. L-BMAA was thought to be a threat only to those few populations whose diet and medicines rely heavily on cycad seeds. However, the recent discovery that cyanobacteria from diverse terrestrial, freshwater, and saltwater ecosystems around the world produce the toxin requires a reassessment of whether it poses a larger health threat. Therefore, it is proposed that monitoring L-BMAA levels in cyanobacteria-contaminated water supplies might be prudent.

Keywords: β-*N*-methylamino-L-alanine; neurodegenerative diseases; neurotoxicity; environmental toxin.

CONTENTS

1. INTRODUCTION

It has been well established that cyanobacterial and other environmental toxins cause and/or promote the development of a vast variety of diseases and

* Corresponding author. E-mail: slopicic@med.bg.ac.rs
doi: 10.2298/JSC100629047L

disturbances in both animals and men.[1–3] Environmentally available excitatory amino acids are a good example. When ingested, or otherwise introduced into an organism, they can induce numerous disturbances of the nervous system. One of the excitatory amino acids that has received a lot of attention lately is *β-N*-methylamino-alanine (BMAA).

β-N-Methylamino-alanine is a highly reactive, low molecular weight amino acid (MW 118 g mol^{-1}) with unusual chemistry, originating as a result of its 2-amino groups being only partially ionized under physiological conditions.[4] It was first isolated by Vega and Bell[5] in 1967 as a result of an effort to isolate a causative agent of the amyotrophic lateral sclerosis/Parkinsonism-dementia complex of the Western Pacific (ALS/PDC).

The Western Pacific amyotrophic lateral sclerosis/Parkinsonism–dementia complex has been reported in three genetically and ethnically distinct population groups residing in Guam (Chamorros of the Marianas Islands), Japan (Japanese residents of the Kii Peninsula, Honshu Island) and New Guinea (indigenous people of South West Papua or Irian Jaya, Indonesia). This disease presents a spectrum of neurological disorders with unusually high incidence, characterized by features of ALS, Parkinsonism, dementia, or a combination of these.[6]

BMAA is proposed to contribute to ALS/PDC based on its presence in Cycad seeds which have been singled out as the strongest epidemiological link to the disease, and constitute a dietary or medicinal item in all the afflicted populations. It is noteworthy that BMAA passes the blood–brain barrier,[7,8] and its bioavailability in primates, when orally administered, is 80 %.[9]

Although the role of BMAA in human neurodegenerative disease is still debated,[10,11] a series of investigations both *in vitro* and *in vivo* has unequivocally established that the amino acid is indeed a neurotoxin.

2. THE BMAA NEUROTOXICITY

The first report describing BMAA-induced neurotoxicity was made the same year the amino acid was first isolated. Bell and colleagues presented the results at the 5th Cycad Conference in 1967. They administered natural and synthetic BMAA intraperitoneally to chicks. The symptoms produced by both natural and synthetic BMAA were general unsteadiness in standing, followed by loss of ability to extend the legs and stand erect. The head was often bend down, the feet were no longer held straight, and the chicks would often fall over and were unable to get up. They showed head circling movements and head retraction. Higher doses of BMAA increased the proportion of chicks affected, decreased the period between injection and the appearance of toxic symptoms and lengthened the period of intoxication.[12]

The landmark paper showing the neurotoxic effects of BMAA in primates was published in 1987 by Spencer and colleagues.[13] One-year-old male cyno-

molgus monkeys received by gavage varying doses of L-BMAA (100–315 mg kg^{-1} daily for up to 12 weeks). They were clinically and neuropathologically examined, and also evaluated neurophysiologically. Neurological deficits appeared insidiously after 2–12 weeks and signs of motor neuron dysfunction developed symmetrically or asymmetrically. Clinical and electrophysiological signs of motor deficit preceded the appearance of physical alterations in the corresponding areas of the CNS. The regional susceptibility to L-BMAA showed a gradation from motor cortex to spinal cord to substantia nigra (from most affected to least affected). In this study, Spencer *et al.*[13] showed clinical, neurophysiological and neuropathological evidence that L-BMAA induces a primate motor system disorder with involvement of the upper and lower motor neurons and the extrapyramidal system.

Numerous investigations that followed confirmed the neurotoxic properties of BMAA. It was shown that in rats, BMAA causes acute motoric and behavioral deficits,[14–18] signs of cerebellar dysfunction,[14,15] and hyperexcitability with body shakes, convulsions and epileptiform activity on EEG.[19,20] Neuropathologically, BMAA has caused postsynaptic vacuolization and neurodegeneration of cortical,[21] spinal cord,[22] and hippocampal[23] neurons in mice, as well as neurodegeneration of cerebellar,[14,24] and monoaminergic[16,25] neurons in rats.

In a recent investigation, Karlsson *et al.*[26] studied the transfer of BMAA to fetal and neonatal brains and the effects of BMAA on the development of behavioral characteristics in rodents. The study revealed transplacental transfer of (3)*H*-BMAA and a significant uptake in fetal mouse brain. The radioactivity was specifically located in the hippocampus, striatum, brainstem, spinal cord and cerebellum of 10-day-old mice. BMAA treatment on postnatal days 9–10 induced acute alterations in the behavior of neonatal rats, such as impaired locomotive ability and hyperactivity. The observed behavioral changes also suggested possible cognitive impairment.[26] The same group reports that rats treated with BMAA during the neonatal period displayed acute but transient motoric disturbances, long-term learning impairments and failed to show habituation at a juvenile age.[27]

Santucci and coworkers[28] provided further evidence supporting a direct causal link between L-BMAA and neuronal damage. The authors studied the effect of L-BMAA on cell viability *in vivo* by measuring the electrophysiological activity of mouse retinal neurons by electroretinography recordings. Intra-ocular injections of L-BMAA selectively reduced the amplitude of the *b*-wave, without affecting either the *a*-wave amplitude or the *a*- and *b*-latencies. Death of retinal cells was evidenced by histology on retina sections, caspase 3 activation, incurporation of propidium iodide and production of reactive oxygen species. Co-injection of the specific NMDA antagonist, MK-801, significantly protected the retinal neurons from L-BMAA/NMDA-induced apoptosis.[28]

Finally, BMAA exhibited toxicity in various aquatic animal species, including zebra fish (*Danio rerio*), brine shrimp (*Artemia salina*) and the protozoan *Nassula sorex*, with the toxic responses presented as clonus convulsions and abnormal spinal axis formation (*D. rerio*), loss of phototaxis (*A. salina*) and mortalities (all species),[29] while dietary intake of BMAA reduced the lifespan as well as the neurological functions of *Drosophila melanogaster* flies.[30]

Of particular relevance to human health, in two independent laboratories where blinded brain tissue samples were tested, both found BMAA in patients who had died of neurodegenerative disease but not in patients who died of causes unrelated to neurodegeneration.

Murch *et al*.[31] showed that BMAA occurs in the brains of Guamanians dying of ALS/PDC (average concentration 627 μg g^{-1}, 5 mM) but not in control brains. Moreover, they reported that BMAA was present in the brain tissues of North American patients who had died of Alzheimer's disease (average concentration 95 μg g^{-1}, 0.8 mM).[31] Although Snyder *et al.*,[32] using a different HPLC method and other assay techniques, were unable to reproduce the findings of Murch *et al.*,[31] Pablo and colleagues,[33] using the original techniques of Murch and coworkers,[31] recently confirmed the presence of protein-bound BMAA in postmortem brain specimens taken from neuropathologically confirmed cases of 13 ALS, 12 Alzheimer's disease (AD), and 8 Huntington's disease North American patients. The authors reported the presence of BMAA in concentrations exceeding 100 μg g^{-1} in patients who had died with sporadic AD and ALS but not in the brains of non-neurological controls or Huntington's disease patients.[33]

3. MECHANISMS OF BMAA NEUROTOXICITY

The greatest initial insight into the mechanisms of BMAA neurotoxicity was provided by electrophysiological studies. In a breakthrough paper, Weiss and Choi reported that the neurotoxic potential of BMAA is greatly enhanced in the presence of physiological concentrations of bicarbonate ions.[34] They went on to show that, in presence of bicarbonate, BMAA acts on NMDA ionotropic glutamate receptors causing marked depolarization of the membrane potential.[35] Allen and coworkers later confirmed these findings, but reported that the effect can be blocked by antagonists of non-NMDA ionotropic glutamate receptors.[36]

Nedeljkov *et al.* investigated the effects of L-BMAA on Retzius nerve cells of isolated ganglia of the leech *Haemopis sanguisuga* and showed that the presence of bicarbonate ions produces a 4-fold increase in BMAA-induced depolarization of the membrane potential.[37] Lopicic and colleagues, using the same model, reported that application of both 1 mmol L^{-1} L-BMAA in Ringer solution containing 20 mmol L^{-1} bicarbonate caused a significant 74 % decrease in the input resistance of directly polarized membrane and that the non-NMDA receptor antagonist 6-cyano-7-nitroquinoxaline-2,3-dione (CNQX) at a concentration of

100 μmol L^{-1} decreased the effect of L-BMAA on membrane potential by 57 %. The authors also presented evidence for a rise in the intracellular Na^+ concentration $(Na^+)_c$ and decrease in the intracellular K^+ concentration $(K^+)_c$ during BMAA induced depolarizations. The application of 2 mmol L^{-1} L-BMAA in bicarbonate Ringer for 4 min led to an average increase of $(Na^+)_c$ by 30.13±13.21 mmol L^{-1}, indicating a rapid influx of sodium into the cell, while the same concentration of L-BMAA produced a decrease of $(K^+)_c$ by 15.76±0.43 mmol L^{-1}, indicating a rapid efflux of K^+ from the cell.[38]

BMAA was also shown to produce a rise in the intracellular Ca^{2+} concentration,[39–41] and induce oxidative stress. Rao *et al.*[40] examined the effects of BMAA on reactive oxygen species (ROS) production in motor neurons from dissociated mouse spinal cord cultures using the oxidant-sensitive fluorophore, hydroethidine (HEt). The cells were loaded with HEt and imaged before and after 30 min exposure to BMAA (1–3 mM). The motor neurons showed significant increases in HEt oxidation several minutes after addition of BMAA and the BMAA-induced ROS generation was dose dependent.[40] Lobner and coworkers[41] investigated the mechanisms of BMAA toxicity on mixed cortical cell cultures containing neurons and astrocytes, prepared from fetal (15–16-day gestation) mice. Cellular oxidative stress was measured with the fluorescent dye dichlorofluorescein (DCF). Exposure to 3 mM BMAA for 3 h caused a significant increase in oxidative stress which was blocked by the free radical scavenger trolox.[41]

The presented evidence that BMAA acts *via* ionotropic glutamate receptors, increases the intracellular Na^+ and Ca^{2+} concentrations and induces oxidative stress all indicate that the amino acid might cause neurodegeneration through the mechanism of excitotoxicity.

Recently, Liu *et al.*[42] proposed that the mechanism of neurotoxicity of BMAA may be three-fold, involving not only direct action on the ionotropic glutamate receptors, but also activation of the metabotropic glutamate receptor 5 (mGluR5) and induction of oxidative stress unrelated to excitotoxicity. They found that BMAA inhibits the cystine/glutamate antiporter (system Xc−) mediated cystine uptake, which in turn leads to glutathione depletion and increased oxidetive stress. BMAA also appears to drive glutamate release *via* the system Xc− and this glutamate induces toxicity through activation of the mGluR5 receptor.[42]

Finally, the latest results by Nunn and Ponnusamy[4] provide evidence that several biochemical mechanisms are also involved in the neurotoxicity of BMAA. The authors showed that BMAA changes the distribution of taurine, glycine and serine between rat brain slices and their incubation medium. The glutamate/glutamine cycle between neurons and glia was also compromised as a result of BMAA administration. In model experiments, BMAA reacted non-enzymatically with pyridoxal-50-phosphate, releasing methylamine, and methylamine was also formed in rat liver and kidney homogenates when incubated with BMAA. The

formation and release of methylamine is significant since chronic administration of methylamine to rats caused oxidative stress.[4]

4. BMAA AND THE ENVIRONMENT

The renewed interest in L-BMAA as an environmental neurotoxin stemmed from a series of papers by Cox *et al.*[4] They first established that the source of L--BMAA in *Cycas* palms are cyanobacteria of the genus *Nostoc* living as endosymbionts in the corraloid roots of the palm.[43] Axenic cultures of *Nostoc* isolated from corraloid roots of *C. micronesica* were found to produce 0.3 μg g^{-1} BMAA, while roots with flourishing cyanobacterial infections had 37 μg g^{-1} BMAA. Uninfected roots contained no BMAA.[43] Furthermore, Cox and coworkers presented evidence for biomagnification of BMAA through the Guamanian ecosystem; from cyanobacteria (0.3 μg g^{-1}) to *Cycad* seeds (up to 1161 μg g^{-1}), to bats *P. mariannus mariannus* (3556 μg g^{-1}), which are consumed as a delicacy in the diet of the people affected by ALS/PDC in Guam.[43]

However, the chemical nature of BMAA would make the molecule seem a poor candidate for bioaccumulation within an ecosystem since, unlike other biomagnified compounds, BMAA is not lipophilic and thus its accumulation in fatty tissues would seem unlikely. This issue was resolved by Murch and colleagues.[31] The group reported that BMAA occurs not only as a free amino acid, but can also be released from a bound form by acid hydrolysis. After first removing free amino acids from tissue samples of various trophic levels in Guam, Murch and coworkers hydrolyzed the remaining fraction and found BMAA concentrations to increase 10- to 240-fold. The authors comment that this protein-bound form of BMAA may function as an endogenous neurotoxic reservoir, accumulating and being transported between trophic levels and subsequently being released during digestion and protein metabolism.[31]

Finally, Cox *et al.* tested 11 *Nostoc* strains isolated from symbioses with lower and higher plants, and 30 laboratory strains of free-living cyanobacteria, covering all major taxonomic groups and found 8 out of 11 *Nostoc* strains, and 29 out of the 30 laboratory strains contained BMAA.[44]

The ubiquity of cyanobacteria in terrestrial, freshwater, brackish and marine environments, combined with the process of biomagnification, opened up an interesting possibility for widespread exposure to BMAA in concentrations sufficient for neurotoxicity. This started a worldwide search for the presence of BMAA in the environment.

Several methods have been reported to detect BMAA in cyanobacterial, plant and animal tissue samples, including high performance liquid chromategraphy (HPLC), gas chromatography–mass spectrometry (GC–MS), liquid chromatography–heated electrospray ionization–mass spectrometry/mass spectrometry

(LC–ESI–MS/MS) and a method for underivatized BMAA using an amino acid analyzer.

Using three different high performance liquid chromatography (HPLC) techniques and two different liquid chromatography/mass spectrometry (LC/MS) techniques, Banack and coworkers demonstrated that the marine *cyanobacterial* species represented by *Nostoc* CCMED-001 produce β-*N*-methylamino-L-alanine. The concentration of BMAA in the specimens ranged from 7 to 25μg g^{-1}.[45]

Metclaf *et al.* analyzed 12 environmental samples, including blooms, scum and mats from waterbodies throughout the United Kingdom, collected over a 14--year period.[46] The waterbodies from which the samples were collected consisted of 11 inland freshwaters and one coastal brackish water. All of the waterbodies are of high, and often multiple usages – seven are abstracted for drinking water treatment, five are used as recreational waters, four as fisheries and one for livestock watering. BMAA was found to be present in all the examined samples in concentrations ranging from 8 to 287 μg g^{-1}. The authors also reported the occurrence of BMAA in waterbodies which are used for drinking water after treatment. Whether the processes of drinking water treatment remove or destroy BMAA requires investigation.

The use of cyanobacteria has also been reported in the Peruvian highlands.[47] The colonies of *Nostoc* commune (locally called llullucha) are harvested by indigenous peoples from high altitude vernal pools and lakes throughout the Peruvian Andes, and sold on the local markets. The colonies are used for food and medicine. As food, the colonies are preferred fresh, but can also be sun-dried to preserve them for the dry season. *Nostoc* commune is also used as a famine food, particularly when potatoes are scarce. Furthermore, llullucha is locally believed to be rich in calcium and is given to children as a milk substitute, and represents an ingredient of a local stew called picante.

Medicinally, *Nostoc* is used in the Peruvian highlands to treat fevers and inflammation; it is drunk after maceration. It is also applied topically by wrapping mashed *Nostoc* in a cloth around the waist overnight to treat stomach, liver, and kidney pain or taken internally after boiling for the same ailments. Large colonies are also macerated and applied topically to assist in the final stages of a difficult labor and delivery.

Johnson and coworkers tested 21 samples of Nostoc commune from seven local markets for the presence of BMAA and found it present in all the samples in concentrations ranging from 2.04 to 21.51 μg g^{-1}.[47]

Esterhuizen and Downing investigated for the presence of BMAA in cyanobacterial cultures representing taxonomic diversity and geographic distribution in southern Africa.[48] The cyanobacteria were collected from various freshwater impoundments that are used for agricultural and recreational activities, as well as from raw water sources for potable water production. All strains, except one,

were reproducibly positive for BMAA, although several cultures were below the limit for quantification. Where BMAA could be quantified, it was found to be present in concentrations of 0.05–2755.6 μg g^{-1}. No correlation between the BMAA concentrations was observed within or between taxonomic groups or geographic locations. However, considerable difference in the BMAA content was found between extracts from different culture phases for the same strain, indicating that a number of factors, such as growth conditions, culture age and history, or nutritional or environmental stress, could influence the BMAA content in cyanobacteria.[49]

Li *et al.* have analyzed axenic cultures of *Microcystis aeruginosa* and Nostoc sp. at various growth stages, isolated from Chinese freshwaters, for BMAA. BMAA was detected in the Nostoc sp., but at very low concentrations (<0.07 pmol on column),[49] and BMAA was also detected in blue-green algae used for food supplements, freshwater fish and bottled water.[50]

Cox and coworkers report that cyanobacterial crusts and mats that are widespread in the deserts of Qatar contain BMAA.[51] These cyanobacterial crusts, which help bind the desert sands, are dormant throughout most of the year, but during brief spring rains actively photosynthesize. When disturbed by vehicular traffic or other activities, the dried crusts and mats can produce considerable amounts of dust, leading to significant exposure to BMAA and other cyanotoxins through inhalation. Since veterans of the 1990–1991 Gulf War younger than 45 years of age were reported to have an increased incidence of ALS compared to personnel who were not deployed, the authors went on to conclude that inhalation of BMAA, and other aerosolized cyanotoxins, may constitute a significant risk factor for the development of ALS and other neurodegenerative diseases.[51]

A cluster of ALS patients with incidence of the disease 10- to 25-times higher than expected, recorded in Enfield, New Hampshire, USA, was also linked to chronic exposure to BMAA and other cyanotoxins, since the town encompasses Lake Mascoma, which has a history of cyanobacteria algal blooms.[52] The authors suggested that possible routes of toxin exposure include inhalation of aerosolized toxins, consumption of fish, or ingestion of lake water.

BMAA-containing cyanobacteria were also found in drinking water sources and small pools within the Gobi Desert. Since such pools of water are crucial resources for wildlife inhabiting the area, the authors suggested assessment of cyanotoxin effects on organisms living in the Gobi Desert and other desert environments.[53]

Faassen and coworkers analyzed mixed species scum material from Dutch urban waters that suffer from cyanobacterial blooms. Free BMAA was detected at nine of the 21 sampled locations with a maximum concentration of 42 μg g^{-1}. Although the BMAA concentrations were relatively low, the authors concluded

that co-occurrence with other cyanobacterial neurotoxins might pose a serious health risk.[54]

Avian vacuolar myelinopathy (AVM) is a neurological disease that produces uncoordinated behavior in affected birds. Feeding and sentinel trials, field surveys and genetic studies implicated the plant species *Hydrilla verticillata* (Hydrocharitaceae) and an associated epiphytic cyanobacterial species (order Stigonematales) as a causal link to AVM. Furthermore, Stigonematales were shown to produce BMAA. It was suggested that if biomagnification of BMAA occurs in these ecosystems, as was observed in the Guam ecosystem, then the consumption of fish and waterfowl from AVM-confirmed reservoirs could represent a significant human health risk.[55]

5. CONCLUSIONS

β-*N*-Methylamino-alanine is a neurotoxic amino acid produced by widespread cyanobacteria. A possible link between this amino acid and neurodegenerative diseases makes it a potential risk for animal and human health. Until more is known about the role of BMAA in progressive neurodegenerative illnesses, it is suggest that monitoring for the presence of BMAA in the environment would be prudent.

NOMENCLATURE

AD	Alzheimer's disease
ALS	Amyotrophic lateral sclerosis
ALS/PDC	Amyotrophic lateral sclerosis/Parkinsonism–dementia complex of the Western Pacific
AVM	Avian vacuolar myelinopathy
BMAA	β-*N*-Methylamino-alanine
CNQX	6-Cyano-7-nitroquinoxaline-2,3-dione
DCF	Dichlorofluorescein
GC–MS	Gas chromatography–mass spectrometry
HEt	Hydroethidine
HPLC	High performance liquid chromatography
$(K^+)_c$	Intracellular K^+ concentration
LC/MS	Liquid chromatography/mass spectrometry
LC–ESI–MS/MS	Liquid chromatography–heated electrospray ionization–mass spectrometry/mass spectrometry
$(Na^+)_c$	Intracellular Na^+ concentration
NMDA	*N*-Methyl-D-aspartate
ROS	Reactive oxygen species

Acknowledgements. The paper was originally presented at the 2nd REP LECOTOX Workshop "Trends in Ecological Risk Assessment", 21–23 September, 2009, Novi Sad, Serbia (EC FP 6 funded project INCO-CT-2006-043559-REP-LECOTOX). This work was supported by grant 145001 from the Ministry of Science and Technological Development of the Republic of Serbia.

И З В О Д

ЕКСЦИТАТОРНА АМИНО КСЕЛИНА *β*-*N*-МЕТИЛАМИНО-L-АЛАНИН ЈЕ ПОТЕНЦИЈАЛНИ НЕУРОТОКСИН

СРЂАН ЛОПИЧИЋ[1], МАРИЈА БРАТИЋ-СТАНОЈЕВИЋ[1], RATNAK DHRUBA[1], ДРАГАН ПАВЛОВИЋ[2], МИЛИЦА ПРОСТАН[3] и ВЛАДИМИР НЕДЕЉКОВ[1]

[1]*Институт за патолошку физиологију, Медицински факултет Универзитета у Београду, 11 000 Београд,* [2]*Ernst Moritz Arndt University, Greifswald, Germany и* [3]*Институт за фармакологију, клиничку фармакологију и токсикологију, Медицински факултет Универзитета у Београду, 11 000 Београд*

Аминокиселина *β*-L-метиламино-L-аланин (L-BMAA) повезана је са комплексом амиотрофичне латералне склерозе/паркинсонизам–деменције који се јавља у три одвојене етничке групе Западног Пацифика. Овај потенцијални неуротоксин производе цијанобактерије које живе у симбиози са кореном палми из рода *Cycas*. Првобитно је владало мишљење да L-BMAA представља ризик само за наведене западнопацифичке популације које у исхрани и лечењу користе велике количине семена палме *Cycas*. Новија истраживања, међутим, показују да цијанобактерије присутне у разнородним екосистемима у земљишту, сланим и слатким водама широм света такође производе ову аминокиселину. Имајући у виду потенцијални ризик који L-BMAA представља за здравље људи, било би важно пратити ниво ове аминокиселине у водама у којима су присутне цијанобактерије.

(Примљено 29. јула, ревидирано 4. октобра 2010)

REFERENCES

1. G. A. Codd, L. F. Morrison, J. S. Metcalf, *Toxicol. Appl. Pharmacol.* **203** (2005) 264
2. Z. Svircev, S. Krstic, M. Miladinov-Mikov, V. Baltic, M. Vidovic, *J. Environ. Sci. Health C. Environ. Carcinog. Ecotoxicol. Rev.* **27** (2009) 36
3. Z. Svircev, V. Baltic, M. Gantar, M. Jukovic, D. Stojanovic, M. Baltic, *J. Environ. Sci. Health C. Environ. Carcinog. Ecotoxicol. Rev.* **28** (2010) 39
4. P. B. Nunn, M. Ponnusamy, *Toxicon* **54** (2009) 85
5. A. Vega, E. A. Bell, *Phytochemistry* **6** (1967) 759
6. R. M. Garruto, Y. Yase, *TINS* **9** (1986) 368
7. M. W. Duncan, N. E. Villacreses, P. G. Pearson, L. Wyatt, S. I. Rapoport, I. J. Kopin, S. P. Markey, Q. R. Smith, *J. Pharmacol. Exp. Ther.* **258** (1991) 27
8. Q. R. Smith, H. Nagura, Y. Takada, M. W. Duncan, *J. Neurochem.* **58** (1992) 1330
9. M. W. Duncan, S. P. Markey, B. G. Weick, P. G. Pearson, H. Ziffer, Y. Hu, I. J. Kopin, *Neurobiol. Aging* **13** (1992) 333
10. G. Miller, *Science* **313** (2006) 428
11. V. T. Karamyan, R. C. Speth, *Life Sci.* **82** (2008) 233
12. M. G. Whiting, *Transcripts of Four Cycad Conferences*, **XI** (1988) 1
13. P. S. Spencer, P. B. Nunn, J. Hugon, A. C. Ludolph, S. M. Ross, D. N. Roy, R. C. Robertson, *Science* **237** (1987) 517
14. A. A. Seawright, A. W. Brown, C. C. Nolan, J. B. Cavanagh, *Neuropathol. Appl. Neurobiol.* **16** (1990) 153
15. S. E. Smith, B. S. Meldrum, *Eur. J. Pharmacol.* **187** (1990) 131
16. H. Lindstrom, J. Luthman, P. Mouton, P. Spencer, L. Olson, *J. Neurochem.* **55** (1990) 941
17. Z. Rakonczay, Y. Matsuoka, E. Giacobini, *J. Neurosci. Res.* **29** (1991) 121
18. Y. C. Chang, S. J. Chiu, K. P. Kao, *Chin J. Physiol.* **36** (1993) 79
19. S. M. Ross, P. S. Spencer, *Synapse* **1** (1987) 248

20. Y. Matsuoka, Z. Rakonczay, E. Giacobini, D. Naritoku, *Pharmacol. Biochem. Behav.* **44** (1993) 727
21. S. M. Ross, M. Seelig, P. S. Spencer, *Brain Res.* **425** (1987) 120
22. P. B. Nunn, M. Seelig, J. C. Zagoren, P. S. Spencer, *Brain Res.* **410** (1987) 375
23. E. J. Buenz, C. L. Howe, *Neurotoxicology* **28** (2007) 702
24. P. C. Staton, D. R. Bristow, *J. Neurochem.* **69** (1997) 1508
25. M. Santiago, E. R. Matarredona, A. Machado, J. Cano, *Toxicol. Lett.* **167** (2006) 34
26. O. Karlsson, N. G. Lindquist, E. B. Brittebo, E. Roman, *Toxicol. Sci.* **109** (2009) 286
27. O. Karlsson, E. Roman, E. B. Brittebo, *Toxicol. Sci.* **112** (2009) 185
28. S. Santucci, N. Zsurger, J. Chabry, *J. Neurochem.* **109** (2009) 819
29. E. L. Purdie, J. S. Metcalf, S. Kashmiri, G. A. Codd, *Amyotroph. Lateral. Scler.* **10** (Suppl. 2) (2009) 67
30. X. Zhou, W. Escala, S. Papapetropoulos, W. G. Bradley, R. G. Zhai, *Amyotroph. Lateral. Scler.* **10** (Suppl. 2) (2009) 61
31. S. J. Murch, P. A. Cox, S. A. Banack, J. C. Steele, O. W. Sacks, *Acta Neurol. Scand.* **110** (2004) 267
32. L. R. Snyder, R. Cruz-Aguado, M. Sadilek, D. Galasko, C. A. Shaw, T. J. Montine, *Neurology* **72** (2009) 1360
33. J. Pablo, S. A. Banack, P. A. Cox, T. E. Johnson, S. Papapetropoulos, W. G. Bradley, A. Buck, D. C. Mash, *Acta Neurol. Scand.* **120** (2009) 216
34. J. H. Weiss, D. W. Choi, *Science* **241** (1988) 973
35. J. H. Weiss, C. W. Christine, D. W. Choi, *Neuron* **3** (1989) 321
36. C. N. Allen, P. S. Spencer, D. O. Carpenter, *Neuroscience* **54** (1993) 567
37. V. Nedeljkov, S. Lopicic, D. Pavlovic, D. Cemerikic, *Ann. N. Y. Acad. Sci.* **1048** (2005) 349
38. S. Lopicic, V. Nedeljkov, D. Cemerikic, *Comp. Biochem. Physiol. A* **153** (2009) 284
39. D. M. Brownson, T. J. Mabry, S. W. Leslie, *J. Ethnopharmacol.* **82** (2002) 159
40. S. D. Rao, S. A. Banack, P. A. Cox, J. H. Weiss, *Exp. Neurol.* **201** (2006) 244
41. D. Lobner, P. M. Piana, A. K. Salous, R. W. Peoples, *Neurobiol. Dis.* **25** (2007) 360
42. X. Liu, T. Rush, J. Zapata, D. Lobner, *Exp. Neurol.* **217** (2009) 429
43. P. A. Cox, S. A. Banack, S. J. Murch, *Proc. Natl. Acad. Sci. USA* **100** (2003) 13380
44. P. A. Cox, S. A. Banack, S. J. Murch, U. Rasmussen, G. Tien, R. R. Bidigare, J. S. Metcalf, L. F. Morrison, G. A. Codd, B. Bergman, *Proc. Natl. Acad. Sci. USA* **102** (2005) 5074
45. S. A. Banack, H. E. Johnson, R. Cheng, P. A. Cox, *Mar. Drugs* **5** (2007) 180
46. J. S. Metcalf, S. A. Banack, J. Lindsay, L. F. Morrison, P. A. Cox, G. A. Codd, *Environ. Microbiol.* **10** (2008) 702
47. H. E. Johnson, S. R. King, S. A. Banack, C. Webster, W. J. Callanaupa, P. A. Cox, *J. Ethnopharmacol.* **118** (2008) 159
48. M. Esterhuizen, T. G. Downing, *Ecotoxicol. Environ. Saf.* **71** (2008) 309
49. A. Li, Z. Tian, J. Li, R. Yu, S. A. Banack, Z. Wang, *Toxicon* **55** (2009) 947
50. P. M. Scott, B. Niedzwiadek, D. F. Rawn, B. P. Lau, *J. Food Prot.* **72** (2009) 1769
51. P. A. Cox, R. Richer, J. S. Metcalf, S. A. Banack, G. A. Codd, W. G. Bradley, *Amyotroph. Lateral. Scler.* **10** (Suppl. 2) (2009) 109
52. T. A. Caller, J. W. Doolin, J. F. Haney, A. J. Murby, K. G. West, H. E. Farrar, A. Ball, B. T. Harris, E. W. Stommel, *Amyotroph. Lateral. Scler.* **10** (Suppl. 2) (2009) 101

53. D. Craighead, J. S. Metcalf, S. A. Banack, L. Amgalan, H. V. Reynolds, M. Batmunkh, *Amyotroph. Lateral. Scler.* **10** (Suppl. 2) (2009) 96
54. E. J. Faassen, F. Gillissen, H. A. Zweers, M. Lurling, *Amyotroph. Lateral. Scler.* **10** (Suppl. 2) (2009) 79
55. R. R. Bidigare, S. J. Christensen, S. B. Wilde, S. A. Banack, *Amyotroph. Lateral. Scler.* **10** (Suppl. 2) (2009) 71.

Journal of the Serbian Chemical Society
JSCS-info@shd.org.rs • www.shd.org.rs/JSCS
J. Serb. Chem. Soc. 76 (4) 491–497 (2011)
JSCS–4135
UDC 542.913:549.52+547.564.7+547.572
Original scientific paper

Evaluation of the radical scavenging activity of a series of synthetic hydroxychalcones towards the DPPH radical

IVA T. TODOROVA, DANIELA I. BATOVSKA*, BISTRA A. STAMBOLIYSKA and STOYAN P. PARUSHEV

Institute of Organic Chemistry, Centre of Phytochemistry, Bulgarian Academy of Sciences, Acad. G. Bonchev Str. Bl. 9, Sofia, 1113, Bulgaria

(Received 23 August, revised 15 November 2010)

Abstract: Sixteen hydroxychalcones were synthesized in sufficient purity by the Claisen–Schmidt condensation between appropriate acetophenones and aromatic aldehydes. All the compounds were evaluated for their ability to scavenge the stable free 2,2-diphenyl-1-picrylhydrazyl (DPPH) radical. Important structure–activity relationships were observed that strongly contribute to the knowledge for the design of DPPH radical scavenging chalcones. Relevant theoretical parameters were computed in an attempt to understand and explain the obtained experimental results.

Keywords: hydroxychalcones; 4'-chlorohydroxychalcones; synthesis; radical--scavenging activity; DPPH free radical.

INTRODUCTION

Chalcones (1,3-diarylprop-2-en-1-ones) are open-chain flavonoids consisting of two aromatic rings **A** and **B** that are joined by a three-carbon α,β-unsaturated carbonyl system. These compounds display a large number of biological activities, some of which are believed to correlate with their antioxidant potential.[1,2] For this reason, up-to-now many chalcones have been assessed[2] for their radical scavenging activity (*RSA*) towards various radicals. In this respect, the stable 2,2--diphenyl-1-picrylhydrazyl (DPPH) radical was the most employed target. The DPPH radical scavenging activity of chalcones was found to be favoured by the presence of the α,β-unsaturated carbonyl system,[3] and one or more phenolic groups, particularly arranged in either a pyrogallol or catechol moiety.[3–7] In addition, the introduction of an electron donating functionality, such as a prenyl or methoxy group, next to the phenolic group was regarded as important because these substituents increase the rate of hydrogen atom transfer from the phenolic

* Corresponding author. E-mail: danibat@orgchm.bas.bg
doi: 10.2298/JSC100517043T

group.[6,8] However, the influence of the methoxy group on the RSA of hydroxychalcones was studied mainly in ring **A** because of the structural similarity of these compounds to many naturally-occurring chalcones.[1]

In the present study, a set of various hydroxychalcones possessing one or two phenolic groups in ring **B** and their analogues in which a methoxy substituent was inserted next to the phenolic group was synthesized. Ring **A** was unsubstituted or contained a *p*-chloro group. The RSA of all the chalcones was studied against the free DPPH radical using relevant theoretical parameters.

EXPERIMENTAL

General

The hydroxylated chalcones were synthesized in high yields (Table I) by variants of the Claisen–Schmidt condensation.[9,10] The melting points were obtained using a Mel-Temp 1102D-230 VAC instrument and are reported uncorrected. The radical scavenging activity of chalcones toward DPPH was determined on a Helios gamma UV–Vis spectrophotometer.

TABLE I. Substitution pattern, yields, melting points (m.p.), SC_{50}, bond dissociation enthalpy (*BDE*) and ionization potential (*IP*) values of the investigated chalcones **1**–**16**

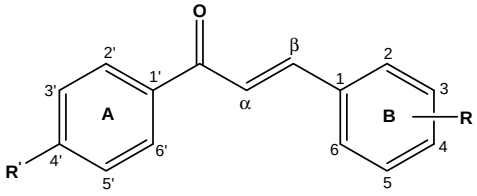

Compound	R'	R	Yield[a] %	M.p. °C	SC_{50}[b] mM	*BDE* kJ mol^{-1}	*IP* kJ mol^{-1}
1	H	2-OH	68	154–155	437.44	314.5	7.52
2	Cl	2-OH	73	143–145	465.60	316.6	7.58
3	H	3-OH	68	130–133	180.50	329.9	7.54
4	Cl	3-OH	78	106–109	181.25	330.8	7.62
5	H	4-OH	81	184–185	47.23	315.4	7.30
6	Cl	4-OH	83	175–176	111.29	317.1	7.38
7	H	3,4-OH	38	179–180	0.05	280.0	7.13
8	Cl	3,4-Di-OH	56	201–202	0.87	281.5	7.21
9	H	2-OH-3-OCH_3	69	112–113	12.19	312.4	7.19
10	Cl	2-OH-3-OCH_3	74	129–131	9.71	313.0	7.27
11	H	3-OH-4-OCH_3	72	92–94	264.38	317.9	7.05
12	Cl	3-OH-4-OCH_3	74	195–196	53.76	327.4	7.12
13	H	4-OH-3-OCH_3	70	91–95	158.74	314.4	7.01
14	Cl	4-OH-3-OCH_3	79	268–270	4.50	311.9	7.09
15	H	4-OH-3,5-di-OCH_3	80	powder	18.93	295.2	6.78
16	Cl	4-OH-3,5-di-OCH_3	83	119–121	2.31	296.1	6.86
Caffeic acid[c]	–	–	–	–	0.05	279.8	7.55

[a]Isolated yields; [b]the SC_{50} value refer to the chalcone concentration providing 50 % scavenging of DPPH radicals present in the test medium; [c]used as a positive control

The quantum chemical calculations were performed using the Gaussian 09 package[11] on a MADARA grid. The geometries of all possible conformational isomers of the studied compounds, radicals, radical cations were fully optimized by application of the UB3LYP functional in conjunction with the 6-31G* basis set. The optimized structures were further characterized by analytic computations of harmonic vibrational frequencies at the same level. Only the results for the most stable conformers according to the calculation were employed in the analysis of the structure–activity relationship.

DPPH radical scavenging assay

The radical-scavenging activity (*RSA* / %) of the chalcones **1**–**16** was determined using the DPPH radical in ethanol (0.1 mM), as described by Nenadis and Tsimidou.[12] Briefly, an aliquot (2960 μL) of a 0.1 mM ethanolic DPPH solution was mixed with 40 μL of each ethanolic sample solution to achieve concentrations of 0.5, 0.9, 1.8, 3.6 and 7.2 mM. The decrease of the light absorption at 516 nm of the DPPH radical solution was measured 20 min after addition of each chalcone sample. Caffeic acid was used as a positive control. The results were expressed as $RSA = (A(t = 0) - A(t = t'))\times 100/A(t = 0)$. The absorbance ($A$) values were corrected for radical decay using blank solutions. Each measurement was performed in triplicate at 25 °C. The SC_{50} value for each compound, representing its millimolar concentration providing 50 % scavenging of the DPPH radicals present in the test medium, was calculated from the $RSA = f$(concentration) curves. The standard deviations were below 10 %. The SC_{50} values were used in the structure–activity relationship study.

Statistical analysis

The correlation between the theoretical and experimental data was studied in terms of the correlation coefficient, r, also known as the Pearson product–moment correlation coefficient, which was computed using Excel software. The significance of the correlation was also calculated. The Ward method was used for clustering of the hydroxychalcones based on their radical scavenging ability (SC_{50}) and computed molecular descriptors. The aim was to find a theoretical parameter that discriminates between active and inactive chalcones.

RESULTS AND DISCUSSION

Sixteen chalcones with a hydroxycinnamoyl motif in their molecules were selected for evaluation of the RSA towards the DPPH radical. The chalcones possessed either a phenolic group or a combination of a phenolic and a methoxy group at various positions on the ring **B**, and had either a *p*-chloro group or no substituent on ring **A** (Table I). All the chalcones were obtained in sufficient purity by the Claisen–Schmidt condensation between acetophenone derivatives and the appropriate aromatic aldehyde (see Experimental).

The DPPH radical scavenging ability of all the chalcones was evaluated spectrophotometrically and compared to those of the well-known antioxidant caffeic acid (3,4-dihydroxycinnamic acid) (Table I). It was observed that the activity of chalcones having one or two phenolic groups in their ring **B** decreased in the following order depending on the position of the phenolic group: 3,4-di-OH (**7**) >> >> 4-OH (**5**) > 3-OH (**3**) > 2-OH (**1**). Insertion of a *p*-chloro group in ring **A** of these compounds did not affect their activity when 2-OH (**2**) and 3-OH (**4**) substituents were present in ring **B** but led to a 2- and 17-fold decrease in the *RSA* of

the chalcones with 4-OH (**6**) and 3,4-di-OH (**8**) groups, respectively. The two most active chalcones, **7** and **8** showed a RSA commensurable with that of caffeic acid, which was due to the presence of the 3,4-dihydroxycinnamoyl (catechol) moiety in their molecules. In particular, the electron-donating hydroxyl group at C-3 in the phenyl ring of caffeic acid is known[13] to increase the rate of hydrogen atom transfer from the phenolic group at C-4 to the DPPH radicals, resulting in the formation of an *o*-hydroxyl phenoxyl radical. This radical is more stable due to the delocalization of the unpaired electron across the entire molecule and the intramolecular hydrogen bonding interaction. The *o*-hydroxyl radical is also easier to oxidize further to the final product *o*-quinone.[14] Methoxylation of one of the hydroxyl groups of 3,4-dihydroxychalcone **7** to form 3-hydroxy-4--methoxy- (**11**) and 4-hydroxy-3-methoxychalcones (**13**) led to a great loss in activity because the chalcones **11** and **13** cannot form quinone oxidation products. The presence of a methoxy group was favourable when it was next to the 2-OH group (compound **9**) and when two methoxy groups were inserted from both sides of 4-OH group (compound **15**). It was also found that insertion of chlorine at the *p*-position in ring **A** enhanced the *RSA* of all chalcones substituted with a combination of phenolic and methoxy groups and these chalcones were more active than the chlorinated chalcones having hydroxyl groups only.

In order to understand the experimental results, the structure of the studied molecules and their radicals were studied using the Density functional theory (DFT) employing the UB3LYP functional and the 6-311G* basis set. It was taken into consideration that the two generally accepted mechanisms[15] for the antioxidant action of phenolic compounds (ArOH) are hydrogen atom transfer (HAT, Eq. (1)) and single-electron transfer followed by proton transfer (SET–PT, Eqs. (2) and (3)).

$$\mathrm{ArOH} \rightarrow \mathrm{ArO}^{\bullet} + \mathrm{H}\cdot \quad (1)$$

$$\mathrm{ArOH} \rightarrow \mathrm{ArOH}^{+\bullet} + \mathrm{e}^{-} \quad (2)$$

$$\mathrm{ArOH}^{+\bullet} \rightarrow \mathrm{ArO}^{\bullet} + \mathrm{H}^{+} \quad (3)$$

The corresponding reaction enthalpies, bond dissociation enthalpy (*BDE*, related to Eq. (1)) and the ionization potential (*IP*, related to Eq. (2)), were calculated (Table I) and used as theoretical parameters to elucidate the substituent effect on the antioxidant activity. While the *IP* values were found not to discriminate between the active and inactive compounds, a moderate but statistically significant positive correlation ($r = 0.47$, $p < 0.05$) was obtained between the *BDE* and SC_{50} values. A hierarchical cluster analysis of these data yielded a dendrogram with horizontal lines representing the chalcones and vertical lines showing the similarity between pairs of chalcones based on their SC_{50} and *BDE* values (Fig. 1). Two main clusters were observed showing that in fact the *BDE* discriminated between the active ($SC_{50} < 2.31$ mM) and the inactive chalcones ($SC_{50} >$

> 4.50 mM). The *BDE* values calculated for the active compounds were all below 300 kJ mol^{-1} (Table I). However, an outlier was present in the cluster of the active chalcones, namely compound **15**, which had a *BDE* value of 295.2 kJ mol^{-1} but did not show RSA (Table I, Fig. 1). The reason for this phenomenon remains unclear.

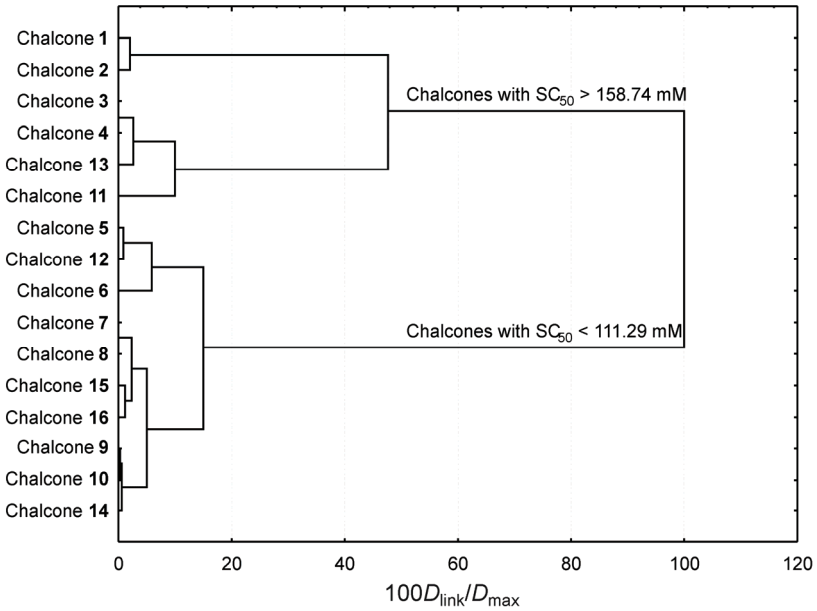

Fig. 1. Hierarchical dendrogram obtained by the method of complete linkage. The dendrogram shows that the bond dissociation enthalpy values discriminate between the active and inactive chalcones (D_{link} – linkage distance; D_{max} – maximal linkage distance.

With the BDE values in mind, another observation was made indicating that the electronic effects of *p*-chloro group in ring A did not influence the RSA of chalcones. This non-influential behaviour of the *p*-chloro group was in agreement with the results reported by Kim *et al.*[5] However, in our study, it was found that the *p*-chloro group did not affect the RSA only of the chalcones having *o*-OH and *m*-OH functionalities in ring B. Insertion of *p*-chloro group in ring A of the chalcones with *p*-OH and 3,4-di-OH groups decreased their RSA. When attached to the chalcones having a combination of hydroxyl and methoxy groups in ring B it increased their activities. The course of action of the *p*-chloro group however remains unclear.

An attempt was also made to correlate the SC_{50} results of the chalcones with some other molecular descriptors. However, the parameters refractivity, polarizability, mass, coefficient of molecular partition octanol–water (log *P*), dipole

moments and HOMO and LUMO energies were disregarded due to their inability to differentiate the active compounds (data not given).

The observed relationships between the position and the surrounding of the phenolic groups in ring **B** and the *RSA* of hydroxychalcones may be useful for the design of chalcone-like compounds with radical scavenging abilities.

CONCLUSIONS

A series of hydroxychalcones was synthesized and evaluated for their DPPH radical scavenging activity. Depending on the position of the phenolic group in ring **B**, the radical scavenging activity of the hydroxychalcones decreased in the following order: 3,4-di-OH >> 4-OH > 3-OH > 2-OH. The presence of a methoxy group was favourable when it was next to the 2-OH group and when two methoxy groups were inserted on both sides of the 4-OH group. Insertion of a 4'--chloro group in ring **A** enhanced the activity of all chalcones substituted with a combination of phenolic and methoxy groups and these compounds were more active than 4'-chloro chalcones having hydroxyl groups only. The reported structure–activity observations strongly contribute to the knowledge for design of DPPH radical scavenging chalcones.

Acknowledgments. This work was supported by the Bulgarian National Science Fund (Contracts X-1514 and RNF01/0110).

И З В О Д

ИСПИТИВАЊЕ СПОСОБНОСТИ ХВАТАЊА DPPH РАДИКАЛА СЕРИЈЕ СИНТЕТИЧКИХ ХИДРОКСИХАЛКОНА

IVA T. TODOROVA, DANIELA I. BATOVSKA, BISTRA A. STAMBOLIYSKA и STOYAN P. PARUSHEV

Institute of Organic Chemistry, Centre of Phytochemistry, Bulgarian Academy of Sciences, Acad. G. Bonchev Str. Bl. 9, Sofia, 1113, Bulgaria

Синтетисано је шеснаест хидроксихалкона Клајзен–Шмитовом кондензацијом, полазећи од одговарајућих ацетофенона и ароматичних алдехида. Свим једињењима је испитана способност хватања стабилних слободних радикала 2,2-дифенил-1-пикрилхидразила (DPPH). Утврђени су односи структура–активност који омогућавају дизајн нових халкона као хватача DPPH радикала. Израчунати су релевантни теоријски параметри у циљу разумевања и објашњавања експерименталних резултата.

(Примљено 23. августа, ревидирано 15. новембра 2010)

REFERENCES

1. D. Batovska, I. Todorova, Curr. Clin. Pharmacol. 5 (2010) 1
2. L. Ni, C. Q. Meng, J. A. Sikorski, Expert Opin. Ther. Pat. 14 (2004) 1669
3. Y.-Z. Cai, M. Sun, J. Xing, Q. Luo, H. Corke, Life Sci. 78 (2006) 2872
4. H. Mohamad, F. Abas, D. Permana, N. H. Lajis, A. M. Ali, M. A. Sukari, T. Y. Hin, H. Kikuzaki, N. Nakatani, Z. Naturforsch. 59c (2004) 811
5. B.-T. Kim, K.-J. O, J.-C. Chun, K.-J. Hwang, Bull. Korean Chem. Soc. 29 (2008) 1125

6. J. Nishida, J. Kawabata, Biosci. Biotechnol. Biochem. 70 (2006) 193
7. D. Kozlowski, P. Trouillas, C. Calliste, P. Marsal, R. Lazzaroni, J.-L. Duroux, J. Phys. Chem. A 111 (2007) 1138
8. G. V. Rao, B. N. Swamy, V. Chandregowda, G. C. Reddy, Eur. J. Med. Chem. 44 (2009) 2239
9. D. Batovska, S. Parushev, A. Slavova, V. Bankova, I. Tsvetkova, M. Ninova, H. Najdenski, Eur. J. Med. Chem. 42 (2007) 87
10. K. Lahtchev, D. Batovska, S. Parushev, V. Ubiyvovk, A. Sibirny, Eur. J. Med. Chem. 43 (2008) 2220
11. Gaussian 98 Revision A.7, Gaussian, Inc., Pittsburgh, PA, 1998
12. N. Nenadis, M. Tsimidou, J. Am. Oil Chem. Soc. 79 (2002) 257
13. P. Terpinc, H. Abramovič, Food Chem. 121 (2010) 366.
14. W.-M. Wu, L. Lu, Y. Long, T. Wang, L. Liu, Q. Chen, R. Wang, Food Chem. 105 (2007) 107
15. E. Klein, V. Lukeš, M. Ilčin, Chem. *Phys.* **336** (2007) 51.

Journal of the Serbian Chemical Society
JSCS-info@shd.org.rs • www.shd.org.rs/JSCS
J. Serb. Chem. Soc. 76 (4) 499–504 (2011)
JSCS–4136
UDC 547.235+547.828+547.491:
66.095.3.095.252
Short communication

SHORT COMMUNICATION

Synthesis of 5-(substituted phenylazo)-6-hydroxy-4-methyl-3--cyano-2-pyridones from ethyl 3-oxo-2-(substituted phenylazo)butanoates

JASMINA DOSTANIĆ[1], NATAŠA VALENTIĆ[2#], GORDANA UŠĆUMLIĆ[2#] and DUŠAN MIJIN[2*#]

[1]*Institute of Chemistry, Technology and Metallurgy, University of Belgrade, Department of Catalysis and Chemical Engineering, Njegoševa 12, 11000 Belgrade and* [2]*Faculty of Technology and Metallurgy, University of Belgrade, Karnegijeva 4, 11120 Belgrade, Serbia*

(Received 11 June, revised 22 November 2010)

Abstract: A new procedure for the synthesis of known azo pyridone dyes is presented. A series of 5-(substituted arylazo)-6-hydroxy-4-methyl-3-cyano-2--pyridones were prepared from ethyl 3-oxo-2-(substituted phenylazo)butanoates and cyanoacetamide in acetone using potassium hydroxide as a catalyst by simple refluxing the reaction mixture. The structure of these dyes was confirmed by FT-IR, NMR and UV–Vis spectroscopy.

Keywords: azo compounds; cyclocondensation reaction; cyanoacetamide; pyridone.

INTRODUCTION

Azo pyridone dyes are important pyridone derivatives that have largely replaced yellow disperse dyes based on pyrazolones due to their bright hues.[1,2] Pyridone disperse yellow dyes, such as C.I. Disperse Yellows 114, 119 and 211, are used for dyeing polyester fabrics.[3,4] The conventional reaction route for the preparation of these azo dyes comprises the reaction of pyridone as a coupling component and various diazonium salts.[5–16] Alternatively, arylazo colorants containing pyridone rings can also be prepared from β-diketones and various diazonium salts followed by condensation with cyanoacetamide.[17,18] Recently, a microwave procedure for the synthesis of azo pyridone dyes using the second reaction route was reported.[19]

* Corresponding author. E-mail: kavur@tmf.bg.ac.rs
# Serbian Chemical Society member.
doi: 10.2298/JSC100618044D

Herein, a conventional synthesis of certain 5-(substituted phenylazo)-6-hydroxy-4-methyl-3-cyano-2-pyridones from ethyl 3-oxo-2-(substituted phenylazo)-butanoates, obtained from ethyl acetoacetate and diazonium salts, and cyanoacetamide is reported (Scheme 1).

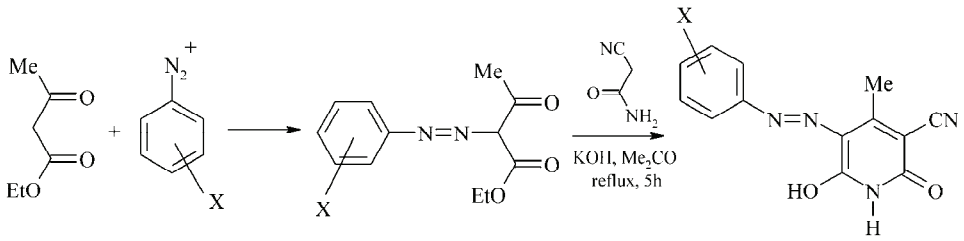

Scheme 1. Reaction route for the synthesis of certain 5-(substituted phenylazo)-6-hydroxy-4--methyl-3-cyano-2-pyridones *via* ethyl 3-oxo-2-(substituted phenylazo)butanoates (X = H (**3**), 4-Me (**3**), 4-MeO (**3**), 4-Cl (**4**), 4-Br (**5**), 4-NO_2 (**6**), 3-Me (**7**), 3-Cl (**8**), 2-MeO (**9**), 2-Cl (**10**)).

RESULTS AND DISCUSSION

Characteristic and spectroscopic data of the prepared compounds

*1,2-Dihydro-6-hydroxy-4-methyl-2-oxo-5-(phenylazo)-3-pyridinecarbonitrile (**1**)*. Orange powder; yield: 33 %; m.p. 285–286 °C (lit. m.p. 288.1 °C,[2] 278––279 °C,[8] 278–280 °C[12]). FTIR (KBr, cm^{-1}): 3447 (NH hydrazo), 3189 (NH heterocyclic), 2231 (CN), 1688, 1667 (C=O). ^{1}H-NMR (200 MHz, DMSO-d_6, δ / / ppm): 2.51 (3H, *s*, CH_3), 7.29 (1 H, *t*, J = 7.2 Hz, Ar–H), 7.48 (2H, *t*, J = 7.5 Hz, Ar–H), 7.66 (2H, *d*, J = 7.2 Hz, Ar–H), 12.04 (1H, *s*, N–H heterocyclic), 14.55 (1H, *s*, N–H hydrazone form). UV–Vis (EtOH) (λ_{max} / nm (log ε)): 399 (4.37).

*1,2-Dihydro-6-hydroxy-4-methyl-5-[(4-methylphenyl)azo]-2-oxo-3-pyridine-carbonitrile (**2**)*. Orange powder; yield: 12 %; m.p. 277–278 °C (lit. m.p. 284.4 °C,[2] 285–286 °C,[8] 252–254 °C[12]). FTIR (KBr, cm^{-1}): 3478 (NH hydrazo), 3176 (NH heterocyclic), 2225 (CN), 1680, 1648 (C=O). ^{1}H-NMR (200 MHz, DMSO––d_6, δ / ppm): 2.50 (3H, *s*, CH_3), 3.34 (3H, *s*, $ArCH_3$), 7.29 (2H, *d*, Ar–H, J = 8.4 Hz), 7.57 (2H, *d*, Ar–H, J = 8.4 Hz), 12.00 (1H, *s*, N–H heterocyclic), 14.65 (1H, *s*, N–H hydrazone form). UV–Vis (EtOH) (λ_{max} / nm (log ε)): 433 (4.03), 399 (4.12).

*1,2-Dihydro-6-hydroxy-5-[(4-methylphenyl)azo]-4-methyl-2-oxo-3-pyridine-carbonitrile (**3**)*. Dark red powder; yield: 11 %; m.p. 270–271 °C (lit. m.p. 272––273 °C[8]). FTIR (KBr, cm^{-1}): 3435 (NH hydrazo), 3189 (NH heterocyclic), 2225 (CN), 1682, 1659 (C=O). ^{1}H-NMR (200 MHz, DMSO-d_6, δ / ppm): 2.51 (3H, *s*, CH_3), 3.36 (3H, *s*, OCH_3), 7.40 (2H, *d*, J = 7.8 Hz, Ar–H), 7.60 (2H, *d*, J = 7.8 Hz,

Ar–H), 12.08 (1H, *s*, N–H heterocyclic), 14.36 (1H, *s*, N–H hydrazone form). UV–Vis (EtOH) (λ_{max} / nm (log ε)): 447 (3.70), 393 (3.90).

*5-[(4-Chlorophenyl)azo)-1,2-dihydro-6-hydroxy-4-methyl-2-oxo-3-pyridine-carbonitrile (**4**)*. Orange powder; yield: 61 %; m.p. 302–303 °C (lit. m.p. 301––302 °C,[8] 288–289 °C[12]). FTIR (KBr, cm^{-1}): 3438 (NH hydrazo), 3142 (NH heterocyclic), 2227 (CN), 1673, 1642 (C=O). ^{1}H-NMR (200 MHz, DMSO-d_6, δ / / ppm): 2.48 (3H, *s*, CH_3), 7.51 (2H, *d*, *J* = 9.0 Hz, Ar–H), 7.69 (2H, *d*, *J* = 9.0 Hz, Ar–H), 12.06 (1H, *s*, N–H heterocyclic), 14.16 (1H, *s*, N–H hydrazone form); UV–Vis (EtOH) (λ_{max} / nm (log ε)): 396 (4.12).

*5-[(4-Bromophenyl)azo)-1,2-dihydro-6-hydroxy-4-methyl-2-oxo-3-pyridine-carbonitrile (**5**)*. Orange powder; yield: 53 %; m.p. 308–309 °C (lit. m.p. >300 °C[19]). FTIR (KBr, cm^{-1}): 3444 (NH hydrazo), 3136 (NH heterocyclic), 2227 (CN), 1673, 1664 (C=O). ^{1}H-NMR (200 MHz, DMSO-d_6, δ / ppm): 2.48 (3H, *s*, CH_3), 7.57 (2H, *d*, *J* = 9.0 Hz, Ar–H), 7.67 (2H, *d*, *J* = 9.0 Hz, Ar–H), 12.07 (1H, *s*, N–H heterocyclic), 14.43 (1H, *s*, N–H hydrazone form). UV–Vis (EtOH) (λ_{max} / / nm (log ε)): 396 (4.32).

1,2-Dihydro-6-hydroxy-4-methyl-5-[(4-nitrophenyl)azo]-2-oxo-3-pyridinecar-bonitrile (**6**). Dark orange powder; yield: 54 %; m.p. >320 °C (lit. m.p. 324.0 °C,[2] 326–327 °C,[8] 326–328 °C[12]). FTIR (KBr, cm^{-1}): 3431 (NH hydrazo), 3116 (NH heterocyclic), 2227 (CN), 1696, 1672 (C=O). ^{1}H-NMR (200 MHz, DMSO-d_6, δ / / ppm): 2.52 (3H, *s*, CH_3), 7.86 (2H, *d*, *J* = 9.0 Hz, Ar–H), 8.30 (2H, *d*, *J* = 9.0 Hz, Ar–H), 12.19 (1H, *s*, N–H heterocyclic), 14.35 (1H, *s*, N–H hydrazone form). UV–Vis (EtOH) (λ_{max} / nm (log ε)): 340 (4.29).

*1,2-Dihydro-6-hydroxy-4-methyl-5-[(3-methylphenyl)azo]-2-oxo-3-pyridine-carbonitrile (**7**)*. Orange powder; yield: 51 %; m.p. 257–258 °C (lit. m.p. 266––268 °C[12]). FTIR (KBr, cm^{-1}): 3454 (NH hydrazo), 3150 (NH heterocyclic), 2218 (CN), 1671, 1645 (C=O). ^{1}H-NMR (200 MHz, DMSO-d_6, δ / ppm): 2.35 (3H, *s*, CH_3), 2.49 (3H, *s*, $ArCH_3$), 7.09 (2H, *t*, *J* = 7.2 Hz, Ar–H), 7.21–7.45 (2H, *m*, Ar–H), 12.02 (1H, *s*, N–H heterocyclic), 14.57 (1H, *s*, N–H hydrazone form). UV–Vis (EtOH) (λ_{max} / nm (log ε)): 429 (4.37), 399 (4.31).

*5-[(3-Chlorophenyl)azo)-1,2-dihydro-6-hydroxy-4-methyl-2-oxo-3-pyridine-carbonitrile (**8**)*. Orange powder; yield: 33 %; m.p. 298–300 °C (Lit. m.p. 288––290 °C[12]). FTIR (KBr, cm^{-1}): 3444 (NH hydrazo), 3155 (NH heterocyclic), 2221 (CN), 1673, 1642 (C=O). ^{1}H-NMR (200 MHz, DMSO-d_6, δ / ppm): 2.47 (3H, *s*, CH_3), 7.27 (1H, *d*, *J* = 9.0 Hz, Ar–H), 7.45 (1H, *t*, *J* = 8.0 Hz, Ar–H), 7.57 (2H, *d*, *J* = 9.0 Hz, Ar–H), 12.07 (1H, *s*, N–H heterocyclic), 14.34 (1H, *s*, N–H hydrazone form). UV–Vis (EtOH) (λ_{max} / nm (log ε)): 399 (4.51).

*1,2-Dihydro-6-hydroxy-5-[(2-methylphenyl)azo]-4-methyl-2-oxo-3-pyridine-carbonitrile (**9**)*. Red powder; yield: 61 %; m.p. 314–315 °C (lit. m.p. 324–325 °C[8]). FTIR (KBr, cm^{-1}): 3457 (NH hydrazo), 3142 (NH heterocyclic), 2226 (CN), 1672, 1658 (C=O). ^{1}H-NMR (200 MHz, DMSO-d_6, δ / ppm): 2.50 (3H, *s*,

CH_3), 3.92 (3H, *s*, OCH_3), 7.00–7.33 (2H, *m*, Ar–H), 7.61 (1H, *d*, *J* = 7.2 Hz, Ar–H), 7.75 (1H, *d*, *J* = 7.4 Hz, Ar–H), 12.06 (1H, *s*, N–H heterocyclic), 14.91 (1H, *s*, N–H hydrazone form). UV–Vis (EtOH) (λ_{max} / nm (log ε)): 379 (4.23).

*5-[(2-Chlorophenyl)azo)-1,2-dihydro-6-hydroxy-4-methyl-2-oxo-3-pyridine-carbonitrile (**10**)*. Orange powder; yield: 28 %; m.p. >320 °C (lit. m.p. 347–348 °C[8]). FTIR (KBr, cm^{-1}): 3447 (NH hydrazo), 3168 (NH heterocyclic), 2223 (CN), 1675, 1660 (C=O). ^{1}H-NMR (200 MHz, DMSO-d_6, δ / ppm): 2.50 (3H, *s*, CH_3), 7.31 (1H, *t*, *J* = 8.0 Hz, Ar–H), 7.51 (1H, *t*, *J* = 7.4 Hz, Ar–H), 7.63 (1H, *d*, *J* = 8.0, Hz Ar–H), 7.90 (1H, *d*, *J* = 7.8 Hz, Ar–H), 12.22 (1H, *s*, N–H heterocyclic), 14.95 (1H, *s*, N–H hydrazone form). UV–Vis (EtOH) (λ_{max} / nm (log ε)): 423 (4.36).

In comparison to the conventional reaction route for the preparation of the studied pyridone dyes, which requests the preparation of the starting pyridone (which usually takes about 8 h),[20] and the synthesis of azo compounds (which also takes several hours),[2] the employed reaction route takes less time (about 2–3 h for the synthesis of the arylazo keto ester and 5 h for the condensation step) but gives, according to literature,[12] lower yields. Although obtained yields are lower (low to moderate), the obtained raw products were generally of high purity and the arylazo dyes obtained in such a manner do not contain unreacted pyridone material, which is present in the first reaction route.

According to the obtained results, electron-attracting substituents in phenyl group give higher yields while electron-donating substituents give lower yields, which is in accordance with the reaction mechanism of pyridone formation.[21] The unreacted intermediate can be isolated by washing the solid residue (obtained from the filtrate after isolation of the product) with hot ethanol and used again for the synthesis of the wanted azo pyridone dye by simple introduction in a new reaction mixture.

The arylazo pyridone dyes prepared in this work may exist in two tautomeric forms: the hydrazone and azo form[8,15] (Fig. 1). The infrared spectra of all syn-

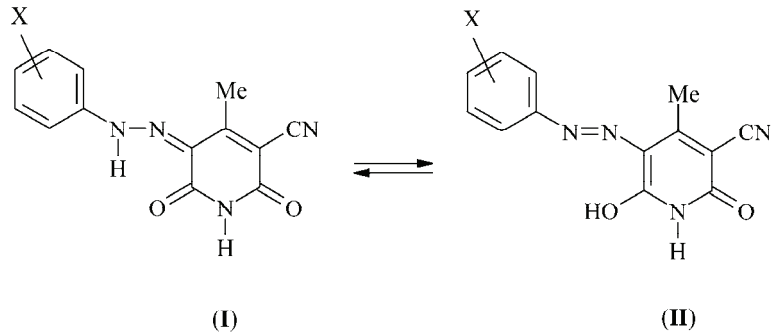

(**I**) (**II**)

Fig. 1. The equilibrium between the hydrazone form (**I**) and the azo form (**II**) of 5-(substituted phenylazo)-6-hydroxy-4-methyl-3-cyano-2-pyridones.

thesized dyes showed two intense carbonyl bands at about 1642 and 1696 cm^{-1}, which were assigned to the diketohydrazone form. The spectra exhibited a broad N–H hydrazone band in the region 3434–3457 cm^{-1} which suggests that these compounds dominantly exist in the solid state in the hydrazone tautomeric form.

The ^{1}H-NMR spectra of the dyes exhibited a signal near 14.16–14.99 ppm. This signal corresponds to the imino N–H proton resonance of the hydrazone form. The obtained results are in agreement with the data obtained by Ertan and Gurkan[12] (hydrazone form with N–H peaks in the range of 15.1–15.6 ppm) and also by Peng *et al*.[22,23] (hydrazone form with N–H peaks in the range of 14.30––16.09 ppm).

EXPERIMENTAL

Materials

All the used materials were obtained commercially, mostly from Fluka, and were used without further purification.

Equipment

The IR spectra were recorded on a Bomem FTIR Spectrophotometer, MB series, in the form of KBr pellets. The ^{1}H-NMR spectra were recorded as solutions in DMSO-d_6 using a Varian Gemini-200 instrument, with tetramethylsilane as the internal standard. The UV–Vis absorption spectra were taken using a Shimadzu 1700 UV–Vis spectrophotometer in 1.00 cm cells at 25±0.1 °C in ethanol at a concentration of 5×10^{-5} mol dm^{-3}.

Synthesis of azo pyridone dyes

To a solution of ethyl acetoacetate (0.01 mol) in 30 cm^3 of ethanol, sodium acetate (3.0 g) was added. The mixture was cooled to 0 °C and a cooled solution of arenediazonium chloride (prepared from 0.01 mol of substituted aniline in 5 cm^3 of dilute HCl (6 M) and a solution of $NaNO_2$ (0.0105 mol) in water (4.2 cm^3) was added under stirring. The stirring was continued for one hour after which the solid was collected, washed with 2×5 cm^3 of water and 2×5 cm^3 of ethanol, and dried in air.

The obtained product (0.01 mol), potassium hydroxide (0.017 mol) and cyanoacetamide (0.02 mol) were dissolved in 15 cm^3 of acetone and stirred and refluxed for 5 h. The resulting mixture was acidified using dilute HCl, and the solid product was collected by filtration and washed with 2×5 cm^3 of water and 2×5 cm^3 acetone. The obtained crystals were then recrystallized from acetone.

CONCLUSIONS

A new simple procedure for the synthesis of 5-(substituted phenylazo)-6-hydroxy-4-methyl-3-cyano-2-pyridones is presented. Synthesis from ethyl 3-oxo-2--(substituted phenylazo)butanoates in acetone gave products in low to moderate yields. These dyes exist in the hydrazone tautomeric form in the solid state and in solvent DMSO-d_6.

Acknowledgments. The authors are grateful to the Ministry of Science and Technological Development of the Republic of Serbia for financial support (Projects 172013 and III 45001).

ИЗВОД

СИНТЕЗА 5-(СУПСТИТУИСАНИХ ФЕНИЛАЗО)-6-ХИДРОКСИ-4-МЕТИЛ-3-ЦИЈАНО-2--ПИРИДОНА ИЗ ЕТИЛ-3-ОКСО-2-(СУПСТИТУИСАНИХ ФЕНИЛАЗО)БУТАНОАТА

ЈАСМИНА ДОСТАНИЋ[1], НАТАША ВАЛЕНТИЋ[2], ГОРДАНА УШЋУМЛИЋ[2] и ДУШАН МИЈИН[2]

[1]*Институт за хемију, технологију и металургију, Универзитет у Београду, Центар за катализу и хемијско инжењерство, Његошева 12, 11000 Београд и* [2]*Катедра за органску хемију, Технолошко–металуршки факултет, Универзитет у Београду, Карнегијева 4, 11120 Београд*

Нови поступак за синтезу познатих азо-пиридонских боја је описан у раду. Серија 5-(супституисаних фенилазо)-6-хидрокси-4-метил-3-цијано-2-пиридона је припремљена из етил-3-оксо-2-(супституисаних фенилазо)бутаноата и цијаноацетамида у ацетону коришћењем калијум-хидроксида као катализатора уз загревање.

(Примљено 11. јуна, ревидирано 22. новембра 2010)

REFERENCES

1. H. Zollinger, *Colour Chemistry*, VCH, Weinheim, 1987, p. 85
2. C.C. Chen, I. J. Wang, *Dyes Pigm.* **15** (1991) 69
3. W. Huang, H. Qian, *Dyes Pigm.* **77** (2008) 446
4. W. Huang, *Dyes Pigm.* **79** (2008) 69
5. L. Cheng, X. Chen, K. Gao, J. Hu, *Dyes Pigm.* **7** (1986) 373
6. A. Cee, B. Horakova, A. Lycka, *Dyes Pigm.* **9** (1988) 375
7. D. Rangnekar, R. Parekh, *Dyes Pigm.* **9** (1988) 475
8. P. Y. Wang, I. J. Wang, *Text. Res. J.* **60** (1990) 519
9. I. Wang, Y. Hus, J. Tian, *Dyes Pigm.* **16** (1991) 83
10. M. Matsui, B. Joglekar, Y. Ishigure, K. Shibata, H. Muramatsu, Y. Murata, *Bull. Chem. Soc. Jpn.* **66** (1993) 1790
11. N. Ertan, F. Eyduran, *Dyes Pigm.* **27** (1995) 313
12. N. Ertan, P. Gurkan, *Dyes Pigm.* **33** (1997) 137
13. H. Song, K. Chen, H. Tian, *Dyes Pigm.* **53** (2002) 257
14. M. Wang, K. Funabiki, M. Matsui, *Dyes Pigm.* **57** (2003) 77
15. G. Ušćumlić, D. Mijin, N. Valentić, V. Vajs, B. Sušić, *Chem. Phys. Lett.* **397** (2004) 148
16. D. Mijin, G. Ušćumlić, N. Perišić-Janjić, N. Valentić, *Chem. Phys. Lett.* **418** (2006) 223
17. G. El-Zanate Elgemeie, A. Mansour, *Bull. Chem. Soc. Jpn.* **66** (1993) 555
18. D. Mijin, G. Ušćumlić, N. Perišić-Janjić, I. Trkulja, M. Radetić, P. Jovančić, *J. Serb. Chem. Soc.* **71** (2006) 435
19. D. Ž. Mijin, M. Baghbanzadeh, C. Reidlinger, C. Oliver Kappe, *Dyes Pigm.* **85** (2010) 73
20. J. M. Bobbit, D. A. Skola, *J. Org. Chem.* **25** (1960) 560
21. M. Mišić-Vuković, M. Radojković-Veličković, *J. Serb. Chem. Soc.* **63** (1998) 585
22. Q. Peng, M. Li, K. Gao, L. Cheng, *Dyes Pigm.* **14** (1990) 89
23. Q. Peng, M. Li, K. Gao, L. Cheng, *Dyes Pigm.* **15** (1991) 236.

Journal of the Serbian Chemical Society
JSCS-info@shd.org.rs • www.shd.org.rs/JSCS
J. Serb. Chem. Soc. *76* (4) 505–512 (2011)
JSCS–4137
UDC *Oxytropis pilosa*:577.151.6:547.972.2:535.379:615.27
Original scientific paper

A study of the antioxidants in *Oxytropis pilosa* (L.) DC.

DRAGOLJUB MILADINOVIĆ[1]*, LJILJANA MILADINOVIĆ[2] and STEVO NAJMAN[3]

[1]*Department of Pharmacy, School of Medicine, University of Niš, Bulevar dr Zorana Đinđića 81, 18000 Niš,* [2]*High school "B. Stanković", Voždova 27, 18000 Niš and* [3]*Department of Biology, School of Medicine, University of Niš, Bulevar dr Zorana Đinđića 81, 18000 Niš, Serbia*

(Received 1 July, revised 27 August 2010)

Abstract: The objective of this study was to estimate the antioxidative potential of *Oxytropis pilosa* (L.) DC. during the active vegetative period. The activities of the antioxidant enzymes (superoxide dismutase, catalase, peroxidase), the quantities of malonyldialdehyde, superoxide and hydroxyl radicals and reduced glutathione and the content of total flavonoids, chlorophylls *a* and *b*, carotenoids and soluble proteins were determined. The results showed that extracts from all plant organs exhibited antioxidant activity. The highest antioxidant ability was observed in the leaves where all the investigated antioxidant enzymes were active in a specific way: During the spring season, peroxidase showed the maximum activity 18.54 U mg^{-1} protein, catalase peaked in summer 9.04 U mg^{-1} protein, whereas, during the autumn season, superoxide dismutase showed maximum activity, 54.28 U mg^{-1} protein. Reduced glutathione, pigments and carotenoids present in the leaves contribute to the high antioxidant activity. Furthermore, inhibition of chemiluminescence activity of Balb/c mice blood phagocytes by crude leaf extracts at concentrations of 3.5 and 7.0 μg cm^{-3} were 30.2 and 36.5 %, respectively.

Keywords: *Oxytropis pilosa*; superoxide dismutase; catalase; peroxidase; antioxidant activity; total flavonoids, chemiluminescence.

INTRODUCTION

Oxytropis pilosa (L.) DC. is a widespread but disjunct relict species that originated in the Altai, Siberia, from where it extended to the West. The species is frequently found from the Russian and Ukrainian steppes to the Alps and thins out on its ways to Scandinavia, the Baltic States and East Europe.[1] In Serbia, it can be found with scattered distribution in the southeastern parts of the country.[2]

* Corresponding author. E-mail: dragoljubm@gmail.com
doi: 10.2298/JSC100701045M

Oxytropis species are well known as the "King of Herbs" in Chinese Tibetan medicine.[3] However, some *Oxytropis* species contain very toxic indolle alkaloids.[4] Current knowledge about the antioxidant properties of *O. pilosa* (L.) DC. are not supported by the available reference data.

This research was designed to study the antioxidant activity of *Oxytropis pilosa* (L.) DC. The antioxidative properties of leaf, stalk and root of *O. pilosa* (L.) DC. during the vegetative period were investigated by determining the activities of the antioxidant enzymes superoxide dismutase (SOD), catalase (C-ase) and peroxidase (P-ase); the quantities of malonyldialdehyde (MDA), the reactive oxygen species (ROS) superoxide (O_2^-) and hydroxyl radicals (·OH) and reduced glutathione (GSH), and the contents of total flavonoids, chlorophylls *a* and *b*, carotenoids and soluble proteins. The paper also describes the inhibition of the chemiluminescence activity of Balb/c mice blood phagocytes by leaves extracts.

EXPERIMENTAL

Plant material

The entire plants of *Oxytropis pilosa* (L.) DC. were collected in 2008 during the active vegetative period (April to October) from Subotinac, southeastern Serbia. The plant material was collected at three stages of growth (SG) as follows:

– 1st SG – the initial vegetation stage (April 2008)
– 2nd SG – the blooming stage (June 2008)
– 3rd SG – the seed forming stage (October 2008)

Botanical identification was made by Dr. N. Randjelović of the Botany Department, Faculty of Science, University of Niš, Serbia, where a voucher specimen is deposited.

Methods

One g of plant material was ground with quartz sand in a cold mortar. The ground material was suspended in 5 cm^3 0.1 mol dm^{-3} K_2HPO_4 at pH 7. After 10-min centrifugation at 4 °C and 15000 g, aliquots of the supernatant were used for SOD activity measurements. 20 µl of Tsuchiashi solution (chloroform/ethanol 3/5) were added to the supernatant before measurement of the enzyme activity. The SOD activity was determined in aliquots by the method of Misra and Fridovich[5] based on the inhibition of the transformation of adrenaline to adrenochrome at pH 10.2. For the other antioxidant enzymes and other biochemical determinations, the plant material was treated in the same way but the medium was 0.1 mol dm^{-3} phosphate buffer (K_2HPO_4/KH_2PO_4, pH 7) with a plant material to medium ratio of 1:5, centrifuged for 10 min at 15000 *g*. After the centrifugation, the supernatant was evaluated for:

– C-ase activity spectrophotometrically at 240 nm;[6]
– P-ase activity, using guacol as substrate;[7]
– lipid peroxidation (LP) by the thiobarbituric acid (TBA) method; the values are given as equivalent amounts of malonyldialdehyde (MDA);
– the calibration curve was prepared with malonyldialdehyde bis-diacetal; [8]
– the superoxide radical was determined by the auto-oxidation of adrenaline;[9]
– the hydroxyl radical by the inhibition of deoxyribose degradation.[10]

Moreover, the amount of GSH was determined with Ellman reagent[11] and protein by Folin reagent[12]. Total flavonoids were estimated according to Marckam.[13] The pigments were extracted with acetone and determined spectrometrically using molar extinction coefficients reported by Wettstein.[14]

The experimental results are expressed as the mean±standard deviation of three replicates.

Chemiluminescence assay

The chemiluminescence (CL) assay was performed to measure the total antioxidant potential of plant origin. The CL intensity in phagocytosis of mouse's blood leukocytes served as a measure of the oxidant activity.[15] The CL intensities were measured on a liquid scintillation counter Beckman LS 3200 in the "out of coincidence" mode. Blood samples of Balb/c mice were prepared as previously described.[16] Luminol (5-amino-2,3-dihydrophthalazine-1,4-dione) solution, 0.1 mol dm^{-3} in dimethyl sulfoxide (Sigma) was used as the chemiluminogenic probe. The CL mixture was diluted with phosphate buffer (pH 7.2) to a final concentration of 10^{-5} mol dm^{-3}. In order to estimate enzymatic and non-enzymatic compounds of plant and their antioxidant activity, two manners of extract preparation were used. Crude leaf extract was prepared simultaneously as for the determination of the enzymatic activity. Leaves collected in the blooming stage of vegetation were used. A boiled leaf extract was obtained after cooling of the crude one (95 °C, 30 min). Blood sample without a test extract served as a control. Butylated hydroxytoluene (BHT) was used as a standard common antioxidant. The measurements of CL were performed in duplicate.

RESULTS AND DISCUSSION

Significant OH accumulation in the leaves (1.74 nmol mg^{-1} protein) contributes to a high level of LP (14.31 nmol mg^{-1} protein), but does not contribute to O_2^- accumulation in the same plant organ. The highest amount of O_2^- was detected in the root during all observed SG (Table I). The different responses of LP and O_2^- accumulation between root and leaf may be associated with the intensity level of environmental stress and different protective mechanisms.[17]

TABLE I. Quantities of reduced glutathione, malonyldialdehide, O_2^-, $^{\bullet}OH$ and protein in the organs of *Oxytropis pilosa* (L.) DC.

SG	Plant organ	Content				
		GSH U mg^{-1} prot.	MDA nmol mg^{-1} prot.	O_2^- nmol mg^{-1} prot.	$^{\bullet}OH$ nmol mg^{-1} prot.	Protein mg g^{-1}
1st	Leaf	1.98±0.18	9.74±0.97	152.68±9.76	1.70±0.33	7.95±0.60
	Stalk	0.51±0.06	5.76±0.89	251.73±8.42	1.38±0.29	7.84±0.50
	Root	0.85±0.08	6.94±0.79	276.32±11.04	1.29±0.23	7.24±0.40
2nd	Leaf	2.10±0.23	13.10±1.56	168.56±9.58	1.82±0.29	10.87±0.89
	Stalk	0.62±0.08	7.29±0.91	230.78±8.69	1.61±0.31	8.60±0.60
	Root	0.94±0.19	8.92±0.79	332.79±10.21	1.24±0.21	7.96±0.84
3rd	Leaf	1.32±0.15	14.31±2.76	214.78±10.71	1.74±0.28	7.24±0.50
	Stalk	0.34±0.05	8.10±0.82	243.44±8.89	1.43±0.22	5.25±0.70
	Root	1.15±0.14	12.56±2.05	323.56±11.04	1.05±0.19	6.24±0.41

The GSH quantity in the leaves was the highest in the blooming stage (2.10 μmol mg^{-1} protein). The present results, in comparison with literature data,[18] suggest that the research plant species was not dramatically exposed to the negative influences of $^{\bullet}OH$ and O_2^-. Of course, the low quantity of GSH does not

automatically mean low activity of the other components of the antioxidant system.

The protein contents in the plant organs were significantly higher in blooming stage than in other SGs. A different variation of protein over the seasons was observed by Bogdanović[19] in *Picea omorika* (Panč.) Purkinye. In the study of the antioxidant defence system of high mountain and steppe plants, the average protein concentration was 29 mg g^{-1} dry in steppe plants of the family Fabaceae and 38 mg g^{-1} dry in alpine plants. This may be important under the low temperature and inadequate water conditions of alpine regions.[20]

TABLE II. Contents of total flavonoids, chlorophylls *a* and *b* and carotenoids in the leaves of *Oxytropis pilosa* (L.) DC.

SG	Flavonoids mg g^{-1} dry	Chlorophyll *a* mg g^{-1}	Chlorophyll *b* mg g^{-1}	Carotenoids mg g^{-1}
1st	0.126±0.005	1.54±0.46	0.70±0.05	0.52±0.07
2nd	0.232±0.008	1.76±0.61	0.71±0.08	0.63±0.08
3rd	0.091±0.007	1.39±0.38	0.52±0.04	0.41±0.06

The quantity of total flavonoids and the contents of pigments are presented in Table II. The highest values of all the investigated parameters were found in the blooming vegetation stage. The lower quantities of O_2^- in the leaves (Table I), where the total flavonoids (0.232 mg g^{-1} dry) and carotenoids contents (0.63 mg g^{-1}) were the highest, may support the assertion of the high antioxidant ability of leaves.

The changed antioxidant enzyme activities in plant organs of *O. pilosa* (L.) DC. show a different antioxidant metabolism in response to environmental stress. The leaves exhibited the highest SOD, C-ase and P-ase activities in all SG (Table III). The vegetation stage had a significant effect on the SOD activity in *O. pilosa* (L.) DC. the activity being significantly higher in the seed forming stage than in the other two vegetation stages. The SOD activity in the leaves of *Astragalus vulneria* (Fabaceae) was 60 U g^{-1} FW.[20] The SOD activity in *Allium ursinum*[18] was found to be as low as the activity detected in leaves of *O. pilosa* (L.) DC. (54.28 U mg^{-1} protein). SOD plays a central role in the enzymatic defence system in removing O_2^-.[21] The accumulation of O_2^- occurred in the root, together with changes in the SOD activity. The increased O_2^- production in the roots under environmental stress is correlated with the decreased SOD activity. Since enhanced information of ROS under stress conditions induce both protective responses and cellular damage,[22] the obtained results indicate that O_2^- accumulation in the root involves a protective mechanism under environmental stress in *O. pilosa* (L.) DC.

The C-ase activity in the researched plant was influenced by seasonal conditions (Table III). The highest activity in the blooming stage (9.04 U mg^{-1} protein) shows that catalase may also be involved in the protection from intense light

and high temperature. The combined action of C-ase and SOD converts O_2^- and H_2O_2 to water and molecular oxygen, thus averting cellular damage under unfavourable conditions such as water stress.[23]

TABLE III. Activities of the antioxidant enzymes in the organs of *Oxytropis pilosa* (L.) DC.

SG	Plant organs	*SOD* U mg^{-1} prot.	C-ase U mg^{-1} protein	P-ase U mg^{-1} protein
1st	Leaf	51.43±5.78	8.32±0.87	18.54±1.20
	Stalk	25.41±3.82	5.16±0.58	14.89±0.54
	Root	23.70±3.46	6.96±0.51	5.46±0.43
2nd	Leaf	48.26±6.27	9.04±0.82	16.23±0.98
	Stalk	24.12±3.56	6.28±0.56	12.33±0.49
	Root	25.21±2.36	6.26±0.34	7.54±0.36
3rd	Leaf	54.28±4.55	7.64±0.52	15.76±0.71
	Stalk	25.89±3.24	3.85±0.28	10.64±0.51
	Root	27.36±3.82	6.14±0.31	8.72±0.43

The vegetation stage had no significant influence on peroxidase activity in the examined plant organs. The very small changes in the P-ase activity in the leaves of *O. pilosa* (L.) DC. (15.76–18.54 U mg^{-1} prot.) may indicate its physiological importance in all vegetation stages. On the other hand, literature data report significant differences in P-ase activity in some plant species.[24,25] The reason for this is several isoenzymes that have separate physiological functions. For example, in *Minium affine* exposed to extreme drought conditions, two isoenzymes were found after rehydration. The first responsible for drought protection and second involved in the cell repair system.[26]

The parameters of CL inhibition of blood phagocytes by leaf extracts of *O. pilosa* (L.) DC. (collected in the blooming vegetation stage) are given in Table IV and presented in Figs. 1 and 2. The extract of *O. pilosa* (L.) DC. reduced chemiluminiscence emission at both employed concentrations in a dose-dependent manner. Compared to the common antioxidant BHT, the inhibition was lower, but compared to commercial vegetal extracts of Isoflavin Beta and red clover, the extracts of *O. pilosa* (L.) DC. demonstrated higher levels of inhibition.[27] Sin-

TABLE IV. Parameters of the inhibition of the CL activity of blood phagocytes by *Oxytropis pilosa* (L.) DC. extracts

Sample	Inhibition[a], %	Index of inhibition[b]
BHT (3.5 μg cm^{-3})	49.1	–
BHT (7.0 μg cm^{-3})	55.8	–
Crude leaves extract (3.5 μg cm^{-3})	30.2	61.6
Crude leaves extract (7.0 μg cm^{-3})	36.5	65.5
Boiled leaves extract (3.5 μg cm^{-3}	24.4	49.6
Boiled leaves extract (7.0 μg cm^{-3})	45.8	82.0

[a]100×CL sample/CL control; [b]100×CL sample/CL BHT

ce BHT is known to be a free radical scavenger, it can be concluded that the CL inhibitory effect of the *O. pilosa* (L.) DC. leaf extract included the scavenger effect. According to the results obtained for peroxidase activity in leaves (Table III), a high level of activity in the initial and blooming vegetation stages could be seen. It is possible that peroxidase was "responsible" for high antioxidant activity of the crude leaf extract.

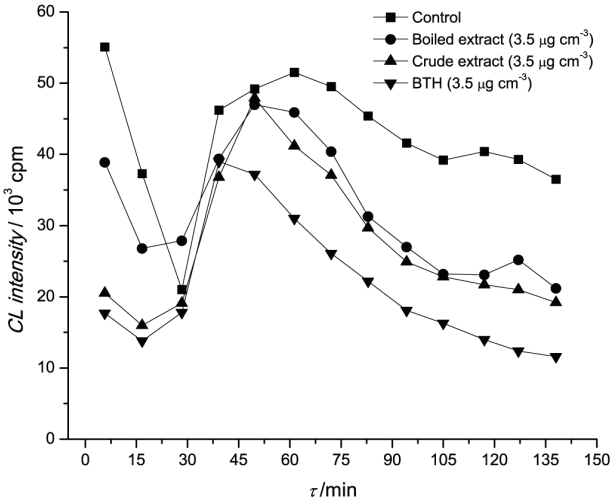

Fig. 1. Antioxidant activity of *O. pilosa* (L.) DC. extracts at lower doses.

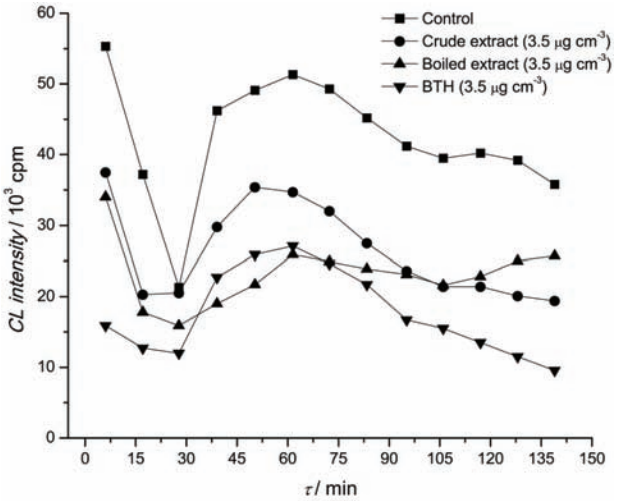

Fig. 2. Antioxidant activity of *O. pilosa* (L.) DC. extracts at higher doses.

There were some differences between the crude and boiled extracts. The crude extract showed an approximate inhibition by 33 %, while the boiled one

inhibited by about 35 %. The lower inhibition of CL intensity in the crude leaf extract could be due to a deficit in antioxidant compounds in the reaction mixture, in contrast to the persistence of substances with pro-oxidant activity. The inhibitory activity of the boiled extract was more dose-specific than those of the crude extracts, which is in accordance with the previous explanation. The opposite effects could involve direct stimulating action on the phagocyte cell, chemical pro-oxidant action and anti-inhibitory action in different ways.[28]

CONCLUSIONS

The results reported herein can be considered as initial information on the antioxidant properties of *O. pilosa* (L.) DC. The examined antioxidant enzymes changed the levels of their activities in the vegetative period in specific way. During the spring season P-ase showed maximum activity, C-ase peaked in the summer, whereas SOD showed maximum activity during the autumn season. This suggests a complementary action of these enzymes, in response to external changes. The examined antioxidant enzymes may be used as indicators of the antioxidant ability of *O. pilosa* (L.) DC. to environmental changes. All the investigated organs possessed effective antioxidants, especially the leaves. Furthermore, the inhibition of the chemiluminiscence activity of Balb/c mice blood phagocytes by crude leaf extracts at concentrations of 3.5 and 7.0 μg cm^{-3} were 30.2 and 36.5 %, respectively. Therefore, the leaves could be used as a source of natural antioxidants and in the pharmaceutical industry for the manufacture of products with a potent oxygen radical scavenger activity.

Acknowledgements. We thank Prof. Dr Novica Ranđelović for the botanical determination of the plant species.

ИЗВОД

ПРОУЧАВАЊЕ АНТИОКСИДАНАТА У *Oxytropis pilosa* (L.) DC.

ДРАГОЉУБ МИЛАДИНОВИЋ[1], ЉИЉАНА МИЛАДИНОВИЋ[2] и СТЕВО НАЈМАН[3]

[1]Катедра за фармацију, Медицински факултет, Универзитет у Нишу, Булевар др Зорана Ђинђића 81, 18000 Ниш, [2]Гимназија „Бора Станковић“, Вождова 27, 18000 Ниш и [3]Катедра за биологију, Медицински факултет, Универзитет у Нишу, Булевар др Зорана Ђинђића 81, 18000 Ниш

У раду су приказани резултати проучавања антиоксидантних ензима супероксид-дисмутазе, каталазе и пероксидазе у листу, стаблу и корену самоникле популације *Oxytropis pilosa* (L.) DC. из југоисточне Србије. Такође су проучавани садржаји малонил-диалдехида, супероксид- и хидрокси-радикала, редукованог глутатиона, као и садржај укупних флавоноида, хлорофила *а* и *б*, каротеноида и растворљивих протеина. Највиша антиоксидантна активност је забележена у лишћу, у коме су антиоксидантни ензими активни на специфичан начин: у пролеће пероксидаза испољава максималну активност, 18,54 U mg^{-1} протеина; максимум активности каталазе је у лето, 9,04 U mg^{-1} протеина; док је супероксид-дизмутаза у јесен најактивнији ензимски систем, 54,28 U mg^{-1} протеина. Редуковани глутатион, пигменти и каротеноиди присутни у лишћу доприносе високој антиоксидантној активности проучаване биљне врсте. У прилог овоме је инхибиција хемилуминесцентне активности фагоцита Balb/c мишева свежим екстрактом лишћа у концентрацијама од 3,5 и 7,0 μg cm^{-3} од

30,2, односно 36,5 %. Из овог разлога лишће *O. pilosa* (L.) DC. се може користити као извор природних антиоксиданата и бити сировинска база за производњу фармаколошких препарата значајне антиоксидантне активности.

(Примљено 1. јула, ревидирано 27. августа 2010)

REFERENCES

1. M. Schlee, M. Göker, G. W. Grimm, W. Sauer, V. Hemleben, in *Relict Species Phylogeography and Conservation Biology*, J. C. Habel, T. Assmann, Eds., Springer-Verlag, Berlin, 2010, p. 105
2. N. Diklić, in *Flora of SR Serbia*, Vol. IV, M. Josifović, Ed., Serbian Academy of Sciences and Arts, Belgrade, 1974, p. 301
3. C. Lou, M. Wang, G. Yang, H. Cai, Y. Li, F. Zao, H. Yang, L. Tong, *Toxicol. in Vitro* **23** (2009) 906
4. R. J. Molyneux, S. T. Lee, D. R. Gardner, K. E. Panter, L. F. James, *Phytochemistry* **68** (2007) 2973
5. H. P. Misra, I. Fridovich, *J. Biol. Chem.* **247** (1972) 3170
6. L. M. Simon, Z. Fatrai, D. E. Jonas, B. Matkovics, *Biochem. Physiol. Pflanzen* **166** (1974) 387
7. B. Matkovics, R. Novak, H. D. Hanh, L. Szabo, I. Varga, A. Zalesna, *Comp. Biochem. Physiol. B* **56** (1977) 31
8. Z. A. Placer, L. Custman, B. C. Hohnson, *Anal. Biochem.* **16** (1968) 359
9. R. A. Greenwald, *Handbook of Methods for Oxygen Radical Research*, CRC Press Inc., Boca Raton, Fl, 1985, p. 230
10. K. H. Cheesman, A. Beavis, H. Esterbauer, *Biochem. J.* **252** (1988) 649
11. I. Sedlak, R. H. Lindsay, *Anal. Biochem.* **25** (1968) 192
12. O. H. Lowry, N. J. Rosebrought, A. L. Randal, *J. Biol. Chem.* **193** (1951) 265
13. K. R. Markam, *Methods in Plant Biochemistry*, Academic Press, London, 1989, p. 48
14. D. Wettstein, *Exp. Cell Res.* **12** (1957) 427
15. O. Hirayama, M. Takagi, K. Hukumoto, S. Katoh, *Anal. Biochem.* **247** (1997) 237
16. S. Rais, A. Perianin, M. Lenoir, A. Sadak, D. Rivollet, M. Paul, M. Denian, *Antimicrob. Agents Chemother.* **44** (2000) 2406
17. B. Shaomin, Y. Jiang, *Scient. Horticult.* **120** (2009) 264
18. D. Štajner, B. M. Popović, J. Čanadanović-Brunet, M. Štajner, *Fitoterapia* **79** (2008) 303
19. J. Bogdanović, N. Milosavić, R. Prodanović, T. Dučić, K. Radotić, *Biochem. Syst. Ecol.* **35** (2007) 263
20. I. Öncel, E. Yurdakulol, Y. Keles, L. Kurt, A. Yildiz, *Acta Oecol.* **26** (2004) 211
21. G. Bartosz, *Biochem. Pharmacol.* **30** (2008) 13
22. O. Blokhina, E. Virolainen, K. V. Fagerstedt, *Ann. Bot.* **91** (2003) 179
23. K. V. Chaitanya, D. Sundar, S. Masilamani, A. Ramachadra Reddy, *Plant Growth Regul.* **36** (2002) 175
24. D. Štajner, B. M. Popović, M. Gavrilović, *Arh. Farm.* **5** (1997) 612
25. D. Štajner, J. Čanadanović-Brunet, *Phytother. Res.* **13** (1999) 333
26. K. Christov, N. Bakardijeva, *Plant Perox. News Lett.* **11** (1998) 35
27. S. R. Georgetti, R. Casagrande, V. M. Di Mambro, A. E. Azzolini, M. J. Fonseca, *AAPS PharmSci.* **5** (2003) 1
28. J. Ngoupayo, T. K. Tabopda, M. S. Ali, *Bioorg. Med. Chem.* **17** (2009) 5688.

Journal of the Serbian Chemical Society
JSCS-info@shd.org.rs • www.shd.org.rs/JSCS
J. Serb. Chem. Soc. *76* (4) 513–522 (2011)
JSCS–4138
UDC 66.091.8+547.56+620.266.1
Original scientific paper

Removal of aqueous phenol and phenol derivatives by immobilized potato polyphenol oxidase

NIKOLA LONČAR[1#], NATAŠA BOŽIĆ[2#], IVAN ANĐELKOVIĆ[1], ALEKSANDRA MILOVANOVIĆ[2#], BILJANA DOJNOV[2#], MIROSLAVA VUJČIĆ[2#], GORAN ROGLIĆ[1#] and ZORAN VUJČIĆ[1*#]

[1]*Faculty of Chemistry, University of Belgrade, Studentski trg 12–16, Belgrade and* [2]*Institute of Chemistry, Technology and Metallurgy – Center of Chemistry, University of Belgrade, Studentski trg 12–16, Belgrade, Serbia*

(Received 19 July, revised 6 September 2010)

Abstract: Phenols containing halogens, which tend to deactivate the aromatic nuclei, constitute a significant category of highly toxic and difficult-to-degrade pollutants, which arise from a wide variety of industries. The main purpose of this study was to obtain an inexpensive immobilized enzyme for the removal of phenols. Partially purified potato polyphenol oxidase (PPO) was immobilized onto different commercial and laboratory produced carriers. Three of the obtained biocatalysts, with the highest PPO activities, namely Eupergit C250L––PPO; Celite–PPO and CelluloseM–PPO, were tested in a batch reactor for the removal of phenol, 4-chlorophenol and 4-bromophenol. In the case of 2.5 mM substrates with Eupergit C250L–PPO, an around 45 % removal of 4-bromophenol was achieved, while the removals 4-chlorophenol and phenol were 35 and 20 %, respectively. The reusability of Eupergit C250L–PPO for the removal of 4-chlorophenol was tested. After eight repeated tests, the efficiency of 4-chlorophenol removal by Eupergit C250L–PPO immobilisate had decreased to 55 %.

Keywords: polyphenol oxidase; potato; phenol; immobilization; Eupergit.

INTRODUCTION

Increased production of plastics, dyes, pesticides and other chemicals has resulted in the generation of hazardous chemical wastes and hence environmental pollution. A few persistent pollutants, including several pesticides, are carried in air and water over several hundred kilometers, affecting the wildlife and general population.[1] These pollutants are non-biodegradable and are known to have carcinogenic, mutagenic or chronic toxic effects.

* Corresponding author. E-mail: zvujcic@chem.bg.ac.rs
# Serbian Chemical Society member.
doi: 10.2298/JSC100619046L

Chlorinated organic compounds, in particular, are found to be resistant to biochemical degradation. Monochlorophenols, among others phenol compounds, serve as intermediates in the production of pesticides.[2] These are also used as antimicrobial agents in a wide array of products, such as adhesives, oils, textiles and pharmaceutical products. Phenols are present in the wastewater of various industries, such as refineries up to 6–500 mg L^{-1}, coking operations (28–3900 mg L^{-1}), coal processing (9–6800 mg L^{-1}) and the manufacture of petrochemicals (2.8–1220 mg L^{-1}).[3,4] Other sources of wastewater streams containing phenols are pharmaceuticals, plastics, wood products, paint and pulp, and paper industries (0.1–1600 mg L^{-1}).[3,4] The release of phenol-containing wastewater into open water is forbidden without prior treatment because of the toxicity of phenol and its derivatives. Due to the toxic nature of some of these compounds, the Environmental Protection Agency, EPA, has set a water purification standard of less than 1 μg L^{-1} of phenol in drinking waters.[5] Moreover, EPA studies have shown that the usage of chlorine for disinfection of phenol-containing water may yield toxic 2-chlorophenol.[5]

Biological treatment methods are generally cheaper than physical or chemical treatment methods for lowering phenol concentrations.[6] The microorganisms used are usually aerobes, including *Pseudomonas* sp., *Alcaligenes* sp., *Azotobacter* sp., *Rhodococcus* sp. and *Cryptococcus* sp.[7,8] Most of these studies were performed with pure cultures. The inherent toxicity of chlorophenols, or of the intermediates produced during their degradation, compromises the ability of such pure cultures to completely mineralize the chlorophenols present in wastewater. In addition, bromophenols are actually used as effective disinfection reagents. Therefore, biological treatment techniques, if used alone, have a serious limitation in treating non-biodegradable/toxic chemicals. Another alternative is to use enzymes, such as polyphenol oxidases and peroxidases. Nevertheless, the major obstacle in the commercial application of soluble enzymes for environmental purposes is their limited operational stability, which means that a continuous supply of large amounts of fresh and partially purified enzyme is required.

However, enzyme immobilization is an excellent technique to overcome this problem due to its high storage stability and better control of the catalytic process.[9] The potential advantages of enzymatic treatment as compared with conventional treatments include among others: application to recalcitrant materials, operation at high and low contaminant concentrations over a wide pH range, including extreme values (pH 2 or 11), and temperature and salinity ranges, and easy control of the process.

A number of oxidative enzymes from bacteria, fungi and plants have been reported to play an important role in numerous waste treatment applications. Peroxidases and polyphenol oxidases can act on specific recalcitrant pollutants by precipitation or transforming to other products and permitting a better final treat-

ment of the waste. Improvement of the enzyme operational stability and half-life and thereby a reduction in treatment cost was accomplished through enzyme immobilization.[10]

For the treatment of large volumes of waste-waters, reactors containing immobilized enzymes are desirable because of the high cost of enzymes. Enzyme immobilization techniques usually provide, in addition to the desired reuse of the enzyme, unexcelled advantages such as product separation and continuous operation.[11] Cheaper supports and enzymes for the preparation of immobilized enzyme preparations for such applications are always been sought after. Polyphenol oxidase (PPO) from potato is an exceptionally cheap enzyme because it can be purified from potato waste of the food industry. It was shown previously[12] that PPO activity was the greatest at the exterior of the tuber, including the skin and cortex tissue 1 to 2 mm beneath the skin.

Therefore, in this work, the possible use of several commercial carriers, as well as a few non-conventional carriers, for potato PPO immobilization was examined. Three of them, Eupergit C250L, Celite and CelluloseM, which had the highest percentage of bound PPO activity, were tested in batch reactors for the removal of phenol, 4-chlorophenol (CP) and 4-bromophenol (BP) from synthetic wastewater.

EXPERIMENTAL

Reagents

Potato *(Solanum tuberosum*) tubers were obtained from the local market. Commercially available carriers: Eupergit C250L, Celite, Cellulose (MTM®, Green Sand and Birm), as well as laboratory modified carriers: MTM® enriched with 10 % Ti, cellulose enriched with 1 % Ti, cellulose enriched with 0.7 % Ti, cellulose enriched with 0.25 % Ti and CelluloseM prepared by Meng *et al.*[13] were used in this study. All employed reagents and solvents were of the highest available purity but at least analytical grade. They were purchased unless otherwise stated from Merck (Darmstadt, Germany) and Sigma-Aldrich (St. Louis, MO, USA).

Preparation of crude extract

Potato tubers were kept at 3 °C for 12 h. Potato tubers were chilled to 3 °C. Thereafter, whole tubers were homogenized in a commercial juicer. The homogenate (1 L) was centrifuged at 3500 rpm at 4 °C. 600 mL of clear supernatant was desalted against 10 mM Na phosphate buffer pH 7.3 using a Sephadex G25 coarse column.

Purification of polyphenol oxidase

60 g of preswollen QAE Sephadex A-50 was equilibrated with 10 mM Na phosphate buffer, pH 7.3. The equilibrated ion-exchanger was added to the extract and mixed with a magnetic stirrer for 30 min in an oxygen-free atmosphere. Then the matrix was washed with starting buffer and the enzyme was eluted with 500 mL of 0.75 M NaCl in starting buffer. The partially purified enzyme preparation was stored at –20 °C until use.

Polyphenol oxidase activity assay

PPO activity was determined using L-DOPA as the substrate at 25°C by measuring the initial rate of dopachrome formation.[14] The standard assay mixture contained 0.1 ml of en-

zyme in 1.5 ml of 9.3 mM L-DOPA in 50 mM Tris-HCl pH 7.0. The absorbance at 475 nm was measured using a Philips UV–VIS–NIR PU 8630 spectrophotometer. One unit of PPO activity was defined as the amount of enzyme that catalyzes an increase in absorbance of 0.001 per min at 25 °C.

Immobilization of polyphenol oxidase onto the various carriers

10 mg of each carrier was measured in triplicate and added into 200 µL of enzyme preparation (8471 U ml^{-1}). 10 mg of each carrier was added in 0.9 % NaCl as a blank probe. Mixtures were left for 24 h on IKA orbital shaker at 400 rpm. Biocatalysts were removed by centrifugation at 14000 rpm and washed six times with 0.9 % NaCl. For further study, three biocatalysts with the highest activity were scaled up to 1 g and produced using the above-described procedure.

Immobilized polyphenol oxidase activity assay

The activity of the immobilized enzyme was assayed using a modified version of the method of Kwon and Kim.[14] Ten milligrams of partially dried biocatalyst (enzyme + support) was added to 800 µL of 2.325 mM L-DOPA in 50 mM Tris HCl buffer pH 7.0 at 25 °C. The mixture was shaken for 3 min and then centrifuged at 14000 rpm. The increase in the absorbance due to the formation of dopaquinone in the resulting supernatant was measured at 475 nm. The blank sample contained 10 mg of blank carrier instead of biocatalyst besides the other components of activity assay mixture. This was necessary because some carriers: MTM®, MTM® enriched with 10 % Ti, Green Sand and Birm, possess an inherent ability to oxidise L-DOPA. The specific activity of the immobilized PPO is defined as an increase in absorbance of 0.001 per min per gram of immobilisate under the given assay conditions.

Preliminary application study of the immobilized PPO using a batch reactor

Removal of phenolic compounds from synthetic wastewater was investigated with 100 mg of semidry biocatalyst that was added to 3 mL of 2.5 and 10 mM solutions of phenol, CP and BP and incubated for 5 h on an IKA orbital shaker to allow continuous oxygenation. After 5 h, the solutions were tested for the remaining phenol content using the 4-aminoantipyrine (AAP) assay.[15] The concentrations of phenols were measured using a colorimetric assay in which the phenolic compounds react with 2.08 mM AAP and 8.34 mM potassium ferricyanide in 0.25 M sodium bicarbonate solution to form a red quinone-type dye that absorbs light with a peak wavelength of 510 nm. The extent of color generation at 510 nm after a 6-min incubation time is proportional to the concentration of phenols in the assay solution. Absorbance readings were converted to phenolic concentrations using calibration lines.

pH optimum of soluble PPO and Eupergit C250L–PPO immobilizate

To determine the optimum pH of soluble and immobilized PPO activity against L--DOPA, 0.1 ml of the soluble enzyme and 10 mg of partially dried biocatalyst and a series of 50 mM buffers in the pH range from 3.0 to 10.5 were used (acetate, pH 3.0–5.0; phosphate, pH 6.0–10.5) and the residual activity was determined under the above-described enzyme assay conditions.

The reusability of Eupergit C250L–PPO immobilizate for 4-chlorophenol removal

The reusability of Eupergit C250L–PPO immobilizate for CP removal was tested by repeating the above-described 5 h incubation experiment 8 times. Between these 8 cycles, the immobilizate was collected by centrifugation and washed three times in assay buffer.

RESULTS AND DISCUSSION

Potato is an inexpensive source of enzymes for biotechnology.[16] Horseradish and turnip peroxidases have been employed in phenol removal.[17] The sources of peroxidases are available in abundance in Serbia, but these are seasonal and expensive plants; thus, using potatoes which are available during the whole year represent an advantage. PPOs from potato are the most suitable enzymes with respect to their availability and cost.[18] The efficiency of the enzymatic treatment was found to be independent of the enzyme purity and, therefore, it was possible to utilize a crude or partially purified preparation that is protected from deactivation due to the significant quantity of protein present instead of a purified one.[17] This feature leads to a significant reduction in treatment costs.

The polyphenol oxidases were partially purified using ion-exchange chromatography on QAE Sephadex with a yield of 69 %. The results of the purification are presented in Table I.

TABLE I. Partial purification of polyphenol oxidase from potato tuber

Property	Crude extract	Desalted crude extract	QAE-Sephadex eluted fraction
A_{475}	1.000	1.060	0.860
V / mL	600	650	480
Activity, U ml^{-1}	10000	10600	8600
Total activity, U ml^{-1}	6000000	6890000	4128000

In spite of the intrinsic ability to oxidize L-DOPA, judging by the instantaneous change in the color of the reaction mixture after mixing the carrier with the substrate, MTM®, MTM® enriched with 10% Ti, Birm and Green Sand were used for the immobilization, since the oxidizing ability of the carrier was subtracted by the use of a blank. Titanium modified cellulose beads (90 μm) with different amounts of bound titanium (0.25, 0.7 and 1.0 %, w/w) and titanium cellulose prepared according to Meng *et al.*[13] were also used in this study. In addition, some commercially available carriers, Eupergit C250L, Celite and unmodified cellulose, were also tested. MTM®, MTM® enriched with 10 % Ti, Birm and Green Sand were found not appropriate carriers for PPO immobilization due to the negligible or very low bound PPO activity. Furthermore, regarding the cellulose carriers, only CelluloseM showed a reasonably high bound activity of PPO, while the other four cellulose materials had very similar (low) values for the activity towards L-DOPA. Significant activities were detected with Celite–PPO, CelluloseM–PPO and Eupergit C250L–PPO biocatalysts (Fig. 1). The Eupergit C250L–PPO biocatalyst had the highest activity according to its specific activity.

As model pollutants, phenol, BP and CP were chosen. During the experimental removal of these three compounds from aqueous solution, the best results were obtained with PPO immobilized on Eupergit C250L. Comparison of the im-

mobilizates gave “ladder” histograms in the case of 2.5 mM substrates (Fig. 2) and a similar histogram with lower values in the case of 10 mM substrates (Fig. 3).

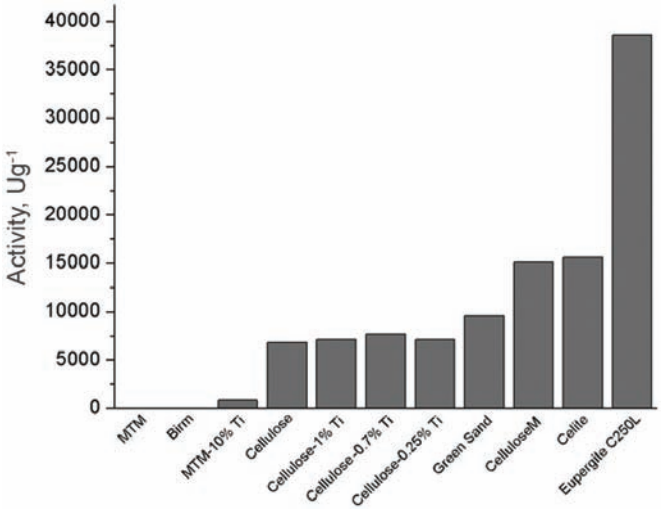

Fig. 1. Comparison of activity of produced biocatalysts towards 2.325 mM L-DOPA. Values represent specific activity of each produced biocatalyst (U g^{-1} of dry carrier).

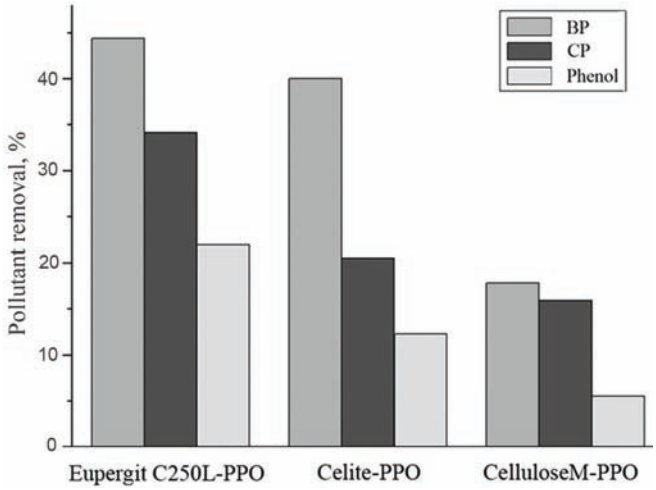

Fig. 2. Removal of 2.5 mM of 4-bromophenol, 4-chlorophenol and phenol after 5 h in a batch reactor.

Removal was the highest with the Eupergit C250L–PPO immobilizate, then with Celite–PPO immobilizate and the lowest with CelluloseM–PPO immobilizate. Although the removal of phenol can be considered as poor, due to low monophenolase activity of potato PPO,[19] it is comparable with the results obtained

by others for immobilized laccase activity.[20] In the case of 2.5 mM substrates with Eupergit C250L biocatalyst, around 45 % removal of BP was achieved, while 35 % and 20 % of the CP and phenol were removed, respectively. In the study of Levy *et al*.,[21] in which horseradish peroxidase immobilized on cellulose was used for the removal of BP, only 17 % removal was obtained with an initial BP concentration of 0.2 mM. Usually, a higher percent removal was obtained when a lower initial pollutant concentration was used. Bearing this in mind, it can be concluded that the Eupergit C250L–PPO biocatalyst used in the present study showed high efficiency for the removal of BP and CP. When 10 mM concentrations were used, the biocatalysts still showed removal abilities but it seems that in possible application, dilution of such wastewater would be useful.

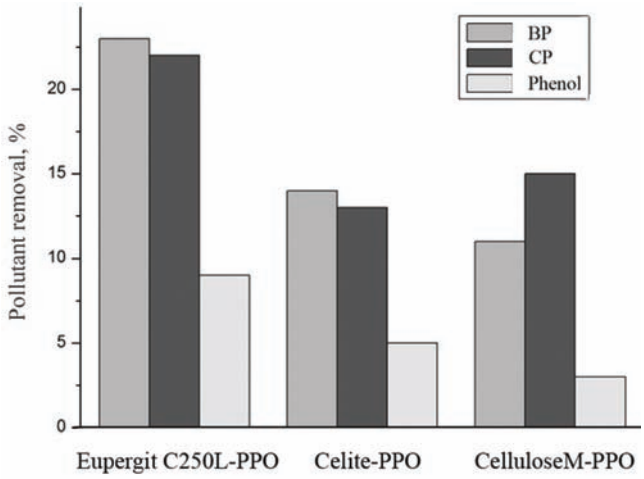

Fig. 3. Removal of 10 mM 4-bromophenol, 4-chlorophenol and phenol after 5 h in a batch reactor.

The optimum pH of free and Eupergit C250L–PPO immobilizate was studied since the pH value is one of the most influential parameters altering enzyme activity in an aqueous medium. The optimum pH values for free PPO and Eupergit C250L–PPO immobilizate were 7–9 and 8–9, respectively (Fig. 4). The difference in the optimal pH values of the soluble and immobilized enzyme might be a consequence of a change in the ionic environment of the carrier around the active sites of the enzyme.

In order to attain a better practical employment of the Eupergit C250L–PPO immobilizate in a batch reactor, it was necessary to investigate the reusability of the immobilizate. The reusability of Eupergit C250L–PPO for the removal of CP was considered. After eight repeated tests, each of 5 h duration, the efficiency of CP removal by Eupergit C250L–PPO immobilizate had decreased to 55 % (Fig. 5). The formation and accumulation of dark precipitates on immobilizates were

observed. Further studies should examine the application of continuous reactors, which would prevent the accumulation of reaction products on the biocatalyst. The reusability of an immobilized enzyme is one of its important advantages, which influences the cost of industrial applications.[22] Similar studies in which immobilized peroxidase had retained 40 % of its activity after eight repeated applications was considered as a significant reusability.[23]

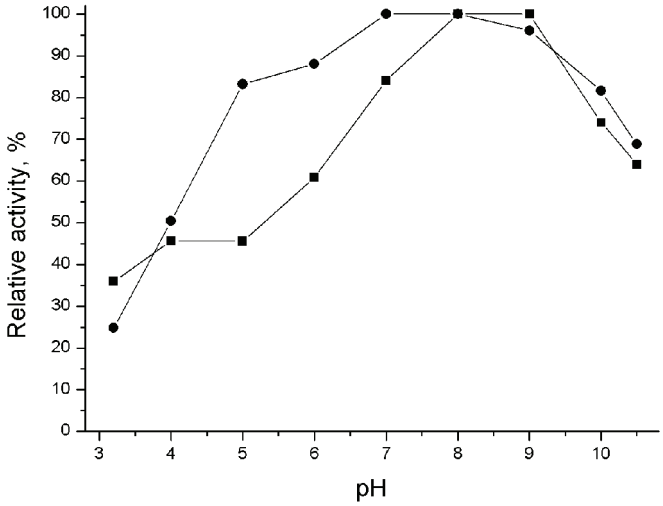

Fig. 4. Effect of pH on the activity of soluble PPO (●) and Eupergit C250L–PPO immobilizate (■).

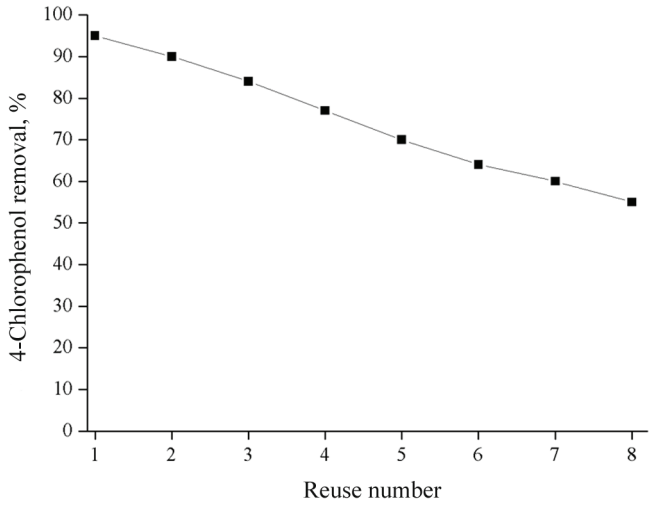

Fig. 5. 4-Chlorophenol removal reusability of Eupergit C250L–PPO immobilizate.

Khan *et al.*[18] investigated PPO immobilized on Celite and showed that the immobilized enzyme was more resistant to denaturation induced by pH, temperature, urea, the detergents SDS and Triton X-100 and Tween 20, and the water-miscible organic solvents acetonitrile, dimethylformamide, dioxane and *n*-propanol as compared to its soluble counterpart. In conjunction with these results, the present results give rise to a spectrum of possible carriers for PPO and other enzymes that might be used for wastewater treatment.

CONCLUSIONS

PPO enzymes from a low purity source, *i.e.*, partially purified potato preparation, showed good potential for phenol removal by polymerization. The experimental results indicated that phenol conversion in synthetic wastewaters is possible using Eupergit C250L, Celite and CelluloseM carriers. The Eupergit C250L––PPO biocatalyst used in this study showed high efficiency for the removal of BP and CP and significant reusability for removal of CP after 8 cycles of application. The presented immobilization method is a very economic procedure for the immobilization of PPO. Thus, the proposed process can be considered as a first step in further explorations for possible PPO carriers for the removal of phenol and phenol derivatives from wastewater.

Acknowledgements. This work was supported by the Ministry of Science and Technological Development of the Republic of Serbia (Grant No. 172048).

ИЗВОД

УКЛАЊАЊЕ ФЕНОЛА И ФЕНОЛНИХ ДЕРИВАТА ИЗ ВОДЕ ИМОБИЛИЗОВАНОМ ПОЛИФЕНОЛ-ОКСИДАЗОМ ИЗ КРОМПИРА

НИКОЛА ЛОНЧАР[1], НАТАША БОЖИЋ[2], ИВАН АЊЂЕЛКОВИЋ[1], АЛЕКСАНДРА МИЛОВАНОВИЋ[2], БИЉАНА ДОЈНОВ[2], МИРОСЛАВА ВУЈЧИЋ[2], ГОРАН РОГЛИЋ[1] и ЗОРАН ВУЈЧИЋ[1]

[1]*Хемијски факултет, Универзитет у Београду, Студентски трг 12–16, Београд и* [2]*Институт за хемију, технологију и металургију – Центар за хемију, Универзитет у Београду, Студентски трг 12–16, Београд*

Халогеновани феноли имају дезактивирано ароматично језгро и чине значајну категорију веома токсичних и тешко разградивих загађивача у разним индустријским гранама. Главни циљ овог рада је био добијање јефтиног имобилизованог ензима за уклањање фенола. Делимично пречишћена полифенол-оксидаза (ПФО) из кромпира је имобилизована на различитим комерцијалним и лабораторијски синтетизованим носачима. Од добијених биокатализатора, три са највећим активностима ППО, названи Еупергит Ц250Л–ПФО; Целит–ПФО и ЦелулозаМ–ПФО, тестирани су у реактору за уклањање фенола, 4-хлорфенола и 4-бромфенола. У случају 2,5 mM супстрата са Еупергит Ц250Л–ПФО, постигнуто је око 45 % разградње 4-бромфенола, док су 4-хлорфенол и фенол разграђени 35, односно 20 %. Тестирана је и способност вишеструке употребе Еупергит Ц250Л–ПФО имобилизата за уклањање 4-хлорфенола. Након осам поновљених циклуса ефикасност Еупергит Ц250Л–ПФО имобилизата за уклањање 4-хлорфенола је пала на 55 %.

(Примљено 19. јула, ревидирано 6. септембра 2010)

REFERENCES

1. R. Hakulinen, S. Woods, J. Ferguson, M. Benjamin, *Water Sci. Technol.* **17** (1985) 289
2. D. K. Zuzana, T. Livia, *World J. Microbiol. Biotechnol.* **25** (2008) 243
3. S. Contrerasa, M. Rodriguez, F. Al Momania, C. Sansa, S. Esplugasa, *Water Res.* **37** (2003) 3164
4. G. Busca, S. Berardinelli, C. Resini, L. Arrighi, *J. Hazard. Mater*. **160** (2008) 265
5. United States Environmental Protection Agency, EPA, http://nepis.epa.gov/Adobe/PDF/ /2000LNAI.PDF (accessed April, 2011)
6. A. Goi, M. Trapido, T. Tukhanen, *Adv. Environ. Res.* **8** (2004) 303
7. P. M. D. Armenante, D. Kafkewitz, G. A. Lewandowski, C. J. Jou, *Water Res.* **33** (1999) 681
8. J. Valenzuela, U. Bumann, R. Cespedes, L. Padilla, B. Gonzalez, *Appl. Environ. Microbiol.* **63** (1997) 227
9. S. Wada, H. Ichikawa, K, Tatsumi, *Biotechnol. Bioeng*. **42** (1993) 854
10. N. Duran, E. Esposito, *Appl. Catal. B* **28** (2000) 83
11. K. Tatsumi, S. Wada, H. Ichikawa, *Biotechnol. Bioeng*. **51** (1996) 126
12. P. W. Thygesen, S. P. Robinson, *Plant Physiol.* **109** (1995) 525
13. L. Z. Meng, C. Q. Du, Y. Y. Chen, Y. B. He, *J. Appl. Polym. Sci.* **84** (2002) 61
14. D. Y. Kwon, W. Y. Kim, *J. Biochem. Mol. Biol.* **29** (1996) 163
15. M. Wagner, J. A. Nicell, *Water Res.* **35** (2001) 485
16. Z. Vujčić, N. Lončar, B. Dojnov, A. Milovanović, M. Vujčić, N Božić, *Food Chem*. **121** (2010) 418
17. V. A. Cooper, J. A. Nicell, *Water Res.* **30** (1996) 954
18. A. A. Khan, S. Akhtar, Q. Husain, *J. Mol. Catal. B* **40** (2006) 58
19. E. Selinheimo, D. NiEidhin, C. Steffensen, J. Nielse, A. Lomascolo, S. Halaouli, E. Record, D. O'Beirne, J. Buchert, K. Kruus, *J. Biotechnol.* **130** (2007) 471
20. L. Cordi, R. C. Minussi, R. S. Freire, N. Duran, *Afr. J. Biotechnol.* **6** (2007) 1255
21. I. Levy, G. Ward, Y. Hadar, O. Shoseyov, C. Dosoretz, *Biotechnol. Bioeng.* **82** (2003) 223
22. S. Akhtar, A. A. Khan, Q. Husain, *Chemosphere* **60** (2005) 291
23. M. Matto, Q. Husain, *Ecotoxicol. Environ. Safety* **72** (2009) 965.

Journal of the Serbian Chemical Society
JSCS-info@shd.org.rs • www.shd.org.rs/JSCS
J. Serb. Chem. Soc. *76* (4) 523–528 (2011)
JSCS–4139
UDC *Laggera crispata*+582.998.1:665.52/.54+543.51+543.544.3(540)
Short communication

SHORT COMMUNICATION

Chemical investigation of the essential oil of *Laggera crispata* (Vahl) Hepper & Wood from India

RAM S. VERMA[1]*, RAJENDRA C. PADALIA[1], CHANDAN S. CHANOTIYA[2], AMIT CHAUHAN[1] and ANJU YADAV[2]

[1]*Central Institute of Medicinal and Aromatic Plants (CIMAP, CSIR), Research Centre, Pantnagar, P. O. – Dairy farm Nagla, Udham Singh Nagar, Uttarakhand-263149 and* [2]*Central Institute of Medicinal and Aromatic Plants (CIMAP, CSIR), P. O. CIMAP, Lucknow-226015, India*

(Received 1 August, revised 22 September 2010)

Abstract: Hydrodistilled essential oil of the aerial parts of *Laggera crispata* (Vahl) Hepper & Wood, collected from the Kumaon region of the western Himalayas was analysed by gas chromatography and gas chromatography–mass spectrometry. Eighty constituents, accounting for 83.9 % of the total oil composition, were identified. The oil was mainly dominated by sesquiterpenoids (45.3 %) and benzenoid compounds (33.9 %). Among them, 2,5-dimethoxy-*p*--cymene (32.2 %), 10-*epi*-*γ*-eudesmol (14.7 %), *β*-caryophyllene (6.9 %) and caryophyllene oxide (5.4 %) were major components of the oil.

Keywords: *Laggera crispata*; Asteraceae; essential oil; GC–MS; 2,5-dimethoxy-*p*-cymene; 10-*epi*-*γ*-eudesmol.

INTRODUCTION

The genus *Laggera* Sch.-Bip. *ex* Koch, belonging to the Asteraceae family, is represented by over 10 species prevalent in the tropical Asia and African continents. In India, it is represented by 3 species commonly found in tropical regions in both plains and altitudes up to 1500 m. The three species representing the genus are *Laggera alata*, *Laggera aurita* and *Laggera crispata*, of which *L. aurita* is characterized with stems not having wings while the other 2 species possess winged stems. In *L. alata*, the wings are broad, entire and continuous, while in *L. crispata*, they are narrow, toothed and interrupted. However, all three species are aromatic in nature.[1]

Laggera crispata (Vahl) Hepper & Wood (Syn. *Laggera pterodonta* (DC.) Sch.-Bip. *ex* Oliver is an annual, erect, highly branched, strongly aromatic and

* Corresponding author. E-mail: rswaroop1979@yahoo.com
doi: 10.2298/JSC100801048V

viscid pubescent plant. The leaves paste of *L. crispata* is used in the treatment of inflammation and swelling in north-east India and it is also said to possess anthelminthic properties.[2] In traditional Chinese medicine, the aerial parts of this plant have been used as an anti-inflammatory, antibacterial and anti-leukaemia agent.[3] Recently, great attention has been paid to *Laggera* species because of their diverse chemical components and biological activities.[4] The plants have been noted to possess antiviral activity against Herpes simplex type I and II and anti-tuberculosis activity.[5,6]

Many phytochemical investigations have been performed on the non-volatile and volatile constituents of different species of *Laggera* from various countries.[7–17] In India, *L. aurita* has also been studied on a few occasions.[18–20] However, a literature survey revealed that there are no reports available on the phytochemical aspects of *L. crispata* from India. Therefore, in present research, the essential oil derived from the aerial part of *L. crispata* was investigated by GC and GC–MS.

EXPERIMENTAL

Plant material

Fresh plant material (aerial parts) of *L. crispata* were collected at the vegetative stage from an experimental field of the Central Institute of Medicinal and Aromatic Plants, Research Centre, Purara, Uttarakhand in August, 2009. The plant material was authenticated at the Botany Department of the Centre (voucher specimens No. Cimpant-335). The site is located at an altitude of 1250 m in the Kattyur Valley, western Himalayas. Climatologically, it is categorized as a temperate zone. The monsoon usually breaks in June and continues to September.

Extraction of the essential oil

The essential oil was extracted from fresh aerial parts of *L. crispata* by hydrodistillation, for 3 h using a Clevenger apparatus.[21] The percentage essential oil content (% v/w) was estimated on a fresh weight basis. The obtained oil sample was dehydrated over anhydrous sodium sulphate and kept in a cool and dark place before analyses.

Gas chromatography (GC)

The GC analyses of the oil samples were realised on a Perkin Elmer Auto XL GC and a Nucon gas chromatograph model 5765 equipped with a FID using two different stationary phases, *i.e.*, DB-5 (30 m×0.32 mm; 0.25 µm film coating) and CP-Wax 52 CB (30 m×0.32 mm×0.25 µm film thickness) fused silica columns, respectively. Hydrogen was used as the carrier gas at 1.0 ml min^{-1}. The oven temperature was programmed from 70–250 °C at 3 °C min^{-1} for the DB-5 column and from 70–230 °C at 4 °C min^{-1} for the CP-Wax 52 CB column. The injector and detector temperatures were 210 and 230 °C, respectively. The injection volume was 0.02 µl neat (syringe: Hamilton 1.0 µl capacity, Alltech, USA) and the split ratio was 1: 30.

Gas chromatography–mass spectrometry (GC–MS)

GC–MS analysis of the essential oil sample was performed on a Perkin Elmer Auto-System XL GC interfaced with a turbomass quadrupole mass spectrometer fitted with an Equity-5 fused silica capillary column (60 m×0.32 mm i.d., film thickness 0.25 µm). The oven temperature was programmed from 60–210 ºC at 3 °C min^{-1} using helium as the carrier gas at

1.0 mL min^{-1}. The injector temperature was 210 °C, injection volume 0.1 µl prepared in *n*-hexane (dilution 10 %), split ratio 1: 40. The MS were taken at 70 eV with a mass scan range of 40–450 amu and scan rate 1.0 s with an interscan delay of 0.5 s.

Identification of the components

The constituents were identified based on their Retention Index (*RI*, determined with reference to a homologous series of *n*-alkanes, C_9–C_{24}, run under identical experimental conditions), co-injection with standards (Aldrich and Fluka) or known essential oil constituents, an MS Library search (NIST/EPA/NIH version 2.1 and Wiley registry of MS data 7th edition) and by comparing with MS literature data.[22,23] The relative amounts of the individual components were calculated based on the GC peak area (FID response) without using correction factors.

RESULTS AND DISCUSSION

The fresh plant material of *L. crispata* collected at vegetative stage yielded 0.11 % (v/w) essential oil. GC–FID and GC–MS analyses of the oil enabled the identification of eighty components, representing 83.9 % of the total oil content. The components with their relative percentage are summarized in Table I-S, given in the Supplementary material to this paper. The oil was mainly composed of benzenoid compounds (33.9 %), oxygenated sesquiterpenes (33.9 %), and sesquiterpene hydrocarbons (11.4 %). Monoterpene hydrocarbons and their oxygenated counterparts were detected in small amounts (2.2 and 2.5 %, respectively) in this oil. The benzenoid class of components was mainly represented by 2,5-dimethoxy-*p*-cymene (32.2 %), which was the major component of the oil. The oxygenated sesquiterpenes detected in significant amounts were 10-*epi*-*γ*-eudesmol (14.7 %), and caryophyllene oxide (5.4 %). Moreover, the major sesquiterpene hydrocarbons of the oil were *β*-caryophyllene (6.9 %), *α*-humulene (2.0 %) and bicyclogermacrene (1.8 %). Furthermore, among the oxygenated monoterpenes, only terpinen-4-ol was detected above 1 %. The structures of major constituents of the essential oil are given in Fig. 1.

According to literature surveys, 2,5-dimethoxy-*p*-cymene and 10-*epi*-*γ*-eudesmol have been previously detected in different species of the genus *Laggera* (Table I). The essential oil of *L. alata* grown in Nigeria[12] and Cameroon;[14] *L. aurita* grown in India;[18] *L. gracilis* grown in Cameroon;[14] and *L. pterodonta* grown in Cameroon[13] and West Africa[16] were all dominated by thymol dimethyl ether and eudesmol isomers. However, *L. alata* grown on the Comoros Islands was dominated by sesquiterpene hydrocarbons;[17] *L. oloptera* grown in Cameroon was found to possess mainly sesquiterpene and monoterpene hydrocarbons,[14] while *L. tomentosa* grown in Ethiopia contained the oxygenated monoterpene, chrysanthenone.[15]

TABLE I. Major components in the essential oil of the genus *Laggera* growing in different countries

Species	Plant part	Major compounds	Country
Laggera alata	Leaf	Thymoquinol dimethyl ether (11.17–29.17 %), α-eudesmol (7.68–12.55 %)	Nigeria[12]
L. alata	Leaf	Dimethoxy-*p*-cymene (34.1 %), γ-eudesmol (21.4 %)	Cameroon[14]
L. alata	Leaf	β-Caryophyllene (30.5 %), α-muurolene (21.1 %)	Comoros Islands[17]
L. aurita	Whole plant	2,3-Dimethoxy-*p*-cymene (? %), laggerol (? %)	India[18]
L. gracilis	Leaf	Dimethoxy-*p*-cymene (33.4 %), γ-eudesmol (10.7 %)	Cameroon[14]
L. oloptera	Leaf	β-Caryophyllene (15.2–20.4 %), sabinene (2.9–28.9 %), germacrene D (10.3–17.9 %)	Cameroon[14]
L. pterodonta	Leaf	2,5-Dimethoxy-*p*-cymene (28.2 %), γ-eudesmol (26.2 %)	Cameroon[13]
L. pterodonta	Leaf	2,5-Dimethoxy-*p*-cymene (30.5 %), 10-*epi*-γ-eudesmol (24.6 %)	West Africa[16]
L. tomentosa	Leaf and inflorescence	Chrysanthenone (57.5 %), isochrysanthenone (6.8 %)	Ethiopia[15]

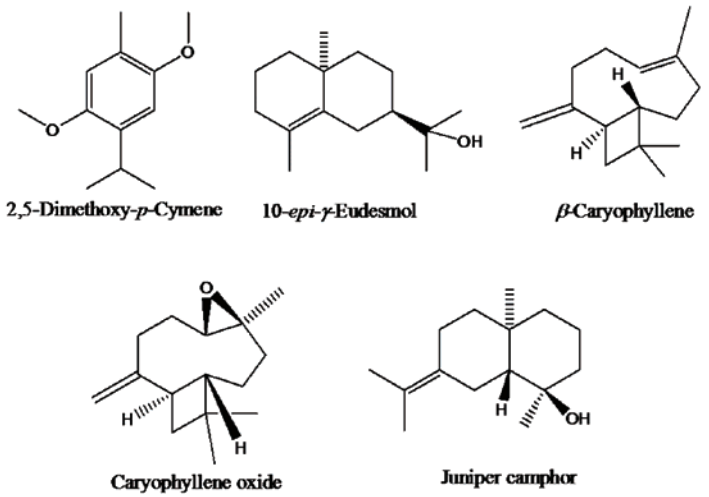

Fig. 1. Chemical structures of marker constituents of the essential oil of *L. crispata*.

CONCLUSIONS

The *L. crispata* collected from the Kumaon region of the Himalayas was rich in thymol derivatives. The thymol derivatives are thought to be responsible for medicinal uses of *Laggera* species. Modern research also showed that phenolic compounds are known for a number of biological activities. Therefore, in light of

the presence of interesting molecules in the essential oil of the *L. crispata*, it can be said that this plant could potentially be used in various food and pharmaceutical preparations.

SUPPLEMENTARY MATERIAL

The components of essential oil with their relative percentage are available electronically at http://www.shd.org.rs/JSCS/, or from the corresponding author on request.

Acknowledgement. The authors are thankful to the Director, Central Institute of Medicinal and Aromatic Plants (CIMAP, CSIR) for providing the necessary facilities and encouragement.

И З В О Д

ИСПИТИВАЊЕ ХЕМИЈСКОГ САСТАВА ЕТАРСКОГ УЉА БИЉКЕ *Laggera crispata* (VAHL) HEPPER & WOOD ИЗ ИНДИЈЕ

RAM S. VERMA[1], RAJENDRA C. PADALIA[1], CHANDAN S. CHANOTIYA[2], AMIT CHAUHAN[1] и ANJU YADAV[2]

[1]*Central Institute of Medicinal and Aromatic Plants (CIMAP, CSIR), Research Centre, Pantnagar, P.O. – Dairy farm Nagla, Udham Singh Nagar, Uttarakhand-263149 и* [2]*Central Institute of Medicinal and Aromatic Plants (CIMAP, CSIR), P.O. CIMAP, Lucknow-226015, India*

Етарско уље изоловано дестилацијом воденом паром из надземних делова биљке *Laggera crispata* (Vahl) Hepper & Wood, сакупљене у западним Хималајима, анализирано је методама гасне хроматогарфије и гасне хроматографије–масене спектрометрије. Идентификовано је осамдесет састојака, који су чинили 83,9 % уља. Доминантни су сесквитерпеноиди (45,3 %) и бензеноидна једињења (33,9 %). Главни састојци уља су 2,5-диметокси-*p*-цимен (32,2 %), 10-*epi*-*γ*-еудезмол (14,7 %), *β*-кариофилен (6,9 %) и кариофилен-оксид (5,4 %).

(Примљено 1. августа, ревидирано 22. септембра 2010)

REFERENCES

1. S. Kumar, in *Flora of India*, Vol. 13, P. K. Hajra, R. R. Rao, D. K. Singh, B. P. Uniyal, Eds., Botanical Survey of India, Kolkata, India, 1995, p. 148
2. H. Tag, A. K. Das, *Indian J. Trad. Know.* **3** (2004) 80
3. Y. Xiao, Q. Zheng, Q. Zhang, H. Sun, F. Gueritte, Y. Zhao, *Fitoterapia* **74** (2003) 459
4. X. C. Li, C. H. Huo, Q. W. Shi, H. Kiyota, *Chem. Biodiv.* **4** (2007) 105
5. T. Kuljanabhagavad, R. Suttisri, T. Pengsuparp, N. Ruangrungsi, *J. Health Res.* **23** (2009) 175
6. O. H. Egharevba, P. Oladosu, E. S. Okhale, I. Ibrahim, K. O. Folashade, K. S. Okwute, I. J. Okogun, *J. Med. Plants Res.* **4** (2010) 1235
7. Y. Zhao, J. M. Yue, Y. N. He, Z. W. Lin, H. D. Sun, *J. Nat. Prod.* **60** (1997) 545
8. Y. Zhao, J. M. Yue, Z. W. Lin, J. K. Ding, H. D. Sun, *Phytochemistry* **44** (1997) 459
9. A. A. Ahmed, H. R. El-Seedi, A.A. Mahmoud, A.E.A. El-Douski, I.F. Zeid, L. Bohlin, *Phytochemistry* **49** (1998) 2421
10. P. Raharivelomanana, J. P. Bianchini, A. R. P. Ramaneolina, J. R. E. Rasoarahona, R. Faure, A. Cambon, *Phytochemistry* **47** (1998) 1085
11. Q. Zheng, Z. Xu, X. Sun, W. Yao, H. Sun, C. H. K. Cheng, Y. Zhao, *Phytochemistry* **63** (2003) 835

12. O. Ekundayo, B. Oguntimein, I. Laakso, R. Hiltunen, *Planta Med.* **55** (1989) 573
13. M. B. Ngassoum, L. Jirovetz, G. Buchbauer, W. Fleischhacker, *J. Essent. Oil Res.* **12** (2000) 345
14. J. R. Kuiate, J. M. Bessiere, P. H. Amvam Zollo, *Flav. Fragr. J.* **17** (2002) 105
15. N. Asfaw, H. J. Storesund, A. J. Aasen, L. Skattebol, *J. Essent. Oil Res.* **15** (2003) 102
16. K. D. Sohounhloue, A. U. Sagbo, C. Menut, J. M. Bessiere, *J. Essent. Oil Res.* **16** (2004) 193
17. H. M. Said, A. B. Said, S. Zrira, B. Benjilali, *J. Essent. Oil-Bear. Plants* **8** (2005) 15
18. S. K. Zutshi, B. K. Bamboria, M. M. Bokadia, *Curr. Sci.* **44** (1975) 571
19. S. K. Zutshi, M. M. Bokadia, *Indian J. Chem. B* **14B** (1976) 711
20. S. K. Zutshi, M. M. Bokadia, *Indian J. Chem. B* **14B** (1976) 64
21. J. F. Clevenger, *J. Am. Pharm. Assoc.* **17** (1928) 345
22. R. P. Adams, *Identification of essential oil components by gas chromatograph/mass spectrometry*, Allured Publishing Corporation, Carol Stream, IL, USA, 1995
23. N. W. Davies, *J. Chromatogr.* **503** (1990) 1.

Journal of the Serbian Chemical Society
JSCS@tmf.bg.ac.rs • www.shd.org.rs/JSCS
J. Serb. Chem. Soc. 76 (4) S1–S3 (2011) *Supplementary material*

SUPPLEMENTARY MATERIAL TO

Chemical investigation of the essential oil of *Laggera crispata* (Vahl) Hepper & Wood from India

RAM S. VERMA[1]*, RAJENDRA C. PADALIA[1], CHANDAN S. CHANOTIYA[2], AMIT CHAUHAN[1] and ANJU YADAV[2]

[1]*Central Institute of Medicinal and Aromatic Plants (CIMAP, CSIR), Research Centre, Pantnagar, P. O. – Dairy farm Nagla, Udham Singh Nagar, Uttarakhand-263149 and* [2]*Central Institute of Medicinal and Aromatic Plants (CIMAP, CSIR), P. O. CIMAP, Lucknow-226015, India*

J. Serb. Chem. Soc. 76 (4) (2011) 523–528

TABLE I-S. Essential oil composition of *L. crispata* from the Kumaon region of Uttarakhand, India

Compound	Class	*RI*[a]	*RI*[b]	*RI*[c]	Peak area[d], %
α-Thujene	MH	932	931	1028	tr
α-Pinene	MH	941	939	1022	tr
Sabinene	MH	978	976	1124	0.2
β-Pinene	MH	982	980	1109	tr
β-Myrcene	MH	989	991	1164	0.1
(*Z*)-3-Hexenyl acetate	AC	998	1004	–	tr
α-Phellandrene	MH	1000	1005	1167	0.5
δ-3-Carene	MH	1007	1011	1153	tr
α-Terpinene	MH	1012	1018	1179	0.3
p-Cymene	BC	1019	1026	1274	0.4
Limonene	MH	1024	1031	1198	0.1
β-Phellandrene	MH	1029	1031	1210	tr
(*Z*)-*β*-Ocimene	MH	1042	1040	1242	tr
(*E*)-*β*-Ocimene	MH	1055	1050	1265	0.5
γ-Terpinene	MH	1066	1062	1248	0.4
Terpinolene	MH	1087	1088	1284	0.1
(*E*)-Sabinene hydrate[e]	OM	1100	1097	1559	0.8
Linalool	OM	1103	1098	1555	tr
(*Z*)-*p*-Menth-2 en-1-ol	OM	1120	1121	1636	0.1
(*E*)-*p*-Menth-2 en-1-ol	OM	1137	1140	1570	0.1
(*E*)-Pinocamphone	OM	1157	1160	–	tr
Terpinen-4-ol	OM	1172	1177	1611	1.5
p-Cymen-8-ol	BC	1184	1183	1865	0.1

* Corresponding author. E-mail: rswaroop1979@yahoo.com

TABLE I-S. Continued

Compound	Class	*RI*[a]	*RI*[b]	*RI*[c]	Peak area[d], %
α-Terpineol	OM	1187	1189	1705	tr
Myrtenol	OM	1188	1194	1887	tr
Thymol methyl ether	BC	1234	1235	1597	0.1
Carvacrol methyl ether	BC	1245	1244	1618	0.1
Thymol	BC	1293	1290	–	tr
β-Caryophyllene	SH	1426	1418	1589	6.9
2,5-Dimethoxy-*p*-cymene[f]	BC	1431	1423	1877	32.2
Aromadendrene	SH	1440	1439	–	tr
(*Z*)-*β*-Farnesene	SH	1445	1443	1666	0.1
α-Humulene	SH	1456	1454	1685	2.0
(*E*)-*β*-Farnesene	SH	1460	1458	1673	tr
β-Acoradiene	SH	1466	1466	–	tr
γ-Gurjunene	SH	1474	1473	–	tr
γ-Muurolene	SH	1478	1477	–	tr
Germacrene D	SH	1481	1480	1728	tr
2-Phenylethyl propionate	BC	1483	–	–	0.9
β-Selinene	SH	1486	1485	1713	0.1
α-Selinene	SH	1491	1494	1742	0.1
Bicyclogermacrene	SH	1496	1495	1754	1.8
α-Muurolene	SH	1500	1499	1737	tr
Germacrene A	SH	1502	1503	–	tr
β-Bisabolene	SH	1508	1509	1743	tr
γ-Cadinene	SH	1512	1513	–	tr
Cubebol	OS	1516	1514	1954	0.1
δ-Cadinene	SH	1527	1524	1771	0.1
(*Z*)-Nerolidol	OS	1533	1534	–	0.1
α-Cadinene	SH	1537	1538	1813	tr
α-Calacorene	SH	1542	1542	1937	0.3
Elemol	OS	1545	1549	2092	1.1
Thymohydroquinone	BC	1549	1553	–	tr
Germacrene B	SH	1559	1556	1854	tr
(*E*)-Nerolidol	OS	1563	1564	2048	tr
Germacrene D-4-ol	OS	1572	1574	2068	0.1
Caryophyllene oxide	OS	1583	1581	2005	5.4
Guaiol	OS	1596	1595	2100	0.1
Humulene epoxide II	OS	1607	1606	–	0.3
1,10-*di*-*epi*-Cubenol	OS	1611	1612	–	tr
10-*epi*-*γ*-Eudesmol	OS	1621	1619	2112	14.7
1-*epi*-Cubenol	OS	1627	1627	2085	0.3
γ-Eudesmol	OS	1629	1630	2184	0.6
epi-*α*-Cadinol	OS	1637	1640	–	0.4
epi-*α*-Muurolol	OS	1641	1641	2206	1.4
β-Eudesmol	OS	1647	1649	2253	0.5
α-Eudesmol	OS	1651	1652	2247	0.9
7-*epi*-*α*-Eudesmol	OS	1656	1658	–	2.4
Bulnesol	OS	1667	1666	–	0.2

TABLE I-S. Continued

Compound	Class	*RI*[a]	*RI*[b]	*RI*[c]	Peak area[d], %
β-Bisabolol	OS	1672	1671	2166	0.2
Eudesma-4(15),7-dien-1-*β*-ol	OS	1684	1685	–	tr
Juniper camphor	OS	1692	1691	2319	3.4
(*Z*,*Z*)-Farnesol	OS	1715	1713	–	tr
Curcuphenol	BC	1717	1715	–	tr
(*E*,*E*)-Farnesol	OS	1721	1722	2366	tr
Oplopanone	OS	1735	1733	–	0.2
(*E*,*Z*)-Farnesol	OS	1745	1742	–	tr
Benzyl benzoate	BC	1762	1762	–	0.1
8-*α*-Acetoxyelemol[g]	OS	1790	1789	–	1.4
iso-Acorone	OS	1806	–	–	0.1
Unidentified[h]	–	1844	–	–	11.5
Class composition					
Monoterpene hydrocarbons (MH)	–	–	–	–	2.2
Oxygenated monoterpenes (OM)	–	–	–	–	2.5
Sesquiterpene hydrocarbons (SH)	–	–	–	–	11.4
Oxygenated sesquiterpenes (OS)	–	–	–	–	33.9
Benzenoid compounds (BC)	–	–	–	–	33.9
Aliphatic compound (AC)	–	–	–	–	tr
Total identified, %	–	–	–	–	83.9

[a]Retention indices determined on the DB-5 column using an *n*-alkane homologous series (C_9–C_{24}); [b]retention indices from the literature;[22] [c]retention indices determined on the CP-WAX 52 CB column; [d]peak area calculated on the DB-5 column; [e]*cis*/*trans* related to methyl *vs*. isopropyl groups; [f]also known as thymohydroquinone dimethyl ether; tr: trace (<0.05 %); [g]tentative identification based on the comparison of the retention indices with literature values; [h]mass spectrum (70 eV): 234 (M^+), 219, 173, 145, 117, 93, 91 (100 %), 55, 53

Journal of the Serbian Chemical Society
JSCS-info@shd.org.rs • www.shd.org.rs/JSCS
J. Serb. Chem. Soc. *76* (4) 529–537 (2011)
JSCS–4140
UDC 547.461.2+547.831+546.472:548.7
Original scientific paper

Crystal structure of an oxalate-bridged tetranuclear 8-hydroxyquinoline Zn(II) cluster: $[Zn_4Q_6(Ox)]_{0.5n}$

JIAJUN WANG[1], QIANG WANG[2], YANJUN SUN[3], YUEMEI WANG[4], GUOSHENG ZHAO[1] and YUNCHENG CUI[1]*

[1]*Chemistry College of Jilin Normal University, Key Laboratory of Preparation and Application of Environmentally Friendly Materials (Jilin Normal University), Ministry of Education, Siping, 136000,* [2]*Department of Biological Medicine and Chemical Engineering, Liaoning Institute of Science and Technology, Benxi, 117004,* [3]*Boda College of Jilin Normal University, Siping, 136000 and* [4]*Xi'an Modern Chemistry Research Institute, Xi'an, 710065, China*

(Received 22 August, revised 22 October 2010)

Abstract: The chain structure of a tetranuclear zinc(II) cluster $[Zn_4Q_6(Ox)]_{0.5n}$ ($[Zn_4(C_9H_6NO)_6(C_2O_4)]_{0.5n}$) (**1**) (Q = 8-hydroxyquinoline anion, Ox = oxalate dianion) was determined by X-ray crystallography and characterized by elemental analysis, IR spectroscopy and thermal analysis. It crystallizes in the monoclinic system, space group $P2_1/n$ (No. 14), with the lattice parameters a = = 13.2222(15) Å, b = 11.0566(12) Å, c = 16.2224(18) Å, β = 92.1770(10)°, V = = 2369.9(5) Å^3, Z = 4, M_r = 607.23 g mol^{-1}, Dc = 1.702 g cm^{-3}. The tetranuclear zinc(II) clusters form 1D polymeric chains parallel to the b-axis. The π–π stacking interactions involving aryl rings support the formation of the 1D polymeric structure. The neighboring polymeric chains are connected by C–H···π interactions.

Keywords: 8-hydroxyquinoline; zinc(II) cluster; single crystal structure.

INTRODUCTION

The rapid development of supramolecular chemistry and metal–organic coordination polymer research *via* crystal engineering have produced many new polymers with unique, well-defined structures,[1,2] which are of great interest for potential applications in catalysis,[3] adsorption,[4] ion-exchange,[5] sensor technology,[6] optoelectronics,[7] and nanowires.[8] These metal–organic network structures depend on the judicious selection of metal centers and organic ligands that may afford the desirable covalent bonds, hydrogen-bonding linkages, or π–π interactions for the construction of new supramolecules or polymers. 8-Hydroxy-

* Corresponding author. E-mail: yccuisp@yahoo.cn
doi: 10.2298/JSC100822049W

quinoline is a well-known molecule which due to its metal-complexation ability is frequently used for analysis or metal precipitation.[9] To date, in the research field of organic luminescent materials, many molecules, such as metal based quinoline derivatives, have shown promising results as strong contenders for future display technology.[10] Extensive work has been performed on tris-(8-hydroxyquinoline) aluminum (AlQ_3) and ZnQ_2 due to their properties, such as excellent flexibility, high photoconductivity and high life time of devices.[11] Zinc(II), as a d^{10} ion, has been used as the metal center in building coordination polymers in the search for non-linear optical materials.[12] Zinc(II) complexes also show luminescence, which is typically red shifted compared to the corresponding Al(III) compounds.[13] In supramolecular chemistry, 8-hydroxyquinoline derivatives can be used for the formation of hydrogen bonded networks[14,15] as well as of supramolecular aggregates.[16] In coordination chemistry, simple 8-hydroxyquinolines coordinated with zinc(II) ions are very versatile and they can form 2:1 and 3:1 complexes.[16,17] To further research zinc(II) complexes, in the presented study, an oxalate bridged, ternary tetranuclear 8-hydroxyquinoline zinc(II) coordination polymer **1** was obtained.

EXPERIMENTAL

Synthesis

All reagents employed were of analytical grade. $Zn(OAc)_2 \cdot H_2O$ (0.235 g, 1 mmol), 8-hydroxyquinoline (0.146 g, 1 mmol) and oxalic acid (0.050 g, 0.5 mmol) in water (17 ml) were mixed with stirring. The pH was adjusted to 8.0, then the mixture was sealed in a 25 ml stainless steel reactor equipped with a Teflon liner and heated at 170 °C for 96 h whereby dark yellow crystals of the title polymer were obtained (yield 27 %, based on Zn). Upon cooling, the C H N contents were determined by elemental analysis: Calcd. for $C_{28}H_{18}N_3O_5Zn_2$: C, 55.34; H, 2.96, N, 6.92 %. Found: C, 54.91; H, 2.84; N, 6.70 %; IR (KBr, cm^{-1}): 3052*w*, 1674*s*, 1642*sh*, 1640*s*, 1619*s*, 1512*s*, 1455*m*, 1352*w*, 1304*m*, 1103*m*, 1033*m*, 807*m*, 755*m*.

Crystal structure determination and physical measurements

A yellow block crystal with dimensions of 0.25 mm×0.20 mm×0.17 mm was chosen for X-ray diffraction analysis. Crystal structure measurement for polymer **1** was performed on a Bruker Smart Apex II CCD diffractometer using the ω scan technique with MoKα radiation (λ = 0.71073 Å) at room temperature (293(2) K). Absorption corrections were applied using the multi-scan technique[18] (the crystal data and refinement relative parameters are listed in Table I). A total of 19891 reflections were obtained in the range of $2.20 \leq \theta \leq 26.00°$, of which 4654 were independent (R_{int} = 0.0831) and 2777 observed reflections with $I > 2\sigma(I)$ were employed for the structure determination and refinement. The structure was solved by the direct method and refined with full-matrix least-squares techniques using the SHELXTL program[19] within WINGX.[20] All non-hydrogen atoms were refined anisotropically with the final R_1 = 0.0943, ωR_2 = 0.0939 ($\omega = 1/[\sigma^2(Fo^2)+(0.0325P)^2]$ where $P = (Fo^2+2Fc^2)/3$, $(\Delta/\sigma)_{max}$ = 0.011, $F(000)$ = 1228, μ = 2.072 mm^{-1}, S = 0.989, $(\Delta\rho)_{max}$ = 0.691 e $Å^{-3}$ and $(\Delta\rho)_{min}$ = –0.423 e $Å^{-3}$. The hydrogen atoms on the carbon atoms were generated geometrically.

The FT–IR spectrum was recorded from KBr pellets in range 4000–400 cm^{-1} on a Perkin–Elmer 240C spectrometer. Thermogravimetric analysis was performed using a Perkin–Elmer TG-7 analyzer in nitrogen.

TABLE I. Crystal data and refinement relative parameters

Crystal data	
Formula: $C_{28}H_{18}N_3O_5Zn_2$	V = 2369.9 (5) $Å^3$
M_r = 607.19	Z = 4
a = 13.2222 (15) Å	$F(000)$ = 1228
b = 11.0566 (12) Å	D_x = 1.702 Mg m^{-3}
c = 16.2224 (18) Å	Mo K_α radiation, λ = 0.71073 Å
α = 90 °	μ = 2.07 mm^{-1}
β = 92.177 (1)°	T = 298 K
γ = 90°	0.25 mm×0.20 mm×0.17 mm
Data collection	
Radiation source: fine-focus sealed tube	R_{int} = 0.083
Radiation monochromator: graphite	θ_{max} = 26.0°, θ_{min} = 2.2°
Measured reflections: 19891	h = −16→16
Independent reflections: 4654	k = −13→13
Reflections: 2777 (with $I > 2\sigma(I)$)	l = −19→20
Refinement	
Refinement on: F^2	Primary atom site location: structure-invariant direct methods
Least-squares matrix: Full	Secondary atom site location: difference Fourier map
$R[F^2 > 2\sigma(F^2)]$ = 0.044	Hydrogen site location: inferred from neighboring sites
$wR(F^2)$ = 0.094	H atoms treated by a mixture of independent and constrained refinement
S = 0.99	$w = 1/[\sigma^2(Fo^2) + (0.0325P)^2]$, where $P = (Fo^2+2Fc^2)/3$
Reflections: 4654	$(\Delta/\sigma)_{max} < 0.001$
Parameters: 343	$\Delta\rho_{max}$ = 0.69 e $Å^{-3}$
Restraints: 0	$\Delta\rho_{min}$ = −0.42 e $Å^{-3}$

RESULTS AND DISCUSSION

IR spectra

In the IR spectrum, polymer **1** exhibited absorption at 1103 cm^{-1} (*m*), corresponding to the presence of quinoline C–O bonds. The C–H stretching mode for the phenyl ring was relatively weak and was observed at about 3052 cm^{-1}. The peaks at 1640 cm^{-1} (*s*) are attributed to $\nu_{C=N}$ stretching,[21] and the peak at 1455 cm^{-1} is assigned to ν_s(–C=N–C=C–).[22] The peaks at 1619 (*s*) and 1512 cm^{-1} (*s*) are assigned to C=C stretching vibrations of the aryl rings and the peak at 755 cm^{-1} is attributed to the $\nu_{C–H}$ of aryl rings. The strong carboxylic acid peak at 1726cm^{-1} (*s*) diminished and two peaks developed at 1674 (*s*) and 1642cm^{-1} (*sh*)

assigned to the asymmetric stretching of carboxyl (CO_2) and another two peaks at 1352 (*w*) and 1304cm^{-1} (*m*) can be regarded to the symmetric stretching of carboxyl (CO_2), while the peak at 1033cm^{-1} (*m*) can be considered as the stretching of carboxyl (CO). The peak at 807cm^{-1} (*m*) can be assigned to the stretching of the δ band of carboxyl CO_2.

Thermal analysis

The TG curve of the title polymer $[Zn_4Q_6(Ox)]_{0.5n}$ showed two weight loss steps peaking at 375 and 446 °C. Based on the weight changes, the first weight loss process may be related to the loss of one Ox (found 6.4 %; calcd. 7.2 %); the second weight loss event corresponds to the loss of six Qs (found 69.3 %; calcd. 71.1 %). After 560 °C, basically no loss weight occurred while the residual weight of 24.3 % suggests that the residue may be ZnO (calcd. 26.8 %).

*Crystal structure of $[Zn_4Q_6(Ox)]_{0.5n}$)(**1**)*

The structure of the title polymer (**1**) ($[Zn_4Q_6(Ox)]_{0.5n}$) is illustrated in Scheme 1 and Fig. 1.

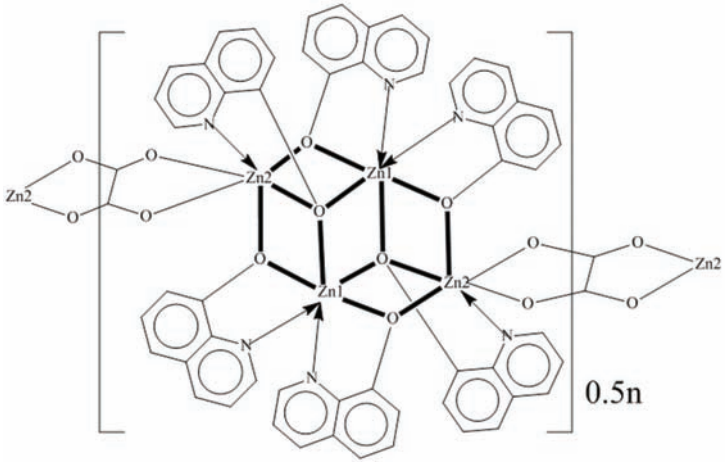

Scheme 1. The structure of the title tetranuclear coordination polymer **1** ($[Zn_4Q_6(Ox)]_{0.5n}$).

The crystal structure consists of tetranuclear dimeric clusters. The centre of inversion is located at the middle of the tetranuclear cluster. There are two crystallographically independent zinc center sites (Zn1 and Zn2) within half of one cluster. The two zinc centers have the same coordination geometry (each zinc center is coordinated by six atoms and is located at the centre of an octahedron). Four 8-hydroxyquinoline anions (Qs) are involved in coordination with Zn1. The coordination is achieved by four O and two N atoms. The N2, O1, O2 and O3 atoms are located in an equatorial plane, while O3^i (*i* stands for the sym-

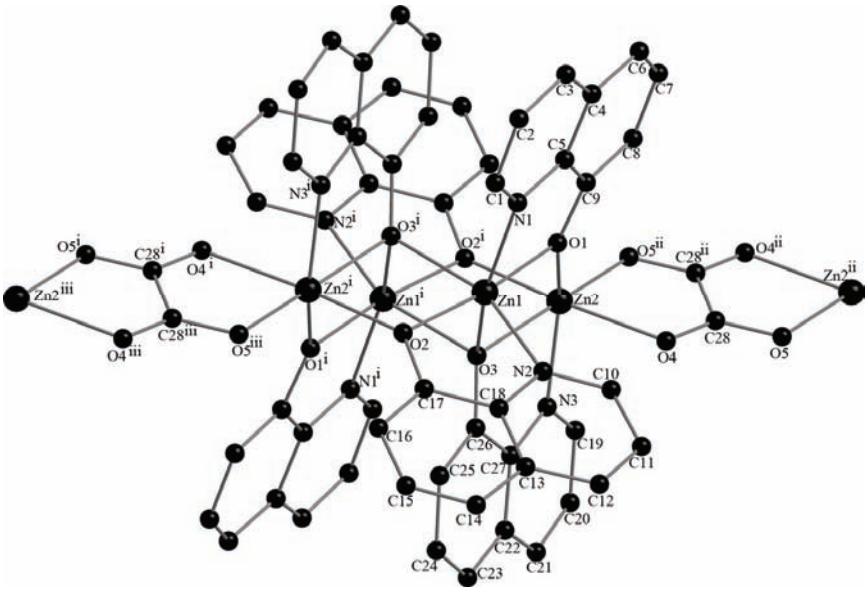

Fig. 1. Coordination geometry of the tetranuclear coordination polymer **1**, hydrogen atoms are omitted for clarity. Symmetry codes for i: 2–*x*, –*y*, –*z*, ii: 2–*x*, 1–*y*, –z and iii: *x*, –1+*y*, *z*.

metry operation 2–*x*, –*y*, –*z*) and N1 occupy the axial sites. Three Qs and one Ox are involved in coordination with Zn2. Zn2 is coordinated with five O atoms (two from oxalate and three from 8-hydroxyquinoline anions) and one N atom. The $O2^{i}$, O3, O4 and $O5^{ii}$ (*ii* stands for the symmetry operation 2–*x*, 1–*y*, –*z*) are located at the equatorial positions, while O1 and N3 occupy the axial sites. The phenolic oxygen atoms O1 and O2 are two-center μ_2-type oxygen atoms; O1 connects Zn1 and Zn2 and O2 connects Zn1 and $Zn2^{i}$. The phenolic oxygen O3 and its symmetry equivalent $O3^{i}$ are two three-center μ_3-type oxygen atoms; O3 connects Zn1, Zn2 and $Zn1^{i}$ and $O3^{i}$ connects the $Zn1^{i}$, $Zn2^{i}$ and Zn1 atoms. The Zn–N distances range between 2.086 and 2.139 Å, which is consistent with reported Zn–N distances, from 2.003[23] to 2.144.[24] The $Zn–O_{phenolic}$ distances range from 2.054 to 2.219 Å (Table II), and are similar to those reported in the literature (from 2.063–2.220 Å).[24,25] The $O4_{Ox}$ and $O5^{ii}_{Ox}$ are two doubly bridging O atoms coordinated to the Zn2 center; the $Zn2–O_{Ox}$ distances are 2.211(3) ($O4_{Ox}$–Zn2), and 2.057(3) Å ($O5^{ii}$–Zn2). The average Zn–O distance is 2.120(5) Å, which is slightly longer than the normal Zn–O distance 2.070 Å.[25] The dihedral angles between the Q rings are 18.88° (ring containing N1 and ring containing N3), 64.62° (ring containing N2 and ring containing N3) and 81.49° (ring containing N1 and ring containing N2). The Zn–Zn distances are 3.324 (Zn1···Zn2), 3.278 ($Zn1^{i}$···Zn2), and 3.264 Å ($Zn1^{i}$···Zn1). These three distances are consistent with the Zn···Zn distances of the related multinuclear 8-hyd-

roxyquinoline Zn(II) clusters (from 3.232 to 3.303 Å (tetranuclear[26a,26b]); 3.397 Å (trinuclear[26c]); 3.240 and 3.496 Å (binuclear[26d,26e])). These distances are longer than the sum of covalent radii of two Zn (2.44 Å, 1.22 Å×2),[27] but clearly shorter than the sum of the van der Waals radii of two Zn (4.20 Å, 2.10 Å×2).[28] These data reveal that there are the metal–metal interactions in the tetranuclear Zn centers in each cluster of the polymer **1**. The oxalate dianion exhibits the bis-bidentate coordination mode bridging two Zn2 atoms, *i.e.*, it chelates two symmetry-related Zn2 atoms. The Ox ligand acts as a spacer between adjacent two tetranuclear clusters, thus linking the clusters into a one-dimensional chain (Fig. 2). In the crystal lattice, the centroid-to-centroid distances to about 4 Å between the aryl-rings and their equivalent symmetry molecules at 2–*x*, –*y*, –*z* are listed in Table II. The data given in Table II suggest the existence of intra-chain offset π-stacking interactions and inter-chains point-to-face (T-shaped) C–H···π interactions. Moreover, in polymer **1** there are intra-chain, non-classic hydrogen bonds[29,30] C(16)–H(16)···O(5)^c (symmetry code *c*: *x*, –1+*y*, *z*) (Table II). It is obvious that in solid state, all these molecular interactions contribute to the stabilization of the supramolecular structure **1**.[31–34]

TABLE II. Selected bond lengths, Å, and bond angles, ° (symmetry transformation: #1: –*x*+2v,–*y*+1,v–*z*; #2: –*x*+2, –*y*, –*z*)

Bond	Length	Bond	Length
N(1)–Zn(1)	2.125(3)	O(3)–Zn(1)	2.120(3)
N(2)–Zn(1)	2.086(3)	O(3)–Zn(1)#2	2.216(2)
N(3)–Zn(2)	2.139(3)	O(3)–Zn(2)	2.219(3)
O(1)–Zn(1)	2.059(3)	Zn(2)–O(2)#2	2.086(3)
O(1)–Zn(2)	2.060(3)	O(4)–Zn(2)	2.211(3)
O(2)–Zn(1)	2.054(3)	O(5)–Zn(2)#1	2.057(3)
Bonds	Angle	Bonds	Angle
O(2)–Zn(1)–O(1)	172.80(11)	O(3)–Zn(1)–O(3)#2	82.36(10)
O(2)–Zn(1)–N(2)	80.54(13)	N(1)–Zn(1)–O(3)#2	94.40(11)
O(1)–Zn(1)–N(2)	106.65(13)	O(5)#1–Zn(2)–O(1)	111.89(11)
O(2)–Zn(1)–O(3)	102.51(10)	O(1)–Zn(2)–O(3)	75.05(10)
O(1)–Zn(1)–O(3)	77.26(10)	O(2)#2–Zn(2)–O(3)	79.51(10)
N(2)–Zn(1)–O(3)	93.60(12)	O(5)#1–Zn(2)–O(2)#2	96.04(10)
O(2)–Zn(1)–N(1)	100.44(13)	O(1)–Zn(2)–O(2)#2	96.40(11)
O(1)–Zn(1)–N(1)	79.05(12)	O(5)#1–Zn(2)–N(3)	99.25(12)
N(3)–Zn(2)–O(4)	85.42(12)	O(1)–Zn(2)–N(3)	144.98(12)
O(5)#1–Zn(2)–O(3)	172.30(11)	O(2)#2–Zn(2)–N(3)	95.83(11)
N(2)–Zn(1)–N(1)	97.35(13)	O(5)#1–Zn(2)–O(4)	78.19(11)
O(3)–Zn(1)–N(1)	155.90(12)	O(1)–Zn(2)–O(4)	85.66(11)
O(2)–Zn(1)–O(3)#2	80.28(10)	O(2)#2–Zn(2)–O(4)	174.23(10)
O(1)–Zn(1)–O(3)#2	92.59(10)	N(3)–Zn(2)–O(3)	75.13(11)
N(2)–Zn(1)–O(3)#2	159.02(12)	O(4)–Zn(2)–O(3)	106.25(10)

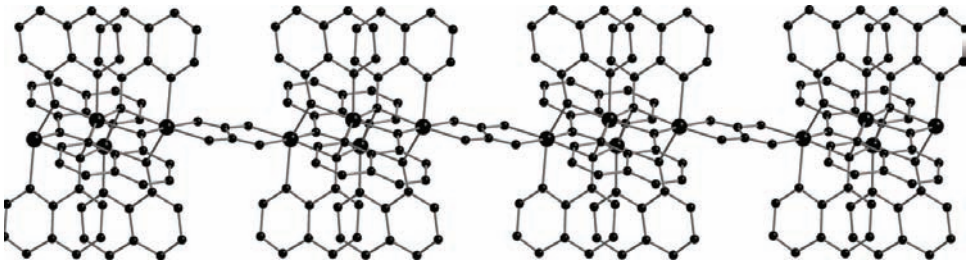

Fig. 2. The 1D infinite chains structure and π–π stacking interactions of polymer **1**, the hydrogen atoms are omitted for clarity.

TABLE III. The relative parameters of the intermolecular π–π interactions (with distinct centroids ≈ 4.0 Å), X–H···Cg (π-ring) interactions (H···Cg < 3.0 Å, γ < 30.0°) and non-classic hydrogen bonds in complex **1** (defined ring and symbol explanations: Cg(1): N(1) → C(1) → C(2) → C(3) → C(4) → C(5) →; Cg(2): N(3) → C(19) → C(20) → C(21) → C(22) → C(27) →; Cg(3): C(4) → C(5) → C(9) → C(8) → C(7) → C(6) →; Cg(4): C(22) → C(23) → C(24) → C(25) → C(26) → C(27) →; Cg(5): C(13) → C(14) → C(15) → C(16) → C(17) → C(18) →; Cg(I) = plane number I (= ring number in () above); dihedral angle = dihedral angle between planes I and J (°); distinct centroids = distance between ring centroids (Å); CgI_Perp = = perpendicular distance of Cg(I) on ring J (Å); γ = angle Cg(I) → Cg(J) vector and normal to plane J (°); symmetry codes: a: 2–*x*, –*y*, –*z*; b: 3/2–*x*, –1/2+*y*, 1/2–*z*; c: *x*, –1+*y*, *z*)

Cg(I) Cg(J)	Distinct centroids, Å	Dihedral angle, °	CgI_Perp, Å	γ / °
Cg(1) → Cg(2)	3.999(3)	17.83	3.563	26.99
Cg(1) → Cg(4)	3.559(3)	19.93	3.523	8.14
Cg(2) → Cg(1)	3.998(3)	17.83	3.331	33.59
Cg(3) → Cg(4)	4.032(3)	20.15	3.523	29.11
Cg(4) → Cg(1)	3.559(3)	19.93	3.400	17.16
Cg(4) → Cg(3)	4.032(3)	20.15	3.422	31.92
X–H(I) Cg(J)	H···Cg distance, Å	H–Perp, Å	X–H···Cg angle, °	γ / °
C(6)–H(6) → Cg(5)	2.93	2.815	157	16.34
C(15)–H(15) → Cg(4)	2.83	2.791	136	9.78
D–H···A	D–H distance, Å	H···A distance, Å	D···A distance, Å	D–H···A angle, °
C(16)–H(16)···O(5)	0.93	2.48	3.254(5)	141

CONCLUSIONS

A catenarian oxalate-bridged ternary tetranuclear 8-hydroxyquinoline zinc(II) coordination polymer of slightly distorted octahedral geometric configuration was obtained in the reaction of $Zn(OAc)_2 \cdot H_2O$ with 8-hydroxyquinoline and oxalic acid. The coordination geometry and the intermolecular interactions (π--stacking interactions, C–H···π interactions and non-classic hydrogen bonds) were investigated. Elemental analysis, TG analysis and FT-IR spectroscopy were also employed to characterize the title coordination polymer in detail.

Supplementary data. Supplementary material is deposited in the Cambridge Crystallographic Data Centre, 12 Union Road, Cambridge CB2 1EZ, UK, as supplementary material No. CDCC 784785 and can be obtained by contacting the CCDC.

Acknowledgements. This work was supported by the Jilin Normal University. The authors thank Ning-Hai Hu and Heng-Qing Jia of the Changchun Institute of Applied Chemistry, Chinese Academy of Sciences, and Guang-Gang Gao.

ИЗВОД

КРИСТАЛНА СТРУКТУРА ТЕТРАНУКЛЕАРНОГ 8-ХИДРОКСИХИНОЛИН Zn(II) КЛАСТЕРНОГ КОМПЛЕКСА СА ОКСАЛАТНИМ АНЈОНОМ У МОСТУ: $[Zn_4Q_6(Ox)]_{0.5n}$

JIAJUN WANG[1], QIANG WANG[2], YANJUN SUN[3], YUEMEI WANG[4], GUOSHENG ZHAO[1] и YUNCHENG CUI[1]

[1]*Chemistry College of Jilin Normal University; Key Laboratory of Preperation and Application of Envirinmental Friendly Materials (Jilin Normal University), Ministry of Education, Siping, 136000,* [2]*Department of Biological Medicine and Chemical Engineering, Liaoning Institute of Science and Technology, Benxi, 117004,* [3]*Boda College of Jilin Normal University. Siping, 136000, China и* [4]*Xi'an Modern Chemistry Research Institute. Xi'an, 710065, China*

Применом рендгенске структурне анализе одређена је структура тетрануклеарног цинк(II) кластерног комплекса $[Zn_4Q_6(Ox)]_{0.5n}$ ($[Zn_4(C_9H_6NO)_6(C_2O_4)]_{0.5n}$) **1** (Q = 8-хидроксихинолински анјон, Ox = оксалат). За карактеризацију овог комплекса употребљени су елементална микроанализа, IR спектроскопија и термална анализа. Комплекс је кристалисао у моноклиничном систему, просторна група $P2_1/n$ (No. 14), са параметрима јединичне ћелије: a = = 13.2222(15) Å, b = 11.0566(12) Å, c = 16.2224(18) Å, β = 92.1770(10)°, V = 2369.9(5) Å^3, Z = 4, M_r = 607.23, Dc = 1.702 g cm^{-3}. Тетрануклеарни цинк(II) кластерни комплекс гради 1D полимерне ланце паралелне са b-осом. Интеракције слагања (π–π) које укључују арилне прстенове доприносе грађењу 1D полимерне структуре. Суседни полимерни ланци су повезани преко CH···π интеракција.

(Примљено 22. августа, ревидирано 22. октобра 2010)

REFERENCES

1. J. Y. Lu, *Coord. Chem. Rev*. **246** (2003) 327
2. J. K. Cheng, Y. G. Yao, J. Zhang, Z. J. Li, Z. W. Cai, X. Y. Zhang, Z. N. Chen, Y. B. Chen, Y. Kang, Y. Y. Qin, Y. H. Wen, *J. Am. Chem. Soc*. **126** (2004) 7796
3. a) K. Endo, T. Kake, T. Sawaki, O. Hayashida, H. Masuda, H. Aoyama, *J. Am. Chem. Soc*. **119** (1997) 4117; b) T. Sawaki, T. Dewa, Y. Aoyama, *J. Am. Chem. Soc*. **120** (1998) 8539; c) J. S. Seo, D. Whang, H. Lee, S. I. Jun, J. Oh, Y. J. Jeon, K. Kim, *Nature* **404** (2000) 982; d) B. G. Lor, E. G. Puebla, M. Iglesias, M. A. Monge, C. R. Valero, N. Snejko, *Inorg. Chem.* **41** (2002) 2429
4. a) B. F. Abrahams, P. A. Jackson, R. Robson, *Angew. Chem. Int. Ed.* **37** (1998) 2656; b) M. Kondo, T. Okubo, A. Asami, S. Noro, S. Kitagawa, T. Ishii, H. Matsuzaka, K. Seki, *Angew. Chem. Int. Ed.* **38** (1999) 140; c) H. Eddaudi, H. L. Li, O. M. Yaghi, *J. Am. Chem. Soc.* **122** (2000) 1391; d) J. W. Ko, K. S. Min, M. P. Suh, *Inorg. Chem.* **41** (2002) 2151
5. a) O. M. Yaghi, H. Li, *J. Am. Chem. Soc.* **118** (1996) 295; b) K. S. Min, M. P. Suh, *J. Am. Chem. Soc*. **122** (2000) 6834

6. a) J. A. Real, E. Andrés, M. C. Muñoz, M. Julve, T. Granier, A. Boussekou, F. Varret, *Science* **268** (1995) 265; b) M. Albrecht, M. Lutz, A. L. Spek, G. van Koten, *Nature* **406** (2000) 970
7. O. R. Evans, W. Lin, *Chem. Mater.* **13** (2001) 2705
8. B. H. Hong, S. C. Bae, C. W. Lee, S. Jeong, K. S. Kim, *Science* **294** (2001) 348
9. a) Z. H. Skraup, *Chem. Monatsschr.* **2** (1881) 139; b) O. Doebner, W. V. Miller, *Chem. Ber.* **16** (1883) 1664; c) R. G. W. Hollingshead, *Oxine and its Derivatives*, Buttersworths, London, UK, 1954
10. C. W. Tang, S. A. Van Slyke, *Appl. Phys. Lett.* **51** (1987) 913
11. V. P. Barberis, J. A. Mikroyannidis, *Synth. Met.* **156** (2006) 865
12. W. B. Lin, O. R. Evans, R. G. Xiong, Z. Y. Wang, *J. Am. Chem. Soc.* **120** (1998) 13272
13. J. Zhang, R. G. Xiong, Z. F. Chen, X. Z. You, G. H. Lee, S. M. Peng, *Chem. Lett.* (2001) 676
14. M. Albrecht, O. Blau, K. Witt, E. Wegelius, M. Nissinen, K. Rissanen, R. Fröhlich, *Synthesis* (1999) 1819
15. a) M. Albrecht, K. Witt, E. Wegelius, K. Rissanen, *Tetrahedron* **56** (2000) 591; b) M. Albrecht, K. Witt, R. Fröhlich, O. Kataeva, *Tetrahedron* **58** (2002) 561
16. M. Albrecht, O. Blau, R. Fröhlich, *Chem. Eur. J.* **5** (1999) 48
17. M. Albrecht, K. Witt, P. Weis, E. Wegelius, R. Fröhlich, *Inorg. Chim. Acta* **341** (2002) 25
18. T. Higashi, *Program for Absorption Correction*, Rigaku Corporation, Tokyo, Japan, 1995
19. G. M. Sheldrick, *SHELXTL, v. 5 Reference Manual*, Siemens Analytical X-Ray Systems, Madison, WI, 1997
20. L. J. Farrugia, *J. Appl. Cryst.* **32** (1999) 837
21. A. R. Oki, J. Sanchez, T. J. Lester, A. Roxburgh. *Synth. React. Inorg. Met.-Org. Chem.* **26** (1996) 1
22. A. K. Tripathi, K. K. Sharma, P. Mathur, *Indian J. Chem.* **30A** (1991) 400
23. F. C. McDonald, R. C. Applefield, C. J. Halkides, J. H. Reibenspies, R. D. Hancock, *Inorg. Chim. Acta* **361** (2008) 1937
24. Y. G. Lu, W. Cheng, X. R. Meng, H. W. Hou, *J. Mol. Struct.* **875** (2008) 183
25. A. G. Orpen, L. Brammer, F. H. Allen, O. Kennard, G. Watson, R. Taylor, *J. Chem. Soc., Dalton Trans. II* (1989) S1
26. a) Y. Kai, M. Morita, N. Yasuoka, N. Kasai, *Bull. Chem. Soc. Jpn.* **58** (1985) 1631; b) E. Sattarzadeh, G. Mohammadnezhad, M. M. Amini, S. W. Ng *Acta Cryst.* **E65** (2009) m712; c) I. García-Santos, J. Sanmartín, A. M. García-Deibe, M. Fondo, E. Gómez *Polyhedron* **28** (2009) 3055; d) L. Xue, H. H. Wang, X. J. Wang, H. Jiang, *Inorg. Chem.* **47** (2008) 4310; e) E. Sattarzadeh, G. Mohammadnezhad, M. M. Amini, S. W. Ng *Acta Cryst.* **E65** (2009) m554
27. B. Cordero, V. Gómez, A. E. Platero-Prats, M. J. Revés, E. Cremades, F. Barragán. S. Alvarez, *J. Chem. Soc., Dalton Trans.* (2008) 2832
28. S. Z. Hu, Z .H. Zhou, Q. R. Cai, *Acta Phys. Chim. Sin.* **19** (2003) 1073
29. T. Steiner, *Cryst. Rev.* **6** (1996) 1
30. G. A. Jeffrey, H. Maluszynska, J. Mitra, *Int. J. Biol. Macromol.* **7** (1985) 336
31. R. H. Hunter, R. H. Haueisen, A. Irving, *Angew. Chem. Int. Engl. Ed.* **33** (1994) 566
32. Y. C. Cui, J. J. Wang, G. B. Che, C. B. Liu, C. B. Li, *Acta Crystallogr. E* **62** (2006) 1633
33. F. F. Jian, H. L. Xiao, P. P. Sun, P. S. Zhao, *Molecules.* **9** (2004) 876
34. Q. Xu, M. Du, Y. M. Guo, X. H. Bu, *Chin. J. Struct. Chem.* **21** (2002) 621.

Journal of the Serbian Chemical Society
JSCS-info@shd.org.rs • www.shd.org.rs/JSCS
J. Serb. Chem. Soc. 76 (4) 539–555 (2011)
JSCS–4141
UDC 544.112:517.544.4:621.376.2
Original scientific paper

On the relationship between molecular spectroscopy and statistical mechanics: calculation of partition functions for triatomic molecules undergoing large-amplitude bending vibrations

MILAN V. SENĆANSKI[1#], JELENA RADIĆ-PERIĆ[2] and MILJENKO PERIĆ[2*#]

[1]*Innovation Centre of the Faculty of Chemistry, University of Belgrade, Studentski Trg 12–16, 11158 Belgrade and* [2]*Faculty of Physical Chemistry, University of Belgrade, Studentski Trg 12–16, P.O. Box 47, 11158 Belgrade, Serbia*

(Received 26 November 2010)

Abstract: The evaluation of partition functions for triatomic molecules undergoing large-amplitude bending vibrations is discussed. It was supposed that the needed molecular structure data were obtained by means of *ab initio* calculations. Special attention is paid to the coupling between the bending and stretching modes and the interplay between bending motions and rotations. An appropriate scheme for variational computation of the energy levels is developed.

Keywords: partition functions; triatomic molecules; large-amplitude bending.

INTRODUCTION

The present study was motivated by the need for partition functions of the molecule BC_2, which plays an important role, *e.g.*, in plasma processes that should lead to the synthesis of boron carbide, B_4C. Since it was not possible to find either numerical data for the partition functions or spectroscopically derived molecular structure parameters needed to calculate partition functions by the machinery of statistical mechanics, *ab initio* quantum mechanical calculations on this species were performed.[1] The results of these investigations showed that BC_2 has a very interesting structure. It is characterized by the ground electronic state having C_2v (X^2A_1) or slightly distorted C_2v (X^2A') symmetry, separated by a barrier of about 2000 cm^{-1} from a local minimum on the potential energy surface, corresponding to the linear molecular geometry ($^2\Sigma^+$). The transition from the one to the other structure occurs in the course of large-amplitude bending vibrations, being strongly coupled to the stretching vibrational modes. Therefore,

* Corresponding author. E-mail: peric@ffh.bg.ac.rs
# Serbian Chemical Society member.
doi: 10.2298/JSC101126052S

if one wishes to compute reliable partition functions for this molecule, one has to solve a number of specific problems that are normally ignored in textbooks on statistical mechanics. In the present paper, the theoretical background of the problem is dealt with. In the following paper,[2] the results of the calculation of the vibrational–rotational energy levels in the ground electronic state and the corresponding partition functions are given.

The paper is organized as follows. In the second section, an evaluation of the energy levels and partition functions of triatomic molecules with linear and bent equilibrium geometries in the harmonic approximation is reviewed. In the third section, a method for *ab initio* handling of the same problem is presented. An approach for the solution of the Schrödinger equation for large-amplitude bending vibrations is briefly described. The last section presents a short conclusion.

HARMONIC APPROXIMATION

At the beginning, it was found sensible to estimate the relationship between characteristic molecular-energy values and the quantity kT, where k is the Boltzmann constant and T the temperature. In the present study, instead of energy, the wave number, $\tilde{\nu} = E/hc$, expressed in cm^{-1} (1 J is equivalent to 5.0364×10^{22} cm^{-1}) is often used; in this case, the Boltzmann constant becomes $k = 0.695$ cm^{-1} K^{-1}. In the temperature interval of interest, *i.e.*, 1000–6000 K, the value of kT will be in the range 700–4000 cm^{-1}. The contribution of excited electronic states to the total partition function is neglected. The stretching vibrational wave numbers for molecules such as BC_2, being the subject of our next paper, are around 10^3 cm^{-1}, whereas the bending wave numbers have values of a few hundred cm^{-1}.[1] The rotational constants are of a few cm^{-1}.

First, the partition functions in the harmonic approximation are handled. Triatomic molecules are considered separately in spatially and spin non-degenerate electronic states with linear and non-linear equilibrium geometry. In both cases, the molecular Hamiltonian can be written in the form:

$$\hat{H} = \hat{H}^{\mathrm{tr}} + \hat{H}^{\mathrm{e}} + \hat{H}^{\mathrm{v}} + \hat{H}^{\mathrm{r}} \quad (1)$$

where $\hat{H}^{\mathrm{tr}}$, $\hat{H}^{\mathrm{e}}$, $\hat{H}^{\mathrm{v}}$ and $\hat{H}^{\mathrm{r}}$ represent the translational, electronic, vibrational and rotational parts, respectively. In the following, the translational part of the Hamiltonian, Eq. (1), is ignored and assume the eigenvalues of the electronic part to be included in $\hat{H}^{\mathrm{v}}$ as the "potential energy surface", calculated within the framework of the Born–Oppenheimer approximation. Writing Eq. (1), it is implicitly assumed that coupling between vibrational and rotational motions is neglected.

Linear equilibrium geometry

Triatomic molecules with linear equilibrium geometry are traditionally handled as species having two rotational and four vibrational degrees of freedom.

According to such a scheme, the vibrational and rotational parts of the Hamiltonian (1) are written in the forms:

$$\hat{H}^{\mathrm{v}} = \hat{H}_{\mathrm{s}} + \hat{H}_{\mathrm{b},z} \tag{2}$$

$$\hat{H}^{\mathrm{r}} = \hat{H}^{\mathrm{r}}_{x,y} \tag{3}$$

The *z*-axis is chosen to coincide with the molecular axis at linear nuclear arrangements. The vibrational Hamiltonian is separated into a stretching ($\hat{H}_{\mathrm{s}}$) and a bending ($\hat{H}_{\mathrm{b,z}}$) part. This can be performed because the stretching and bending coordinates are (in the case of linear molecules) not coupled with one another in the harmonic approximation. $\hat{H}^{\mathrm{r}}_{\mathrm{x,y}}$ is the Hamiltonian for end-over-end rotations.

The stretching part of the vibrational Hamiltonian is in the harmonic approximation represented by:

$$\hat{H}_{\mathrm{s}} = -\frac{\hbar^2}{2\mu_r}\frac{\partial^2}{\partial r^2} - \frac{\hbar^2}{2\mu_R}\frac{\partial^2}{\partial R^2} - \frac{\hbar^2}{\mu_{rR}}\frac{\partial^2}{\partial r \partial R} + \frac{1}{2}k_{rr}r^2 + \frac{1}{2}k_{RR}R^2 + k_{rR}rR \tag{4}$$

where r and R are two stretching vibrational coordinates. In the case of linear molecules, ABC, the usual choice is r = A–B and R = B–C, *i.e.*, the stretching coordinates represent the bond lengths (or their changes with respect to the equilibrium values) – Fig. 1. μ_R and μ_r are the corresponding "reduced masses". k_{rr}, k_{RR} and k_{rR} are the quadratic force constants representing the electronic energy as a function of the stretching coordinates. The eigenvalues of the Hamiltonian (4) are:

$$E_{\mathrm{s}} = \left(v_{\mathrm{s1}} + \frac{1}{2}\right)\hbar\omega_{\mathrm{s1}} + \left(v_{\mathrm{s2}} + \frac{1}{2}\right)\hbar\omega_{\mathrm{s2}} = \left(v_{\mathrm{s1}} + \frac{1}{2}\right)hc\tilde{\nu}_{\mathrm{s1}} + \left(v_{\mathrm{s2}} + \frac{1}{2}\right)hc\tilde{\nu}_{\mathrm{s2}} \tag{5}$$

where ω is the vibrational frequency (in units s^{-1}) and $\tilde{\nu}$ the wave number. The energy spectrum is non-degenerated.

In the harmonic approximation, the bending part of the vibrational Hamiltonian has the form:

$$\hat{H}_{\mathrm{b,z}} = -\frac{\hbar^2}{2\mu_{\mathrm{b}}}\left(\frac{\partial^2}{\partial\theta^2} + \frac{1}{\theta}\frac{\partial}{\partial\theta} + \frac{1}{\theta^2}\frac{\partial^2}{\partial\varphi^2}\right) + \frac{1}{2}k_\theta\theta^2 \tag{6}$$

if the volume element $\mathrm{d}V = \theta\mathrm{d}\theta\mathrm{d}\varphi$ is assumed. For molecules with linear equilibrium geometry, the bending coordinate is usually chosen to be the supplement of the bond angle, *i.e.*, $\theta = \pi - \angle$ A–B–C, expressed in length units. Equation (6) represents the Hamiltonian of an isotropic two-dimensional harmonic oscillator, the eigenvalues of which are:

$$E_{\mathrm{b},z} = \left(v_{\mathrm{b}} + 1\right)\hbar\omega_{\mathrm{b}} = \left(v_{\mathrm{b}} + 1\right)hc\tilde{\nu}_{\mathrm{b}} \tag{7}$$

Each energy level is $v_b + 1$ degenerated, because for every $v_b = 0,1,2,\ldots$ there are sublevels of the same energy corresponding to the value of the vibrational angular quantum number $l = -v_b,-v_b+2,\ldots,v_b$. Beyond the harmonic approximation, this degeneracy is lifted and the energy depends on both v_b and the absolute value of l – for this reason, l is usually considered as an unsigned quantity. Each $E_{v_b,|l|}$ level is in the case of anharmonicity twofold degenerate for $|l| \neq 0$.

The rotational Hamiltonian is usually written as:

$$\hat{H}^{r}_{x,y} = \frac{\hat{J}_x^2}{2I_B} + \frac{\hat{J}_y^2}{2I_B} = \frac{\hat{J}^2}{2I_B} \tag{8}$$

since the z-component of the nuclear angular momentum equals zero and thus:

$$\hat{J}^2 \equiv \hat{J}_x^2 + \hat{J}_y^2 + \hat{J}_z^2 = \hat{J}_x^2 + \hat{J}_y^2 \tag{9}$$

where I_B is the moment of inertia along the axes perpendicular to the molecular axis. The energy levels corresponding to the Hamiltonian (8) are:

$$E^{r}_{x,y} = \frac{J(J+1)\hbar^2}{2I_B} \equiv BhcJ(J+1), \tag{10}$$

where

$$B \equiv \frac{h}{8\pi^2 c I_B} = \frac{\hbar}{4\pi c I_B} \tag{11}$$

is the rotational constant, usually expressed in cm^{-1}. Each J-level is $(2J+1)$--degenerated because the wave functions for a given J are also characterized by the quantum number M ($M = -J,-J+1,\ldots,J$), denoting the projection of the angular momentum along a space-fixed (Z) coordinate axis.

If the above scheme is assumed, the total molecular partition function for the degrees of freedom considered is such as given in the majority of textbooks:[3]

$$Z = Z_{s1} Z_{s2} Z_{b,z} Z^{r}_{x,y} \tag{12}$$

with:

$$Z_{s1} = \left(1 - e^{-\frac{\hbar\omega_{s1}}{kT}}\right)^{-1}, \quad Z_{s2} = \left(1 - e^{-\frac{\hbar\omega_{s2}}{kT}}\right)^{-1} \tag{13}$$

$$Z_{b,z} = \left(1 - e^{-\frac{\hbar\omega_b}{kT}}\right)^{-2} \tag{14}$$

$$Z^{r}_{x,y} = \frac{kT}{\sigma hcB} = \frac{kT}{\sigma 2\pi\hbar cB} \tag{15}$$

In all formulae (13–15), the Boltzmann constant is assumed to have its "normal" value, $k = 1.380 \times 10^{-23}$ J K^{-1}. The "symmetry number" in the present case (asymmetric ABC molecules) is σ = 1. In the following formulae, it will be omitted. It is assumed that the zeroth vibrational–rotational level is taken to be zero on the energy scale. The rotational partition function is derived in the "high--temperature approximation" by replacing the sum with the corresponding integral:

$$Z_{x,y}^{\mathrm{r}} = \sum_{J=0}^{\infty} (2J+1) \mathrm{e}^{-\frac{BhcJ(J+1)}{kT}} \cong \int_{J=0}^{\infty} (2J+1) \mathrm{e}^{-\frac{BhcJ(J+1)}{kT}} \mathrm{d}J = \frac{kT}{hcB} \tag{16}$$

However, when Eq. (9) is written, the fact is ignored that triatomic molecules have a non-vanishing component of the total angular momentum along the molecular axis. This arises from the vibrational angular momentum, and relation (9) has to be replaced by the correct one:

$$\hat{J}^2 \equiv \hat{J}_x^2 + \hat{J}_y^2 + \hat{l}^2 \tag{17}$$

The origin of the vibrational angular momentum becomes clear when the rotational Hamiltonian is formally written in the general form of a prolate symmetric top:

$$\hat{H}_{x,y}^{\mathrm{r}} = \frac{\hat{J}_x^2}{2I_{\mathrm{B}}} + \frac{\hat{J}_y^2}{2I_{\mathrm{B}}} + \frac{\hat{J}_z^2}{2I_{\mathrm{A}}} \tag{18}$$

where I_{A} is the moment of inertia along the z-axis. Since I_{A} = 0 for linear geometry, one prefers to incorporate the last term on the right-hand side in the bending Hamiltonian – it appears in it (Eq. (6)) in the form of:

$$\frac{\hat{J}_z^2}{2I_{\mathrm{A}}} = \frac{\left(-i\hbar \frac{\partial}{\partial \varphi}\right)^2}{2I_{\mathrm{A}}} = -\frac{\hbar^2}{2\mu_{\mathrm{b}}\theta^2} \frac{\partial^2}{\partial \varphi^2} \tag{19}$$

The singularity caused by the term $\hat{J}_z^2 / (2I_{\mathrm{A}})$ is then exactly cancelled by the singularities caused by the remaining two terms in the Hamiltonian (6). The eigenvalues of the operator $\hat{J}_z^2 = -\hbar^2 \partial^2 / \partial \varphi^2$ are $\hat{l}^2 \hbar^2$. Consequently, Eqs. (8) and (10) are replaced, respectively, by:

$$\hat{H}_{x,y}^{\mathrm{r}} = \frac{\hat{J}_x^2}{2I_{\mathrm{B}}} + \frac{\hat{J}_y^2}{2I_{\mathrm{B}}} = \frac{\hat{J}^2 - \hat{J}_z^2}{2I_{\mathrm{B}}} \tag{20}$$

and

$$E_{x,y}^{\mathrm{r}} = \frac{\left[J(J+1) - l^2\right]\hbar^2}{2I_{\mathrm{B}}} \equiv Bhc\left[J(J+1) - l^2\right] \tag{21}$$

The quantum numbers J and l are connected with each other by the relation $J \geq l$. We write now the energy values corresponding to the operator $\hat{H}_{\mathrm{b,z}} + \hat{H}^{\mathrm{r}}_{\mathrm{x,y}}$ as:

$$E_{\mathrm{b},z} = (v_{\mathrm{b}} + 1)\hbar\omega_{\mathrm{b}} + Bhc\left[J(J+1) - l^2\right] = (2n + l + 1)\hbar\omega_{\mathrm{b}} + \\ + Bhc\left[J(J+1) - l^2\right] \tag{22}$$

where the integer n takes the values 0,1,2,... Taking into account that the degeneracy of each J-level is $(2J + 1)$ and that $l = 0$ levels are non-degenerated, whereas for $l \neq 0$, there are two sublevels corresponding to $l = \pm|l|$, one obtains for the corresponding partition function:[4]

$$Z^{\mathrm{b,r}} = \sum_{l=0}^{\infty}\sum_{n=0}^{\infty}\sum_{J=l}^{\infty} g_l (2J+1)\mathrm{e}^{-\frac{(2n+l)\hbar\omega_{\mathrm{b}} + Bhc\left[J(J+1) - l^2\right]}{kT}} \cong \\ \cong \sum_{l=0}^{\infty} g_l \mathrm{e}^{-\frac{l\hbar\omega_{\mathrm{b}} - l^2 Bhc}{kT}} \sum_{n=0}^{\infty} \mathrm{e}^{-\frac{2n\hbar\omega_{\mathrm{b}}}{kT}} \int_{J=l}^{\infty} (2J+1) e^{-\frac{BhcJ(J+1)}{kT}} \mathrm{d}J = \\ = \frac{kT}{Bhc} \frac{\left(1 + \mathrm{e}^{-\frac{\hbar\omega_{\mathrm{b}} + Bhc}{kT}}\right)}{\left(1 - \mathrm{e}^{-\frac{2\hbar\omega_{\mathrm{b}}}{kT}}\right)\left(1 - \mathrm{e}^{-\frac{\hbar\omega_{\mathrm{b}} + Bhc}{kT}}\right)} \tag{23}$$

Since $\hbar\omega_{\mathrm{b}} >> Bhc$, it follows from Eq. (23):

$$Z^{\mathrm{b,r}} \cong \frac{kT}{Bhc} \frac{1}{\left(1 - \mathrm{e}^{-\frac{\hbar\omega_{\mathrm{b}}}{kT}}\right)^2} \tag{24}$$

In this approximation, the same result is obtained as the product of $Z_{\mathrm{b},z}$, Eq. (14) and $Z^{\mathrm{r}}_{\mathrm{x,y}}$, Eq. (15). Therefore, in spite of the fact that the neglect of the relationship between the quantum numbers J and l, representing the heart of the approximation/misconception, Eq. (9), leads to an unreliable energy level scheme, it does not causes serious errors in the partition function.

Nonlinear equilibrium geometry

Triatomic molecules with nonlinear equilibrium geometry have three rotational and three vibrational degrees of freedom. Several sets of internal coordinates can be applied to describe the molecular vibrations. One possibility is to use the same "valence type" coordinates as for triatomic molecules. However, in the case of nonlinear molecules, they loose somewhat their convenience because their employment leads to terms in the Hamiltonian that couple the stretching and

bending vibrational motions. When dealing with large-amplitude bending vibrations and particularly when one atom migrates around a more or less compact skeleton of the other two (as *e.g.*, the H-atom around the N–C moiety in course of the HNC→HCN isomerisation process,[5,6] or the B-atom around the C–C diatomic rest in the BC_2 molecule), it is more convenient to use the "Jacobi coordinates", R, r and θ, where R is the distance between the nuclei building the diatomic part, r the distance between the migrating atom and the midpoint of the diatomic part, and θ is defined as the angle between the vectors $\vec{r}$ and $\vec{R}$ (Fig. 1). An advantage of these coordinates is that there is no coupling between the three vibrational modes through the kinetic energy part of the vibrational Hamiltonian, and the coupling terms in the potential energy part are generally diminished.

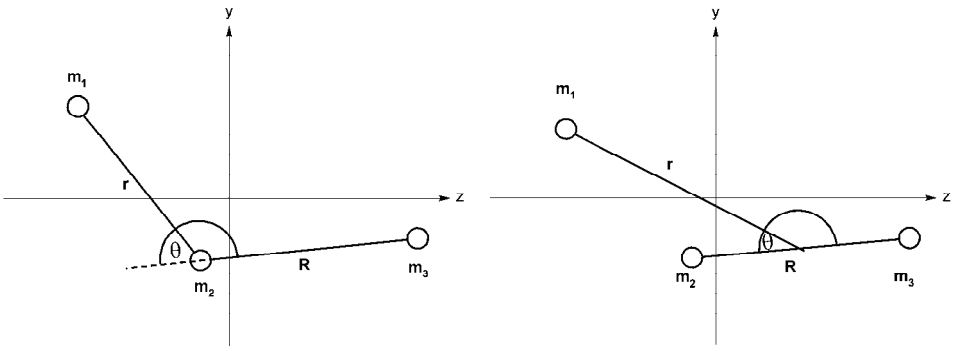

Fig. 1. Vibrational coordinates employed in the present study. Left-hand side: valence coordinates; right-hand side: Jacobi coordinates.

Although the stretching and bending vibrations are mutually coupled in triatomic molecules with nonlinear equilibrium geometry, this coupling is neglected in this subsection, because here the primarily interest lies in bookkeeping concerning the evaluation of the partition functions. The emphasis lies on the consequences of the gradual transformation of the twofold degenerate bending vibration in linear molecules to the one-dimensional bending plus the rotation around the z-axis in bent nuclear arrangements. Thus, the vibrational Hamiltonian in the form:

$$\hat{H}^{\mathrm{v}} = \hat{H}_{\mathrm{s}} + \hat{H}_{\mathrm{b}} \tag{25}$$

is assumed, where the stretching part has the form given by Eq. (4), and the bending part is:

$$\hat{H}_{\mathrm{b}} = -\frac{\hbar^2}{2\mu_{\mathrm{b}}}\frac{\partial^2}{\partial\theta^2} + \frac{1}{2}k_{\theta}\left(\theta - \theta_{\mathrm{e}}\right)^2 \tag{26}$$

The equilibrium value of the coordinate θ is denoted by θ_e. When handling one-dimensional bending vibrations, it is sensible to assume the volume (integration) element $dV = d\theta$. The bending energy corresponding to the operator (26) is:

$$E_b = \left(v_b + \frac{1}{2} \right) \hbar \omega_b \tag{27}$$

and the spectrum is non-degenerated.

Triatomics with bent equilibrium geometry are asymmetric top molecules and thus the corresponding rotational Schrödinger equation cannot be solved analytically. In this subsection, they are handled as if they were symmetric tops, because the primary interest lies in the qualitative features of the partition functions. The rotational Hamiltonian of a symmetric top is given by:

$$\hat{H}^r = \frac{\hat{J}_x^2}{2I_B} + \frac{\hat{J}_y^2}{2I_B} + \frac{\hat{J}_z^2}{2I_A} = \frac{\hat{J}^2 - \hat{J}_z^2}{2I_B} + \frac{\hat{J}_z^2}{2I_A} = \frac{\hat{J}^2}{2I_B} + \frac{\hat{J}_z^2}{2} \left(\frac{1}{I_A} - \frac{1}{I_B} \right) \tag{28}$$

and the corresponding energy is:

$$E^r = Bhc\left[J(J+1) - K^2 \right] + AhcK^2 = BhcJ(J+1) + (A-B)hcK^2 \tag{29}$$

$$A \equiv \hbar^2 / 4\pi c I_A$$

For a given J, the quantum numbers K and M (not appearing in the energy expression, Eq. (29)) take the values $K,M = -J,-J+1,\ldots,J$; since the energy does not depend on the sign of K, the energy levels for a particular combination of J and K are $g_K(2J+1)$-degenerated, with $g_K = 1$ for $K = 0$, and $g_K = 2$ at $K \neq 0$. The quantum number K, determining the projection of the angular momentum on the z-axis of the coordinate system fixed at the molecule, is fully equivalent to the quantum number l defined for linear molecules and, in order to emphasize this equivalence, the symbol l will be used instead of K in this subsection.

The complete vibrational–rotational molecular partition function of a triatomic molecule with non-linear equilibrium geometry is given by:

$$Z = Z_{s1} Z_{s2} Z_b Z^r \tag{30}$$

where the stretching partition functions are of the same forms as those for linear molecules (Eq. (13)). The remaining part of the partition functions can be handled in several different ways:

Case a. The partition function for the (one-dimensional) bending vibrations is:

$$Z_b = \sum_{v_b=0}^{\infty} e^{-\frac{v_b \hbar \omega_b}{kT}} = \left(1 - e^{-\frac{\hbar \omega_b}{kT}} \right)^{-1} \tag{31}$$

The partition function corresponding to the rotational energy expression, Eq. (29), is:

$$Z^{\mathrm{r}} = \sum_{J=0}^{\infty} \sum_{l=-J}^{J} g_l \left(2J+1\right) \mathrm{e}^{-\frac{BhcJ\left(J+1\right)+\left(A-B\right)hcl^2}{kT}} \cong \left(\frac{kT}{hc}\right)^{3/2} \frac{\sqrt{\pi}}{\sqrt{AB}} \qquad (32)$$

The final expression is derived in the high-temperature approximation, taking into account the fact that the term Bl can be neglected in the expression $\exp\left[-(Al^2 + Bl)hc / kT\right]$ and that:

$$\sum_{l=0}^{\infty} g_l \mathrm{e}^{-\frac{Ahcl^2}{kT}} = \sum_{l=-\infty}^{\infty} \mathrm{e}^{-\frac{Ahcl^2}{kT}} \qquad (33)$$

If B is replaced in Eq. (32) by $\sqrt{BC}$, the expression for the rotational partition function of molecules with three unequal moments of inertia (asymmetric tops), as quoted in textbooks, (*e.g.*, Ref. 3), is obtained.

The correlation of the energy levels for bending vibrations plus rotations in a linear and a bent molecule are shown in Fig. 2.

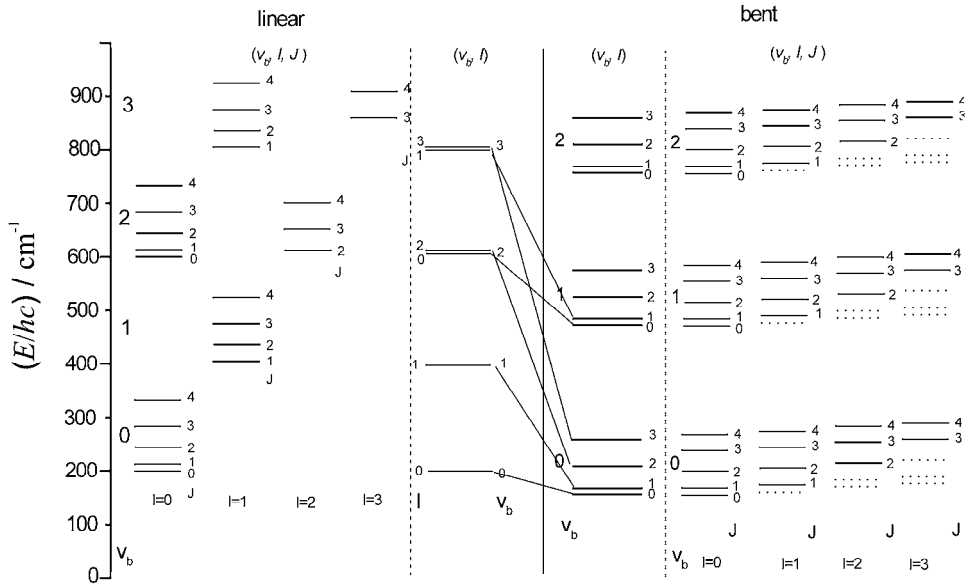

Fig. 2. Correlation between bending vibrational and rotational energy levels of a linear (left-hand side) and a bent (right-hand side) molecule. The levels with the inscription (v_b, l) do not involve a contribution of end-over-end (x,y) rotations. They are computed by means of Eq. (7) for a linear molecule and Eq. (41) for a bent molecule. The levels with the inscription (v_b, l, J) also involve a contribution of x, y rotations (Eqs. (21) and (43)). The values of $\tilde{\nu}_b = 200$ cm^{-1}, $B = 5$ cm^{-1} for linear molecule and $\tilde{\nu}_b = 300$ cm^{-1}, $A = 10$ cm^{-1}, $B = 5$ cm^{-1} for bent molecule are used.

Case b. In order to enable direct comparison of the results for partition functions obtained in the harmonic approximation with their counterparts evaluated beyond that approximation, the rotational partition function is now computed in another way. It will be shown that the partition function of a symmetric top can be replaced in a good approximation by the product of the partition functions of a one-dimensional and a two-dimensional rotator with the quantum numbers being independent of one another.[4] It is thus assumed the rotational Hamiltonian in the form:

$$\hat{H}^{\mathrm{r}} = \hat{H}_1^{\mathrm{r}} + \hat{H}_2^{\mathrm{r}} = \hat{H}_z^{\mathrm{r}} + \hat{H}_{\mathrm{x,y}}^{\mathrm{r}} \tag{34}$$

with

$$\hat{H}_1^{\mathrm{r}} = \frac{\hat{J}_z^2}{2I_{\mathrm{A}}}, \quad \hat{H}_2^{\mathrm{r}} = \frac{\hat{J}_x^2 + \hat{J}_y^2}{2I_{\mathrm{B}}} \tag{35}$$

The corresponding energy levels are:

$$E_1^{\mathrm{r}} = Ahcl^2, \quad l = 0,1,2,..., \; g_{\mathrm{l}} = 1(l=0);2(l\neq 0) \tag{36}$$

$$E_2^{\mathrm{r}} = Bhc \cdot j(j+1), \quad j = 0,1,2,..., \quad g_{\mathrm{j}} = 2j+1 \tag{37}$$

Note that the quantum number j appearing in Eq. (37) does not have the same sense as the quantum number J for the magnitude of the total angular momentum. The partition functions are now

$$Z_1^{\mathrm{r}} = \sum_{l=0}^{\infty} g_{\mathrm{K}} \mathrm{e}^{-\frac{Ahcl^2}{kT}} \cong \int_{-\infty}^{\infty} \mathrm{e}^{-\frac{Ahcl^2}{kT}} \mathrm{d}l = \sqrt{\frac{\pi kT}{Ahc}} \tag{38}$$

$$Z_2^{\mathrm{r}} = \sum_{j=0}^{\infty} (2j+1)\mathrm{e}^{-\frac{BhcJ(J+1)}{kT}} \cong \int_0^{\infty} (2j+1)\mathrm{e}^{-\frac{Bhcj(j+1)}{kT}} \mathrm{d}j = \frac{kT}{Bhc} \tag{39}$$

Multiplying Eq. (38) with Eq. (39), the result of Eq. (32) is indeed obtained. Comparison of the rotational-energy levels of the symmetric top and the sum of the corresponding one-dimensional and two-dimensional rotators is presented in Fig. 3.

Case c. According to the last statement above, when evaluating the partition functions, the term $\hat{J}_z^2 / (2I_{\mathrm{A}})$ from the last but one expression for the rotational Hamiltonian, Eq. (28), can be extracted and put together with the bending Hamiltonian, Eq. (26), into the operator $\hat{H}_{\mathrm{b,z}}$:

$$\begin{aligned} \hat{H}_{\mathrm{b,z}} &= -\frac{\hbar^2}{2\mu_{\mathrm{b}}}\frac{\partial^2}{\partial\theta^2} + \frac{1}{2}k_\theta(\theta-\theta_0)^2 + \frac{\hat{J}_z^2}{2I_{\mathrm{a}}} = \\ &= -\frac{\hbar^2}{2\mu_{\mathrm{b}}}\frac{\partial^2}{\partial\theta^2} + \frac{l^2\hbar^2}{2I_{\mathrm{a}}} + \frac{1}{2}k_\theta(\theta-\theta_0)^2 \end{aligned} \tag{40}$$

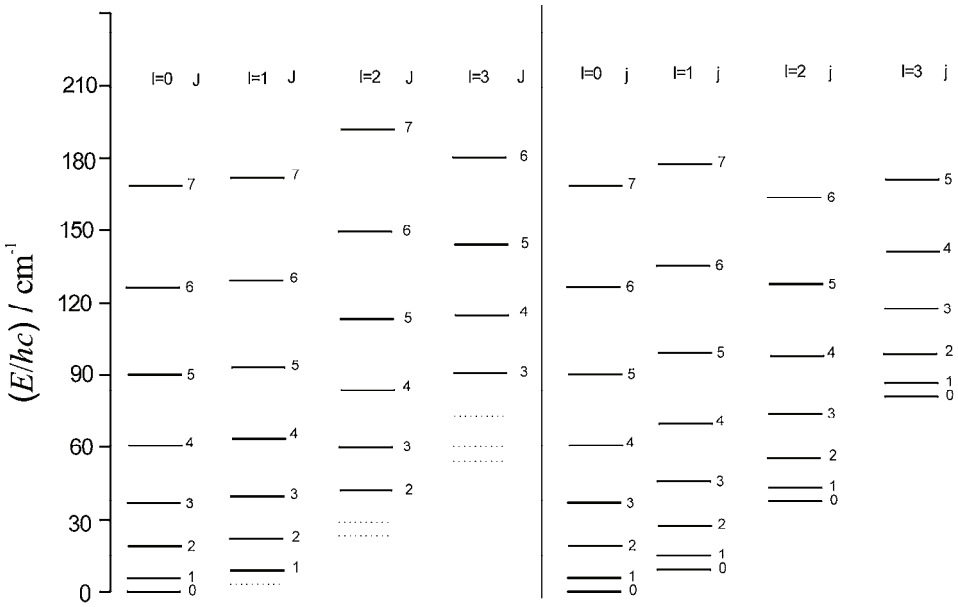

Fig. 3. Correlation between the rotational states of a symmetric top (left-hand side), and the sum of a one-dimensional and a two-dimensional rotator (right-hand side). The values of A = 3 cm^{-1} and B = 1 cm^{-1} are used.

Such a partitioning of the Hamiltonian is performed in order to enable a correlation of the results obtained in the harmonic approximation with those generated by employing the *ab initio* approach described below. The eigenvalues of the Hamiltonian, Eq. (40), are:

$$E_{\mathrm{b},z} = \left(v_{\mathrm{b}} + \frac{1}{2}\right)\hbar\omega_{\mathrm{b}} + Ahcl^2 \tag{41}$$

and the partition function is:

$$\begin{aligned} Z_{\mathrm{b},z} &= \sum_{v_{\mathrm{b}}=0}^{\infty}\sum_{l=0}^{\infty} g_l \mathrm{e}^{-\frac{v_{\mathrm{b}}\hbar\omega_{\mathrm{b}}+Ahcl^2}{kT}} \cong \sum_{v_{\mathrm{b}}=0}^{\infty} \mathrm{e}^{-\frac{v_{\mathrm{b}}\hbar\omega_{\mathrm{b}}}{kT}} \int_{-\infty}^{\infty} \mathrm{e}^{-\frac{Ahcl^2}{kT}} \mathrm{d}l = \\ &= \left(1-\mathrm{e}^{-\frac{\hbar\omega_{\mathrm{b}}}{kT}}\right)^{-1} \sqrt{\frac{kT\pi}{Ahc}} \end{aligned} \tag{42}$$

The eigenvalues of the remaining part of the rotational Hamiltonian, $\left(\hat{J}^2 - \hat{J}_Z^2\right)/\left(2I_{\mathrm{B}}\right)$, are:

$$E_{x,y}^{r} = Bhc\left[J\left(J+1\right) - l^2\right] \tag{43}$$

where $l \leq J$. However, when the partition function corresponding to this part of the Hamiltonian is independently evaluated, one has to put $l = 0$ and to sum over all J-values (from 0 to ∞), as was done in Eq. (19). The total bending–rotational partition function is then the product of Eqs. (42) and (19).

The complete bending–rotational energy is the sum of Eqs. (41) and (43):

$$E_{\mathrm{b,r}} = \left(v_{\mathrm{b}} + \frac{1}{2}\right)\hbar\omega_{\mathrm{b}} + Ahcl^2 + Bhc\left[J\left(J+1\right) - l^2\right] \tag{44}$$

and equals, of course, the sum of E_{b} (Eq. (27)) and E_{b} (Eq. (29)) ($l = K$). The partition function corresponding to the energy expression, Eq. (44), equals the product of the partition functions, Eqs. (31) and (32) (case a), as well as the product of Eqs. (31), (38) and (39) (case b). However, recall that the energy spectra are different for the cases a and c on the one hand, and b on the other. In the first case, the energy levels are given by Eq. (44) with the condition $l \leq J$; for a given combination of J and l the energy level is $g_l(2J+1)$-fold degenerated ($g_l = 1$ for $l = 0$ and $g_l = 2$ for $l \neq 0$). In case b, the energy is:

$$E_{\mathrm{b},z} = \left(v_{\mathrm{b}} + \frac{1}{2}\right)\hbar\omega_{\mathrm{b}} + Ahcl^2 + Bhcj\left(j+1\right) \tag{45}$$

where the quantum numbers l = 0,1,2,… and j = 0,1,2… are independent from each other. The energy level for a given combination of j and l is $g_l(2j+1)$-degenerated (Fig. 3).

In this subsection, the triatomic molecules were handled as symmetric tops. In a treatment beyond this approximation, the $g_l = 2$ degeneracy of the rotation levels with $l \neq 0$ would be lifted.

AN *AB INITIO* APPROACH TO TRIATOMIC MOLECULES UNDERGOING LARGE-AMPLITUDE BENDING VIBRATIONS

The complete vibration–rotation Hamiltonian for a triatomic molecule, expressed in terms of the Jacobi coordinates r, R, and θ (Fig. 1) and the Euler angles α, β and φ, which determine the orientation of the instantaneous molecular principal axes of inertia (*ipia*) with respect to a space-fixed coordinate system, was derived in a previous study.[5] Its kinetic energy part can be written as the sum of the vibrational, rotational and vibration–rotational (coupling) terms:

$$\hat{T} = \hat{T}_{\mathrm{v}} + \hat{T}_{\mathrm{vr}} + \hat{T}_{\mathrm{r}} \tag{46}$$

with

$$\begin{aligned}
\hat{T}_{\mathrm{v}} &= -\frac{\hbar^2}{2}\frac{1}{\mu_r}\frac{\partial^2}{\partial r^2} - \frac{\hbar^2}{2}\frac{1}{\mu_R}\frac{\partial^2}{\partial R^2} - \frac{\hbar^2}{2}\left(\frac{1}{\mu_r r^2} + \frac{1}{\mu_R R^2}\right)\left(\frac{\partial^2}{\partial\theta^2} + \cot\theta\frac{\partial}{\partial\theta}\right) \\
\hat{T}_{\mathrm{vr}} &= -\frac{2\hbar\sin\theta}{I_{xx}^2}\left(-\mu_R r R^2\cos\theta\frac{\partial}{\partial r} + \mu_r r^2 R\cos\theta\frac{\partial}{\partial R} + \right. \\
&\quad \left. + \left(\mu_R R^2 - \mu_r r^2\right)\left(\sin\theta\frac{\partial}{\partial\theta} + \cos\theta\right)\right)i\hat{J}_x \\
\hat{T}_{\mathrm{r}} &= \frac{\hat{I}_{xx}}{2\left(I_{yy} - I_{zz}\right)^2}\hat{J}_x^2 + \frac{1}{2I_{yy}}\hat{J}_y^2 + \frac{1}{2I_{zz}}\hat{J}_z^2
\end{aligned} \tag{47}$$

where μ_r and μ_R are the "reduced masses":

$$\mu_r = \frac{m_3\left(m_1+m_2\right)}{M},\ \mu_R = \frac{m_1 m_2}{m_1+m_2} \tag{48}$$

and

$$\begin{aligned}
I_{xx} &= \mu_r r^2 + \mu_R R^2 = I_{yy} + I_{zz} \\
I_{yy} &= \frac{1}{2}\left[\left(\mu_r r^2 + \mu_R R^2\right) + \sqrt{\mu_r^2 r^4 + \mu_R^2 R^4 + 2\mu_r\mu_R r^2 R^2\cos\left(2\theta\right)}\right] \\
I_{zz} &= \frac{1}{2}\left[\left(\mu_r r^2 + \mu_R R^2\right) - \sqrt{\mu_r^2 r^4 + \mu_R^2 R^4 + 2\mu_r\mu_R r^2 R^2\cos\left(2\theta\right)}\right]
\end{aligned} \tag{49}$$

are the instantaneous principal moments of inertia. $\hat{J}_x$, $\hat{J}_y$ and $\hat{J}_z$ are the components of the molecular angular momentum along the axes of the coordinate system bound to the molecule (*ipia*-system):[7]

$$\begin{aligned}
\hat{J}_x &= -i\hbar\left(-\frac{\cos\varphi}{\sin\beta}\frac{\partial}{\partial\alpha} + \sin\varphi\frac{\partial}{\partial\beta} + \cot\beta\cos\varphi\frac{\partial}{\partial\varphi}\right) \\
\hat{J}_y &= -i\hbar\left(\frac{\sin\varphi}{\sin\beta}\frac{\partial}{\partial\alpha} + \cos\varphi\frac{\partial}{\partial\beta} - \cot\beta\sin\varphi\frac{\partial}{\partial\varphi}\right) \\
\hat{J}_z &= -i\hbar\frac{\partial}{\partial\varphi}
\end{aligned} \tag{50}$$

The integration element is assumed in the form $\mathrm{d}V = \sin\beta\sin\theta\prod\mathrm{d}q_i$ (q_i represent the vibrational and rotational coordinates). The potential energy corresponding to the kinetic energy operator, Eq. (47), represents the electronic energy computed within the framework of the Born–Oppenheimer approximation for a set of relevant values of the coordinates *r*, *R* and θ.

To find approximate solutions of the corresponding Schrödinger equation, a procedure resembling the Born–Oppenheimer approximation (normally used for the separation of electronic and nuclear motions) was applied to the stretching––bending problem. Since the stretching vibrations in the species under consideration are characterized by much larger energies ($\tilde{\nu}_{\mathrm{s}} \approx 1000\ \mathrm{cm}^{-1}$) than those for

the other nuclear degrees of freedom (in the case of BC_2, the bending wave number is as small as $\tilde{\nu}_b \approx 200$ cm^{-1}), the stretching Schrödinger equation was first solved with the Hamiltonian:

$$\hat{H}_s = -\frac{\hbar^2}{2\mu_r}\frac{\partial^2}{\partial r^2} - \frac{\hbar^2}{2\mu_R}\frac{\partial^2}{\partial R^2} + \frac{1}{2}k_{rr}(\theta)r^2 + \\ + \frac{1}{2}k_{RR}(\theta)R^2 + k_{rR}(\theta)rR + \ldots \quad (51)$$

The force constants $k_{rr}(\theta), k_{RR}(\theta), k_{rR}(\theta), \ldots$ represent the stretching potential surface. One calculates them separately for a number of values of the bending coordinate, handled as a parameter in the same sense as the nuclear coordinates when the electronic Schrödinger equation is solved in the usual Born–Oppenheimer approximation. Since the stretching vibrations are normally small-amplitude ones, the calculations are restricted to the quadratic field only. The solutions of Eq. (51) are then:

$$E_s(\theta) = \left(v_{s1} + \frac{1}{2}\right)\hbar\omega_{s1}(\theta) + \left(v_{s2} + \frac{1}{2}\right)\hbar\omega_{s2}(\theta) \quad (52)$$

From the above kinetic energy operator are now extracted the terms of central importance when dealing with large-amplitude bending vibrations, namely those describing the bending vibrations and rotations around the *z*-axis, coinciding for linear geometries with the molecular axis:

$$\hat{T}_{b,z} = -\frac{\hbar^2}{2}\left(\frac{1}{\mu_r r^2} + \frac{1}{\mu_R R^2}\right)\left(\frac{\partial^2}{\partial\theta^2} + \cot\theta\frac{\partial}{\partial\theta}\right) + \frac{1}{2I_{zz}}\hat{J}_z^2 \quad (53)$$

Were the coupling between the bending and stretching vibrations negligible, the stretching coordinates r and R could be replaced in Eq. (53) by their equilibrium values, r_e and R_e, respectively. Since this is not the case, it is assumed the stretching coordinates are certain functions of θ, $r_e(\theta) \equiv r(\theta)$, $R_e(\theta) \equiv R(\theta)$. However, r and R cannot be directly replaced by $r(\theta)$ and $R(\theta)$ in Eq. (53), as written in Eq. (17) of Ref. 5, because such a Hamiltonian would not be hermitian. Instead, the symmetrised form thereof must be used:

$$\hat{T}_{b,z} = -\frac{\hbar^2}{4}\{\left(\frac{1}{\mu_r r_{(\theta)}^2} + \frac{1}{\mu_R R_{(\theta)}^2}\right)\left(\frac{\partial^2}{\partial\theta^2} + \mathrm{ctg}\,\theta\frac{\partial}{\partial\theta}\right) + \\ + \left(\frac{\partial^2}{\partial\theta^2} + \mathrm{ctg}\,\theta\frac{\partial}{\partial\theta}\right)\left(\frac{1}{\mu_r r_{(\theta)}^2} + \frac{1}{\mu_R R_{(\theta)}^2}\right)\} - \frac{\hbar^2}{2I_{zz}(\theta)}\frac{\partial^2}{\partial\varphi^2} \quad (54)$$

This operator can be alternatively written as:

$$T = -\frac{\hbar^2}{2}\left[T_1(\theta)\frac{\partial^2}{\partial\theta^2} + T_2(\theta)\frac{\partial}{\partial\theta} - l^2 T_3(\theta) + T_4(\theta)\right] \tag{55}$$

where

$$\begin{aligned}
T_1(\theta) &= \frac{1}{\mu_r r_{(\theta)}^2} + \frac{1}{\mu_R R_{(\theta)}^2} \\
T_2(\theta) &= \left[\frac{1}{\mu_r r_{(\theta)}^2} + \frac{1}{\mu_R R_{(\theta)}^2}\right]\cot\theta - 2\left[\frac{1}{\mu_r r_{(\theta)}^3}\frac{\mathrm{d}r_{(\theta)}}{\mathrm{d}\theta} + \frac{1}{\mu_R R_{(\theta)}^3}\frac{\mathrm{d}R_{(\theta)}}{\mathrm{d}\theta}\right] \\
T_3(\theta) &= \frac{1}{I_{zz}(\theta)} \\
T_4(\theta) &= -\left[\frac{1}{\mu_r r_{(\theta)}^3}\frac{\mathrm{d}r_{(\theta)}}{\mathrm{d}\theta} + \frac{1}{\mu_R R_{(\theta)}^3}\frac{\mathrm{d}R_{(\theta)}}{\mathrm{d}\theta}\right]\cot\theta + \\
&\quad + 3\left\{\frac{1}{\mu_r r_{(\theta)}^4}\left[\frac{\mathrm{d}r_{(\theta)}}{\mathrm{d}\theta}\right]^2 + \frac{1}{\mu_R R_{(\theta)}^4}\left[\frac{\mathrm{d}R_{(\theta)}}{\mathrm{d}\theta}\right]^2\right\} - \\
&\quad - \frac{1}{\mu_r r_{(\theta)}^3}\frac{\mathrm{d}^2 r_{(\theta)}}{\mathrm{d}\theta^2} - \frac{1}{\mu_R R_{(\theta)}^3}\frac{\mathrm{d}^2 R_{(\theta)}}{\mathrm{d}\theta^2}
\end{aligned} \tag{56}$$

The operator $\hat{J}_z^2 = -\hbar^2\left(\partial^2/\partial\varphi^2\right)$ was replaced by $l^2\hbar^2$, because we assume the bending functions in the form:

$$\psi(\theta,\varphi) = \frac{1}{\sqrt{2\pi}}e^{il\varphi}\Theta(\theta) \tag{57}$$

The potential energy part of the bending–z-rotation Hamiltonian $\hat{H}_{b,z}$ is assumed in the form:

$$V(\theta) = V_{r,R}(\theta) + E_s(\theta) = V(\theta) + \left(v_{s1} + \frac{1}{2}\right)\hbar\omega_{s1}(\theta) + \left(v_{s2} + \frac{1}{2}\right)\hbar\omega_{s2}(\theta) \tag{58}$$

where $V_{r,R}(\theta)$ is the bending potential corresponding to the bond lengths optimized at each particular value of the coordinate θ. In the language of reaction kinetics, $V_{r,R}(\theta)$ represents the "minimum-energy path" along the "reaction coordinate" θ. The second and the third term on the right-hand side of Eq. (58) are the stretching energies. The bending Schrödinger equation has to be solved separately for each combination of the bending quantum numbers v_{s1} and v_{s2}. Thus, by solving the Schrödinger equation with the Hamiltonians, Eqs. (55) and (58), the stretching–bending–z-rotational energy levels are obtained with the stretch––bend coupling incorporated through the parametric dependence of r_e, R_e, ω_{s1}

and ω_{s2} on θ. In Eq. (58), the stretching energy contribution is written in the harmonic approximation. A generalization involving anharmonicity of the stretching vibrations is straightforward.

Finally, the contribution of the *x*,*y*-rotations to the total energy can be calculated at different levels of sophistication – the choice depends on the concrete numerical values of the parameters in question. In the case of a HBC molecule, when the hydrogen atom migrates around the relatively heavy BC fragment, $I_{xx} \cong I_{yy} >> I_{zz}$ (Eq. (49)), and I_{xx} and I_{yy} do not dramatically vary with a change of θ. This was the situation in previous works on HNC→HCN isomerisation.[5,6] The *x*,*y*-rotational contribution to the total energy can then be calculated by means of Formula (21). If the above conditions are not fulfilled, the average values of the rotational constants can first be calculated over the bending wave functions and after that the rotational spectrum. When the molecular shape if far from a symmetric top, it might be better not to include the *z*-rotational part in the bending Hamiltonian and calculate the energy levels of the asymmetric top separately, using the averaged rotational constants. Of course, the computation of the partition functions must be performed numerically when the energy levels are calculated beyond the harmonic approximation.

In the next study of this series,[2] the molecular Schrödinger equation is solved employing the variational approach introduced in Ref. 5. The key points thereof are repeated here.

The Hamiltonian of Eqs. (55) and (58) has two features that distinguish it from the usual forms of the vibrational Hamiltonian. It is periodical in θ with the period π and has singularities at θ = 0,π. The periodicity is taken into account if all terms in the kinetic and potential energy operator are expanded into Fourier series in θ. The singularities are caused by the presence of the terms T_2 and T_3 with the asymptotic behaviour $\lim_{\theta\to 0,\pi} T_2 \propto \sin^{-1}\theta$, and $\lim_{\theta\to 0,\pi} T_3 \propto \sin^{-2}\theta$. Since the volume element $dV = \sin\theta d\theta d\varphi$ is used, the first singularity disappears in computations of the matrix elements. The second singularity also vanishes when $l = 0$, but remains for $l \neq 0$. In the first case, one employs for representation of the Hamiltonian, the basis functions:

$$\varphi_n = \cos(n\theta) \tag{59}$$

For $l \neq 0$, the basis consists of the functions:

$$\varphi_n = \sqrt{\sin\theta}\cos(n\theta) \tag{60}$$

One cannot use the same basis (particularly Eq. (60)) for both the cases $l = 0$ and $l \neq 0$ because the $l = 0$ wave functions must have non-vanishing values at θ = = 0,π. Due to the presence of the weight factors sin θ (appearing in the volume element) and $\sqrt{\sin\theta}$ (in the basis functions of Eq. (60)), one has to compute matrix elements of the type:

$$\begin{matrix}\int_0^{\pi}\cos(m\theta)\left[T_i / V\sin\theta\right]\cos/\sin n\theta\,\mathrm{d}\theta\\ \int_0^{\pi}\cos(m\theta)\left[T_i / V\sin^2\theta\right]\sin/\cos(n\theta)\,\mathrm{d}\theta\\ \int_0^{\pi}\cos(m\theta)\left[T_i / V\sin\theta\cos\theta\right]\sin/\cos(n\theta)\,\mathrm{d}\theta\end{matrix} \quad (61)$$

They can be easily calculated when the functions in the square brackets are fitted by sin($k\theta$) or cos($k\theta$) series.

CONCLUSIONS

In the present study, an evaluation of partition functions for linear and bent triatomic molecules in the harmonic approximation was reviewed and a scheme was presented for *ab initio* variational calculation of the vibration–rotational energy levels in triatomics undergoing large-amplitude bending vibrations. The harmonic formulae and the variational approach will be employed in the second paper of this series to obtain the energy levels and the partition functions in the ground electronic state of the BC_2 molecule.

Acknowledgement. We acknowledge the financial support of the Ministry of Science and Technological Development of the Republic of Serbia (Contract Nos. 142074 and 142055).

ИЗВОД

ВЕЗА ИЗМЕЂУ МОЛЕКУЛСКЕ СПЕКТРОСКОПИЈЕ И СТАТИСТИЧКЕ МЕХАНИКЕ: РАЧУНАЊЕ ПАРТИЦИОНИХ ФУНКЦИЈА ТРОАТОМСКИХ МОЛЕКУЛА КОЈИ ВРШЕ САВИЈАЈУЋЕ ВИБРАЦИЈЕ ВЕЛИКИХ АМПЛИТУДА

МИЛАН В. СЕЊАНСКИ[1], ЈЕЛЕНА РАДИЋ-ПЕРИЋ[2] и МИЉЕНКО ПЕРИЋ[2]

[1]Иновациони центар Хемијског факултета у Београду и [2]Факултет за физичку хемију Универзитета у Београду

Разматрано је одређивање партиционих функција троатомских молекула који врше савијајуће вибрације великих амплитуда. Претпостављено је да се сви потребни подаци добијају помоћу *ab initio* рачунања. Посебна пажња посвећена је спрези савијајућих и истежућих вибрационих степена слободе, као и интеракцији савијајућих вибрација и ротација. Развијена је погодна схема за варијационо рачунање енергијских нивоа.

(Примљено 26. новембра 2011)

REFERENCES

1. S. V. Jerosimić, M. V. Senćanski, J. Radić-Perić, *J. Mol. Struct*: *Theochem.* **944** (2010) 53
2. M. V. Senćanski, Lj. Stojanović, S. Jerosimić, J. Radić-Perić, M. Perić, *J. Serb. Chem. Soc*. **76** (2011) 557
3. P. W. Atkins, *Physical Chemistry*, 5th ed., Oxford University Press, Oxford, UK, 1994
4. J. Radić-Perić, M. Perić, *Z. Naturforsch*. **42a** (1987) 103
5. M. Perić, M. Mladenović, S. D. Peyerimhoff, R. J. Buenker, *Chem. Phys*. **82** (1983) 317
6. M. Perić, M. Mladenović, S. D. Peyerimhoff, R. J. Buenker, *Chem. Phys.* **86** (1984) 85
7. P. R. Bunker, *Molecular Symmetry and Spectroscopy*, Academic Press, New York, 1979.

Journal of the Serbian Chemical Society
JSCS-info@shd.org.rs • www.shd.org.rs/JSCS
J. Serb. Chem. Soc. 76 (4) 557–573 (2011)
JSCS–4142
UDC 536.722:517.544.4:533.912
Original scientific paper

On the relationship between molecular spectroscopy and statistical mechanics: calculation of vibrational–rotational energy levels and partition functions in the ground electronic state of BC_2

MILAN V. SENĆANSKI[1#], LJILJANA STOJANOVIĆ[2], STANKA JEROSIMIĆ[2], JELENA RADIĆ-PERIĆ[2] and MILJENKO PERIĆ[2*#]

[1]*Innovation Centre of the Faculty of Chemistry, University of Belgrade, Studentski Trg 12–16, 11158 Belgrade and* [2]*Faculty of Physical Chemistry, University of Belgrade, Studentski Trg 12–16, P. O. Box 47, 11158 Belgrade, Serbia*

(Received 26 November 2010)

Abstract: The results of extensive *ab initio* calculations of the vibrational–rotational energy spectrum in the ground electronic state of the BC_2 molecule are presented. These data were employed to discuss the evaluation of the corresponding partition functions. Special attention was paid to the problems connected with the calculation of the partition functions for the bending vibrations and rotations about the axis corresponding to the smallest moment of inertia.

Keywords: vibrational–rotational energy; partition functions; BC_2.

INTRODUCTION

In the preceding paper[1] (in further text: Paper I), the evaluation of the partition functions in triatomic molecules undergoing large-amplitude bending vibrations was outlined. In the present paper, the results of *ab initio* calculations of the vibrational–rotational energy levels are reported and the evaluation of the corresponding partition functions for the ground electronic state of the BC_2 molecule is discussed. A major part of the data required for these calculations was generated in a previous study.[2] They were completed in the present work by stretching vibrational frequencies computed at several values of the bending coordinates in order to construct the effective bending potential curves, which were employed in the subsequent handling of large-amplitude bending vibrations and rotations.

* Corresponding author. E-mail: peric@ffh.bg.ac.rs
# Serbian Chemical Society member.
doi: 10.2298/JSC101126053S

In the present study, the Jacobi coordinates *r*, *R* and θ were employed. R is the distance between the C nuclei, r the distance between the B atom and the midpoint of the C–C diatomic and θ is defined as the angle between the vectors $\vec{r}$ and $\vec{R}$ (Fig. 1 of Paper I; in the present case, the *z*-axis lies at the C_{2v} molecular geometry along $\vec{r}$). These coordinates were also used in an extensive *ab initio* study of the rovibrational spectrum in the ground state of BC_2 performed by Leonard *et al.*[3] There is some confusion concerning the assignment of the vibrational modes in BC_2 (see Section 3.1.4 of Ref. 2). Here, the notation consistent with that introduced in Paper I will be used.[1] The stretching modes will be denoted by subscripts *s*1 and *s*2, where *s*1 stands for the higher-frequency mode (predominately C–C) and *s*2 for the lower-frequency one (predominately B–C_2). The name "angular" or "bending" coordinate is used for θ. However, it should be born in mind that this angle is not the bending angle usually used in spectroscopy, namely the angle between the B–C and C–C bonds (or its supplement) – around the equilibrium geometry (roughly of C_{2v} symmetry) the Jacobi coordinate θ in the present case (B and C atoms of similar mass) is even more similar to the antisymmetric stretching than to the bending valence coordinate.

CALCULATION OF THE EFFECTIVE BENDING POTENTIAL CURVES

The potential energy surface (PES) for the ground electronic state of BC_2 was calculated[2] at various levels of sophistication, by means of the MOLPRO *ab initio* software package.[4] In the present study, the data obtained at the RCCSD(T) level of theory, with the cc-pVQZ atomic orbital basis set, were employed. Instead of computing a complete three-dimensional PES by systematically varying all three Jacobi coordinates, as Leonard *et al.*[3] did, attention was concentrated on the angular variable θ, *i.e.*, an effective bending potential curve was computed by optimizing the values of the stretching coordinates *r* and *R* at a number of values of θ. At this level of theory, the global minimum on the PES corresponds to the angle θ = 84.4°, slightly differing from that (90°) of the C_{2v} geometry, at *R*(= C–C) = 1.279 Å, *r*(=B–C2) = 1.379 Å. Thus the ground state is X^2A' (C_s--point group). However, it lies only roughly 20 cm^{-1} below the energy location of the isosceles triangle ($^2A_1$ species of the C_{2v} group). At the linear nuclear arrangement (B–C–C) and C–C and C–B bond lengths of 1.286 and 1.379 Å, respectively (*i.e.*, at *R*(= C–C) = 1.286 Å; *r*(=B–C2) = 2.022 Å), there is a shallow local minimum on the PES; it lies 216 cm^{-1} below the transition state on the minimum energy path towards the global minimum on the PES. This linear species is of $^2\Sigma^+$ symmetry and it is located 2110 cm^{-1} above the global minimum. Leonard *et al.*[3] reported a value of 2204 cm^{-1} for the same quantity. The barrier on the way from the X^2A' to the $^2\Sigma^+$ state was computed to be 2325 cm^{-1} (compared to 2383 cm^{-1} from the literature[3]). At each value of θ where the bond lengths were relaxed, the local harmonic stretching frequencies were calculated

too. All these results are collected in Table I. Graphical presentations of these quantities are shown in Figs. 1–4. It can be noted that the r = B–C2 stretching coordinate and both stretching vibrational frequencies strongly depend on the angular coordinate θ (the variation of the R = C–C stretching coordinate is relatively weak). Therefore, the coupling of the angular and both stretching vibrational modes in the present case is appreciable and cannot be neglected if reliable results for the vibrational energy levels and the corresponding partition functions are be obtained. A consequence of the strong variation of the r = B–C2 distance with θ is an appreciable dependence of the moments of inertia on the angular coordinate. At the equilibrium geometry (X^2A'), the rotational constants are A = = 1.7175, B = 1.1770 and C = 0.6984 cm^{-1}. At the local minimum corresponding to the linear molecular geometry, B = 0.4136 cm^{-1}. These results agree reasonably with those obtained by Leonard *et al.*[3] (A = 1.7224, B= 1.1814, C = 0.6932 cm^{-1} at the global minimum of the PES – indeed, Leonard *et al.* found it to be of C_{2v} symmetry – and B = 0.4232 cm^{-1} at the linear geometry). The same is true for the stretching vibrational frequencies. The present values at the equilibrium geometry of the molecule are $\tilde{\nu}_{s1}$ = 1733 cm^{-1} and $\tilde{\nu}_{s2}$ = 1213 cm^{-1}, while those from the literature[3] are 1678 and 1180 cm^{-1}; the only known experimental result[5] is $\tilde{\nu}$ =1194.6 cm^{-1} for the lower-frequency stretching vibration.

TABLE I. Angular dependence of the electronic energy, internuclear distances and local stretching vibrational frequencies in the ground electronic state of BC2 calculated at the RCCSD(T)/ /cc-pVQZ level of theory

θ / °	R(=C–C) Å	C–B Å	r(=B–C_2) Å	E Hartree	E/hc cm^{-1}	$\tilde{\nu}_{s1}$ cm^{-1}	$\tilde{\nu}_{s2}$ cm^{-1}
0.00	1.2858	1.3792	2.0221	–100.618957	2109	1906	1165
6.82	1.2858	1.3793	2.0156	–100.618864	2130	–	–
13.67	1.2862	1.3797	1.9962	–100.618610	2185	–	–
20.57	1.2867	1.3803	1.9640	–100.618279	2258	–	–
27.55	1.2874	1.3811	1.9193	–100.618006	2318	–	–
34.64	1.2883	1.3821	1.8627	–100.617975	2325	1805	1307
41.88	1.2891	1.3831	1.7944	–100.618399	2232	–	–
49.32	1.2896	1.3844	1.7155	–100.619487	1993	1805	1403
57.04	1.2892	1.3867	1.6275	–100.621407	1571	1748	1440
65.19	1.2875	1.3926	1.5342	–100.624165	966	1705	1439
74.04	1.2844	1.4106	1.4449	–100.627180	304	1700	1353
84.18	1.2793	1.4610	1.3800	–100.628568	0	–	–
84.4044	1.2790	1.4623	1.3789	–100.628569	0	1733	1213
87.04	1.2779	1.4846	1.3734	–100.628544	5	–	–
90.00	1.2771	1.5133	1.3715	–100.628518	11	1746	1200

Adding to the optimized angular potential curve, the stretching vibrational energies $(v_1+1/2)\hbar\omega_{s1} + (v_2+1/2)\hbar\omega_{s2}$, where $\omega_{s1}(\theta)$ and $\omega_{s2}(\theta)$ are the values for the harmonic stretching vibrational frequencies as functions of θ, effective an-

gular potential curves corresponding to the zeroth stretching vibrational level were computed, as well as those for several combinations of the stretching vibrational quantum numbers (v_1 and v_2). Some of them are presented in Fig. 4.

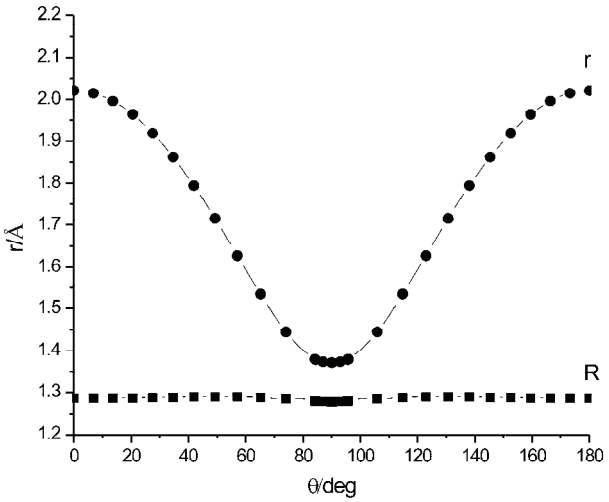

Fig. 1. Dependence of the bond lengths r(=B–C2) and R(C–C) on the bending angle θ in the ground electronic state of BC_2.

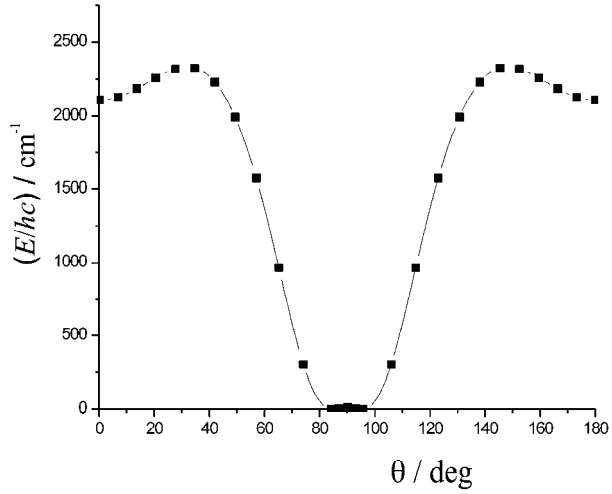

Fig. 2. One-dimensional bending section of the potential energy surface, corresponding to the optimized bond lengths r and R, for the ground electronic state of BC_2.

RESULTS AND DISCUSSION

The energy levels of the Hamiltonian for the angular vibrations and rotations around the z-axis (Eqs. (54)–(56) and (58) from Paper I[1]) were calculated using 100 basis functions, 20 terms in the potential energy expansions, and 15 terms in the expansions of the distances r and R as functions of θ. The results for the l = 0, 1, 2 and 3 quantum numbers are presented in Tables II–VI. Table II comprises the energy levels obtained by employing the minimum-energy angular potential

curve presented in Table I and Fig. 1. The results for four combinations of the stretching quantum numbers (v_{s1} = 0 , v_{s2} = 0; v_{s1} = 0 , v_{s2} = 1; v_{s1} = 1, v_{s2} = 0; v_{s1} = 1 , v_{s2} = 1), obtained by employing the corresponding potentials displayed in Fig. 5, are given in Tables III–VI.

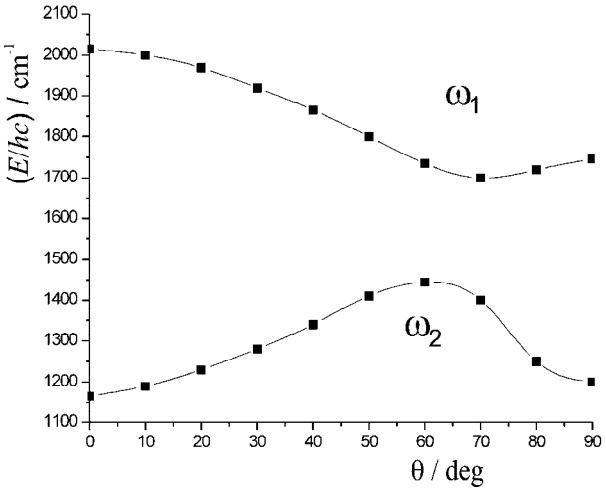

Fig. 3. Dependence of the stretching wave numbers on the bending coordinate θ.

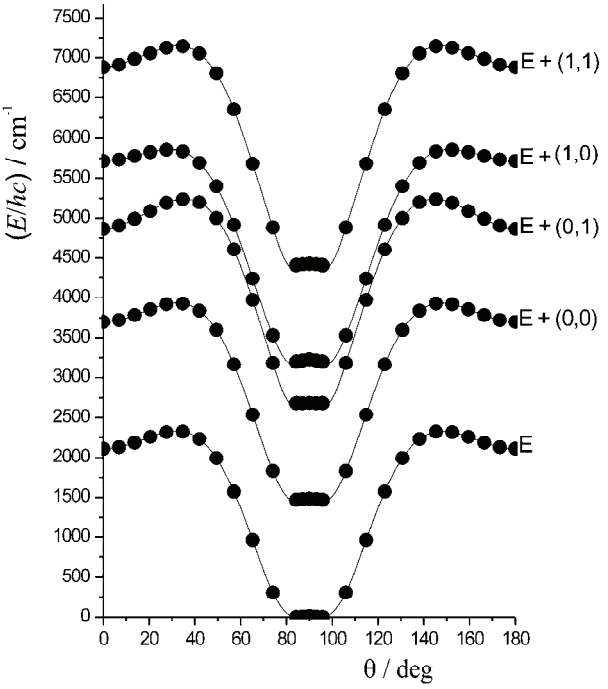

Fig. 4. Effective bending potential curves corresponding to the optimized bond lengths r and R, (E), and the vibrational stretching quantum numbers v_1, v_2, (E + + (v_{s1},v_{s2})).

TABLE II. Bending–*z*-rotational energy levels (in cm^{-1}) calculated using the effective bending potential curve ("minimum") corresponding to the optimized bond lengths. Zero at the energy scale corresponds to the lowest-lying ($v_b = 0$, $l = 0$) vibronic level

Minimum	*l*			
v_b	0	1	2	3
0	0	2	7	16
1	199	200	205	215
2	453	455	461	471
3	710	712	718	728
4	961	963	970	980
5	1200	1202	1209	1220
6	1424	1426	1433	1444
7	1632	1634	1641	1654
8	1821	1824	1832	1845
9	1989	1993	2002	2016
10	2127	2134	2145	2162
11	2130	2216	2252	2276
12	2134	2222	2300	2352
13	2235	2252	2326	2398
14	2282	2323	2382	2453
15	2314	2374	2451	2527
16	2373	2433	2519	2607

TABLE III. Bending–*z*-rotational energy levels calculated using the effective bending potential curve corresponding to the stretching quantum numbers $v_{s1} = 0$, $v_{s2} = 0$. Zero at the energy scale corresponds to the lowest-lying ($v_b = 0$, $l = 0$) vibronic level

(0,0)	*l*			
v_b	0	1	2	3
0	0	2	7	16
1	213	213	218	228
2	481	484	489	499
3	752	754	760	770
4	1015	1017	1023	1034
5	1263	1265	1271	1282
6	1495	1497	1503	1515
7	1710	1712	1720	1732
8	1908	1911	1919	1932
9	2084	2088	2096	2111
10	2234	2237	2247	2264
11	2247	2332	2363	2386
12	2247	2337	2421	2469
13	2347	2360	2445	2517
14	2401	2435	2496	2567
15	2428	2483	2565	2640
16	2484	2538	2630	2721
17	2556	2615	2702	2803
18	2629	2699	2785	2891
19	2708	2786	2877	2986
20	2794	2880	2975	3088

Although it was found that the equilibrium geometry is not exactly C_2v, all energy levels lie above the very small energy barrier (≈ 20 cm^{-1}), so that the molecule behaves effectively as if it had this higher-symmetry configuration. The potential curve has appreciable anharmonicity in the vicinity of the equilibrium geometry as a consequence of the presence of the barrier, which is manifested in the irregular spacing of the vibrational levels – the computed difference between $v_b = 1$ and $v_b = 0$ ($l = 0$) for $v_{s1} = v_{s2} = 0$ (Table III) is much smaller (213 cm^{-1}) than that between $v_b = 2$ and $v_b = 1$ (268), $v_b = 3$ and $v_b = 2$ (271), $v_b = 4$ and $v_b = 3$ (271 cm^{-1}) *etc*. The controversy concerning the question of whether this energy barrier is real will be finally solved when the experimentalists succeed in measuring the energy of the bending fundamental and some of its overtones.

TABLE IV. Bending–*z*-rotational energy levels calculated using the effective bending potential curve corresponding to the stretching quantum numbers $v_{s1} = 0$, $v_{s2} = 1$. Wave number values (in cm^{-1}) are given with respect to the $v_{s1} = 0$, $v_{s2} = 0$, $v_b = 0$, $l = 0$ level

(0,1)	*l*			
v_b	0	1	2	3
0	1224	1225	1231	1239
1	1476	1474	1480	1489
2	1777	1778	1784	1793
3	2077	2080	2086	2096
4	2364	2367	2374	2384
5	2631	2633	2640	2650
6	2876	2876	2883	2894
7	3098	3099	3106	3118
8	3298	3301	3309	3322
9	3437	3478	3487	3502
10	3437	3528	3628	3646
11	3474	3528	3673	3739
12	3614	3618	3679	3770
13	3650	3693	3739	3805
14	3659	3717	3803	3876
15	3727	3762	3852	3952
16	3794	3840	3914	4024
17	3856	3919	3994	4102
18	3927	3999	4082	4190
19	4007	4084	4173	4286
20	4095	4179	4271	4387

Leonard *et al*.[3] performed calculation of all rovibrational states up to the energy of the linear local minimum. We do not find it necessary to compare the present result with theirs; they must differ from one another to some extent because of different handling of the problem (as already mentioned, the approach applied in Ref. 3. was more sophisticated than the present one) and different global-minimum geometry. Instead, the qualitative features of the bending–*z*-ro-

tational spectrum are discussed below, particularly the relationship between the energy-level pattern below and above the potential barrier towards linearity. This topic was not considered in Ref. 3. In the following discussion, the stretching modes are neglected and the results generated employing the minimum-energy angular potential curve are analysed. The results for all vibronic level up to 4000 cm^{-1} are displayed in Fig. 5.

The pattern of the bending plus *z*-rotational levels can be interpreted in an analogous way to the analyses reported in the literature.[6,7] If the bond lengths r and R in the bending–*z*-rotational Hamiltonian, Eqs. (54–56) and (58) of Paper I,[1] are replaced by their equilibrium values r_e and R_e and the following transformation is performed:

$$\begin{aligned} T_3 &= \frac{1}{I_{zz}} = \frac{2}{\mu_r r^2 + \mu_R R^2 - \sqrt{\mu_r^2 r^4 + \mu_R^2 R^4 + 2\mu_r \mu_R r^2 R^2 \cos(2\theta)}} = \\ &= \frac{1}{\sin^2\theta}\left(\frac{1}{\mu_r r^2} + \frac{1}{\mu_R R^2}\right) - \\ &- \frac{2}{\mu_r r^2 + \mu_R R^2 + \sqrt{\mu_r^2 r^4 + \mu_R^2 R^4 + 2\mu_r \mu_R r^2 R^2 \cos(2\theta)}} = \\ &= \frac{1}{\sin^2\theta}\left(\frac{1}{\mu_r r^2} + \frac{1}{\mu_R R^2}\right) - \frac{1}{I_{yy}} \end{aligned} \tag{1}$$

one obtains:

$$\hat{H}_{b,z} = -\frac{\hbar^2}{2\mu_b}\left(\frac{\partial^2}{\partial\theta^2} + \cot\theta\frac{\partial}{\partial\theta} - \frac{l^2}{\sin^2\theta}\right) - Bhcl^2 + V_{r,R}(\theta) \tag{2}$$

with:

$$\frac{1}{\mu_b} = \left(\frac{1}{\mu_r r_e^2} + \frac{1}{\mu_R R_e^2}\right),\ B = \frac{\hbar^2}{2hcI_{yy}} \tag{3}$$

TABLE V. Bending–*z*-rotational energy levels calculated using the effective bending potential curve corresponding to the stretching quantum numbers $v_{s1} = 1$, $v_{s2} = 0$. Wave number values (in cm^{-1}) are given with respect to the $v_{s1} = 0$, $v_{s2} = 0$, $v_b = 0$, $l = 0$ level

(1,0)	*l*			
v_b	0	1	2	3
0	1735	1736	1741	1750
1	1933	1932	1938	1947
2	2198	2200	2206	2216
3	2465	2468	2474	2484
4	2728	2731	2737	2747
5	2979	2981	2987	2998
6	3217	3218	3224	3236
7	3440	3442	3449	3461

TABLE V. Continued

(1,0)	*l*			
v_b	0	1	2	3
8	3648	3651	3659	3672
9	3840	3844	3852	3866
10	4010	4014	4023	4038
11	4155	4157	4168	4186
12	4243	4270	4286	4309
13	4246	4314	4365	4403
14	4272	4327	4406	4466
15	4346	4380	4456	4524
16	4390	4440	4527	4602
17	4443	4498	4597	4688
18	4516	4576	4671	4776
19	4595	4665	4757	4867
20	4678	4757	4852	4966

In this approximation, the kinetic energy operator consists of two terms: the first one is the kinetic energy operator of an isotropic two-dimensional oscillator (when the volume element is: $dV = \sin\theta d\theta d\varphi$) but, at the same time, it represents the complete Hamiltonian of a rigid two-dimensional rotator;[8] the second term can be interpreted as the *l*-dependent correction to it. $V_{r,R}(\theta)$ is the potential for bending vibrations or, alternatively, the potential barrier hindering free rotations of the B-atom around the C–C fragment.

TABLE VI. Bending–*z*-rotational energy levels calculated using the effective bending potential curve corresponding to the stretching quantum numbers $v_{s1} = 1$, $v_{s2} = 1$. Wave number values (in cm^{-1}) are given with respect to the $v_{s1} = 0$, $v_{s2} = 0$, $v_b = 0$, $l = 0$ level

(1,1)	*l*			
v_b	0	1	2	3
0	2960	2961	2966	2975
1	3198	3196	3201	3210
2	3494	3495	3501	3511
3	3791	3794	3800	3810
4	4078	4081	4087	4097
5	4346	4348	4354	4365
6	4595	4595	4602	4614
7	4825	4826	4833	4845
8	5037	5040	5048	5061
9	5230	5234	5242	5256
10	5397	5400	5409	5425
11	5439	5516	5542	5561
12	5439	5518	5622	5661
13	5528	5534	5646	5716
14	5599	5621	5682	5758
15	5622	5666	5753	5827

TABLE VI. Continued

(1,1)	*l*			
v_b	0	1	2	3
16	5667	5711	5813	5910
17	5741	5788	5875	5990
18	5814	5875	5956	6072
19	5890	5962	6047	6163
20	5973	6052	6143	6262

Below the energy corresponding to the linear BCC, particularly around the global minimum of the potential surface, the molecule behaves as a bent one; it is then convenient to write the bending part of the Hamiltonian, Eq. (2), in a form analogous to Eq. (40) of Paper I:[1]

$$\hat{H}_{b,z} = -\frac{\hbar^2}{2\mu_b}\frac{\partial^2}{\partial\theta^2} + Ahcl^2 + V_{r,R}(\theta) \quad (4)$$

where:

$$A = \frac{\hbar^2}{2hcI_{zz}} \quad (5)$$

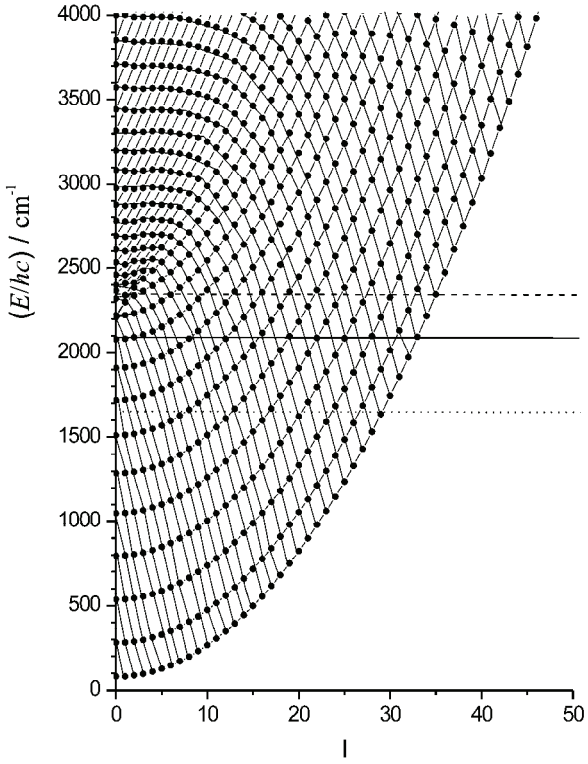

Fig. 5. Bending–*z*-rotational energy levels in the ground electronic state of BC_2. Zero at the energy scale corresponds to the position of the lowest-lying $v_b = 0$, $l = 0$ vibronic level. Full horizontal line: energy position of the local minimum at linear geometry. Dash horizontal line: energy position of the maximum at the barrier between the global and local minimum. Dotted horizontal line: zero energy of the hypothetical free rotator.

This Hamiltonian is obtained from Eq. (2) by replacing the volume element $dV = \sin\theta d\theta d\varphi$ by $dV = d\theta d\varphi$, and absorbing the term (appearing in the transformed kinetic energy operator) $\propto 1/\theta^2 \cong 1/\theta_e^2$ in $V_{r,R}(\theta)$. The first and the third term represent together the Hamiltonian for one-dimensional bending vibrations and the second one, the eigenvalues of the Hamiltonian for rotations about the *z*-axis. In the harmonic approximation, the eigenvalues of the Hamiltonian, Eq. (4), are given by Eq. (41) of Paper I (they are now written without the constant term $\hbar\omega_b/2$):[1]

$$E_{b,z} = \hbar\omega_b v_b + Ahcl^2 \tag{6}$$

Each bending vibrational level is thus accompanied by rotational levels corresponding to $l = 0,1,2,\ldots$, the energies of which depend quadratically on *l*. The $l = 0$ levels are non-degenerated, while the $l \neq 0$ levels are twofold degenerated. The complete approximate bending–rotational energy spectrum can be obtained by adding to these levels the approximate contribution of the *x*,*y* rotations:

$$E^r_{x,y} = \frac{\hbar^2}{2\sqrt{I_{xx}I_{yy}}}\left[J(J+1) - l^2\right] \tag{7}$$

with $J \geq l$. As mentioned in Paper I,[1] if more accurate results are required, we can exclude the second term from the Hamiltonian, Eq. (4), can be excluded and the energy levels of the asymmetric top calculated separately using the properly averaged rotational constants.

Sufficiently far above the potential barrier towards the linear local minimum, there is no potential hindering bending and the Hamiltonian, Eq. (2), effectively reduces to:

$$\hat{H}_{b,z} = -\frac{\hbar^2}{2\mu_b}\left(\frac{\partial^2}{\partial\theta^2} + \cot\theta\frac{\partial}{\partial\theta} - \frac{l^2}{\sin^2\theta}\right) - Bhcl^2 = \frac{1}{2\mu_b}\hat{j}^2 - \frac{l^2\hbar^2}{2I_{yy}} \tag{8}$$

The operator $\hat{j}$ has the same form as the total angular momentum of a linear molecule; a capital (*J*) is not used in order to distinguish this quantity from the total angular momentum involving also *x*- and *y*-rotations. In the harmonic approximation, the eigenvalues of the Hamiltonian, Eq. (8), are:

$$E_{b,z} = E_0 + ahcj(j+1) - Bhcl^2 \tag{9}$$

where E_0 is some reference energy (see below) and:

$$a \equiv \frac{\hbar^2}{2hc\mu_b} = A + B \tag{10}$$

for a given j, the number l takes the values $j, j-1,\ldots,0$. However, the presence of the bending potential reaching a maximum at roughly 2300 cm^{-1} obs-

cures this simple picture. Furthermore, the rotation "constants" cannot be assumed to be constant during large-amplitude motions over all values of θ. For this reason, the values for E_0 (zero point energy of the hypothetical completely free, *i.e.*, without any potential, rotator), a and B in Eq. (9) cannot be derived directly from the *ab initio* computed structural parameters. Instead, one can use, *e.g.*, the computed high-lying $l = 0$ vibronic levels and fit them to Formula (9). In this way, $E_0 = 1634$ cm^{-1}(hc), and $a = 2.51$ cm^{-1} are obtained. Note that this value for a is between those corresponding to the linear geometry ($a_l = 2.245$ cm^{-1}) and the equilibrium (bent) molecular geometry ($a_b = 2.894$ cm^{-1}). The same is true for the effective value for B, which is found to lie between the linear and C_{2v} values of 0.4136 and 1.1770 cm^{-1}, respectively. At small l-values, the values of $j–l$ practically coincide with v_b, the last quantum number playing, in this energy range, solely the role of a running index.

Inspecting the form of the vibronic wave functions, it was found that only the nearly degenerate $l = 0$ levels with $v_b = 10$ and 11 and the $l = 1$ levels with $v_b = 11$ and 12 (Table II and Fig. 5) belong to the local minimum at the linear molecular geometry. The energy difference between the pairs of these $l = 1$ and $l = 0$ levels of roughly 90 cm^{-1}, thus corresponding approximately to the bending frequency of the linear structure. All other vibronic levels belong either to the bent structure with the global minimum close to the C_{2v} geometry (*e.g.*, the v_b from 0 to 9 and 12 levels for $l = 0$, and v_b from 0 to 10 for $l = 1$), or lie above the barrier towards the linearity (among $l = 0$ and $l = 1$ levels, those with $v_b \geq 13$).

The vibronic energy levels below the barrier to linearity (*i.e.*, in the energy region between 0 and roughly 2000 cm^{-1} fit reasonably the energy Formula (6). The lines in Fig. 5 connecting the levels with the same quantum number v_b increase quadratically with increasing l. Small discrepancies are caused by the anharmonicity of the potential, particularly by the presence of the energy hump at the C_{2v} geometry. In Fig. 5, also connected with one another are the energy levels having the same value for $v_b + l \equiv j$ (note that in this energy region, the number j is without any obvious physical meaning, *i.e.*, it is not connected with any real rotational motion). Replacing in Eq. (6) v_b by $j – l$, one obtains:

$$E_{b,z} = \hbar\omega_b j - \hbar\omega_b l + Ahcl^2 \tag{11}$$

For a given j and at a not very large l, the energy given by Eq. (11) linearly decreases with increasing l.

Above the barrier to linearity, the levels with the same "rotational" quantum number j are connected by the lines, which decrease with increasing l. Lines connecting the levels with the same value $j – l = v_b$ with one another are also drawn. According to Eq. (8), they should satisfy the equation:

$$E_{b,z} = E_0 + ahcv_b\left(v_b + 1\right) + ahc\left(2v_b + 1\right)l + Ahcl^2 \tag{12}$$

where again $a = A + B$. At large values of v_b and small l, as in the upper left part of Fig. 5, the energy increases linearly with l. For small values of v_b compared to l, the energy increases quadratically with increasing l in the same manner as the energy of the levels below the barrier with the same quantum number v_b (Eq. (6)). On the other hand, the decreasing curves connecting the levels with the same (high) j value gradually change their second derivative (with respect to l) from $\propto -B$ (Eq. (9)) to $\propto A$ (Eq. (11)) with increasing l.

The complete vibronic energy pattern presented in Fig. 5 is, of course, a combination of both extreme cases discussed above. It gains additional complexity by the presence of the local minimum at the linear geometry and the energy hump at the C_{2v} configuration. Thus, the question is whether partition functions can be reliable computed within the framework of usual approximations such as the harmonic one and that based on the separate handling of the bending vibrations and the z-axis rotations.

The actually computed effective bending potential curve (with a small hump at the C_{2v} geometry), corresponding to the optimized bond lengths and the $l = 0$ and $l = 1$ vibronic levels up to 4000 cm^{-1}, is displayed in Fig. 6. In the same figure, the two lowest-lying $l = 0$ levels computed by using the potential curve

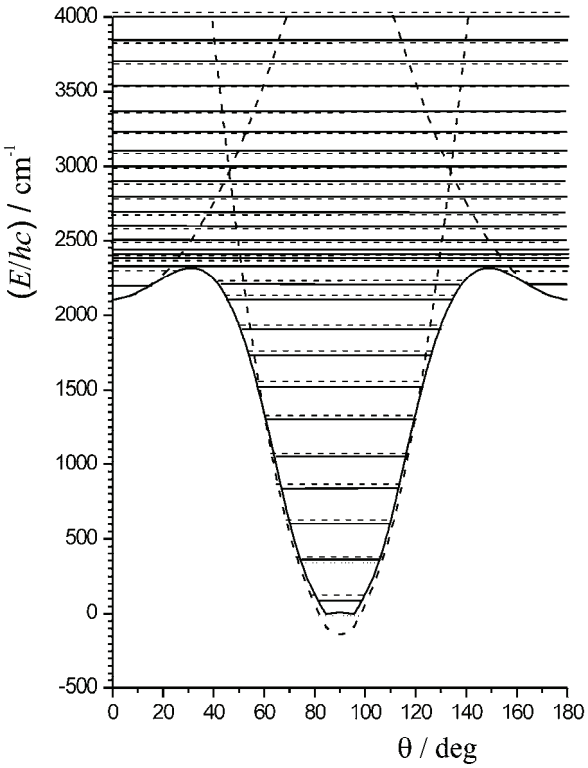

Fig. 6. $l = 0$ (solid horizontal lines) and $l = 1$ (dashed lines) vibronic levels in the ground electronic state of BC_2, calculated employing the effective bending potential curve (with a small hump at the C_{2v} geometry) corresponding to the optimized bond lengths. Dotted horizontal lines denote the two lowest-lying $l = 0$ levels computed using the potential curve having a global minimum at C_{2v} geometry (dotted curve). Dashed potential curves indicate the harmonic approximation of the separate bending potentials for bent and linear equilibrium geometry.

having a global minimum at C_{2v} geometry (as found in some of the previous studies) are presented. Also in Fig. 6, separate harmonic bending potentials having minima at C_{2v} and linear molecular geometry, and the corresponding $l = 0$ and $l = 1$ vibronic levels are shown. In the present case, the partition functions involving bending and *z*-rotational energy levels may be computed at three levels of sophistication: *i*) taking into account only the harmonic potential curve with the minimum at C_{2v} geometry – in this case, the energy is given by Eq. (6), where $\tilde{\nu}_b = 275$ cm^{-1} and the partition function is presented by Eq. (42) of Paper I;[1] *ii*) summing the partition function from the preceding case with that corresponding to the linear two-dimensional harmonic oscillator with the frequency of $\tilde{\nu}_b = 110$ cm^{-1} and the lowest lying vibronic level at $E_0 / hc = 2219$ cm^{-1} above the lowest-lying level of the bent structure – the energy levels of the linear oscillator are given by Eq. (7) of Paper I (without $\hbar\omega_b$ and with the additional E_0), and the corresponding partition function is obtained by multiplying Eq. (14) of Paper I by exp ($-E_0/kT$);[1] *iii*) numerically calculating the partition functions using vibronic levels such as those presented in Fig. 5.

Now, the results obtained by three the procedures described above for two characteristic temperatures, $T = 1000$ K and $T = 5000$ K, are compared with one another. To save time, only partition functions involving energy levels up to 4000 cm^{-1} were computed. This does not ensure full convergence of the results, particularly not for $T = 5000$ K, but gives sufficient information to draw reliable conclusions. Thus, instead of using the analytic formulae for the partition functions in the harmonic approximation, their parts corresponding to the chosen energy region were calculated manually. The double degeneracy of the $l \neq 0$ levels is taken into account and the spin degeneracy (representing a simple multiplicative factor) is ignored. The number of vibronic (bending plus *z*-rotational) energy levels lying in the energy intervals of 100 and 500 cm^{-1} is shown in Fig. 7. It can be seen that the harmonic approximations work reasonably well below the barrier towards the linearity, but they (particularly the first one, in which the presence of the linear structure is ignored) significantly underestimate the number of "rotational" levels above the barrier. Employing the latter set of results (wave number intervals of 500 cm^{-1}), the partition functions were estimated as:

$$Z_{b,z} \cong \sum_{n=1}^{8} N(n) \mathrm{e}^{-\frac{(n-1/2)500\ \mathrm{cm}^{-1} hc}{kT}} \tag{13}$$

where $N(n)$ is the number of levels in the n-th energy interval. At $T = 1000$ K, the partition functions: *i*) 106.5; *ii*) 108.0; *iii*) 118.0 are obtained. The first two numbers are practically identical to those which are obtained by means of the Formulae (42) and (14) of Paper I. The corresponding values at $T = 5000$ K are: *i*) 524.2; *ii*) 582.9; *iii*) 638.4. (Because the energy region between 0 and 4000 cm^{-1} does not ensure convergence of the partition functions at this high temperature,

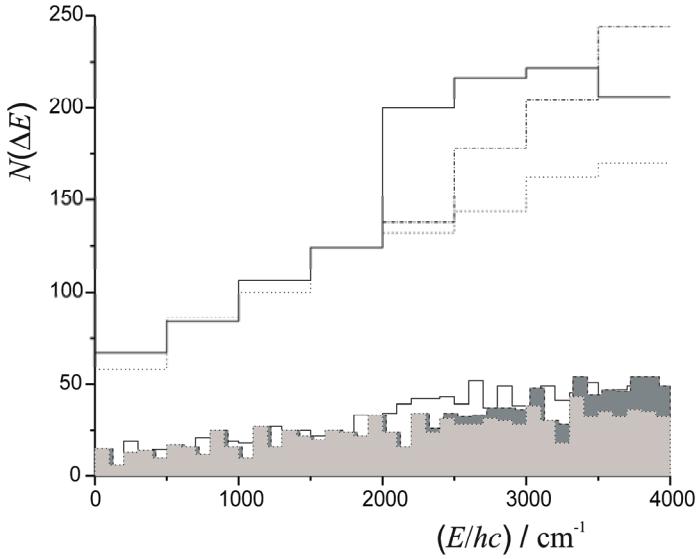

Fig. 7. Numbers of vibronic (bending plus *z*-rotational) energy levels in the ground electronic state of BC_2, lying in the wave number intervals of 100 (bottom) and 500 (top) cm^{-1}. Dotted lines (bright grey in the lower diagram): results obtained with the harmonic approximation only involving C_{2v} configuration. Dash–dotted lines (dark grey in the lower diagram): harmonic approximation, both C_{2v} and linear configurations taken into account. Full lines: results of the variational solution of the Schrödinger equation.

the first two numbers differ considerably from the values obtained employing the analytical Expressions (42) and (14) from Paper I, 1046 and 1592, respectively).

The above analysis leads to the following conclusions. The energy hump at the C_{2v} configuration is too small to cause dramatic irregularities in the bending energy pattern around the equilibrium molecular geometry and, consequently, its presence does not significantly affect the partition functions. On the other hand, the role of the shallow local minimum at linear geometry is completely different in the low- and high-temperature regions. At relatively low temperatures (*e.g.*, at T = 1000 K), the presence of this local minimum, lying about 2000 cm^{-1} above the global minimum, can safely be ignored, because the factor exp ($-E/kT$) strongly quenches its contributions to the partition functions. However, it cannot be ignored if accurate high-temperature partition functions are required. This cannot be clearly seen based on the numbers presented above for T = 5000 K, but becomes quite obvious on comparing Figs. 6 and 8 and inspecting the upper part of Fig. 7. It can be seen that the harmonic approximation in the variant *i* (the presence of the linear structure is ignored) significantly underestimates the number of "rotational" levels above the barrier. On the other hand, approach *ii* tends to overestimate the number of levels in the high-energy region (particularly at T > > 5000 K). Thus, only an approach which takes into account the gradual change

of the structure of the vibrational–rotational spectrum at large-amplitude bending vibrations, such as *iii*, can ensure reliable results in the high-temperature region.

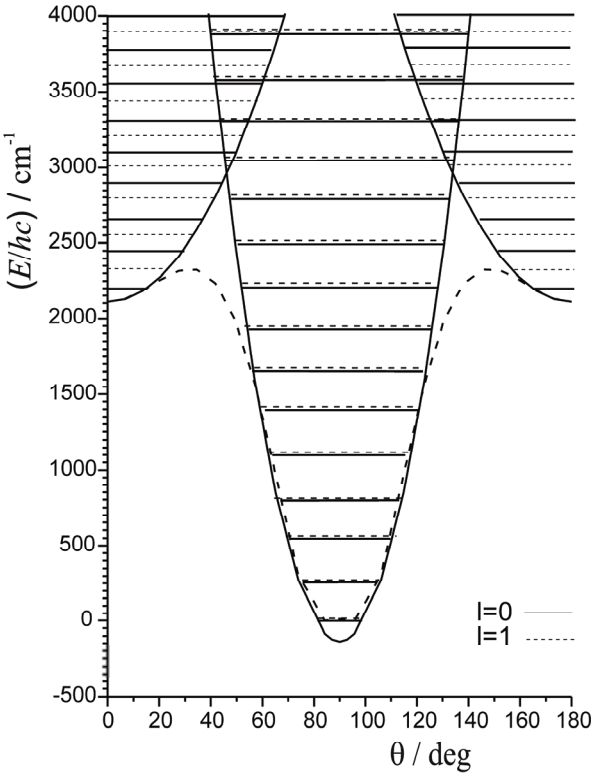

Fig. 8. l = 0 (full horizontal lines) and l = 1 (dashed lines) vibronic levels obtained by replacing the actually computed bending potential (dashed curve) by the harmonic potentials having minima at C_{2v} and linear molecular geometry (solid curves).

It should be stressed once more that the above analysis concerns only the bending–*z*-rotational part of the total partition function. An even more critical point is the evaluation of the contributions of the *x*,*y* rotations. The problems are caused by the much smaller values of the corresponding rotational constants around the linear molecular geometry than in the region close to the global minimum on the potential surface. This part of the partition function cannot be reliably evaluated in harmonic approximations, even at relatively low temperatures.

CONCLUSIONS

In the present paper, the results of extensive *ab initio* calculations of the vibrational–rotational energy spectrum in the ground electronic state of the BC_2 molecule are reported. The corresponding potential energy surface is characterized by a global minimum at slightly distorted C_{2v} geometry, and a local minimum at the linear nuclear arrangement, lying about 2100 cm^{-1} above the global minimum. The potential barrier between these two structures is calculated to be

roughly 2300 cm^{-1}. These facts, as well as the strong stretch–bend coupling cause the vibrational–rotational spectrum to have a rather complex structure. Estimations of the corresponding partition functions, particularly the bending–*z*-rotational one, are discussed in detail.

Acknowledgements. We acknowledge financial support by the Ministry of Science and Technological Development of the Republic of Serbia (Contract Nos. 142074 and 142055).

И З В О Д

ВЕЗА ИЗМЕЂУ МОЛЕКУЛСКЕ СПЕКТРОСКОПИЈЕ И СТАТИСТИЧКЕ МЕХАНИКЕ: РАЧУНАЊЕ ВИБРАЦИОНО–РОТАЦИОНИХ ЕНЕРГИЈСКИХ НИВОА И ПАРТИЦИОНИХ ФУНКЦИЈА У ОСНОВНОМ ЕЛЕКТРОНСКОМ СТАЊУ МОЛЕКУЛА BC_2

МИЛАН В. СЕНЋАНСКИ[1], ЉИЉАНА СТОЈАНОВИЋ[2], СТАНКА ЈЕРОСИМИЋ[2], ЈЕЛЕНА РАДИЋ-ПЕРИЋ[2] и МИЉЕНКО ПЕРИЋ[2]

[1]*Иновациони центар Хемијског факултета Универзитета у Београду и* [2]*Факултет за физичку хемију Универзитета у Београду*

Приказани су резултати опсежних *ab initio* рачунања вибрационо–ротационог енергијског спектра у основном електронском стању молекула BC_2. Ови подаци коришћени су у дискусији о одређивању одговарајућих партиционих функција. Посебна пажња посвећена је проблемима везаним за рачунање партиционих функција за савијајуће вибрације и ротације око осе која кореспондира најмањем моменту инерције.

(Примљено 26. новембра 2010)

REFERENCES

1. M. V. Senćanski, J. Radić-Perić, M. Perić, *J. Serb. Chem. Soc*. **76** (2011) 539
2. S. V. Jerosimić, M. V. Senćanski, J. Radić-Perić, *J. Mol. Struct. Theochem.* **944** (2010) 53
3. C. Leonard, G. Chambaud, P. Rosmus, S. Carter, N. C. Handy, M. Wyss, J. P. Maier, *J. Chem. Phys*. **113** (2000) 5228
4. *MOLPRO, version 2006.1, a package of* ab initio *programs*, http://www.molpro.net
5. J. M. L. Martin, P. R. Taylor, J. P. Yustein, T. R. Burkholder, L. Andrews, *J. Chem. Phys.* **99** (1996) 4927.
6. M. Perić, M. Mladenović, S. D. Peyerimhoff, R. J. Buenker, *Chem. Phys*. **82** (1983) 317
7. M. Perić, M. Mladenović, S. D. Peyerimhoff, R. J. Buenker, *Chem. Phys*. **86** (1984) 85
8. P. R. Bunker, *Molecular Symmetry and Spectroscopy*, Academic Press, New York, 1979.

Journal of the Serbian Chemical Society
JSCS-info@shd.org.rs • www.shd.org.rs/JSCS
J. Serb. Chem. Soc. *76* (4) 575–589 (2011)
JSCS–4143
UDC 546.776+546.824–31:539.12+
541.135.5–039.26:544.4
Original scientific paper

Fabrication and characterization of molybdenum(VI) complex–TiO_2 nanoparticles modified electrode for the electrocatalytic determination of L-cysteine

MOHAMMAD MAZLOUM-ARDAKANI[1]*, HADI BEITOLLAHI[1], ZAHRA TALEAT[1] and MASOUD SALAVATI-NIASARI[2]

[1]*Department of Chemistry, Faculty of Science, Yazd University, Yazd, 89195-741 and* [2]*Department of Inorganic Chemistry, Faculty of Chemistry, University of Kashan, Kashan, I.R. Iran*

(Received 4 May, revised 15 October 2010)

Abstract: A novel voltammetric sensor for the determination of L-cysteine (L-Cys) was fabricated based on a TiO_2 nanoparticles/bis[bis(salicylidene-1,4--phenylenediamine) molybdenum(VI)] carbon paste electrode. The electrochemical behavior of the sensor was investigated in detail by cyclic voltammetry. The apparent electron transfer rate constant (k_s) and charge transfer coefficient (α) of the TiO_2 nanoparticles/molybdenum(VI) complex/carbon paste electrode (CPE) were also determined by cyclic voltammetry and found to be about 4.53 s^{-1} and 0.54, respectively. The sensor displayed good electrocatalytic activity towards the oxidation of L-Cys. The peak potential for the oxidation of L-Cys was lowered by at least 130 mV compared with that obtained at an unmodified CPE. Under optimal conditions, the linear range spans L-Cys concentrations from 1.5×10^{-6} to 1.2×10^{-3} M and the detection limit was 0.70±0.01 μM at a signal-to-noise ratio of 2. In addition, the sensor showed good stability and reproducibility.

Keywords: L-cysteine; TiO_2 nanoparticles; carbon paste electrode; electrocatalysis.

INTRODUCTION

Nano-sized materials have found promising technological applications in many different areas, such as microelectronic devices,[1] photocatalysis,[2] electrocatalysis,[3] biomedical applications[4] and chemical processes.[5] Nanoparticle architectures on electrode supports has attracted substantial research efforts directed to the development of bioelectrochemistry.[6] This is a great opportunity for the chemistry of nanoparticles, as the electronic properties are now tunable *via* particle

* Corresponding author. E-mail: mazloum@yazduni.ac.ir
doi: 10.2298/JSC100504042M

size. With respect to the electrical properties of nanoparticles and of all kind of arrangements constructed from nanoparticles, the most important property is the amount of energy needed to add one extra electron to an initially uncharged particle. This energy is the so-called "charging energy"; it scales roughly with 1/*r* (*r* = radius of the nanoparticle), and it has its atomic analog in the electron affinity of a neutral atom.[7]

The chemical modification of electrodes with a suitable reagent has been widely used for analytical applications. The resulting electrodes were designed to provide the desired selective sites towards the analytes. Chemically modified electrodes (CMEs) have played an important role in studies of electrocatalysis,[8] electron transfer kinetics,[9] membrane barriers,[10] electro-organic syntheses,[11] *etc*. One of the most important electrode modification techniques involves the formation of electrocatalytic systems in which redox species capable of undergoing a rapid and reversible electrode reaction are incorporated onto the electrode surface.[3] These electrodes reduce the overpotential required for either oxidation or reduction of compounds.

L-Cysteine (L-Cys) is an important thio-containing amino acid involved in a variety of important cellular functions, such as protein synthesis, detoxification and metabolism.[12] It has been also used as a radio-protective agent, cancer indicator and is implicated in a number of pathological conditions, including Alzheimer's and Parkinson's diseases as well as autoimmune deficiency syndrome.[13] On the other hand, a deficiency of L-Cys causes many diseases, such as slowed growth in children, depigmentation of hair, edema, lethargy, liver damage, loss of muscle and fat, skin lesion and weakness.[14] Therefore, a sensitive and selective assessment of L-Cys in biological matrices and pharmaceutical preparations is highly demanded.

Electrochemical detection of thiols has been reviewed in the literatures.[15,16] Generally, the responses to thiol oxidation at unmodified electrodes usually suffer from large overpotentials or sluggish electrochemical responses.[16] The chemical modification of inert substrate electrodes with mediators offers significant advantages in the design and development of L-Cys electrochemical sensors. Therefore, biochemists and electroanalytical chemists have shown great interest in the area of modified electrodes to overcome these problems and various modified electrodes have been constructed for this purpose.[17–21]

In continuation of our studies concerning the preparation of chemically modified electrodes,[3,17,19,22–25] in the present work it was found that a TiO_2 nanoparticles/bis[bis(salicylidene-1,4-phenylenediamine) molybdenum(VI)] carbon paste electrode possesses high stability and good electrocatalytic activity toward the electrocatalytic oxidation of L-Cys. Cyclic voltammetry, differential pulse voltammetry and chronoamperometry were used to characterize the elec-

trochemical properties of the electrode and to investigate its electrocatalytic effect on L-Cys oxidation.

EXPERIMENTAL

Apparatus and chemicals

The electrochemical experiments were realized using a computerized potentiostat/galvanostat μAutolab type III (Eco Chemie B.V.A). A conventional three electrode cell was used with an Ag/AgCl/KCl 3.0 M, a platinum wire, and a molybdenum(VI) complex––TiO_2 nanoparticles modified carbon paste electrode (MCTNMCPE) as the reference, auxiliary and working electrodes, respectively. A Metrohm model 691 pH/ mV meter was used for the pH measurements.

All solutions were freshly prepared with doubly distilled water. L-Cys and other reagents were of analytical grade (Merck, Germany). Graphite powder (Merck) and paraffin oil (DC 350, Merck, density 0.88 g cm^{-3}) were used as binding agents for the graphite pastes. Phosphate buffer solutions were prepared from *ortho*-phosphoric acid and its salts in the pH range of 2.0–11.0. TiO_2 nanoparticles (surface area = 84 m^2 g^{-1} and particle size = 6.7 nm) and dioxomolybdenum (VI) complexes, $[MoO_2L]_2$, were synthesized as reported previously.[25]

Preparation of the electrode

The modified electrodes were prepared by dissolving 0.01 g of bis[bis(salicylidene-1,4--phenylenediamine) molybdenum(VI) in CH_3Cl and hand mixing with 95 times its weight of graphite powder and 4 times its weight of TiO_2 nanoparticles using a pestle and mortar. Paraffin (Dc 350, Merck) was added to the above mixture and mixed for 20 min until a uniformly wetted paste was obtained. This paste was then packed into the end of a glass tube (*ca*. 3.4 mm i.d. and 10 cm long). A copper wire inserted into the carbon paste provided for electrical contact. When necessary, a new surface was obtained by pushing an excess of paste out of the tube, which was then polished with weighing paper.

Unmodified carbon paste was prepared in the same manner but without the addition of bis[bis(salicylidene-1,4-phenylenediamine) molybdenum (VI)] and TiO_2 nanoparticles to the mixture. This was used for the purpose of comparison.

Procedures for sample preparation

Human blood serum. Serum was prepared by centrifuging 10 ml of blood after it had been kept in an incubator at 37 °C for 30 min. A 1.0 ml portion of serum was added to 10 ml of 0.1 M phosphate buffer (pH 8.0) in a voltammetric cell and the cyclic voltammograms were recorded.

Acetylcysteine tablets. A 20-mg portion of a finely powdered sample was dissolved in 10 ml of phosphate buffer (pH 8.0) and then 0.1 ml of sample was transferred to a 10 ml voltammetric cell containing 0.1 M phosphate buffer (pH 8.0) and the cyclic voltammograms were recorded.

RESULTS AND DISCUSSION

Electrochemistry of MCTNMCPE

The molybdenum complex was insoluble in aqueous medium and hence it could be easily incorporated into the carbon paste without concern regarding its leaching from the electrode surface. This fabrication process yielded a stable, chemically-modified electrode.

First, the electrochemical behavior of the molybdenum complex modified electrode was studied. The cyclic voltammograms for the modified electrode at different scan rates in 0.1 M phosphate buffer of pH 8.0 were recorded. The cyclic voltammograms of $[MoO_2L]_2$ in the MCTNMCPE showed an anodic and corresponding cathodic peak, whereas the unmodified carbon paste electrodes in the supporting electrolyte showed neither anodic nor cathodic peaks. Experimental investigations show that well-defined and reproducible anodic and cathodic peaks related to the Mo (VI)/Mo (V) redox system (with E_{pa} = 0.760 V, E_{pc} = = 0.58 V, E°' = 0.670 V *vs*. Ag/AgCl/KCl 3.0 M and ΔE_p = 180 mV) can be used as mediators for the electrocatalysis of some important biological compounds with a slow electron transfer. The electrode process was quasi-reversible, with ΔE_p, greater than the (59/n) mV expected for a reversible system. The voltammograms of a quasi-reversible system are more drawn-out and exhibit larger separation of the peak potentials compared to those of a reversible system.[26]

Cyclic voltammograms of the MCTNMCPE were recorded at different scan rates (from 20 to 900 mV s^{-1}). Figure 1A illustrates that the anodic and cathodic peak currents (I_p) were linearly dependent on υ at scan rates in the range 30−200 mV s^{-1}. A linear correlation was obtained between peak currents and the scan rate, indicating that the redox process is not diffusion controlled. With increasing v, the difference between the peak potentials increased. The anodic peak potentials E_{pa} as a function of the scan rate are shown in Fig. 1B. The values of E_p were proportional to the logarithm of the scan rate for scan rates above 200 mV s^{-1}.

The equations of linear potential sweep voltammograms have been derived for any degree of reversibility of the electrochemical reaction for the following methods: surface voltammetry when both the oxidized and the reduced forms are strongly adsorbed and a Langmuir isotherm is obeyed, thin layer voltammetry and linear potential sweep coulometry. If values of ΔE_p larger than 200/n mV can be obtained experimentally, α and k can be easily determined using the following equations:[28]

$$E_{pc} = E^\circ + A \ln [(1 - \alpha)/m] \quad (1)$$

$$E_{pa} = E^\circ + B \ln [\alpha/m] \quad (2)$$

For $E_{pa} - E_{pc} = \Delta E_p$:

$$\log(k_s/s^{-1}) = \alpha \log (1-\alpha) + (1-\alpha) \log \alpha - \log (RT/nFv) - \\ - \alpha (1-\alpha) n_\alpha F \Delta E_p/2.3RT \quad (3)$$

where $A = RT/(1-\alpha)nF$, $B = RT/\alpha nF$ and $m = (RT/F)(k_s/n_\alpha)$.

The transfer coefficient (α) and the apparent charge transfer rate constant (k_s in s^{-1}) for electron transfer between the electrode and the molybdenum complex can be determined by measuring the variation of the peak potentials with scan rate (v). A graph of E_p *vs*. log (v / mV s^{-1}) (Fig. 1B) yields two straight lines with slopes equal to $2.3RT/\alpha n_\alpha F$ and $2.3RT/(1-\alpha)n_\alpha F$ for the cathodic and anodic

peaks, respectively. For scan rates exceeding 200 mV s^{-1}, the values of ΔE were proportional to the logarithm of the scan rate, as indicated by Laviron. Using such graphs and Eq. (3), the values of α and k_s were determined to be 0.54 and 4.53±0.30 s^{-1}, respectively, for the MCTNMCPE in the presence of 0.1 M phosphate buffer.

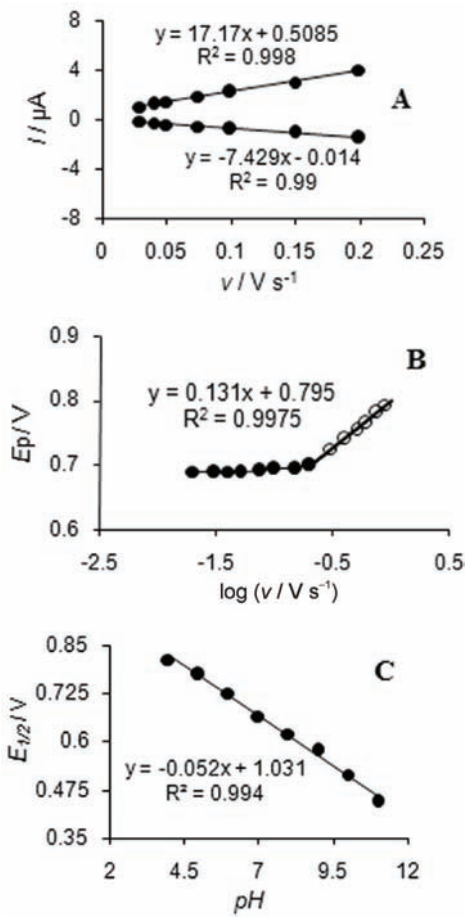

Fig. 1. A) Variation of the peak currents with scan rate; B) variation of E_p *vs.* the log *v*; C) plot of $E_{1/2}$ *vs.* pH for the MCTNMCPE in 0.1 M phosphate buffer solution.

The surface coverage of the electrode was approximately estimated by adopting the method used by Bard.[29] The surface concentration of molybdenum complex (Γ in mol cm^{-2}) was obtained from the integrated charges (Q) of the anodic peak as follows:

$$\Gamma_{EBNBH} = Q/nFA \quad (4)$$

where Q is the charge from the area under the molybdenum complex anodic peak corrected for the baseline and n is the number of electrons exchanged per reactant

molecule. The surface concentration of the molybdenum complex was calculated to be 1.37×10^{-9} mol cm^{-2} for $n = 1$.

pH effect

The electrochemical response of the bis[bis(salicylidene-1,4-phenylene-diamine) molybdenum(VI)] molecule showed a strong dependence on pH. For reversible processes, the number of proton ions participating in the electrochemical reaction can be determined from the pH-dependence of the voltammetric half-wave potential. The anodic and cathodic peak potentials of the MCTNMCPE were shifted to less positive values with increasing pH. The half-wave potential of the MCTNMCPE at various pH values was calculated as the average value of the anodic and cathodic peak potentials of the CVs. The calculated $E_{1/2}$ values as a function of pH are shown in Fig. 1C. This graph presents a straight line with slope = 52 mV/pH. Such a behavior suggests that it obeys the Nernst Equation for a two-electron and proton transfer reaction.[29]

In addition, the electrochemical behavior of L-Cys (pK_{a1} = 1.92, pK_{a2} = = 8.37, pK_{a3} = 10.7) [30] is dependent on the pH value of the aqueous solution, as well as the MC molecule.

Therefore, pH optimization of the solution seemed necessary for the electrocatalytic oxidation of L-Cys. Thus, the electrochemical behavior of L-Cys in 0.1 M phosphate buffered solutions of different pH values (2.0 < pH < 11.0) at the surface of MCTNMCPE was studied by cyclic voltammetry. It was found that the electrocatalytic oxidation of L-Cys at the surface of MCTNMCPE was more favored under basic conditions than in an acidic environment. This appeared as a gradual growth in the anodic peak current and a simultaneous decrease in the cathodic peak current in the cyclic voltammograms of the MCTNMCPE. The results showed that the maximum peak current can be observed at pH 8. Therefore, pH 8.0 was chosen as the optimum pH for the electrocatalysis of L-Cys oxidation at the surface of the MCTNMCPE.

Electrocatalytic oxidation of L-Cys

The cyclic voltammograms from the electrochemical oxidation of 1.0 mM L-Cys at the MCTNMCPE (curve f), a molybdenum(VI) complex-modified CPE (MCMCPE) (curve e), a TiO_2 nanoparticle-modified CPE (TNCPE) (curve d) and the unmodified CPE (curve a) are shown in Fig. 2. As can be seen, the anodic peak potentials for L-Cys oxidation at the MCTNMCPE (curve f) and MCMCPE (curve e) were about 760 mV, while at the TNCPE (curve d), the peak potential was about 835 mV. At the unmodified CPE, the peak potential was about 890 mV (curve b).

From these results, it was concluded that the best electrocatalytic effect for L-Cys oxidation was observed at the MCTNMCPE (curve f). For example, re-

sults show that the peak potential of L-Cys oxidation at the MCTNMCPE (curve f) shifted by about 75 and 130 mV toward negative values when compared with that at the TNCPE (curve d) and unmodified carbon paste electrode (curve b), respectively. Similarly, when comparing the oxidation of L-Cys at the MCMCPE (curve e) and MCTNMCPE (curve f), a dramatic enhancement of the anodic peak current at the MCTNMCPE relative to that obtained at the MCMCPE was observed. In other words, the data clearly show that the combination of TiO_2 nanoparticles and mediator (molybdenum(VI) complex) definitely improve the characteristics of L-Cys oxidation. The MCTNMCPE in 0.1 M phosphate buffer (pH 8.0) and without L-Cys in solution, exhibited a well-behaved redox reaction (curve c). Upon addition of 1.0 mM L-Cys. There was a dramatic enhancement of the anodic peak current (curve f), indicating a strong electrocatalytic effect.

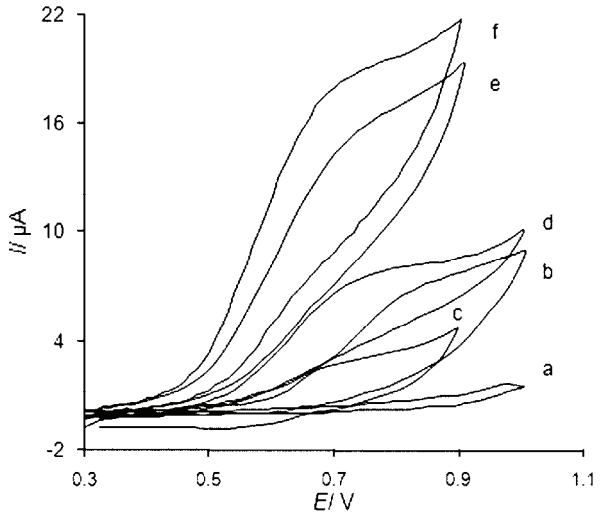

Fig. 2. Cyclic voltammograms of a) CPE in 0.1 M phosphate buffer solution (pH 8.0) at a scan rate 30 mV s^{-1}, b) as a) 1.0 mM L-cysteine, c) as a), d) as b) at the surface of MCTNMCPE and TNCPE, respectively. Also, e) and f) as b) at the surface of MCMCPE and MCTNMCPE, respectively.

Additional information on the rates of these (and other) coupled chemical reactions can be achieved by changing the scan rate (*i.e.*, by adjusting the experimental time scale). In particular, the scan rate controls the time spent between the switching potential and the peak potential.[26] As can be observed from Fig. 3A, the oxidation peak potential shifted with increasing scan rates towards more positive potentials, confirming the kinetic limitation of the electrochemical reaction. In addition, a plot of peak height (I_p) *vs.* $v^{1/2}$, in the range 2–30 mV s^{-1}, was constructed (Fig. 3B). This plot was found to be linear, suggesting that, at sufficient overpotential, the process was diffusion rather than surface controlled. A plot of the sweep rate normalized current ($I_p/v^{1/2}$) *vs.* sweep rate (Fig. 3C) exhibited the characteristic shape typical of an EC process. From the slope of Fig. 3B, the approximate total number of electrons in the overall oxidation of L-Cys

(n) was calculated using the following equation for diffusion-controlled electrochemically irreversible reactions, in which the first electron transfer is rate-determining:[29]

$$I_p = 2.99\times10^5 n((1-\alpha)n_\alpha)^{1/2} A c^* D^{1/2} v^{1/2} \quad (5)$$

where D is the diffusion coefficient of L-Cys (8.54×10^{-5} cm^2 s^{-1}, as obtained by chronoamperometry; see later), c^* is the bulk concentration of L-Cys (0.7 mM), and A is the electrode surface area. A value $\alpha = 0.53$ was obtained from the Tafel plots. To obtain information about the rate-determining step, the Tafel plot was drawn (not shown), as derived from points in the Tafel region of the cyclic voltammogram in Fig. 3A. Therefore, an approximate value for the total number of electrons involved in the anodic oxidation of L-Cys, n in the range from 0.7 to ≈1 was obtained.

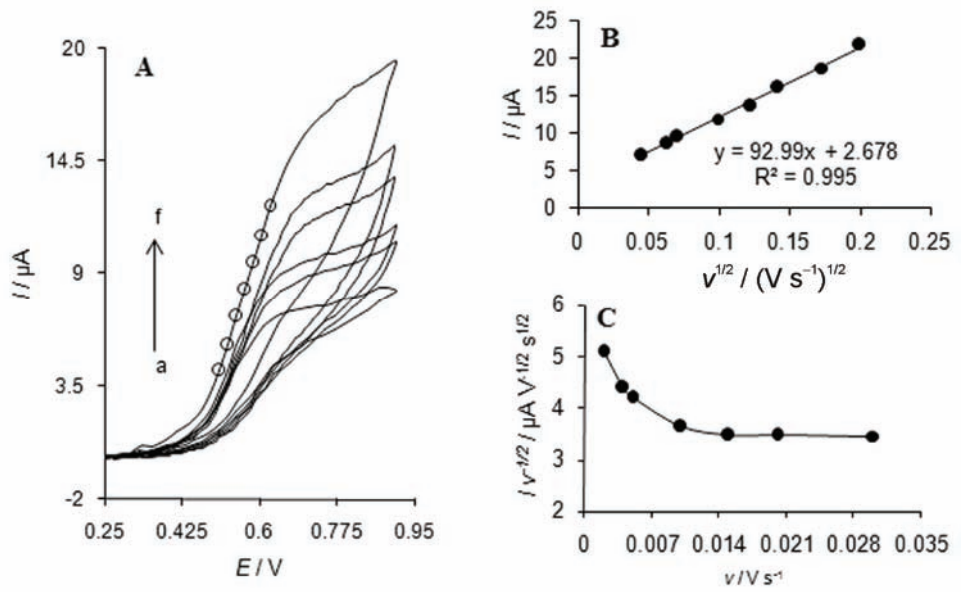

Fig. 3. A) Cyclic voltammograms of the MCTNMCPE in 0.1 M phosphate buffer (pH 8.0) containing 0.7 mM L-cysteine at different scan rates: a) 2, b) 5, c) 10, d) 15, e) 20 and f) 30 mV s^{-1}; B) variation of the electrocatalytic currents *vs.* the square root of scan rate; C) variation of the scan rate-normalized current ($I_p/v^{1/2}$) with scan rate.

Effect of the percent TiO_2 nanoparticles on the behavior of the modified electrode

Figure 4 shows the cyclic voltammograms for 1.0 mM L-Cys in 0.1 M phosphate buffer (pH 8.0) on the surface of molybdenum complex-modified paste electrodes containing various weight percentages of TiO_2 nanoparticles (mixed

with the fine graphite powder to prepare unmodified CPE). As can be seen in Fig. 4, the molybdenum complex-modified electrode without TiO_2 nanoparticles showed a relatively weak and broad wave together with a considerable amount of capacitive current for L-Cys. On the other hand, by addition of 4 mass% of TiO_2 nanoparticles to the graphite powder for preparing the paste, a relatively sharp anodic wave was obtained. The resulting enhancement in the kinetics of L-Cys oxidation together with the remarkable decrease in the capacitive current makes the MCTNMCPE very suitable for the detection of trace amounts of L-Cys in various samples. The maximum sensitivity (anodic peak current) was obtained for the electrode containing 4 mass% TiO_2 nanoparticles, while no enhancement in the current process was obtained with higher amounts. On the contrary, Fig. 4 show that the addition of higher amounts of TiO_2 nanoparticles resulted in lower anodic peak currents. Therefore, in all further electrochemical investigations, 4 mass% TiO_2 nanoparticles was used for preparing the composite pastes.

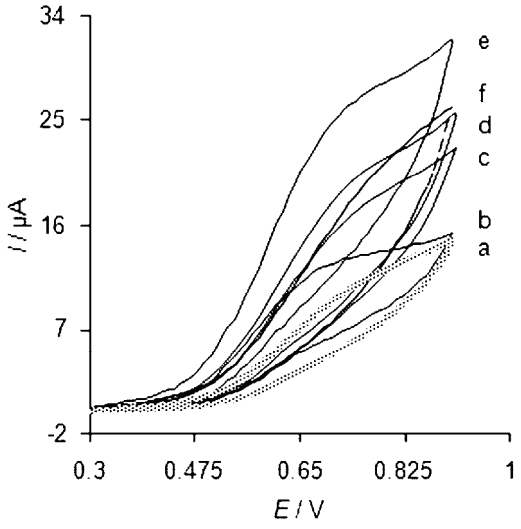

Fig. 4. Cyclic voltammograms of 1.0 mM L-Cys on the surface of a MCMCPE in the absence (a) and presence of TiO_2 nanoparticles in the matrix of the paste: b) 1, c) 2, d) 3, e) 4 and f) 5 mass%.

Chronoamperometric measurements

Chronoamperometry is often used for measuring the diffusion coefficient of electroactive species at the surface area of the working electrode.[26] The chronoamperometry technique was used to investigate catalytic oxidation of L-Cys by a MCTNMCPE. Chronoamperometric measurements of different concentrations of L-Cys at the MCTNMCPE were realized by setting the working electrode potential at 900 mV. In the chronoamperometric studies, the diffusion coefficient, *D*, of L-Cys was determined. The experimental plots of *I vs.* $t^{-1/2}$ with the best fits for different concentrations of L-Cys were employed. The slopes of the resulting straight lines were then plotted *vs.* the L-Cys concentration (Fig. 5A), from the

slope of which and using the Cottrell Equation,[29] a diffusion coefficient of $(8.54\pm0.6)\times10^{-5}$ cm^2 s^{-1} was calculated for L-Cys.

The chronoamperometric method of Galus was also used to evaluate the catalytic rate constant, k / M^{-1}s^{-1}, for the reaction between L-Cys and the MCTNMCPE:[31]

$$I_C / I_L = \gamma^{1/2}(\pi^{1/2}\mathrm{erf}(\gamma^{1/2}) + \exp(-\gamma)/\gamma^{1/2}) \quad (6)$$

where I_C is the catalytic current of L-Cys at the MCTNMCPE, I_L the limited current in the absence of L-Cys and $\gamma = kc^*t$ is the argument of the error function. In the cases where γ exceeds 2, the error function is almost equal to 1 and Eq. (6) can be reduced to:

$$I_C/I_L = \pi^{1/2}\gamma^{1/2} = \pi^{1/2}(kc^*t)^{1/2} \quad (7)$$

where t is the elapsed time. The above equation can be used to calculate the rate constant (k) of the catalytic process. Based on the slope of the I_C/I_L *vs.* $t^{1/2}$ plot (Fig. 5B); k can be obtained for a given L-Cys concentration. Such plots obtained from the chronoamperograms are shown in Fig. 5B. From the values of the slopes, the average value of k was found to be $(6.24\pm0.08)\times10^3$ M^{-1} s^{-1}. The value of k also explains the sharp feature of the catalytic peak observed for the catalytic oxidation of L-Cys at the surface of the MCTNMCPE.

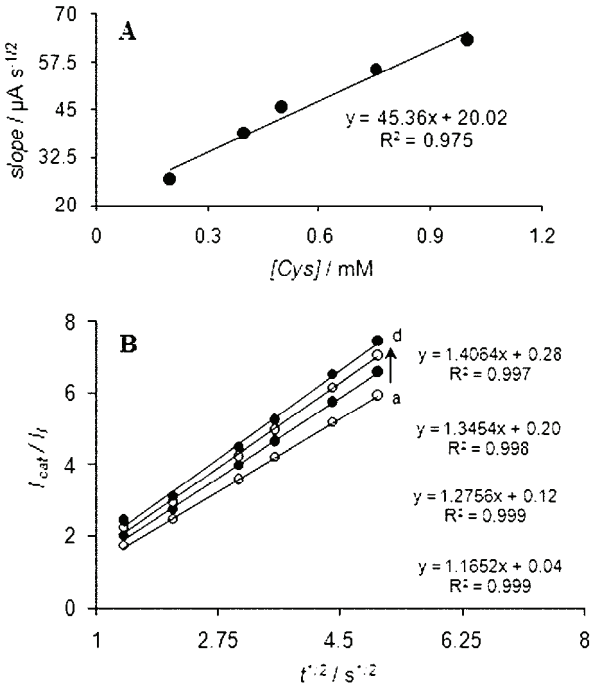

Fig. 5. A) Plot of the slopes of the straight lines against the L-Cys concentration (0.2, 0.4, 0.5, 0.75 and 1.0 mM) obtained from chronoampograms; B) dependence of I_{cat}/I_l on $t^{1/2}$ derived from the data of the chronoamperograms.

Differential pulse voltammetry investigations

Pulse voltammetric techniques are aimed at lowering the detection limits of voltammetric measurements.[26] Since differential pulse voltammetry (DPV) has a much higher current sensitivity and a better resolution than cyclic voltammetry, it was used to estimate the limit of detection of L-Cys. In addition, the contribution of the charging current to the background current, which is a limiting factor in analytical determinations, is negligible in the DPV mode. The responses were linear for L-Cys concentrations in the ranges 1.5–100.0 μM and 100.0–1200.0 μM with current sensitivities of 0.0424 and 0.0082 μA/μM (Fig. 6). The decrease in sensitivity (slope) in the second linear range is probably due to kinetic limitations. From the analysis of this data, the lower limit of detection of L-Cys was estimated to be of the order of 0.70±0.01 μM. This value is comparable to values previously reported by other researchers for the electrocatalytic oxidation of L-Cys at the surface of electrodes chemically modified by other mediators (Table I).[30–33]

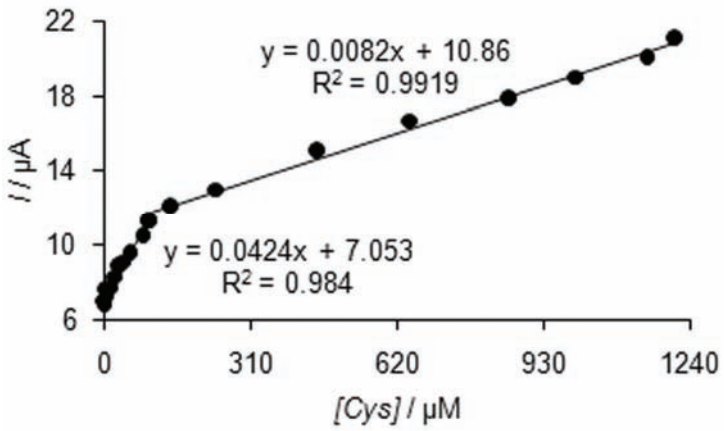

Fig. 6. Plot of the electrocatalytic peak current as a function of L-Cys concentration in the range of 1.5–100.0 μM and 100.0–1200.0 μM obtained from the differential pulse voltammograms.

Interference studies

The influence of various substances, such as $C_2O_4^-$, Br^-, F^-, SO_4^{2-}, NH_4^+, Na^+, EDTA, HPO_4^{2-}, Ca^{2+}, Mg^{2+}, L-cystine, L-phenylalanine, glycine, L-lysine, L-histidine, glucose, SCN^-, L-methionine, L-alanine, L-asparatic acid, L-glutathione, L-tryptophan, tyrosine, ascorbic acid, uric acid and captopril, as compounds that could potentially interfere with the determination of L-Cys under the optimum conditions with 1.0×10^{-5} M L-Cys was studied. The tolerance limit was defined as the maximum concentration of a potential interfering substance that caused an error of less than 5 % for the determination of 1.0×10^{-5} M L-Cys. The

results showed that the peak current of L-Cys was not affected by any of the cations, anions, and organic substances tested.

TABLE I. Comparison of the efficiency of some modified electrodes used in the electrocatalysis of L-Cys

Electrode	Modifier	Method	pH	Peak potential shift, mV	Scan rate mV s^{-1}	Limit of detection M	Dynamic range, M	Ref.
Carbon paste	1-[4-(Ferrocenylethynyl)-phenyl]-1--ethanone	Voltammetry	7.0	350	10	5.0×10^{-6}	2.0×10^{-5}–2.8×10^{-3}	32
Carbon paste	Quinizarine	Voltammetry	7.0	330	50	2.2×10^{-7}	1.0×10^{-6}–1.0×10^{-3}	33
Carbon paste	Ferrocene dicarboxylic acid	Voltammetry	8.0	200	10	1.4×10^{-6}	1.5×10^{-5}–3.2×10^{-3}	34
Carbon paste	Co-complex	Potentiometry	2.4	100	100	5.0×10^{-7}	6×10^{-7}–2×10^{-3}	35
Carbon–TiO_2 nano-particle	Molybdenum(VI) complex	Voltammetry	8.0	130	30	7.0×10^{-7}	1.5×10^{-6}–1.2×10^{-3}	This work

Real sample analysis

To evaluate the applicability of the proposed method to real samples, it was applied to the determination of L-Cys in human blood serum, acetylcysteine tablets (purchased from Hexal Company, Germany (specified content of acetylcysteine was 600 mg per tablet) and water samples. The determination of L-Cys in these samples was performed by the standard addition method in order to prevent any matrix effect. Results are presented in Table II. As the tested water samples were found to be free from L-Cys, synthetic samples were prepared by adding known amounts of L-Cys to water samples. The results are given in Table III.

TABLE II. Determination of L-Cys in human blood serum and acetylcysteine tablets (M)

Sample	Human blood serum	Acetylcysteine tablet
Measured value	$(2.17\pm0.6)\times10^{-4}$	$(5.06\pm0.5)\times10^{-3}$
Real value[a]	$(1.48\pm4.13)\times10^{-4}$	5.09×10^{-3}

[a]Result value at 95 % confidence limits, obtained from five replicated determinations per sample

The repeatability and stability of MCTNMCPE

The electrode capability for the generation of a reproducible surface was examined by cyclic voltammetric data (*i.e.*, E_{pa}, E_{pc}, I_{pa} and I_{pc}) obtained in the optimum solution pH from four separately prepared MCTNMCPEs. The calculated *RSD* for various parameters accepted as the criteria for a satisfactory surface

reproducibility was 1–4 %. This is virtually the same as that expected for the renewal of ordinary carbon paste surfaces.[25] In addition, the long term stability of the MCTNMCPE was tested over a four-week period. Cyclic voltammetry of L-Cys at the surface of MCTNMCPE after the modified electrode had been stored under atmospheric conditions at room temperature showed that the oxidation peak potential of L-Cys was unchanged and the anodic peak current decreased by only less than 1.9 % of the initial oxidation peak current. The antifouling properties of modified electrode toward L-Cys and its oxidation product were investigated by recording the cyclic voltammograms of this modified electrode before and after using in the presence of L-Cys. Cyclic voltammetry of L-Cys at the surface of MCTNMCPE after 15 repetition cycles at a scan rate 30 mV s^{-1} showed that the oxidation peak potential of L-Cys remained changed and the anodic peak current decreased by less than 2.9 %. However, in the present study, the surface of the MCTNMCPE was regenerated before each experiment.

TABLE III. Determination of L-Cys in water samples (n = 5)

Sample	Added, μM	Found, μM	Recovery, %	*RSD* / %
Tap water	0	–	–	–
	5	4.89	97.8	2.8
	10	9.82	98.2	1.4
	15	15.32	10.2.1	3.2
Well water	0	–	–	–
	5	5.09	101.8	2.9
	10	10.28	102.3	2.1
	15	14.83	98.7	1.3

CONCLUSIONS

In the present study, a carbon-paste electrode modified with TiO_2 nanoparticles/bis[bis(salicylidene-1,4-phenylenediamine)molybdenum(VI)] was used for the determination of L-Cys. The CV and DPV investigations showed effective electrocatalytic activity in lowering the anodic overpotential for L-Cys. The high sensitivity and very low detection limit (0.7 μM), together with the ease of preparation and surface regeneration of the modified electrode, and reproducibility of the voltammetric responses are the advantages of the studied modified electrode.

Acknowledgements. The authors wish to thank Yazd University Research Council and IUT Research Council and Excellence in Sensors for financial support of this research. We gratefully acknowledge Dr. N. Taghavinia of Sharif University of Technology, Iran, for the preparation of the nanoparticles.

ИЗВОД

СИНТЕЗА И КАРАКТЕРИЗАЦИЈА ЕЛЕКТРОДЕ МОДИФИКОВАНЕ МОЛИБДЕН(VI) КОМПЛЕКСОМ И TiO_2 НАНОЧЕСТИЦАМА ЗА ЕЛЕКТРОКАТАЛИТИЧКО ОДРЕЂИВАЊЕ L-ЦИСТЕИНА

MOHAMMAD MAZLOUM-ARDAKANI[1], HADI BEITOLLAHI[1], ZAHRA TALEAT[1] и MASOUD SALAVATI-NIASARI[2]

[1]*Department of Chemistry, Faculty of Science, Yazd University, Yazd, 89195-741 и* [2]*Department of Inorganic Chemistry, Faculty of Chemistry, University of Kashan, Kashan, I.R. Iran*

Направљен је нов волтаметријски сензор за одређивање L-цистеина (L-Cys) у виду електроде од угљеничне пасте уз додатак TiO_2 наночестица и бис[бис(салицилидин-1,4--фенилендиамин молибден(VI)] комплекса. Електрохемијско понашање сензора је детаљно испитивано цикличном волтаметријом. Привидна константа брзине преноса електрона и коефицијент прелаза за систем TiO_2 наночестице/комплекс молибдена (VI)/угљенична паста су такође одређени помоћу цикличне волтаметрије и добијене су вредности од око 4,53 s^{-1} и 0,54, редом. Сензор је показао добру електрокаталитичку активност за оксидацију L-Cys. Потенцијал волтаметријског пика оксидације L-Cys био је за 130 mV нижи у поређењу са истим на немодификованој електроди од угљеничне пасте. Под оптималним условима, линеарна област детекције L-Cys обухвата концентрације од $1,5\times10^{-6}$ до $1,2\times10^{-3}$ M, док је граница детекције 0,70±0,01 μM при односу сигнала и шума једнаком два. Поред тога, сензор је показао добру стабилност и репродуктивност.

(Примљено 4. маја, ревидирано 15. октобра 2010)

REFERENCES

1. C. C. Doumanidis, *Microelectron. Eng.* **86** (2009) 467
2. R. Nakamura, Y. Nakato, *J. Am. Chem. Soc.* **126** (2004) 1290
3. H. Beitollahi, M. Mazloum Ardakani, B. Ganjipour, H. Naeimi, *Biosens. Bioelectron.* **24** (2008) 362
4. A. Mehdinia, S. H. Kazemi, S. Z. Bathaie, A. Alizadeh, M. Shamsipur, M. F. Mousavi, *J. Pharmaceut. Biomed.* **49** (2009) 587
5. X. Yang, S. Chen, S. Zhao, D. Li, H. Ma, *J. Serb. Chem. Soc.* **68** (2003) 843
6. R. E. Sabzi, K. Rezapour, N. Samadi, *J. Serb. Chem. Soc.* **75** (2010) 1
7. G. Schmid, *Nanoparticles*, Wily-VCH, New York, 2005
8. Z. Dursun, S. Ulubay, B. Gelmez, F. N. Ertas, *Catal. Lett.* **132** (2009) 127
9. Y. Zhou, S. Wang, B. Ding, Z. Yang, *Catal. Lett.* **118** (2007) 86
10. A. Tiehm, S. T. Lohner, T. Augenstein, *Electrochim. Acta* **54** (2009) 3453
11. D. Orata, F. Segor, *Catal. Lett.* **58** (1999) 157
12. S. Mishra, R. D. Tripathi, S. Srivastava, S. Dwivedi, P. Kumar Trivedi,O. P. Dhankher, A. Khare, *Bioresour. Technol.* **100** (2009) 2155
13. G. N. Yin, H. W. Lee, J. Y. Cho, K. Suk, *Brain Res.* **1265** (2009) 158
14. R. Relienea, M. E. P. Goadd, R. H. Schiestl, *DNA Repair* **5** (2006) 1392
15. J. Kruusma, A. M. Benham, J. A. G. Williams, R. Kataky, *Analyst* **131** (2006) 459
16. P. C. White, N. S. Lawrence, J. Davis, R. G. Compton, *Electroanal.* **14** (2002) 89
17. M. Mazloum-Ardakani, P. Rahimi, P. Ebrahimi Karami, H. R. Zare, H. Naeimi, *Sens. Actuators B* **123** (2007) 763
18. C. Deng, J. Chen, X. Chen, M. Wang, Z. Nie, S. Yao, *Electrochim. Acta* **54** (2009) 3298

19. M. Mazloum-Ardakani, P. Ebrahimi Karami, H. Naeimi, B. B. F. Mirjalili, *Turk. J. Chem.* **32** (2008) 571
20. A. Abbaspour, A. Ghaffarinejad, *Electrochim. Acta* **53** (2008) 6643
21. H. Razmi, H. Heidari, *Anal. Biochem.* 388 (2009) 15
22. Z. Taleat, M. Mazloum-Ardakani, H. Naeimi, H. Beitollahi, M. Nejati, H. R. Zare, *Anal. Sci.* **24** (2008) 1039
23. M. Mazloum-Ardakani, H. Beitollahi, Z. Taleat, H. Naeimi, N. Taghavinia, J. *Electroanal. Chem.* **644** (2010) 1
24. M. Mazloum Ardakani, H. Beitollahi, B. Ganjipour, H. Naeimi, M. Nejati, *Bioelectrochem.* **75** (2009) 1
25. M. Mazloum Ardakani, Z. Taleat, H. Beitollahi, M. Salavati-Niasari, B. B. F. Mirjalili, N. Taghavinia, *J. Electroanal. Chem.* **624** (2008) 73
26. J. Wang J, *Analytical Electrochemistry*, 2nd ed., Wiley-VCH, New York, 2000
27. P. W. Geno, K. Ravichandran, R. P. Baldwin, *J. Electroanal. Chem.* **183** (1985) 155
28. E. Laviron, *J. Electroanal. Chem.* **101** (1979) 19
29. A. J. Bard, L. R. Faulkner, *Electrochemical Methods: Fundamentals and Applications*, 2nd ed., Wiley, New York, 2001
30. W. T. Tan, A. M. Bond, S. W. Ngooi, B. Lim, J. K. Goh, *Anal. Chim. Acta* **491** (2003) 181
31. Z. Galus, *Fundamentals of Electrochemical Analysis*, Ellis Horwood, New York, 1976
32. J. B. Raoof, R. Ojani, H. Beitollahi, R. Hosseinzadeh, *Anal. Sci.* **22** (2006) 1213
33. M. Mazloum-Ardakani, Z. Taleat, H. Beitollahi, H. Naeimi, *J. Iran. Chem. Soc.* **7** (2010) 251
34. J. B. Raoof, R. Ojani, H. Beitollahi, *Electroanalysis* **19** (2007)1822
35. S. Griveau, J. Pavez, J. H. Zagal, F. Bedioui, *J. Electroanal. Chem.* **497** (2001) 75.

Journal of the Serbian Chemical Society
JSCS-info@shd.org.rs • www.shd.org.rs/JSCS
J. Serb. Chem. Soc. 76 (4) 591–606 (2011)
JSCS–4144
UDC 665.32/.33:547.56:66.095.253:66.095.26–128.4
Original scientific paper

Phenolation of vegetable oils

MIHAIL IONESCU and ZORAN S. PETROVIĆ*

Pittsburg State University, Kansas Polymer Research Center, 1701 South Broadway, Pittsburg, Kansas, 66762, USA

(Received 20 August, revised 8 December 2010)

Abstract: Novel bio-based compounds containing phenols suitable for the synthesis of polyurethanes were prepared. The direct alkylation of phenols with different vegetable oils in the presence of superacids (HBF_4, triflic acid) as catalysts was studied. The reaction kinetics was followed by monitoring the decrease of the double bond content (iodine value) with time. In order to understand the mechanism of the reaction, phenol was alkylated with model compounds. The model compounds containing one internal double bond were 9-octadecene and methyl oleate and those with three double bonds were triolein and high oleic safflower oil (82 % oleic acid). It was shown that the best structures for phenol alkylation are fatty acids with only one double bond (oleic acid). Fatty acids with two double bonds (linoleic acid) and three double bonds (linolenic acid) lead to polymerized oils by a Diels–Alder reaction, and to a lesser extent to phenol alkylated products. The reaction product of direct alkylation of phenol with vegetable oils is a complex mixture of phenol alkylated with polymerized oil (30–60 %), phenyl esters formed by transesterification of phenol with triglyceride ester bonds (<10 %) and unreacted oil (30 %). The phenolated vegetable oils are new aromatic–aliphatic bio-based raw materials suitable for the preparation of polyols (by propoxylation, ethoxylation, Mannich reactions) for the preparation of polyurethanes, as intermediates for phenolic resins or as bio-based antioxidants.

Keywords: vegetable oils; phenol; alkylation; aromatic electrophilic substitution; cationic polymerization.

INTRODUCTION

The constant quest for new materials from renewable resources is driven by environmental and sustainability concerns. Vegetable oils are one of the most important groups of renewable raw materials because they are relatively inexpensive and allow a range of chemical reactions at double bonds, ester groups and

* Corresponding author. E-mail: zpetrovi@pittstate.edu
doi: 10.2298/JSC100820050I

allylic positions. Vegetable oils having hydroxyl groups and phenyl rings are multifunctional components useful for the preparation of polyurethanes and phenolic resins. They can be prepared economically in one step by Friedel–Crafts alkylation of phenols with different oils or fatty acids. The objective of this work was to study the feasibility of the preparation of phenolated oils, determine the reaction conditions for the highest yield and examine the reaction mechanism. Particular attention was paid to the side reactions occurring simultaneously with the phenol alkylation reaction.

The internal double bonds in vegetable oils are of low reactivity, thus the introduction of different functional groups is necessary to create useful monomers for polymerization.[1–8] The double bonds of fatty acids can be observed as 1,2--disubstituted olefins.[1–7] Due to the electron-releasing alkyl groups, they are relatively rich in electrons and capable of reacting with electrophilic species, such as protons, carbocations and free radicals. The Friedel–Crafts alkylation of phenols with olefins is a well-known reaction used on an industrial scale for the production of many important chemicals, including a range of antioxidants by alkylation of phenols with isobutylene, octene, diisobutylene, propylene trimers (nonene) and tetramers.[9–12] The ethoxylated long chain alkylated phenols represent one of the most important class of nonionic surfactants (*e.g.*, ethoxylated nonyl phenol).[13] Using this general concept, the Friedel–Crafts alkylation of phenol with vegetable oils, in the presence of acid catalysts was investigated in this study (Scheme 1).

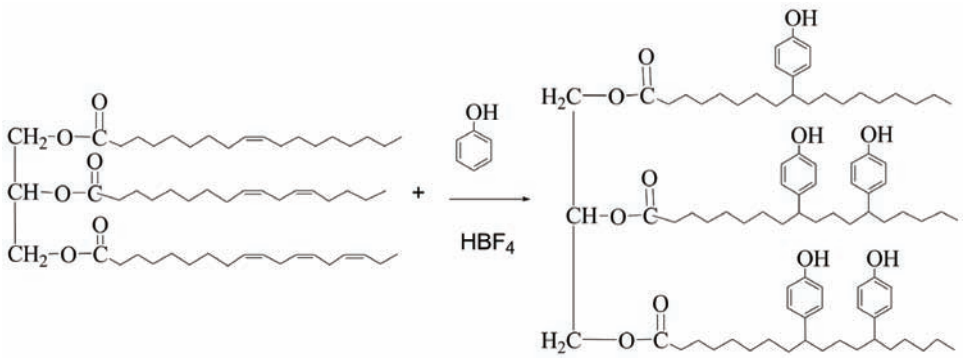

Scheme 1. Friedel–Crafts alkylation of phenol with soybean oil (ideal reaction pathway).

The idea of phenol alkylation with vegetable oils or derivatives of vegetable oils (fatty acids, fatty acid methyl esters, *etc.*) is not new. Generally, the alkylation of phenol with free fatty acids are preferred.[12,14–23] Direct alkylation of linseed oil with phenol or cresols in the presence of triflic acid and the use of the alkylated product for the synthesis of modified phenolic resins is described in a patent.[15] The first direct alkylation of phenol with soybean oil was also des-

cribed.[1] Neither the patents nor the publications gave detailed information about the mechanism, side reactions, composition of the molecular species in the alkylated product or the reactivity of the double bonds.

EXPERIMENTAL

Materials

Refined, bleached and deodorized (RBD) soybean oil (SBO) supplied by Cargill had an iodine value (*IV*) of 129 g I_2/100g. High oleic safflower oil (HOSO) having 82 % oleic acid and an *IV* of 85 g I_2/100g was supplied by Cargill (Minneapolis, MN, USA). Triolein was purchased from NU-CHEK Prep. Inc. (Elysian, MN, USA) and 9-octadecene, purity 97 %, was purchased from Alfa Aesar (Ward Hill, MA, USA). Methyl oleate, purity >99 % and methyl linoleate, purity >99 %, were purchased from NU-CHEK Prep, Inc. Phenol (purity 99 %), melting point (m.p.) 40–42 °C, tetrafluoroboric acid (HBF_4) as a 54 % solution in diethyl ether, and trifluoromethanesulfonic (triflic) acid (CF_3SO_3H) of purity 99 % were purchased from Aldrich (St. Louis, MO, USA).

Methods

The *IV* was determined by the Hanus method.[24] The molecular weights (MW) and MW distribution were determined using a Waters gel permeation chromatograph (Waters Corporation, Milford, MA, USA) consisting of a 510 pump, 410 differential refractometer and a data collection system. Tetrahydrofuran (THF) was used as the eluent at 1.00 mL min^{-1} at 30 °C. Four Phenogel 5 μm columns (50, 100, 1000 and 10,000 Å) plus a Phenogel guard column from Phenomenex (Torrance, CA, USA) covering a MW range of 10^2–10^6 were used. The concentration of investigated compounds in THF was 5 %.

The viscosity was measured at 25 °C on a Rheometrics Scientific Inc. (Piscataway, NJ) SR-500 dynamic stress rheometer, with parallel plates of 25 mm in diameter and gap of 0.2 mm. The infrared spectra were recorded with a Perkin Elmer FTIR Spectrometer 1000 (Waltham, MA, USA)

The ^{1}H-NMR and ^{13}C-NMR spectra were recorded with a 7.05 Bruker Avance DPX-300 NMR spectrometer (Bruker, Rheinstetten, Germany) using 10 % solutions of the investigated compounds in deuterated chloroform ($CDCl_3$). Eight scans for the ^{1}H-NMR spectra and 1000 scans for the ^{13}C NMR spectra were used.

Phenolation reaction

SBO or model compounds (9-octadecene, methyl oleate, HOSO or triolein) were mixed with molten phenol under nitrogen at 50–60 °C. The molar ratio of phenol to double bonds was 1:1. The catalyst was added to the reaction mixture (1 % w/w) and the reaction was maintained for 4–6 h at 90 °C under nitrogen. The reaction mass became red–brown and after 10–20 min a marked increase in the viscosity was observed. The final product was a red––brown viscous liquid. The unreacted phenol was removed by high vacuum distillation.

RESULTS AND DISCUSSION

The accepted general mechanism of the alkylation of phenols with olefins consists of three steps.[10,11,16,25–28] In the first step, a proton from the catalyst attacks a double bond forming a carbocation (Scheme 2a). In the second step, the phenolic hydroxyls, the most nucleophilic groups in the reaction system, react with the carbocation generated in the first step, giving a protonated phenyl ether

(Scheme 2b). In the third step, the protonated phenyl ether rearranges to the *ortho* and *para* alkylated phenol and to a small extent to the non-protonated free phenyl ethers (Scheme 2c).[10,27,28]

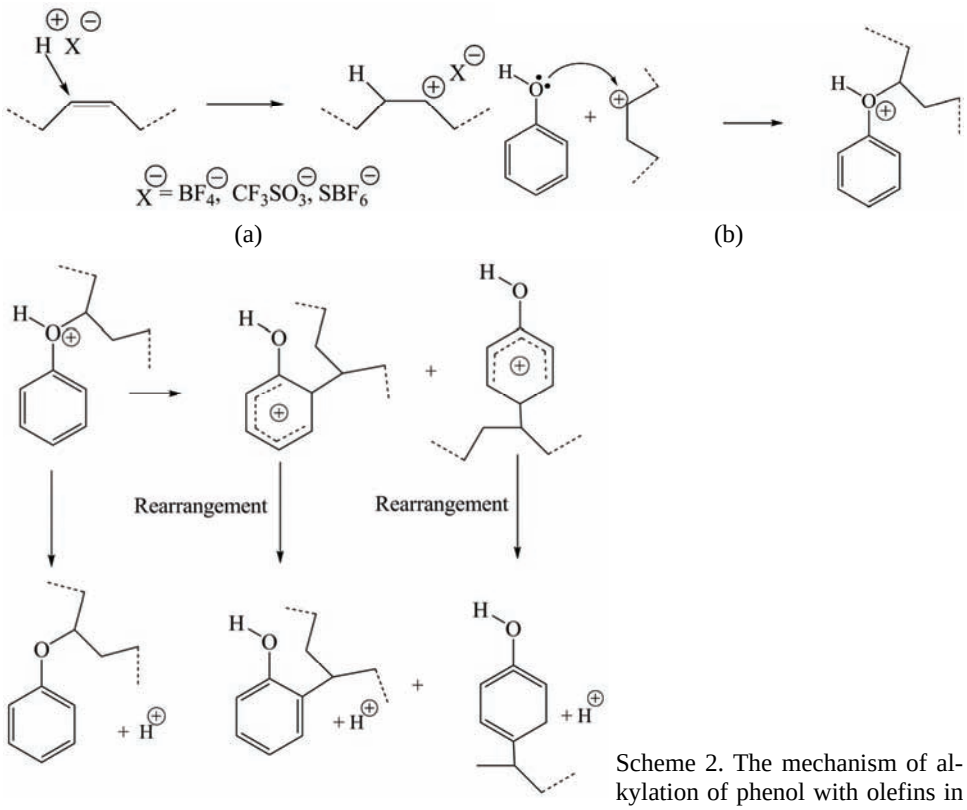

Scheme 2. The mechanism of alkylation of phenol with olefins in three consecutive steps (a, b and c).

The *IV* gives direct information on the disappearance of double bonds. The changes of *IV* with time during the reaction of soybean oil with phenol and in the absence of phenol are shown in Fig. 1. The decreasing *IV* with SBO only is the consequence of the polymerization reaction, but the much stronger decrease of *IV* in the presence of phenol is direct proof that the alkylation reaction has occurred.

A strong decrease in the double bond content and the appearance of alkylated phenol products in the reaction of SBO with phenol was observed in the ^{1}H--NMR spectra. The peaks at 5.2–5.8 ppm, characteristic of double bond protons, which were very strong in the soybean oil (Fig. 2), become very small after the reaction of soybean oil with phenol (Fig. 3). Figure 3 also displays peaks at 6.7––7.4 ppm, characteristic of the protons of the phenol ring alkylated at various positions, again indicating that the alkylation of phenol had occurred. A strong de-

crease of mono-allylic protons of SBO at 2.0–2.1 ppm and of bis-allylic protons at 2.7–2.8 ppm can also be seen in Fig. 3, proving their participation in the process.

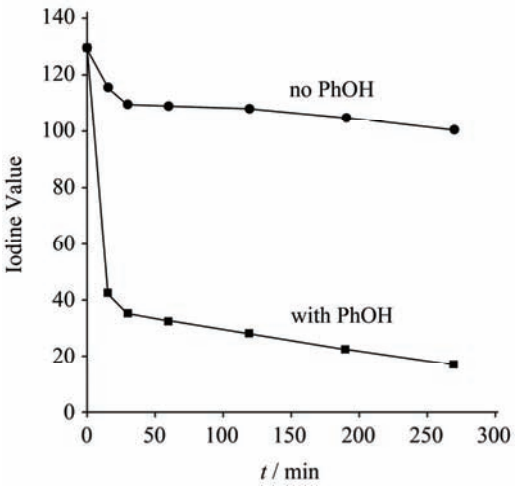

Fig. 1. Variation of iodine value of oil in the absence and the presence of phenol. Catalyst: HBF_4 (1 %); T = 90 °C.

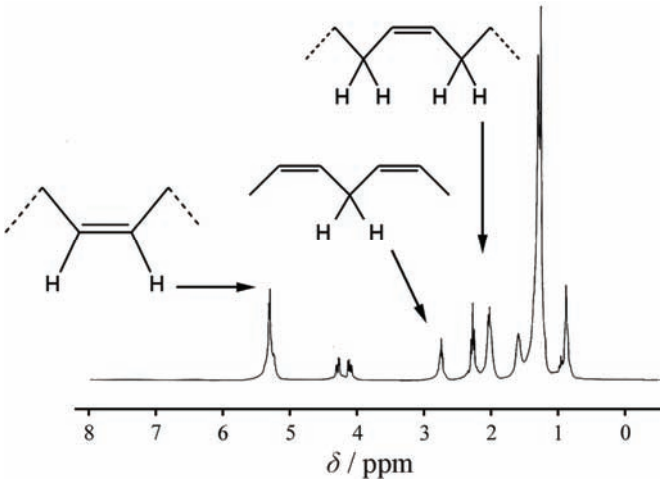

Fig. 2. ^{1}H-NMR Spectrum of soybean oil.

The ^{13}C-NMR spectrum of the phenolated products displayed specific peaks at 132.2 and 127 ppm, characteristic of carbon atoms from the aromatic rings alkylated in the *para* and *ortho* positions, respectively.

A strong (300–550 times) increase in the viscosity at 25 °C of the reaction mass during the phenolation reaction of SBO, from initial values of 0.06 Pa s to 19–33 Pa s after 5–6 h of reaction at 90 °C, is illustrated in Fig. 4.

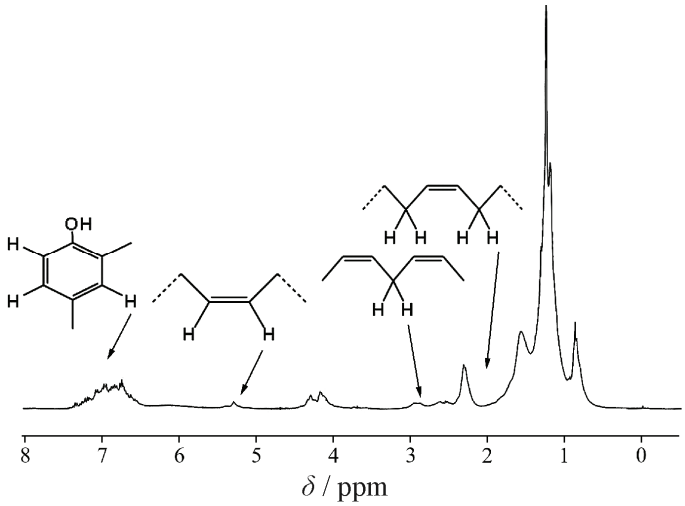

Fig. 3. ^{1}H-NMR Spectrum of phenolated SBO.

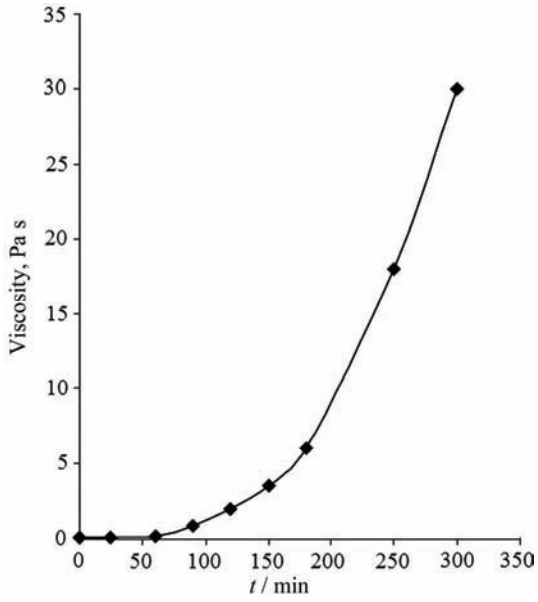

Fig. 4. Variation of the viscosity of the reaction mass during the alkylation reaction of phenol with soybean oil. Catalyst HBF_4 (1 %), T = 90 °C.

A gel permeation chromatogram of the product resulting from the phenolation of SBO under conditions of Friedel–Crafts alkylation reactions (catalyst HBF_4 as a 54 % solution in diethyl ether) is shown in Fig. 5. The chromatogram revealed unreacted phenol, phenyl esters of fatty acids, unreacted soybean oil and alkylated phenol products.

The FTIR spectra of phenolated high oleic safflower oil prepared using two catalysts, HBF_4 and triflic acid, together with the FTIR spectra of the initial HOSO

and phenol are displayed in Fig. 6. The double bond content of the phenolated oil (the peak at 3010 cm^{-1}) decreased significantly compared with the initial oil. The formation of phenyl esters as products of side reactions was observed. The peak at 1746 cm^{-1} is characteristic of the carbonyl from the triglyceride ester groups, while the peak at 1719 cm^{-1} is assigned to carbonyl groups from the phenyl esters of fatty acids. Two superacids were used to test their catalytic effect on the phenolation reaction. Triflic acid is stronger than HBF_4 but no significant difference in the phenolation reactions was observed. In earlier experiments, triflic acid gave a slightly more rapid cationic polymerization reaction of oils in the absence of phenols.

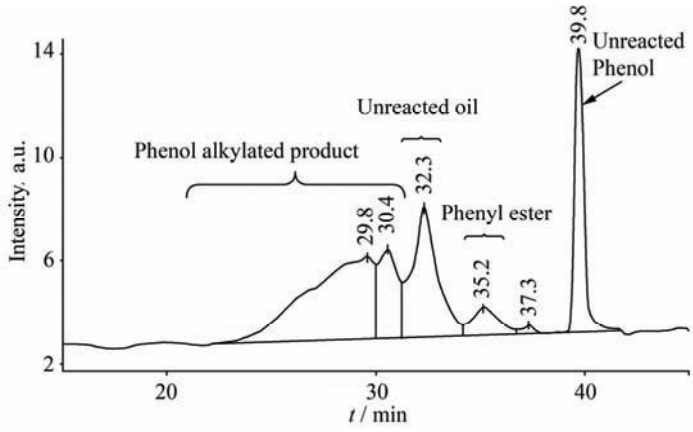

Fig. 5. Typical GPC chromatogram of phenol alkylated with soybean oil.

Phenyl esters were formed to a small extent (less than 10 % in the final phenolated product as measured by the peak area in GPC) by transesterification reactions of triglycerides with phenol, catalyzed by acids (Scheme 3). The position of the peak characteristic of fatty acid phenyl esters was established with a model compound synthesized by transesterification of methyl soyate (methyl esters of soybean fatty acids) with phenol in the presence of a strong transesterification catalyst (stannous octoate), which does not catalyze alkylation or polymerization reactions. It is well known that transesterification of phenols with alkyl esters does not proceed easily, but using an excess of phenol, long reaction time and the continuous removal of methanol resulting from the condensation reaction, it was possible to obtain in a high yield the desired model compound: phenyl ester of soybean fatty acids.

Before running the reaction of phenols with soybean oil, the effect of the catalyst (HBF_4 or triflic acid) on the oil in the absence of phenol was examined under the same experimental conditions. Both superacids polymerized SBO to highly viscous liquids and, at longer reaction times (>7 h), to crosslinked solids.

The cationic polymerization of vegetable oils with superacids is described in detail in a patent.[29] The patent showed that the most important fatty acids involved in the cationic polymerization of vegetable oils are the ones with two (linoleic acid) or three (linolenic acid) double bonds and not oleic acid itself. The polymerization of oils differs from the conventional cationic polymerization of olefins since it involves Diels–Alder and "ene" reactions.[29,30] The structure of polymerized soybean oil presented in Scheme 4 shows that the triglycerides are predominantly linked by cyclic structures as a consequence of Diels–Alder reactions.[30]

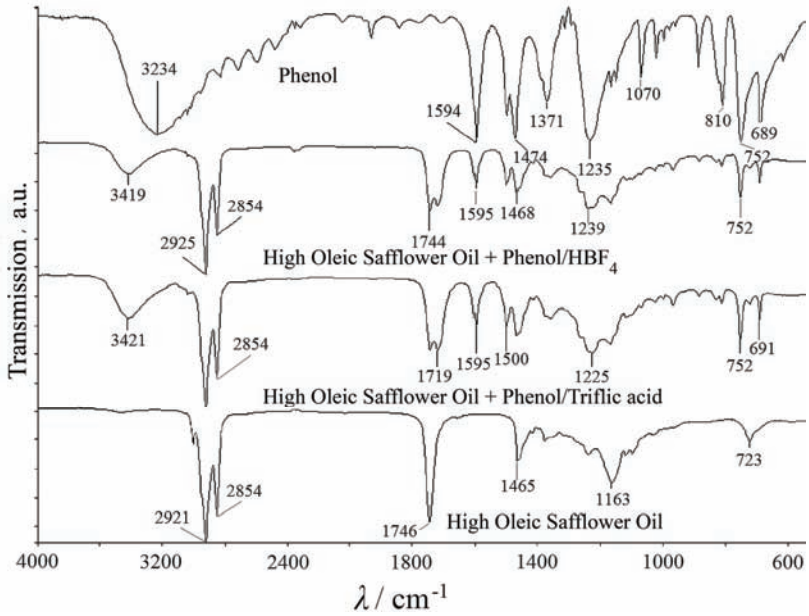

Fig. 6. FTIR Spectra of phenol alkylated with HOSO using HBF_4 and CF_3SO_3H catalysts together with the FTIR spectra of the initial compounds: phenol and HOSO.

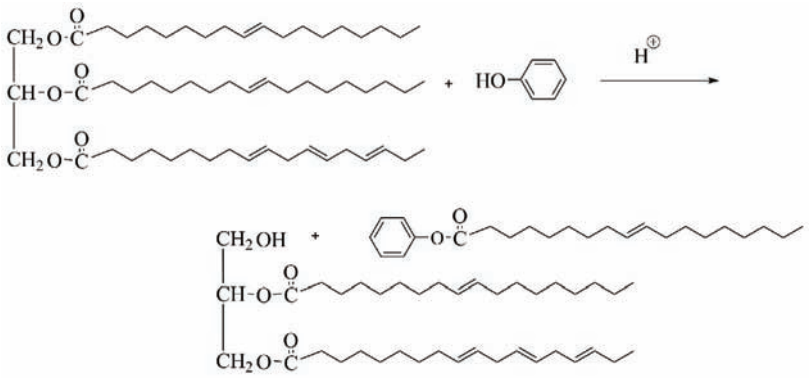

Scheme 3. Formation of phenyl esters by transesterification of triglyceride with phenol.

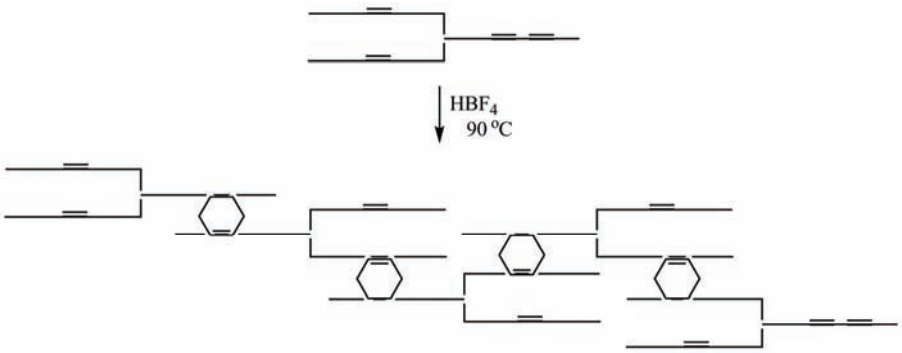

Scheme 4. Structure of cationically polymerized soybean oil in the absence of phenol. The triglyceride units were linked by the Diels–Alder reaction.

The reaction of oils with phenols results in polymerized phenolated oils because of the simultaneous reactions of cationic polymerization of the oils and the alkylation of phenols with by the oils.

In order to better understand the chemistry, model compounds containing internal double bonds similar to the double bonds in oils were used. The model compounds employed for the alkylation of phenol, presented in Scheme 5, were 9-octadecene, methyl oleate, triolein and HOSO.

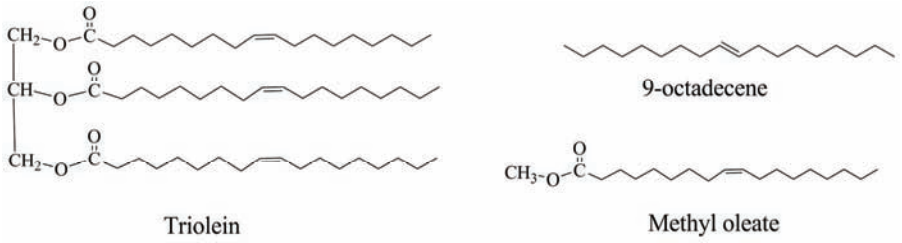

Scheme 5. Model compounds containing internal double bonds used to study the Friedel–Crafts alkylation of phenols.

In a similar way, the possibility of the occurrence of cationic polymerization of the compounds with one internal double bond in the presence of superacid catalysts but absence of phenol at the temperature of alkylation was tested. Figure 7 shows only a monomer peak, *i.e.*, 9-octadecene practically does not polymerize in the presence of superacids.

A similar behavior was observed with methyl oleate (Fig. 8), another model compound with only one internal double bond. After 6 h of reaction at 90 °C in the presence of triflic acid, only a very small quantity of dimers of methyl oleate (0.8 %) was obtained.

When triglyceride model compounds with high content of oleic acid (triolein or HOSO) were polymerized under the same reaction conditions, the major com-

ponent after 6 h was the unreacted oil (≈90 %), accompanied by a small amount of oligomeric oil (less than 10 %), as observed in Fig. 9. The composition of this and later mixtures were determined from the GPC peak areas. The reported values are approximate since the detector response factors for each compound are not known.

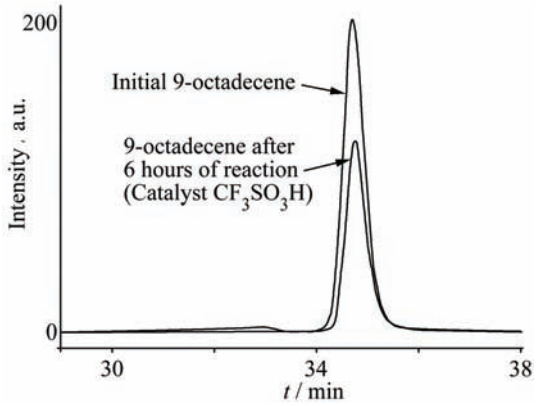

Fig. 7. GPC Chromatogram of 9-octadecene before and after heating for 6 h in the presence of 0.5 % triflic acid.

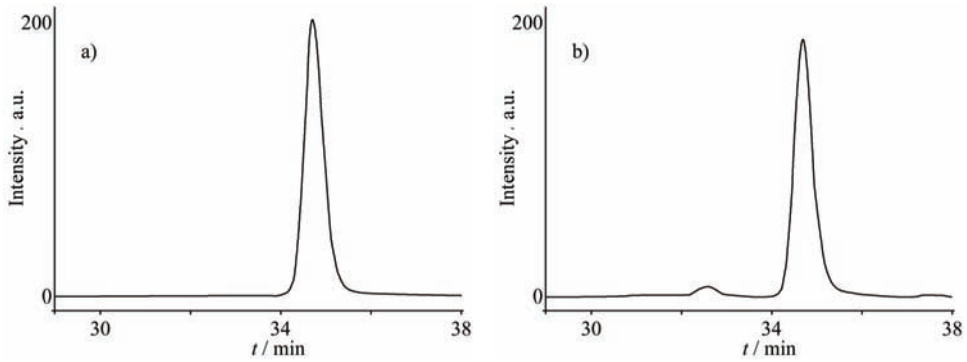

(a) (b)

Fig. 8. GPC Chromatogram of a) methyl oleate before and b) after heating of 6h at 90 °C in the presence of HBF_4 as a catalyst.

These experiments led to the conclusion that fatty acids with a single internal double bond do not undergo cationic polymerization. On the contrary, methyl linoleate, having two double bonds, produced 76 % oligomers and polymers and only 24 % unreacted species after 6 h of heating at 90 °C in the presence of triflic acid. The cationic polymerization of soybean oil with superacids under the same reaction conditions produced around 70 % of polymerized oil, due to the high content of fatty acids with two double bonds (linoleic, 52 %) and three double bonds (linolenic acid, 6–9 %).[29] Thus, the cationic polymerization of vegetable oils is due to fatty acids with two and three double bonds. On the other hand,

both 9-octadecene and methyl oleate are very reactive in the presence of phenols, leading to very good yields of alkylated phenol products (Figs. 10 and 11).

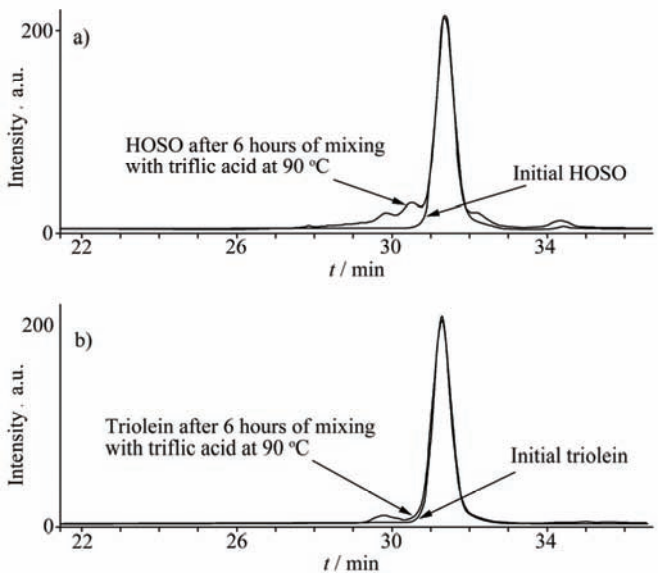

Fig. 9. GPC Chromatogram of a) HOSO and b) triolein before and after mixing for 6 h 90 °C with 1 % triflic acid.

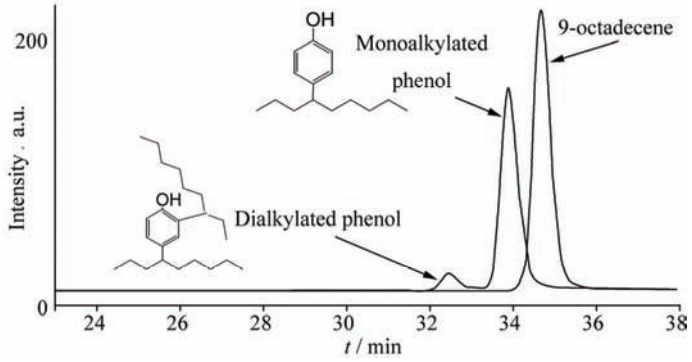

Fig. 10. GPC Chromatogram of 9-octadecene and of alkylated phenol products.

In the case of the phenolation of 9-octadecene, the *IV* decreased from 101 to 10.5 g I_2/100 g, representing a conversion of double bonds of around 90 %. In the case of the phenolation of methyl oleate, the *IV* decreased from 85.7 to 29 g I_2/100g (65 % conversion of the double bonds). The preferred sites for aromatic ring substitution in the Friedel–Crafts alkylation of phenols are the *ortho* and *para* positions (phenol is a trifunctional compound in alkylation reactions having two *ortho* positions and one *para* position available for alkylation). Since the

model compounds with only one internal double bond (9-octadecene, methyl oleate) did not produce oligomers or polymers in the absence of phenol under the same reaction conditions, the only explanation for the formation of oligomers in the alkylation reaction of phenol with 9-octadecene is the Friedel–Crafts mono- and dialkylation of the aromatic ring and mono-, di- and trialkylation in the case of methyl oleate. Both chromatograms presented in Figs. 10 and 11 show the formation of small quantities of di- or even trialkylated products. By analogy, it is possible that during cationic polymerization of oils, di-substitution of the phenolic ring occurs to a small extent, as shown in Scheme 6.

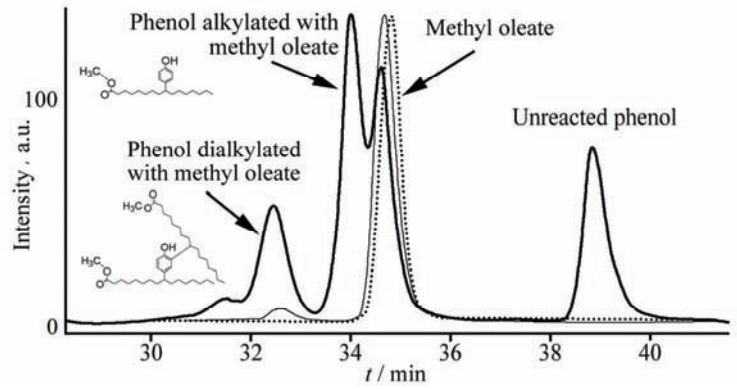

Fig. 11. GPC Chromatograms of methyl oleate, methyl oleate heated with triflic acid (thin line) and phenol alkylated with methyl oleate.

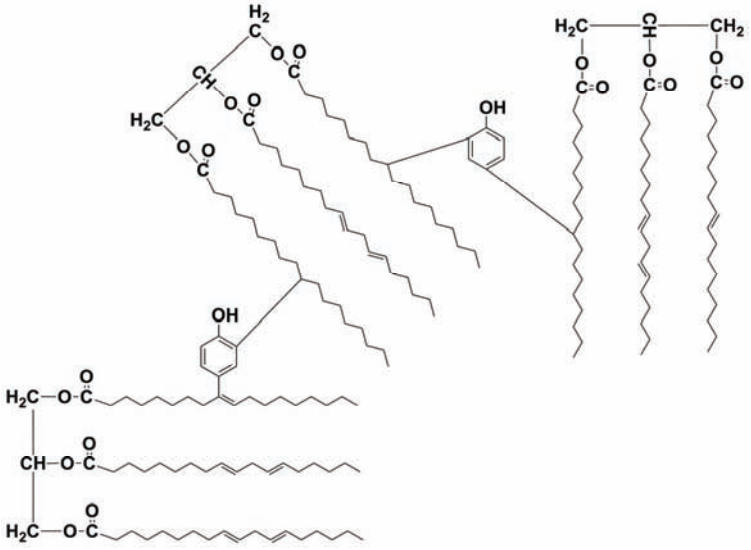

Scheme 6. Formation of vegetable oil oligomers as a consequence of phenol di-alkylation reactions.

Alkylation of phenols with model compounds revealed that the reaction proceeds predominantly with fatty acids having only one internal double bond (oleic acid). Thus, the best oils for Friedel–Crafts alkylation of phenols are those with a high content of oleic acid. The behavior of fatty acids with two or three double bonds under the same reaction conditions is different. Both linoleic and linolenic acids have bis-allylic positions (Scheme 7).

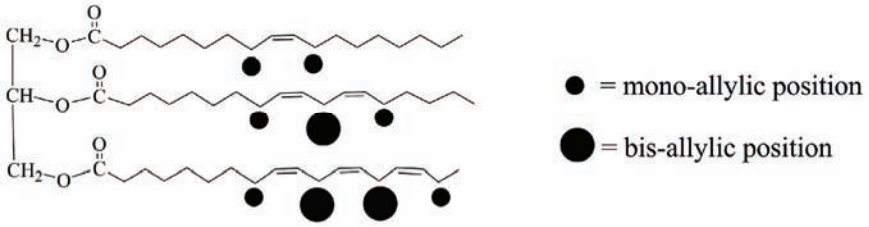

Scheme 7. Mono-allylic and bis-allylic positions in soybean oil.

Hydrogen atoms from these bis-allylic positions are easily transferred (as hydride anions) to the carbocations formed by the addition of protons to double bonds (Scheme 2a). As a consequence, very stable allyl cations of low reactivity due to resonance hybrids are formed (Scheme 8). Allyl cations easily form conjugated double bonds which participate in Diels-Alder reactions.

a)

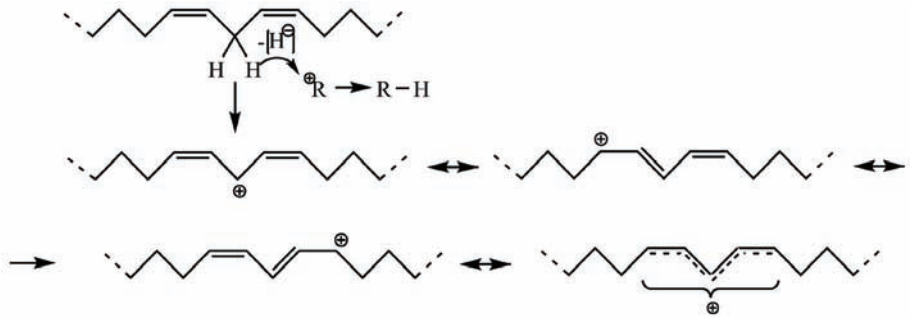

b)

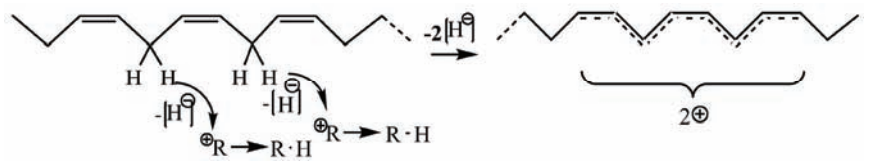

Scheme 8. Formation of stable and low reactivity allyl cations by transfer of bis-allylic hydrogens to carbocations in linoleic and linolenic acids.

Thus, the alkylation of phenols is due to the fatty acids with only one double bond and the polymerization of the oils is due to the fatty acids with two or three internal double bonds and to a small extent due to the phenol di-alkylation reaction.

The most important conclusion of these experiments is that the final product of the Friedel–Crafts alkylation of phenol with the double bonds of vegetable oils is a complex mixture of a polymeric vegetable oil containing phenol units (30–60 %), fatty acid phenyl ester (<10 %) and unreacted vegetable oil (≈30 %), as is displayed in Scheme 9.

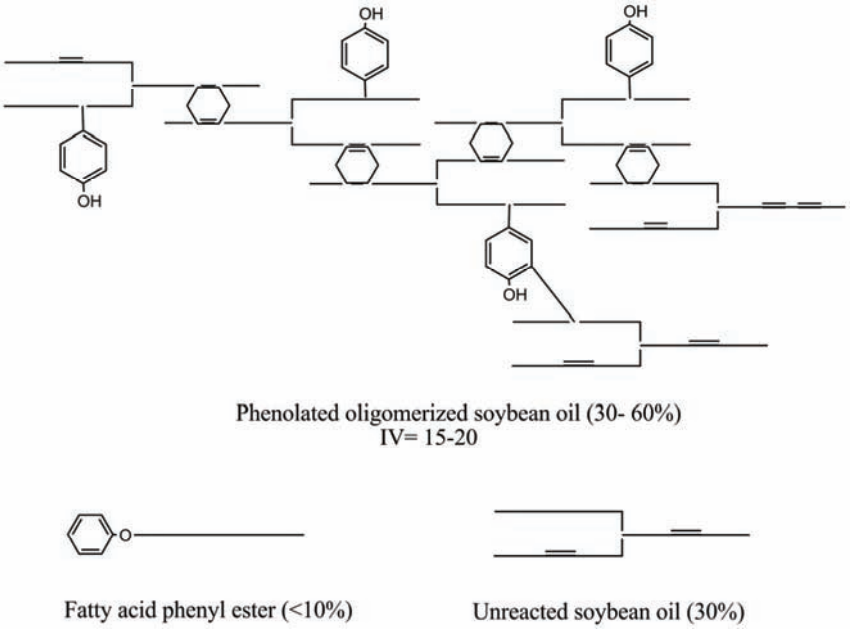

Scheme 9. Composition of the product resulting from the alkylation of phenol with soybean oil.

CONCLUSIONS

The alkylation of phenols with vegetable oils in the presence of a superacid as a catalyst is a process consisting of two simultaneous reactions: the cationic polymerization of the oils and Friedel–Crafts alkylations.

The product is a complex mixture of alkylated phenol oligomers, fatty acid phenyl esters and unreacted vegetable oil.

The fatty acid structures with one internal double bond (18:1) are more reactive in the alkylation of phenols than the structures with two (18:2) or three (18:3) non-conjugated double bonds. Thus, oils with a high oleic content are much better reagents for phenol alkylation than soybean or linseed oils.

Fatty acids with two non-conjugated double bonds (linoleic) or three non--conjugated double bonds (linolenic) lead preferentially to oligomers and polymers by Diels–Alder reactions and to a lesser extent to alkylated products.

Transfer reactions of carbocations with the bis-allylic hydrogens of 18:2 and 18:3 fatty acids lead to stable and low reactivity allyl cations, inefficient in the alkylation of the phenyl nucleus, but very efficient in the polymerization of oils by Diels–Alder reactions.

The dialkylation reaction of phenols proceeds simultaneously with the cationic polymerization of oils leading to the formation of oligomers and polymers. The phenol rings may link two or more triglyceride units.

Ester bonds are not inert in the presence of phenols, resulting in the formation of phenyl esters to a small extent (<10 %) by transesterification of triglyceride ester bonds with phenols.

The synthesized phenolated vegetable oils are suitable for the preparation of new valuable compounds, such as bio-based aromatic-aliphatic polyols for the synthesis of polyurethanes (by propoxylation, ethoxylation and Mannich reactions); as intermediates for the synthesis of phenol–aldehyde resins with high vegetable oil content, such as bio-based antioxidants, *etc*.

Acknowledgment. This work was supported by research funding from the U.S. Department of Agriculture, Award No. 2008-38924-19200.

И З В О Д

БИЉНА УЉА МОДОФОКОВАНА ФЕНОЛОМ

MIHAIL IONESCU и ЗОРАН С. ПЕТРОВИЋ

Pittsburg State University, Kansas Polymer Research Center, 1701 South Broadway, Pittsburg, Kansas, 66762, USA

У овом раду је приказана синтеза нових биоматеријала модификованих фенолом који су погодни за израду полиуретана. Изучавана је реакција алкиловања фенола различитим уљима биљног порекла у присуству суперкиселина (HBF_4, “triflic” односно трифлуорометансулфонске киселине) као катализатора. Кинетика реакције је праћена преко смањења садржаја двоструких веза (јодни број) током времена. Да би се боље разумео и објаснио механизам реакције, алкиловање фенола је анализирано коришћењем модел једињења. Као модел једињења са једном унутрашњом двоструком везом су послужили 9-октадецен и метил-олеат, а једињења са три двоструке везе су била три-олеати, као и шафраново уље са великим садржајем олеинске киселине (82 %). Показано је да су масне киселине са само једном двоструком везом као што је олеинска киселина најпогодније за алкиловање фенола. У присуству масних киселина са две двоструке везе (линолна киселина) и три двоструке везе (линолеинска киселина) одиграва се полимеризација уља преко Дилс–Алдерове реакције, што смањује степен одигравања реакције и принос фенил–алкилованих једињења. Производи реакције алкиловања фенола биљним уљима су комплексана смеша фенола алкилованих полимеризованим уљима (30–60 %), фенолних естара насталих трансестерификацијом фенола са триглицеридима (<10 %) и непрореаговалих уља (30 %). Фенилована биљна уља могу се посматрати као нове ароматско–алифатске биосировине погодне за израду полиола за поли-

уретане (пропоксиловањем, етоксиловањем, Mannich-овом реакцијом), или као интермедијери у производњи фенолних смола или као антиоксиданси.

(Примљено 20. августа, ревидирано 8. децембра 2010)

REFERENCES

1. Z. S. Petrović, K.-H. Hong, W. Shirley, M. Ionescu, *Polym. Prepr. (Am. Chem. Soc., Div. Polym. Chem.)* **46** (2005) 294
2. K.- H. Hong, *M. Sc. Thesis*, Pittsburg State University, 2004
3. Z. S. Petrović, A. Guo, W. Zhang., *J. Polym. Sci. A* **34** (2000) 4062
4. Z. S. Petrović, A. Guo (Pittsburg State University) US Pat. 6,107,433 (2000)
5. Z. S. Petrović, A. Zlatanić, C. C. Lava, S. Sinadinović-Fiser, *Eur. J. Lipid. Sci. Tech.* **104** (2002) 293
6. A. Zlatanić, Z. S. Petrović, K. Dušek, *Biomacromolecules* **3** (2002) 1048
7. A. Zlatanić, C. Lava, W. Zhang, Z. S. Petrović, *J. Polym. Sci. B* **42** (2004) 809
8. T. Abraham, J. Malsam, X. A. Guo, M. Ionescu, I. Javni, Z. S. Petrović, WO 2007127379 (2007)
9. B. Devassy, G. V. Shanbhag, S. P. Mirajkar, W. Bőringer, J. Fletcher, S. B. Halligudi, *J. Mol. Catal. A*, **233** (2005) 141
10. A. de Klerk, R. J. J. Nel, *Ind. Eng. Chem. Res.* **46 (**2007) 7066
11. B. Chaudhuri, M. Sharma, *Ind. Eng. Chem. Res.* **30** (1991) 227
12. N. Farhad, *Bisphenol A and Alkylated phenols*, SRI Process Economics Program Report 192, SRI: Menlo Park, CA, USA, 1988
13. M. Arne, *Nonionic Surfactants*, SRI Process Economics Program Report 168, SRI-Menlo Park, CA, USA, 1984
14. V. L. Larimer, U.S. Pat. 3,468,920 (1969)
15. M. Inoue, K. Nanaumi, M. Nomoto, T. Horiuchi, U.S. Pat. 5,380,789 (1995)
16. J. B. Niederl, S. Natelson, *J. Am. Chem. Soc.* **53 (**1931) 272
17. J. B. Niederl, R. A. Smith, M. E. McGreal, *J. Am. Chem. Soc.* **53** (1931) 3390
18. J. B. Niederl, C. Liotta, *J. Am. Chem. Soc.* **55** (1933) 3025
19. W. C. Ault, E. Abner, U.S. Pat. 3, 192, 239 (1965)
20. F. O. Barrett, C. G. Goebel, U.S. Pat. 3,074,983 (1963)
21. N. B. Niederl, U.S. Pat. 2,082,459 (1937)
22. W.C. Ault, A. Eisner, *J. Am. Oil Chem. Soc.* **39 (**1962) 132
23. A. Eisner, T. Perlstein, W. C. Ault, *J. Am. Oil. Chem. Soc.* **39 (**1962) 290
24. *IUPAC 2,205/1, in Standard Methods for the Analysis of Oils, Fats and Derivatives*, Blackwell Scientific Publications, London, 1992
25. M. Attina, F. Cacace, G. Ciranni, P. Giacomello, *J. Am. Chem. Soc.* **99** (1977) 5022
26. P. Kovacic, J. Hiller, *J. Org. Chem.* **30** (1965) 1581
27. P. A. Spanninger, J. L. von Rosemberg, *J. Am. Chem. Soc.* **94** (1972) 1970
28. P. A. Spanninger, J. L. von Rosemberg, *J. Am. Chem. Soc.* **94** (1972) 1973
29. M. Ionescu, Z. S. Petrovic, in *Proceedings of 101st American Oil Chemists Society Annual Meeting & Expo*, (2010), Phoenix, AZ, USA, , 2010, p. 8
30. M. Ionescu, Z. S. Petrović, U.S. Pat. 7,501,479 (2009).

Journal of the Serbian Chemical Society
JSCS-info@shd.org.rs • www.shd.org.rs/JSCS
J. Serb. Chem. Soc. 76 (4) 607–624 (2011) UDC 667.2+541.42:66.081+582.998.2+54–145.2
JSCS–4145 *Original scientific paper*

Removal of Orange 16 reactive dye from aqueous solutions by waste sunflower seed shells

DANIELA SUTEU[1]*, CARMEN ZAHARIA[2] and TEODOR MALUTAN[3]

[1]Technical University "Gh. Asachi", Faculty of Chemical Engineering and Environmental Protection, Department of Organic and Biochemical Engineering, 71A Blv. Prof. D. Mangeron, 700050, Iasi, [2]Technical University "Gh. Asachi", Faculty of Chemical Engineering and Environmental Protection, Department of Environmental Engineering and Management, 71A Blv. Prof. D. Mangeron, 700050, Iasi and [3]Technical University "Gh. Asachi", Faculty of Chemical Engineering and Environmental Protection, Department of Natural and Synthetic Polymers, 71A Blv. Prof. D. Mangeron, 700050, Iasi, Romania

(Received 21 July, revised 1 October 2010)

Abstract: In this work, the use of an agro-industrial waste, *i.e.*, sunflower seed shells, was investigated as a sorbent for the removal of Orange 16 reactive dye from aqueous environments. Batch experiments were performed as a function of pH, sorbent dose, dye concentration, temperature and contact time. The percent dye removal increased with increasing sorbent dose and temperature of the aqueous solution, and decreased with increasing dye concentration; the required contact time was five hours. The Freundlich, Langmuir, Dubinin–Radushkevich and Tempkin adsorption isotherms were used to describe the equilibrium sorption data and to determine the corresponding isotherm constants. The thermodynamic parameters, ΔG, ΔH and ΔS, were also determined. These parameters indicated that the sorption of reactive dye onto sunflower seed shells was a spontaneous, endothermic and entropy-driven process. The kinetic data were evaluated by pseudo-first order, pseudo-second order and intra-particle diffusion kinetic models. The results of the kinetic study indicated that the sorption of Orange 16 reactive dye onto sunflower seed shells is a complex process and both chemical surface sorption and intra-particle diffusion contribute to the rate-limiting step. Therefore, the sunflower seed shell showed itself to be a promising cheap sorbent for the decolourization of aqueous coloured solutions or effluents.

Keywords: sorption; sunflower seed shell; reactive dye; Orange 16; equilibrium study.

* Corresponding author. E-mail: danasuteu67@yahoo.com
doi: 10.2298/JSC100721051S

INTRODUCTION

The present environment protection policy imposes, among other requirements, not only the ensuring of water quality and protection of all water resources (together with the treatment technologies of industrial or municipal wastewater), but also the integrated management of wastes in the larger context of the depletion of raw materials as priority directions for the recognized organisms or organisations, both on the international and European level. In this context, an attempt was made to combine these two priorities: wastewater treatment and waste valorisation by solving the water depollution problem (water decolourization) using an industrial waste as an adsorptive material.

In the industrial sector, a high water consumer and wastewater producer is the textile industry, mainly textile chemical finishing processing. These industrial wastewaters have a very complex and heterogeneous composition, containing both inorganic and organic compounds in different amounts. For their treatment before discharge into the sewage system or for recycling in technological processes, many different methods, such as adsorption, ion exchange, reverse osmosis, chemical oxidation, precipitation, coagulation–flocculation, extraction and gas stripping, *etc*. have been implemented.[1–6] Many of these procedures are often complicated and time consuming, generate mud or other toxic wastes and may be ineffective or expensive for dilute dye systems.

From these procedures, adsorption is highlighted because of its numerous advantages, such as easiness of achievement and reduced implementation costs.[5] However, the most important advantage in dye removal is the possibility to employ a large variety of adsorptive materials that can be selected based on the known structure of the textile dye. These materials can be synthetic (ion exchange polyamides, polyacrylonitrile fibres, celluloses, ion exchanger resins) and/or natural (peat, seashell, algae, lignite, wood, *etc*.).[1,5,7–11] The high costs of adsorbent preparation re-directed research to the testing of low cost materials, included in the category of "non-conventional" or "low cost" materials, such as: *i*) industrial/agricultural/domestic waste or industrial/agricultural by-products (ash, sludge, sawdust, textile fibbers, mud, bark, seed, husk, straw, *etc*.) and *ii*) natural materials.[5,11–15] The important advantages are: ease of preparation, potentially simple and economic "end-of-pipe" solution to the challenges set by new legislation covering effluent discharges, especially textile effluents.

Thus, the sorption of reactive dyes (*i.e*., a reduction of the textile dye content in final textile effluents to a maximum of 200 mg dye L^{-1}) by agricultural by-products and wastes has been intensively studied and some of the obtained data are summarized in Table I. These sorptive materials can be used in their natural form or can be transformed into charcoal. The sorption capacity depends on the dye concentration in solution, temperature, and sorbent composition.

The results of these studies suggest that sorption onto agricultural by-products and wastes are progressing towards a perspective method.

TABLE I. Application of agricultural wastes as biosorbent for removal of different dyes

Type of agricultural waste	Retained dyes	Sorption capacity, q / mg g^{-1}	Ref.
Almond shell	Rhodamine 6G	32.6 (20 °C)	16
Sunflower seed hull (*Helianthus annuus* L.)	Methyl violet	92.59 (30 °C)	17
Sunflower seed shell	Reactive black 5	0.873	18
Palm shell powder	Methylene blue	121.5 (25 °C)	19
	Rhodamine 6G	105.0 (25 °C)	
Dehydrated peanut hull	Methylene blue	(92.0–108.0) (25 °C)	20
Untreated olive pomace	Reactive red 198	52.21 (20 °C)	21
Sawdust, two size fractions:	Brilliant red HE-3B	11.61 (20 °C)	22
SD-1 (particle size 1–2 mm)	Methylene blue	7.215 / 14.025 (20 °C)	
SD-2 (powder <0.1 mm)	Rhodamine B	7.309 / 10.764 (20 °C)	
	Crystal violet	12.594 / 20.877 (20 °C)	

Therefore, this paper presents the results of a study concerning the utilization of sunflower seed shells (agricultural waste) as a low-cost sorbent for the decolourization of different textile effluents which contain high molecular weight synthetic textile dyes (*i.e.*, to a maximum of 50–200 mg dye L^{-1} in the final textile effluents). Moreover, the operational parameters of the sorption process were established. In addition, equilibrium, kinetic and thermodynamic studies were performed in order to establish all favourable conditions for the uptake of reactive dyes with large molecules.

EXPERIMENTAL

Materials and reagents

Sunflower seed shell was procured from the local oil industry. The seed shells were air-dried at room temperature for two days. Afterwards, they were grounded and sieved to obtain a particle size of 0.8 mm and stored in a plastic bottle for further use. No other chemical or physical treatments were used. The constituents of the sunflower shells were cellulose (≈ 20 %), lignin (≈ 23 %), pentosan (≈ 12 %), hexosane (≈ 23 %), polyuronic acids (≈ 6 %), furfurol (≈ 9 %) and SR (solid residues) obtained from a total hydrolysis (≈ 56 %).

The commercial textile reactive Orange 16 dye ($C_{22}H_{17}O_{11}N_3S_3Na_2$, MW = 617.54, λ_{max} = = 495 nm,) was used. Working solutions with concentration of 24.7–197.6 mg L^{-1} were prepared by appropriate dilution with bidistilled water of a stock solution (500 mg L^{-1}).

Equilibrium studies

Sorption experiments were performed under batch conditions by suspending weighed samples of sorbent (usually 0.3 g) in 25 mL of aqueous dye solution of known initial concentration in flasks placed in a thermostated bath at the desired temperature. The initial solution pH was adjusted by adding 1 M HCl solution, and measured with a pH/EC/TDS Hanna Instruments pH–ion meter. After a determined time (usually 24 h), the phases were separated and the amount of dye in the supernatant was determined by measurement of the absorbance

at 495 nm, the λ_{max} of the dye, using an UV–Vis digital spectrophotometer, model Jasco V-550, and calculation from a dye calibration curve.

The sorption capacity of the sorbent was evaluated from the amount of sorbed dye, q (mg of per g of sorbent):

$$q=10^{-3}(c_0-c)V/G \quad (1)$$

and from the percent dye removal, $R\%$:

$$R\% = 100(c_0 - c)/c_0 \quad (2)$$

where c_0 and c are the initial and the equilibrium concentration of dye in aqueous solution (mg L^{-1}), respectively, G is the amount of sorbent (g), and V is the volume of the solution (mL).

Equilibrium modelling (sorption isotherms)

The relationship between the amount of sorbed dye and its equilibrium concentration was described by four sorption isotherm equations, *i.e.*, the Freundlich, Langmuir, Dubinin–Radushkevich and Tempkin equations.[23,24] The best-fit equilibrium model was established based on the linear regression correlation coefficients, R^2.

The Freundlich isotherm, one of the most used empirical equations, assumes surface heterogeneity and exponential distribution of the active sites of the sorbent:[24]

$$q = K_F c^{1/n} \quad (3)$$

where K_F and n are constants related to the adsorption capacity and sorption intensity (efficiency), respectively.

The Freundlich constants, K_F and n, were evaluated from the slope and intercept of corresponding plots of the graphical representation of the liniarized equation.

In the Langmuir isotherm model, adsorption is based on the assumption that maximum adsorption corresponds to a monolayer of solute molecules on the sorbent surface, containing a finite number of energetically equivalent sites.[23] The Langmuir Equation can be used in the following form:

$$q = \frac{K_L c q_0}{1 + K_L c} \quad (4)$$

where q_0 is the maximum amount of solute sorbed (mg g^{-1}) and KL is the constant related to the binding energy of solute (L mg^{-1}).

The numerical values of Langmuir constants were evaluated from the graphical presentation of $1/q$ *vs.* $1/c$.

In order to appreciate the nature of the sorption process, physical or chemical, the isotherm data were analyzed by the Dubinin–Radushkevich (DR) model,[24] expressed by the following equation:

$$\ln q = \ln q_0 - B\varepsilon^2 \quad (5)$$

where q_0 is the maximum sorption capacity, B is the activity coefficient related to the mean sorption energy and ε is the Polanyi potential, given by:

$$\varepsilon = RT \ln (1 + \frac{1}{c}) \quad (6)$$

The sorption energy can be determined using the following equation:

$$E = \frac{1}{\sqrt{2B}} \tag{7}$$

The Tempkin equation has the following form:[23]

$$q = \frac{RT}{b_T} \ln K_T + \frac{RT}{b_T} \ln c \tag{8}$$

where b_T is the heat of sorption (kJ mol^{-1}), K_T is the intensity of sorption (L g^{-1}), R is the universal gas constant and T is the absolute temperature.

Kinetic studies

The effect of contact time on the sorption of reactive dye onto sunflower seed shells was determined by the "limited bath" technique. A sample of 0.3 g sorbent was added under stirring to 25 mL of dye solution at pH 1.0 and with an initial concentration of 49.4 mg L^{-1}. The temperature of solutions was maintained at 20 °C. After different contact times (30–400 min), volumes of supernatant were removed for absorbance measurement and calculation of the dye content. The extent of sorption was expressed by the fractional attainment of equilibrium:

$$F = \frac{q_t}{q} \tag{9}$$

where q_t and q (mg g^{-1}) are the amount of dye sorbed at time t and at equilibrium (24 h), respectively.

Kinetic modelling

In order to analyze the sorption of Orange 16 reactive dye onto sunflower seed shells and to understand the dynamics of the sorption process in terms of the rate order, pseudo-first order, pseudo-second order and intra-particle diffusion kinetic models were applied to the experimental data.[16,17,25,26]

The pseudo first-order model (Lagergren, 1898) is usually expressed as:

$$\log (q - q_t) = -\frac{k_1}{2.303} t + \log q \tag{10}$$

where q and q_t are the amounts of sorbed dye (mg g^{-1}) at equilibrium (24 h) and respectively any time t (min), and k_1 is the Lagergren rate constant of the first-order sorption (min^{-1}).

The pseudo-second order model (Ho model, 1999) assumes that the sorption follows a second order mechanism and the rate-limiting step may be chemical sorption involving valence forces or covalent forces between sorbent and adsorbate.[27] The rate of a pseudo-second order reaction is expressed by the equation:

$$\frac{t}{q_t} = \frac{1}{k_2 q^2} + \frac{1}{q} t \tag{11}$$

where k_2 is the rate constant of second order sorption (g mg^{-1} min^{-1}) and $q^2 k_2 = h$ can be regarded as the initial sorption rate (mg g^{-1} min^{-1}) as t approaches zero.

The intra-particle diffusion model (Webber and Morris, 1963) assumes that sorption is a multi-step process involving transport of adsorbate from the aqueous solution to the sorption sites of the sorbent (surface sorption) and the diffusion into pores (intra-particle diffusion). The validity of model is confirmed by linear plots of the Weber and Morris Equation:[28]

$$q = k_p t^{0.5} \tag{12}$$

where k_p is the rate constant for intra-particle diffusion (mg g^{-1} min$^{-0.5}$).

RESULTS AND DISCUSSION

Effect of pH on dye sorption

The effect of pH on the sorption of Orange 16 reactive dye was studied from solutions with different initial dye concentrations and a sunflower seed shells dose of 12 g L^{-1}. The results presented in Fig. 1a show that the removal efficiency was maximal in acidic media (pH > 1) and decreased sharply with increasing solution pH.

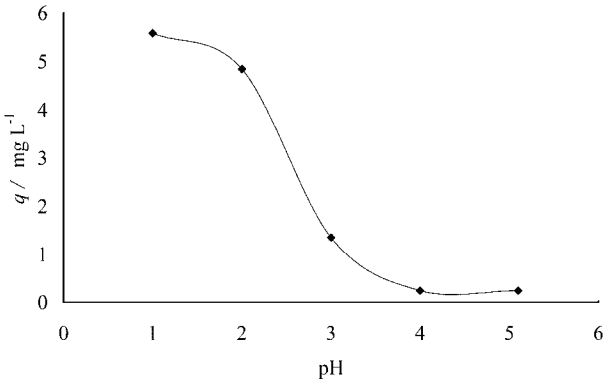

(a)

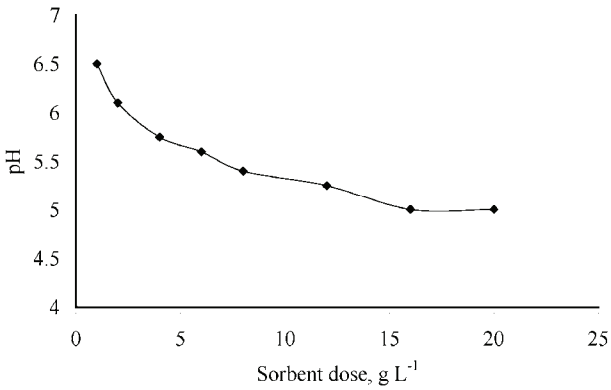

(b)

Fig. 1. a) Effect of pH on the sorption of the reactive dye onto sunflower seed shells. Conditions: 12 g sorbent L^{-1}, 24 h, t = = 25 °C; b) The value of pH_{PZC} (pH of zero charge) for sunflower seed shells.

This behaviour may be correlated with the variation of the sunflower seed shell surface charge in dependence of the solution pH. The pH_{PZC} (pH of zero charge) of sunflower seed shells was determined by the method described by Nouri and Haghseresht[29] (Fig. 1b); the limiting pH 5 was considered as the pH_{PZC} value, when the sorbent surface was neutral. At values of pH < pH_{PZC}, the sorbent surface is positively charged and susceptible to electrostatic interactions with the polar portions of the Orange 16 reactive dye molecules (dissociated

sulphonic groups). At pH > pH_{PZC}, the sorbent surface was negatively charged and was not available to bind the anionic dye.

Effect of sorbent dose on dye sorption

The effect of sorbent dose on the removal of the reactive dye (*R%*) and the sorption capacity (*q*) of sunflower seed shells were examined from solutions containing 86.45 mg dye L^{-1} and pH 1.0 (Fig. 2).

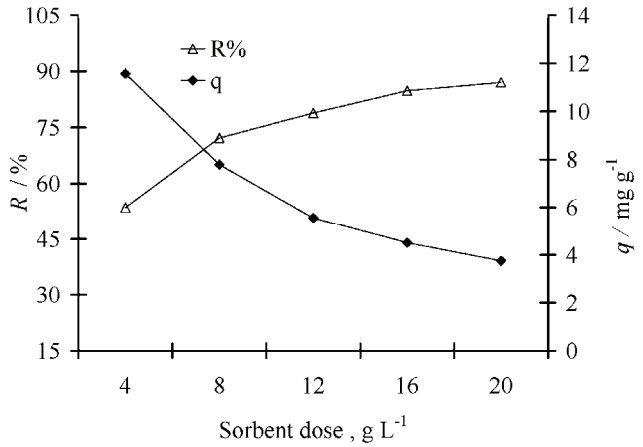

Fig. 2. Effect of sunflower seed shells dose on the sorption of the reactive dye. Conditions: 86.45 mg dye L^{-1}, pH 1.0, 24 h, t = 25 °C.

It can be seen that the increasing of the sunflower seed shells dose from 2 to 20 g L^{-1} increased the percentage of dye removal from 53.53 to 87.07 %, due to the increasing number of available sorption sites. Simultaneously, the amount of reactive dye retained per unit weight of sorbent decreased from 11.57 to 3.75 mg g^{-1}, indicating a moderate sorptive capacity of the sunflower seed shells.

Effect of initial dye concentration and temperature on dye sorption

The effect of initial reactive dye concentration *vs*. the sorption capacity of sunflower seed shells was investigated from solutions of pH 1.0, for a sorbent dose of 12 g L^{-1} and the results are presented in Fig. 3. As can be seen, the amount of dye retained increased with the increasing initial dye concentration.

The amount of sorbed dye per unit mass of sunflower seed shells increased from 1.65 to 13.24 mg L^{-1} when the initial dye concentration was increased from 24.7 to 197.6 mg L^{-1} at 278 K temperature. This is probably due to the enhancement of dye molecules migration into the internal macroporous and mesoporous structure of the sorbent at high initial dye concentrations in the aqueous solutions.

The dye sorption onto sunflower seed shells was also dependent on solution temperature. It can be clearly observed in Fig. 3 that the amount of Orange 16 reactive dye sorbed from solutions of pH 1.0 with different initial dye concen-

trations increased with increasing temperature; the effect being more pronounced at high concentrations.

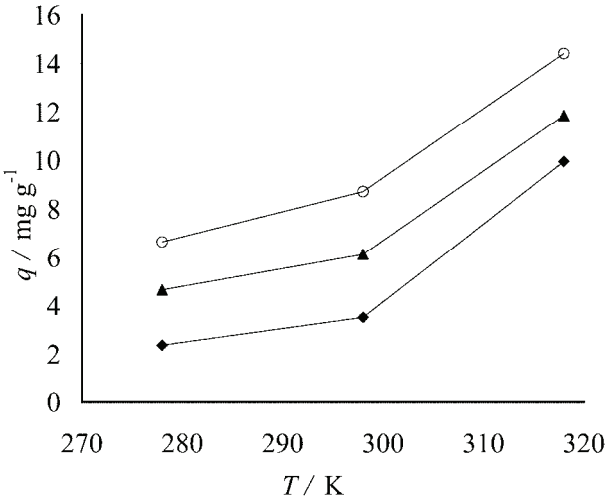

Fig. 3. Effect of the initial dye concentration on the sorption of the reactive dye. Conditions: pH 1.0, 12 g sorbent L^{-1}, 24 h; ○ – c = 37.05 mg L^{-1}; ▲ – c = 86.45 mg L^{-1}; ♦ – c = 123.5 mg L^{-1}.

Effect of contact time on dye sorption

The effect of contact time of the phases on the sorption of Orange 16 reactive dye onto sunflower seed shells is presented in Fig. 4.

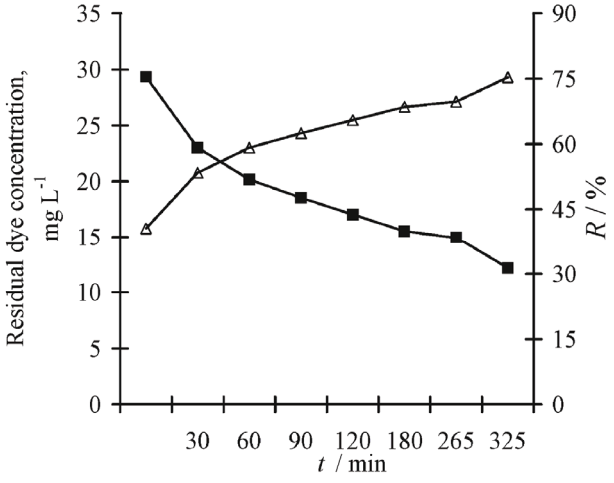

Fig. 4. Effect of the contact time on the removal of Orange 16 reactive dye by sunflower seed shells. Conditions: pH 1.0, 12 g sorbent L^{-1}, 25 °C; ■ – residual dye concentration; Δ – R.

The obtained data showed that the removal of reactive dye was faster in the initial stages of the contact period; the residual concentration of reactive dye in the solution rapidly decreased *vs.* time up to 300 minutes, and thereafter slowly decreases to the equilibrium value. This fact can be explained by the large num-

ber of vacant surface sites available for dye sorption during the initial stages of sorption. The increasing dye removal percent with increasing contact time (Fig. 4) suggests a more rapid dye removal from solutions with higher initial concentrations, because of the increased concentration gradient between the solution and the sorbent surface.

Sorption equilibrium

An analysis of the equilibrium data by fitting them to different isotherm models (Eq. (3)–(5) and (8)) is very important for an estimation of the practical sorption capacity and for optimization of the design of the sorption system. The isotherms of Orange 16 reactive dye sorption onto sunflower seed shells at three temperatures (5, 25 and 45 °C) are presented in Fig. 5.

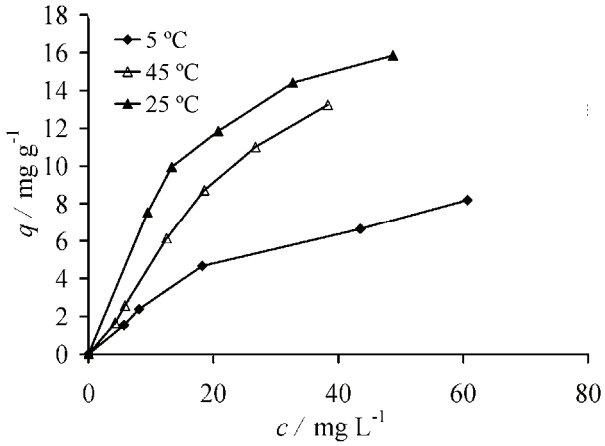

Fig. 5. The sorption isotherms of Orange 16 reactive dye onto sunflower seed shells at three temperatures. Condition: pH 1.0, 12 g sorbent L^{-1}.

In the studied dye concentration range (27.7–197.6 mg L^{-1}), the obtained isotherms were concave to the concentration axis, indicating an affinity for sunflower seed shells and a saturation trend at high dye concentrations. An increase in temperature increased the amount of sorbed dye.

The parameters related to each isotherm, calculated from the intercepts and slopes of the corresponding linear plots (Figs. 6a–6d) together with their correlation coefficients (R^2) are presented in Table II.

As can be seen from Table II, the value of Freundlich parameters, K_F and n, increase with increasing temperature, showing that the sorption of the reactive dye was more favourable at high temperatures. In all cases, the value of n was greater than unity, indicating a beneficial adsorption.

The values of the correlation coefficients from Table II show that the experimental data were better fitted by the Langmuir model of monolayer coverage of the sorbent with reactive dye molecules. This is in accordance with the shape of the sorption isotherms, which correspond to type L2 (Langmuir type) in the Giles

classification.[30] The values of q_0, which reflect the accessibility of sorption sites, and the Langmuir constant K_L, which reflect the binding energy between reactive dye molecules and sunflower seed shells, increase with increasing temperature, indicating that the sorption is an endothermic process.

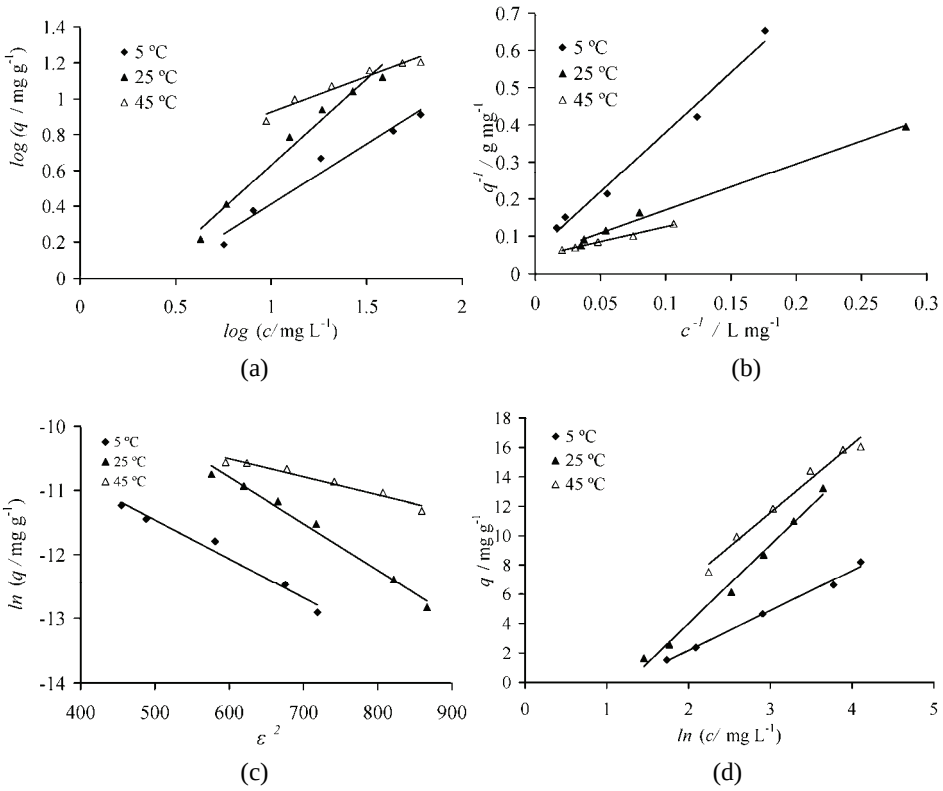

Fig. 6. Freundlich (a), Langmuir (b), DR (c) and Tempkin (d) plots for the sorption of Orange 16 reactive dye onto sunflower seed shells at three temperatures.

The sorption energy determined in the DR equation (Table II) revealed a possible ion exchange mechanism for the reactive dye sorption onto sunflower seed shells (the sorption energy was between 8 and 16 kJ mol^{-1}).[24] Mean free energy values lower than 8 kJ mol^{-1} characterize a physical sorption mechanism, while values between 8 and 16 kJ mol^{-1} indicate an ion exchange mechanism.[24]

The values of the correlation coefficients for the Tempkin isotherm model were between 0.9804 and 0.99 at all studied temperatures, which confirms the better fit of equilibrium data as compared with the Freundlich isotherm model. The Tempkin isotherm takes into account some indirect sorbate–sorbent interactions, and assumes that because of these interactions the heat of sorption is li-

near rather logarithmic, as implied in the Freundlich equation and decreases linearly with coverage.[17,25,31]

TABLE II. Isotherm parameters for the sorption of reactive dye Orange 16 onto sunflower seed shells

Parameter	T / K		
	278	298	318
	Freundlich		
K_F/ (mg g^{-1})(L mg^{-1})$^{1/n}$	0.545	0.4627	3.3799
n	1.486	1.0375	2.516
Linear regression equation	$y = 0.6739x - 0.2623$	$y = 0.9638x - 0.3347$	$y = 0.3974x + 0.5289$
R^2	0.9683	0.9773	0.9495
	Langmuir		
q_0 / mg g^{-1}	17.036	21.74	22.12
K_L / L mg^{-1}	0.0182	0.0206	0.0579
Linear regression equation	$y = 3.2159x + 0.0587$	$y = 1.244x + 0.046$	$y = 0.7807x + 0.0469$
R^2	0.9852	0.9923	0.9884
	Dubinin–Radushkevich (DR)		
q_0 / mg g^{-1}	13.661	1007.406	91.21
B / mol^2 kJ^{-1}	0.0061	0.0073	0.0028
E / kJ mol^{-1}	9.05	8.276	13.36
Linear regression equation	$y = -0.0061x - 8.4122$	$y = -0.0073x - 6.4183$	$y = -0.0028x - 8.8203$
R^2	0.9757	0.9848	0.9576
	Tempkin		
b_T / kJ mol^{-1}	850.67	462.561	569.16
K_T / L g^{-1}	0.301	0.286	0.599
Linear regression equation	$y = 2.7157x - 3.2566$	$y = 5.3562x - 6.7025$	$y = 4.6452x - 2.3738$
R^2	0.9931	0.99	0.9804

Study of thermodynamic parameters

To evaluate the effect of temperature on the Orange 16 reactive dye sorption onto sunflower seed shells and to understand the nature of the sorption, it is necessary to determine the apparent thermodynamic parameters using the values of binding Langmuir constant, K_L (L mol^{-1}), and the Gibbs and van't Hoff equations.[16,32]

The negative values of apparent free energy change (ΔG in the range –27.7 to –21.6 kJ mol^{-1}) indicate that sorption of the reactive dye onto sunflower seed shells is spontaneous and thermodynamically feasible in the studied temperature range (278–318 K). The values of ΔG decreased with increasing tempe-

rature, showing that the spontaneity of sorption process is inversely proportional to the temperature.[25]

The positive value of the enthalpy change (ΔH = 21.0 kJ mol^{-1}) confirmed the endothermic nature of sorption process of Orange 16 reactive dye onto sunflower seed shells.

The positive value of entropy change (ΔS= 152.0 J mol^{-1}K^{-1}) suggests increased randomness at the solid–liquid interface during the sorption of reactive dye and some structural changes in the sorbate and the sorbent.[16] It could be suggested that the driving force of sorption is an entropy effect.

Moreover, the magnitudes of ΔH and ΔG give information about the nature of the sorption process. The literature data indicate that physical sorption is determined by weak forces, and is characterized by ΔH value no higher than 4.2 kJ mol^{-1} and, respectively, ΔG values lower than –16 kJ mol^{-1}; chemical sorption is determined by forces much stronger than those implicated in physical processes, and is characterized by ΔH values higher than 21 kJ mol^{-1} and ΔG values higher than 20 kJ mol^{-1}.[16,32]

The obtained data show that the sorption of Orange 16 reactive dye onto sunflower seed shells occurred by weak physical interaction and ion exchange between the surface of the sorbent and the dye molecules, as a consequence of surface charge on the sorbent at pH values lower than pH_{PZC}. The forces involved in the sorption can range from weak van der Waals forces to electrostatic attractions between the ionized sulphonyl groups of the dye molecule and the positively charged surface of the sunflower shells (SSS):

$$SSS–OH + H^+ + {}^-O_3S–Dye \rightarrow SSS–OH_2^+ \, {}^-O_3S–Dye \quad (12)$$

Infrared study of Orange 16 reactive dye binding onto sunflower seed shells

In order to obtain more information about the mechanism of dye binding onto sunflower seed shells, an infrared analysis was performed. The FTIR spectra of the sunflower seed shells before and after sorption of Orange 16 reactive dye from aqueous solutions of pH 1.0 are presented in Fig. 7.

Sunflower seed shells spectra present many overlapped bands, whose intensity depend on the origin and isolation method.

A comparison between spectra of sunflower seed shells before and after loading with the Orange 16 reactive dye, in accord with literature data, indicates that:

– the appearance of a specific band at 2854.64 cm^{-1} (2924.09 cm^{-1} is specific for the Orange reactive dye) with a different peak height to the corresponding band in the spectrum of seed shells alone in case (1) and the association of seed shell – Orange reactive dye in case (2) suggest the formation of ionic associations between sunflower seed shells and Orange 16 reactive dye;

– at acidic pH values, due to the presence of hydroxyl groups from the lateral chain (*i.e.*, sunflower seed shell – OH + H^+), the sunflower seed shells can be associated in conjugated structures with the reactive dye (^-O_3S–Dye), highlighted by the band of 2854.64 cm^{-1}. The height increase of the specific band at 2854.64 cm^{-1} in the IR spectrum, due to sunflower seed shell – dye association (line 2, Fig. 7), confirms the establishment of ionic bonds between the sunflower seed shells and sorbed dye (a charged organic molecule consisting of polar and non-polar regions);

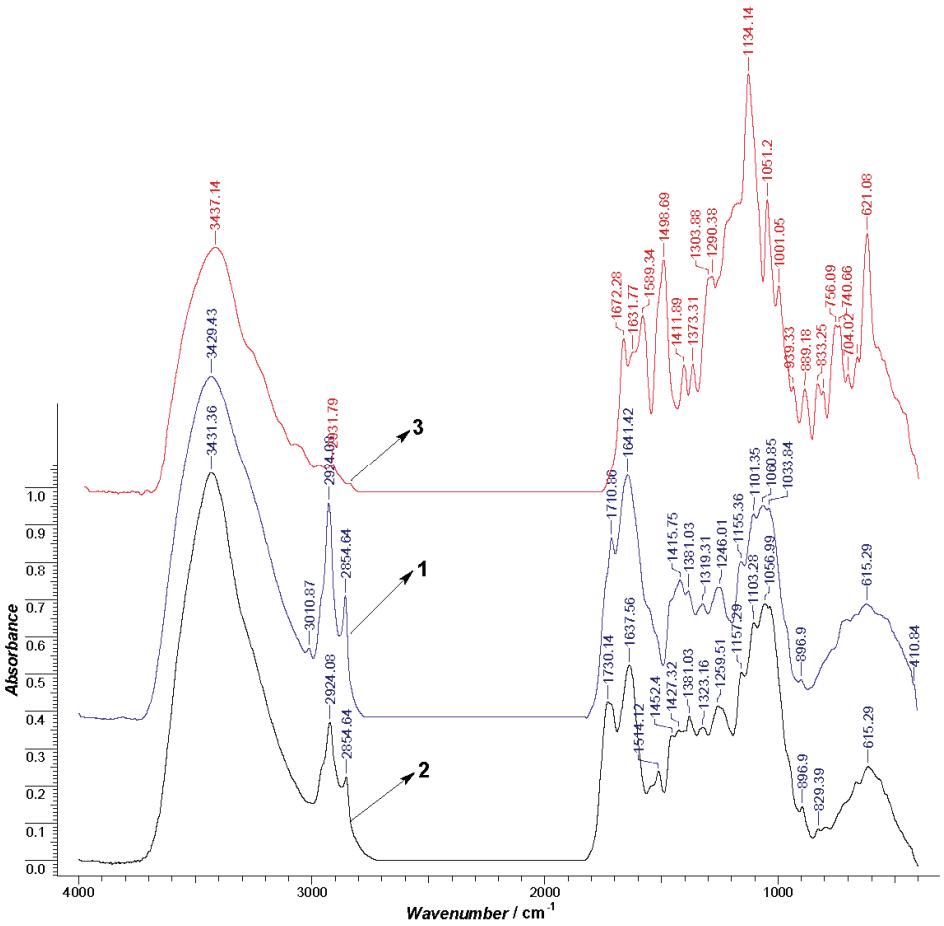

Fig. 7. FTIR Spectra of sunflower seed shells (1), Orange 16-sunflower seed shells (2) and Orange 16 dye (3) samples.

– the intensity and position of peaks assigned to characteristic functional groups from the sunflower seed shells were either minimized or slightly shifted after sorption of the reactive dye; these changes can be attributed to electrostatic

interactions between the positively charged functional groups of the sorbent (oxygen is easily protonated in acidic conditions) and the anionic dye;

– the FTIR spectra suggest that the adsorption mechanism could be considered as a combination of electrostatic interaction and physical sorption.

Kinetics study

It was seen from Fig. 8 that the kinetics of sorption of the tested dye onto sunflower seed shells is composed of two ranges: 1) an initial rapid range in which the sorption was fast on the external surface of the sorbent and the equilibrium was achieved rapidly (within 300 minutes) and 2) a slower second range during which the sorption process of Orange 16 reactive dye onto sunflower seed shells was completed.[25]

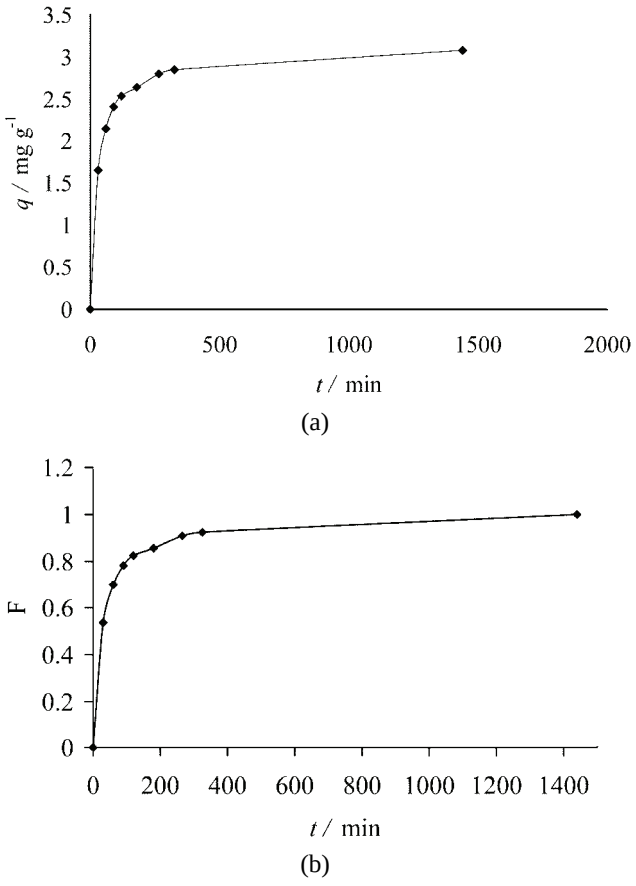

Fig. 8. Effect of contact time on the sorption capacity (a) of sunflower seed shells for Orange 16 fractional attainment of equilibrium (*F*) *vs*. time (b). Conditions: pH 1.0, 12 g sorbent L^{-1}, 25 °C.

The constants of the pseudo first-order model (Lagergren, 1898) calculated from the linear plots of log ($q_e - q$) *vs.* t (Fig. 9) and the corresponding correlation coefficients are presented in Table III. The R^2 value of 0.861 suggested that the Lagergren model was not well fitted in the modelling of kinetic data; also, the estimated values of q_e were not in very good agreement with the experimental ones. The constants of the pseudo-second order model (Ho model, 1999) were determined from plots t/q *vs.* t (Fig. 9) and the corresponding values are presented in Table III.

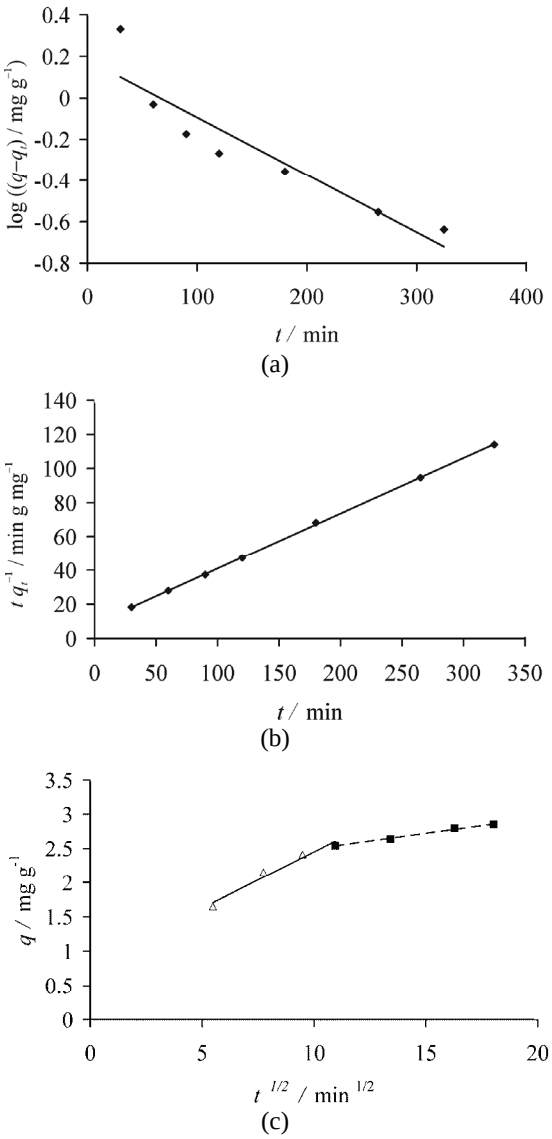

Fig. 9. Pseudo-first (a) and pseudo-second (b) order kinetics and intraparticle diffusion model (c) of Orange 16 reactive dye sorption onto sunflower seed shell: T = 20 °C; pH 1.0; c_0 = 49.4 mg L^{-1}; 12 g sorbent L^{-1}.

TABLE III. The kinetic parameters of the sorption process of Orange 16 reactive dye onto sunflower seed shells

Kinetic model	Parameter	Value
Lagergren model – pseudo-first kinetic model	k_1 / min^{-1}	0.00645
	q_0 /mg g^{-1}	1.529
	R^2	0.861
Ho model – pseudo-second kinetic model	k_2 / g mg^{-1}.min^{-1}	0.0105
	h / mg g^{-1}.min^{-1}	0.1191
	q_0 /mg g^{-1}	3.07
	R^2	0.9998
Intra-particle diffusion model	k_{p1} / mg g^{-1} min$^{-0.5}$	0.1643
	R_1^2	0.9684
	k_{p2} / mg g^{-1} min$^{-0.5}$	0.0456
	R_2^2	0.9903

The extremely high value of the correlation coefficient (Table III) shows a good compliance of the data with the pseudo-second order kinetic model and suggests that chemical sorption instead of mass transfer may be the rate-limiting step for the sorption process. It can be seen in Fig. 9 that the regression does not pass through the origin, which suggests that intraparticle diffusion is not the only rate-limiting step.

It can be observed in Fig. 9c that, after saturation of the surface (within the first 120 min), the data fit a linear equation of the form q *vs.* $t^{0.5}$ ($R_2^2 > R_1^2$), indicating diffusion of sorbate species through the internal porous structure of the sunflower seed shell.

It can be concluded that the sorption of Orange 16 reactive dye onto sunflower seed shell is a complex process and both surface sorption and intraparticle diffusion contributes to the rate limiting steps.

CONCLUSIONS

Sunflower seed shell as a waste material can be considered an effective sorbent for the removal of Orange 16 reactive dye from aqueous solutions at pH 1.0.

The sorption of reactive dye onto sunflower seed shell is dependent on the initial solution pH, the dose of sunflower seed shell, the dye concentration and temperature. The best pH value was 1 for the sorption of the tested anionic dye. The sorption of dye increases with increasing of the sunflower seed shell dose, dye concentration and temperature.

The experimental data were analyzed using Freundlich, Langmuir, Dubinin–Radushkevich and Tempkin models. The Langmuir isotherm model characterized the equilibrium sorption data the best; the monolayer sorption capacities were 21.7 and 22.1 mg g^{-1} at 25 and 45 °C, respectively. The value of sorption energy determined by the DR model suggested a combined mechanism of phy-

sical sorption and electrostatic interactions between sorbent surface and the dye molecules.

The values of thermodynamic parameters suggest a feasible, spontaneous and endothermic sorption process between the surface of the sorbent and the dye molecules.

The kinetic of the reactive dye sorption onto sunflower seed shell was found to follow a pseudo-second-order rate equation. The Orange 16 reactive dye sorption onto sunflower seed shell is a complex process and both chemical surface sorption and intraparticle diffusion contribute to the rate-limiting step.

A comparison between the obtained values of the maximum sorption capacity of the sunflower seed shell for reactive dye removal with those reported in literature for other ligno–cellulose sorbents (Table I) confirms the conclusion that this material has a good sorption capacity and can be used for the treatment of coloured wastewaters or effluents containing moderate amount of dye.

ИЗВОД

УКЛАЊАЊЕ РЕАКТИВНЕ БОЈЕ ОРАНЖ 16 ИЗ ВОДЕНОГ РАСТВОРА ОТПАДНИМ ЉУСКАМА СУНЦОКРЕТА

DANIELA SUTEU[1], CARMEN ZAHARIA[2] и TEODOR MALUTAN[3]

[1]Technical University "Gh. Asachi", Faculty of Chemical Engineering and Environmental Protection, Department of Organic and Biochemical Engineering, 71A Blv. Prof. D. Mangeron, 700050, Iasi, [2]Technical University "Gh. Asachi", Faculty of Chemical Engineering and Environmental Protection, Department of Environmental Engineering and Management, 71A Blv. Prof. D. Mangeron, 700050, Iasi и [3]Technical University "Gh. Asachi", Faculty of Chemical Engineering and Environmental Protection, Department of Natural and Synthetic Polymers, 71A Blv. Prof. D. Mangeron, 700050, Iasi, Romania

У овом раду испитана је употреба агроиндустријског отпада у виду љуски сунцокрета као сорбента за уклањање реактивне боје Оранж 16 из водених средина. Изведени су шаржни експерименти у функцији pH, дозе сорбента, концентрације боје, температуре и времена контакта. Проценат уклоњене боје увећава се са растом дозе сорбента и температуре воденог раствора, а опада са порастом концентрације боје: потребно време контакта је пет часова. Коришћене су адсорпционе изотерме Freundlich, Langmuir, Dubinin–Radushkevich и Tempkin за описивање података о сорпционој равнотежи и за одређивање одговарајућих изотермских константи. Такође су одређени термодинамички параметри (ΔG, ΔH и ΔS), који су указали на то да је сорпција ове боје на љускама сунцокрета спонтан и ендотермички процес вођен ентропијом. Кинетички подаци су тестирани моделима псеудопрвог, псеудодругог реда и моделом интрачестичне дифузије. Резултати кинетичког проучавања указују на то да је сорпција Оранж 16 на љускама сунцокрета сложен процес, у којем ступњу ограничавања брзине доприносе и површинска хемисорпција и интрачестична дифузија. Стога, љуска сунцокрета може бити обећавајући јефтин сорбент за обезбојавање водених раствора или ефлуената.

(Примљено 21. јула, ревидирано 1. октобра 2010)

REFERENCES

1. D. Suteu, C. Zaharia, D. Bilba, R. Muresan, A. Popescu, A. Muresan, *Textile Ind.* **60** (2009) 254

2. Y. Anjaneyulu, N. Sreedhara Chary, D. Samuel Suman Raj, *Rev. Environ. Sci. Bio/Technol.* **4** (2005) 245
3. R. Babu, B. Parande, A. K. Prem, T. Kumar, *J. Cotton Sci.* **11** (2007) 141
4. M. Surpateanu, C. Zaharia, *Environ. Eng. Manage. J.* **3** (2004) 629
5. S. J. Allen, B. Koumanova, *J. University Chem. Technol. Metall. (Bulgary)* **40** (2005) 75
6. E. Forgacs, T. Cserhati, G. Oros, *Environ. Internat.* **30** (2004) 953
7. D. Suteu, D. Bilba, C. Zaharia, A. Popescu, *Scientific Study & Research*, **IX** (2008) 293
8. D. Suteu, C. Zaharia, *Bull. Inst. Polytech. Iasi* **LIV** (**LVIII**) (2008) 81
9. D. Suteu, C. Zaharia, M. Harja, in *Proceeding of International Scientific Conference*, Gabrovo, Bulgaria, 2008, p. 475
10. G. Crini, *Bioresour. Technol.* **97** (2006) 399
11. V. K. Gupta, S. Suhas, *J. Environ. Manage*. **90** (2009) 2313
12. G. Crini, P. M. Badot, *Prog. Polym. Sci*. **33** (2008) 399
13. D. Suteu, I. Volf, M. Macoveanu, *J. Environ. Eng. Manage.* **5** (2006) 119
14. D. Suteu, C. Zaharia, D. Bilba, M. Surpateanu, *Bulletin of the Transilvania University of Brasov* **IV** (2007) 692
15. D. Suteu, C. Zaharia, A. Muresan, R. Muresan, A. Popescu, *J. Environ. Eng. Manage.* **8** (2009) 1471
16. H. B. Senturk, D. Ozdes, C. Duran, *Desalination* **252** (2010) 81
17. B. H. Hameed, *J. Hazard. Mater.* **154** (2008) 204
18. J. F. Osma, V. Saravia, J. L. Toca-Herrera, S. R. Couto, *J. Hazard. Mater*. **147** (2007) 900
19. G. Sreelatha, P. Padmaja, *J. Environ. Prot. Sci.* **2** (2008) 63
20. D. Ozer, G. Dursun, A. Ozer, *J. Hazard. Mater.* **144** (2007) 171
21. T. Akar, I. Tosun, Z. Kaynak, E. Ozkara, O. Yeni, *J. Hazard Mater.* **166** (2009) 1417
22. V. Jaikumar, V. Ramamurthi, *Int. J. Chem.* **1** (2009) 2
23. M. Wawrzkiewicz, Z. Hubicki, *J. Hazard. Mater.* **172** (2009) 868
24. D. Kavith, C. Namasivayam, *Bioresour. Technol.* **98** (2007) 14
25. R. Han, J. Zhang, P. Han, Y. Wang, Z. Zhao, M. Tang, *Chem. Eng. J.* **145** (2009) 496
26. S. Senthilkumaar, P. Kalaamani, K. Porkodi, P. R. Varadarajan, C. V. Subburaam, *Bioresour. Technol.* **97** (2006) 1618
27. Y. S. Ho, G. McKay, *Water Res.* **34** (2000) 735
28. W. J. Weber Jr., J. C. Morris, *J. Sanit. Eng. Div. ASCE* **89** (1963) 31
29. S. Nouri, F. Hageseresht, *Adsorption* **10** (2004) 79
30. C. H. Giles, T. H. MacEwan, S. Nakhwa, D. J. Smith, *J. Chem. Soc. London* (1960) 3973
31. K. Vijayaraghavan, T. V. N. Padmesh, K. Palanivelu, M. Velan, *J. Hazard. Mater.* **133** (2006) 304
32. C. H. Weng, Y. C. Sharma, S. H. Chu, *J. Hazard. Mater.* **155** (2008) 65.

Journal of the Serbian Chemical Society
JSCS-info@shd.org.rs • www.shd.org.rs/JSCS
J. Serb. Chem. Soc. 76 (4) 625–641 (2011) UDC 669.04+669.3:504.53.054+669.4/.5(497.11)
JSCS–4146 *Original scientific paper*

Multi-criteria analysis of soil pollution by heavy metals in the vicinity of the Copper Smelting Plant in Bor (Serbia)

DJORDJE NIKOLIĆ[1]*, NOVICA MILOŠEVIĆ[2], ŽIVAN ŽIVKOVIĆ[1], IVAN MIHAJLOVIĆ[1#], RENATA KOVAČEVIĆ[2] and NEVENKA PETROVIĆ[2]

[1]*University of Belgrade, Technical Faculty in Bor, Vojske Jugoslavije 12, 19210 Bor and* [2]*Institute for Mining and Metallurgy Bor, Zeleni bulevar 35, 19210 Bor, Serbia*

(Received 28 March, revised 23 September 2010)

Abstract: This study highlights the consequences on soil pollution of one hundred years of manufacturing in the Copper Mining and Smelting Complex RTB-Bor (Serbia). Soil sediments were taken *via* a probe from the surface layer of the soil at twelve different measuring points. The measuring points were all within 20 km of the smelting plant, which included both urban and rural zones. Soil sampling was performed using a soil core sampler in such way that a core of a soil of radius 5 cm and depth of 30 cm was removed. Subsequently, the samples were analyzed for pH and heavy metal concentrations (Cu, Pb, As, Cd, Mn, Ni and Hg) using different spectrometric methods. The obtained results for the heavy metal contents in the samples show high values: 2,540 mg kg^{-1} Cu; 230 mg kg^{-1} Pb; 6 mg kg^{-1} Cd; 530 mg kg^{-1} Ni; 1,300 mg kg^{-1} Mn; 260 mg kg^{-1} As and 0.3 mg kg^{-1} Hg. In this study, critical zones of polluted soil were identified and ranked according to their metal contents by the multi-criteria decision method Preference Organization Method for Enrichment Evaluation/Geometrical Analysis for Interactive Assistance – PROMETHEE/GAIA, which is the preferred multivariate method commonly used in chemometric studies. The ranking results clearly showed that the most polluted zones are at locations holding the vital functions of the town. Therefore, due to the high bioavailability of heavy metals through complex reactions with organic species in the sediments, consequences for human health could drastically emerge if these metals enter the food chain.

Keywords: heavy metals; soil; pollution; multi-criteria; PROMETHEE /GAIA.

INTRODUCTION

At the onset of the new millennium, more and more attention is being devoted to the quality of air and soil in urban and rural areas in Europe.[1–4] Nume-

* Corresponding author. E-mail: djnikolic@tf.bor.ac.rs
# Serbian Chemical Society member.
doi: 10.2298/JSC100823054N

rous studies provide various data about the content of heavy metals such as: Cu, Pb, Zn, As, Cd and Hg in air and soil in the vicinity of non-ferrous metal smelters, especially copper smelting plants which are a significant source of environmental pollution.[5–13] In studies of this type, high concentrations of heavy metals have been reported. These metals are discharged with the smelting gases in the form of airborne particles (PM_{10}), their concentrations decreasing as distance from the smelter plant chimney increases. Soil contamination has sometimes been detected at locations at a long distance from the smelter. For example, in the case of the Canadian smelting plant Flin Flon, the maximum distance on which contamination with copper was registered is 33 km and in the case of zinc, 217 km.[14]

The size of the contaminated area, distance from the copper smelter plant and the period of soil exposure to heavy metals contamination, as well as their concentration, depend on numerous factors, such as: direction and speed of the wind, terrain configuration, dimensions of the airborne particles, concentration of the airborne particles at the smelter plant chimney, height of the stack, *etc*. Copper smelter plants discharge with their gasses heavy metal particles (Cu, Pb, As Cd, Ni, Mn, Hg and other toxic elements). These air-born pollutants have detrimental effects on human health. In addition, the precipitation of these particles onto the soil over a long period increases its pollution, which causes contamination of crops with heavy metals, making them hazardous for animal and human health.[15–18]

Due to increasing urbanization and the development of non-ferrous metallurgy in Europe, a special EU Commission was formed which regulates threshold values for heavy metals and gases within industrial, urban and rural zones. Special international regulations oblige many countries to protect particular regions from pollution. For instance, the Danube countries through which the Danube River flows are determined to protect this river from all kinds of pollution. Representatives of the Serbian government have also signed several such legal acts.

In this paper, the results of a study of the content of heavy metals in the soil in the vicinity of the Copper Smelting Plant in Bor after a centenary-long production of copper are presented. During the period 1970–1980, this smelting plant was one of the largest copper smelting plants in Europe according to its capacity.[19] The locations from which soil samples were taken were located in the urban zone of the town, which has a population of more than 40,000. In addition to the urban zones, the nearby rural zones are also considerably inhabited, with more than 20,000 residents living within a range of approximately 20 km from the smelter (the source of air pollution).[20] The following fact should be emphasized: 200,000 t of SO_2 are discharged annually, *i.e*., approximately 3.33 t per resident on average, as a result of company operations.[21] Furthermore, approximately 2.25 kg of dust is discharged per ton of processed raw material, which lead to annual emission of 5.3–19.6 kg As, 4.86–7.99 kg Zn and 6.27–25.11 kg

Pb per resident, and these already high values are frequently exceeded, presenting extremely large numbers if compared to other industrial zones in Europe.[22] These facts indicate that this is highly polluted region, which, besides endangering human health in the region, represent a particular threat for a broad region of southeastern Europe as well. Regardless of the size of this region, the attitude of the company's management towards pollution should be based on a global approach for solving this problem concerning the results obtained during investigations of soil, air and water pollution on the local scale.[23,24] The authors of this paper believe that the results of the investigations presented herein could be useful for achieving such a goal.

The objective of this study was to indicate the potential threats from increased content of heavy metals in the soil within a rather wide area around the Bor Copper Smelting Plant, which is showing a tendency to expand while utilizing the same smelting technology. Simultaneously, this zone is defined as one of the most polluted zones in Serbia, which, therefore, represents a zone of great threat to human health in this part of Europe. The influence of heavy metals in food chains in this region has not been studied specifically but, on the other hand, increased contents of As, Cu and Pb in some plants and increased contents of As and Pb in the organisms of the employees of the RTB-Bor Company and citizens of Bor have been registered.[22] According to this report, waste gases from the smelter plant have destroyed to various extents the soil in almost all villages around Bor. The total affected surface of damaged soil in the Municipality of Bor is estimated at some 25,500 ha, which constitutes 60 % of all agricultural soils.[22] The high extent of damaged soil in the Bor area has both economical and health-related consequences, such as decreased agricultural production, production of lower-quality food, further impoverishment of farmers, higher food prices on the local market with a consequential drop in living standards and inadequate nutrition, affecting growth and development of children, and health in general. For example, copper is an essential element for the growth of plants but the high copper content in the soil around Bor is toxic for plants as it reduces the growth of their roots. High As concentrations also have an adverse impact on the growth of plants.

EXPERIMENTAL

Study area

The Municipality of Bor encompasses an area of 856 km^2 in the central part of Eastern Serbia; around 100 km from the Romanian and 30 km from the Bulgarian border (Fig. 1). The population density of the Municipality is 67.2 inhabitants per km^2. The altitude of the town Bor, 378 m, is low compared with the surrounding high mountains (Stol 1156 m, Veliki Krs 1146 m and Crni Vrh 1043 m). Bor is located in the valley of the Homonym River. Wood soil covers 45 % of the area of the Municipality of Bor; the remainder is 49 % agricultural soil and 6 % infertile soil. The climate is moderate continental. The average mean annual rainfall is

around 469.2 mm m^{-2}, snow coverage lasts about 60 days and the annual average temperature is 11.7 °C. The annual average mean relative air humidity is 73 %, while the average atmospheric pressure is 971 mbar. The prevailing wind is WNW with an average velocity of 0.5 m s^{-1}; the wind still period is over 50 %.

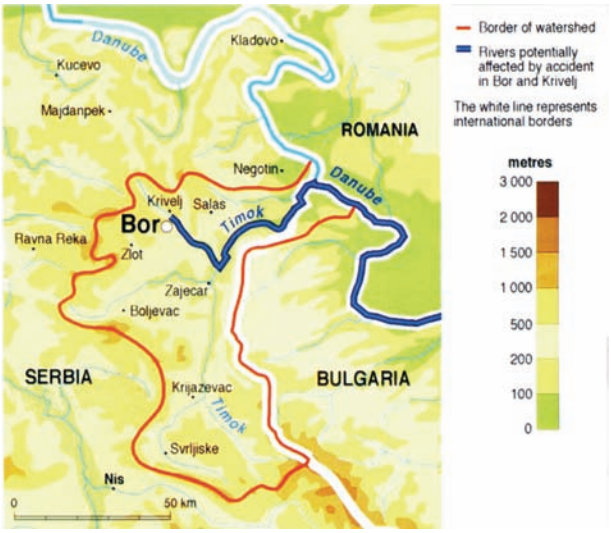

Fig. 1. Map of the studied area in the surroundings of the Copper Smelter Bor, Serbia.

The RTB Bor Copper Smelting Plant, a part of the RTB Mining and Smelting Complex, is located in the town Bor. Production in Bor commenced in 1903 by underground mining. The mine is located on the north-eastern rim of the town; the open pit, the metallurgical--smelting complex and the flotation tailings pond make a boundary between the urban and the industrial zone. Due to the fact that the town was built in the near vicinity of the mine, as well as near the location of the copper smelting plant and two further mines close by, the town itself represents a serious environmental hot spot of Serbia and Europe.[25] The Bor River (industrial river), representing one of the most polluted rivers in the world, flows into the Timok River, a tributary of the Danube River (Fig. 1).

In addition to industrial practice, this region has considerable tourist potentials which are located near Bor. Certainly the most remarkable natural and tourist region is the National Nature Park "Djerdap" to the northeast on the banks of the Danube. Closer to Bor are the Bor Lake and the mountain complex "Homoljske Mountains" to the WNW. All these areas have preserved nature and considerable flora and fauna species with some endemic characteristics. All are endangered with the technology currently employed for copper production in the RTB Bor.

The technology process employed in the RTB Bor Copper Smelting Plant

Degradation of a huge soil area, a huge volume of the soil waste and pollution of underground and surface water are the main attribute for most activate or closed mines and copper smelting plants. The technology used for copper production in the Smelting Plant in Bor is outdated.[26] This technology is based on classical pyrometallurgy,[27] with smelting in reverberatory furnaces and a relatively low degree of SO_2 gas utilization (< 50 %) for the pro-

duction of sulfuric acid. The technical limitations of such technology leads to pollution of the environment with large concentrations of SO_2 and airborne particles of PM10 dust, as well as aero-sediments even larger than the PM_{10} particles.[20] The ores used in this process are of the chalcopyrite and pyrite type with an increased content of As, which is found in the form of FeAsS and Cu_3AsS_4. During oxidative roasting and smelting of these minerals, heavy metal oxides, As and SO_2 gas are formed which exit through the chimneys of the smelter plant and pollute the environment.[28–29] The geographical ranges with a concentration level of SO_2 lower than the approved maximum value are 15 km from the factory chimney. Copper ore smelting in Bor with high sulfur dioxide emissions has caused erosion, high acidity of soils and destruction of the vegetation in the nearby areas. Acid soil affects fertility and also increases the mobility of heavy metals that could reach vegetation. Around the mining and metallurgical industrial complex, the acidity values of the agricultural soils are the highest. Sulfur dioxide damages plant and tree leaves in either an acute or chronic manner. Acute damages are caused by a short impact of very high sulfur dioxide concentrations and are manifested by damage to cells and/or the drying of leaves. Chronic damages occur after longer exposure of plants to lower sulfur dioxide concentrations, and this causes a decrease in organic growth.[22]

Contamination by PM_{10} particles is present up to 15 km from the smelter smokestack which emits the harmful substances. The concentration of SO_2 gas and heavy metals in the PM_{10} are largely above the threshold concentrations regulated by EU directives.[20,25,30,31] The concentrations are also above the limits prescribed by the local Serbian Regulative that defines the maximum allowed heavy metal content in the air.[22]

The main reason for such a situation is the failed opportunity for implementation of new technology at a time when it was financially feasible (during 1980s). At that point, this should be considered as the most important step in the life cycle of the company.[32] During 2003, a continuous operational real-time monitoring system (CORTMS) for tracking air pollution was installed in Bor. This system enables the continuous measurement of the SO_2 concentration in air (values are read at 15 min intervals) and the cumulative measurement of the heavy metals content in airborne particles at two measuring points in the urban part of the city of Bor. In addition, a mobile station is operational, which allows the measurement of the PM_{10} content and aero-sediments at 15 different locations.[20]

Sampling

Soil samples were taken from the locations indicated in Fig. 2, between July and August 2008. These locations were not farmed; therefore, contamination of the ground through the use of agricultural measures was excluded. Ten samples were taken from each location. The soil samples were taken *via* a soil core sampler in such a way that a core of a soil was removed of radius 5 cm and depth 30 cm. A 5-cm surface layer of the core was stripped off and the rest of the sample was dried at 50 °C for 2 h and its weight measured. In the next step soil, the samples were ground and homogenized until the required size was obtained and then the pH and heavy metals contents were determined. The obtained reproducibility for the metals contents in the samples were relatively high (0.87–0.95).

Chemical analysis

The pH value of the samples was realized using a pH–conductivity/°C meter, PC_{10}/ /EUTECH Instrument. For determination of the heavy metals contents in the soil, each sample was dissolved in an acidic mixture consisting of $HF+HClO_4$, while HCl was used for filling up to the volume of the flask. The contents of Cu, Pb, Cd, Ni and Mn content were determined by atomic adsorption spectrophotometry (AAS),[33] using a Perkin Elmer model 2380 instru-

ment. The As content was determined by inductively coupled plasma atomic emission spectrophotometry (ICP–AES) employing an ARL 3410 instrument, while mercury content in the samples was determined by flameless atomic adsorption spectrophotometry–mercury analyzer (A–Hg) using a Perkin Elmer FIMS-100 instrument. All chemical analyses were performed in a certified chemical laboratory of the Institute for Mining and Metallurgy in Bor.

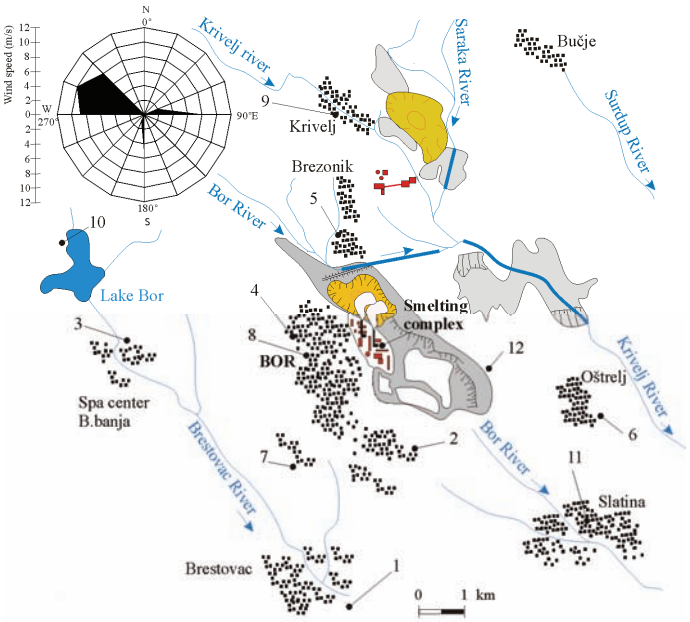

Fig. 2. Map of sites from which the samples were taken (1 – Village of Brestovac; 2 – Industrial zone "Elektroistok"; 3 – Spa center "B. banja"; 4 – Hospital; 5 – Village of Brezonik; 6 – Village of Ostrelj; 7 – Suburban area "Bor 2"; 8 – City location "Šumska sekcija"; 9 – Village of Krivelj; 10 – Lake Bor; 11 – Village of Slatina; 12 – Zone behind the industrial waste-yard).

Data analysis

There are many statistical methods used in chemometric studies.[34,35] For the purpose of ranking the zones of the studied region (Fig. 2) according to the soil contamination, it was decided to use the method of multi-criteria decision making, MCDM.[36] Many authors use MCDM for analyzing the problem of air and soil pollution.[37–40] In this study, the PROMETHEE method was used for ranking the locations from which the soil samples were taken in accordance with the heavy metals contents, while GAIA plane was used for graphical interpretation of the PROMETHEE results. In other words, GAIA plane provides a clear picture of a decision making problem by visualization of the PROMETHEE ranking.[41] The GAIA visual modeling method provides the decision maker with information about the conflicting character of the criteria and the impact of the weights of the criteria on the final results. The GAIA plane is defined by corresponding unit eigenvectors u and v, resulting from a unicriterion net flows covariance matrix, obtained using principal components analysis (PCA). Using PCA, it is possible to define a plane having the minimal amount of information lost by projection (Δ).[42] Main reason for implementing PROMETHEE/GAIA for processing the acquired data was the

specific advantages of this method in regards to other MCDM methods. These advantages are mostly attributable to the way of structuring the problem; high quantity of data which can be processed; ability to quantify qualitative values, good software support and presentation of processed data.[20,4344]

The PROMETHEE method presents an outranking method for a fixed set of alternatives.[45] For the application of this method, it is necessary to define a specific preference function and to assign a weight of significance (weight coefficient) to each criterion. The preference function defines the rank of one option with respect to another and translates deviation between two parallel alternatives into a unique parameter which is associated with the degree of preference. The degree of preference presents a growing deviation function, whereby, in case of small deviation, it refers to a weak preference and in the case of large deviation, it represents a strong preference associated with a reference alternative. The PROMETHEE method has at its disposal six possible shapes of preferential functions (usual, U-shape, V-shape, level, linear and gaussian), whereby every shape depends on two thresholds (Q and P). The indifference threshold (Q) represents the maximum deviation which the decision maker considers as unimportant, while the preference threshold (P) represents the minimum deviation which is considered to be decisive for the decision maker, where P is not allowed to be smaller than Q. The Gaussian threshold (S) represents a mean value between the thresholds P and Q.[45-49]

The PROMETHEE method is based on determining the positive (Φ^+) and the negative flow (Φ^-) for each alternative towards outranking relations and in correlation with the acquired weight coefficients for each criterion-attribute. In the case of the investigations presented in this paper, the alternatives were the investigated locations, while the criterions were the heavy metals content detected at the locations. The positive preference flow expresses how much an alternative dominates over the others; therefore, the greater the value ($\Phi^+ \rightarrow 1$), the more significant is the alternative. The negative preference flow expresses the preference of all the other alternatives compared to the analyzed one. An alternative is more important if the value of the output flow is smaller ($\Phi^- \rightarrow 0$). The complete ranking of PROMETHEE II is based on the calculation of a net outranking flow value (Φ) that represents the balance between the positive and the negative outranking flows. The higher the net flow is, the better the alternative.[42,50,51] Accordingly, if the alternative has a greater positive (Φ^+) and a lower negative flow (Φ^-), then the net outranking flow (Φ) for this alternative is higher. For the investigations presented in this paper, this would mean that such a location (alternative) has a larger significance compared to the other, which means that this location is less contaminated with heavy metals (criterions) compared to the other investigated locations.[20]

RESULTS AND DISCUSSION

Chemical analysis

The obtained results for the heavy metals contents in the samples taken from the urban zones of town site Bor and surroundings are presented in Table I for 12 locations in total, the positions of which are shown in Fig. 2. Maybe the most important finding that should be considered by the local authorities and stakeholders is a fact that according to legislation,[52] 100 % of the analyzed samples were contaminated with copper (maximum allowed concentration for copper in soil is 36 mg kg^{-1}); 100 % of the samples were contaminated with cadmium (maximum allowed concentration for cadmium in soil is 0.8 mg kg^{-1});[52] 58.3 %

of the samples were contaminated with arsenic (maximum allowed concentration for arsenic in soil is 29 mg kg^{-1})[52] and 25 % of the samples were contaminated with lead (maximum allowed concentration for lead in soil is 85 mg kg^{-1}).[52]

The highest contents of some heavy metals were found in the samples taken from the locations near to the town center (Table I). The wind "rose" (Fig. 2) for the period 2005–2008 indicates that the WNW (west–northwest) wind direction is prevalent during the year (approximately 30 %) which led to the highest degree of air pollution in this part of the town (measuring points 4 and 8 – City Hospital and the city location "Šumska sekcija – Forest Section", respectively). The following objects are located in this part of the town: the old town center, a hotel, the town market, the town hall building, the faculty campus, an elementary school and the city hospital. With increasing distance from the plant stacks, the soil pollution decreased and it is minimal was at a distance of 20 km (measuring point 10 – Lake Bor); however the influence of pollution was still apparent.

TABLE I. Evaluation table. Heavy metals concentrations (mg kg^{-1}) in the soil at 12 locations in the urban area of the town Bor and its surroundings, with given preference function and respective thresholds for each criterion

Alternatives	Criteria-metal concentrations in sediments							
	pH	Cu	Pb	Cd	Ni	Mn	As	Hg
Analytic method	pH-Meter	AAS	AAS	AAS	AAS	AAS	ICP–AES	A–Hg
Minimum/Maximum	–	Min	Min	Min	Min	Min	Min	Min
Preference Function	–	Linear	Linear	Linear	Linear	Linear	Linear	Linear
Indifference threshold (*Q*)	–	116	10	0	2	42	12	0.0101
Preference threshold (*P*)	–	696	57	1	12	252	73	0.0603
Location 1	7.7	530	70	2	45	1100	17	< 0.1
Location 2	7.6	1050	100	4	33	880	68	0.1
Location 3	7.5	550	60	2	33	1300	52	0.1
Location 4	7.4	2540	180	6	49	1200	260	0.3
Location 5	7.9	770	80	2	12	1200	33	0.1
Location 6	7.8	390	40	2	41	1200	15	< 0.1
Location 7	6	1000	40	< 2	37	1200	23	< 0.1
Location 8	7.2	2140	230	5	53	1100	140	0.3
Location 9	6	580	60	2	16	1200	25	0.1
Location 10	7.5	220	50	3	37	460	19	< 0.1
Location 11	7.7	930	80	3	49	900	41	0.1
Location 12	7.7	260	50	< 2	37	1100	16	0.1
Max. value		2540	230	6	53	1300	260	0.3
Average value		913.33	86.67	2.92	36.83	1070	59.08	0.133
Min. value		220	40	< 2	12	460	15	< 0.1
Limit values according to the soil quality standard of the Netherlands[52]		< 36	< 85	< 0.8	< 35	–	< 29	< 0.3
Limit values according to the National Legislation of the Republic of Serbia[53]		< 100	< 100	< 3	< 50	–[a]	< 25	< 2

[a]Manganese limit value is not regulated in the National Legislation of the Republic of Serbia

The heavy metals found in the analyzed soils from these sampling locations are in such concentrations that they can only be explained to be the result of atmospheric precipitations of airborne particles and aero-sediments from gases produced by the Copper Smelting Plant located in Bor. To confirm this assumption, soil samples from five locations which are more than 20 kilometers from the Copper Smelting Plant were analyzed. Three of the five samples contained copper but less than the limiting value of 100 mg kg^{-1}). The presence of As and the other investigated heavy metals was not registered at a significant level at any of the locations. The contents of the heavy metals at the investigated locations presented in Table I are much higher compared to these more distant locations, which corroborated the assumption that atmospheric precipitations of airborne particles and aero-sediments from the Copper Smelting Plant stacks in Bor was responsible for the high levels of pollutants found in the near vicinity of the plant.

On settling at pH values between 6 and 8 over many years, these materials became mineralized. However, as their concentrations were not high enough for classical mineralogical analysis, possible mineralogical forms of the heavy metals in the analyzed soils were determined utilizing the HSC Chemistry 4.0 software package (chemical reaction and equilibrium software) by analyzing the areas of stability for the possible phases in the *Eh*–pH equilibrium diagram calculated for room temperature. The stability field diagrams calculated the presence of a range of metal oxide, hydroxide and sulfate minerals in the analyzed soil: Cu (CuO; Cu_2O; Cu); As (H_2AsO_4; $HAsO_4$; AsO_4; $HAsO_3$); Cd (Cd^{2+}; $Cd(OH)_2$; $CdSO_4 \cdot 2.67H_2O$; CdS; Cd); Pb (PbO_2; $Pb_4(OH)_4$; $Pb_6(OH)_8$; $PbSO_4$; $PbO \cdot PbSO_4$; Pb); Hg (Hg; HgO); Ni ($Ni(OH)_3$; NiO; Ni; $NiHO_{0.68}$; $NiSO_4 \cdot 4H_2O$); Mn (MnO_4; MnO_2; Mn_2O_3; Mn_3O_4; $Mn(OH)_2$; Mn^{2+}; Mn; $MnSO_4$; MnS). In addition, presence of Cu_2S, CdS and FeS is possible. The presence of oxides, hydroxides and sulfates of heavy metals in the contaminated soil indicates a large probability of their transition into ground waters and the human food chain.[17]

Also, the determined values of the heavy metals contents in the surface layer cannot originate from primary mineralization of the ore deposit in this region because minerals of the heavy metals are found at depths deeper than 100 m, from where the ore deposit exploited by the Copper Smelting Plant is obtained.

When comparing the values given in Table I with the values at other urban regions in the surroundings of industrial zones, Sophia (Bulgaria):[12,54] Cu, 40 mg kg^{-1}; Pb, 32 mg kg^{-1} and Cd, 0.4 mg kg^{-1}, Palermo (Italy):[55] Pb, 202 mg kg^{-1}; Cu, 63 mg kg^{-1} and Hg, 0.68 mg kg^{-1}, Manresa (Spain):[56] Cu, 20.3 mg kg^{-1}; Cd, 0.28 mg kg^{-1} and Pb, 0.18 mg kg^{-1}, Port Kembria (Australia):[8] Cu, 49 mg kg^{-1}; As, 3.2 mg kg^{-1} and Pb, 20 mg kg^{-1}, the present results indicate that the soil pollution in the studied zone is very high. Continuing the operation of the Copper Smelting Plant in the present manner is cumulatively increasing the heavy metal

content in the soil and presents a severe threat to human health in this part of Europe.

PROMETHEE and GAIA ranking analysis

The obtained values of the heavy metals Cu, Pb, Cd, Ni, Mn, As and Hg contents in the soil in the examined urban zone of the town of Bor and its surroundings (20 km in diameter from plant smokestacks) are given in Table I for 12 locations, the positions of which are shown in Fig. 2. These results represent the average values of heavy metal contents in 10 samples obtained from each location. Additionally, data was provided regarding chosen preference functions and indifference and preference thresholds which are necessary for multi-criteria ranking of locations by the degree of contamination with heavy metals using the PROMETHEE/GAIA method. The model implies the ranking of the best alternatives – locations with the lowest presence of heavy metals according to given set of preference functions and weight criteria. In all cases a linear function is used as the preferential one. The reason for such a consideration results from the fact that the heavy metal content in the soil decreases with increasing distance from the factory chimney in the direction of wind flow. The simplest mathematical expression that can explain this pattern is a linear function.

Consequently, the locations were ranked according to their degree of contamination with heavy metals in the studied area using the aforementioned PROMETHEE/GAIA method. Considering that the data in Table I have a quantitative character, a linear function was chosen for the preference function, Fig. 3. (example for Cu), for all the defined criteria with indifference and preference thresholds (Q and P) in the 5 and 30 % zones, respectively.[45]

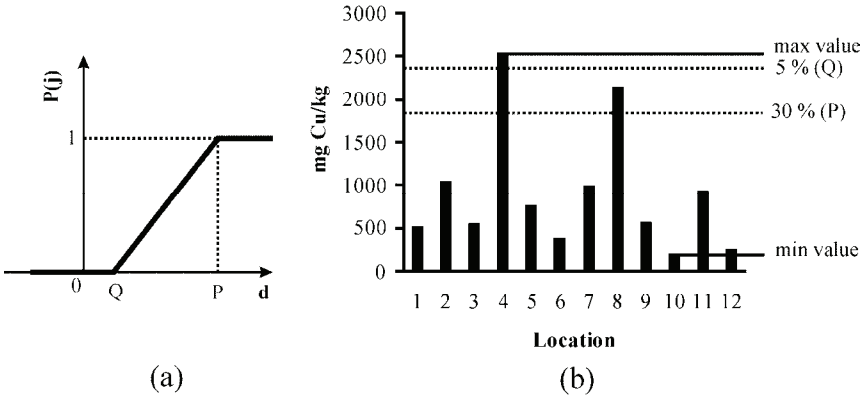

Fig. 3. a) Determination of the preference function values based on the indifference and preference thresholds for a linear preference function; b) defining the indifference and preference thresholds zones for the copper concentration as a criterion.

For the purpose of defining the weight coefficients, it was taken into account that the heavy metals do not have the same significance, *i.e.*, each of them has a different effect on human health and the environment, which is defined in Table II. The weight of significance assigned to each metal was determined considering the reference dose of exposure, toxicity and damage to human health. By utilizing the Decision Lab 2000 software package, with the PROMETHEE/GAIA method, based on the data in Tables I and II, values were acquired for the positive (Φ^+) and negative (Φ^-) flows, (Table III).

TABLE II. Given weights for each criterion

Criteria-dangerous metal	Weight	Influence on health
Pb	22.5	I Category, retained in the human organism and is carcinogenic
Cd	22.5	I Category, retained in the human organism and is carcinogenic
As	15	I Category, easily removed from the organism within 3–5 days
Hg	10	Poisonous, not carcinogenic, removed from the organism with in 1 month
Ni	15	Carcinogenic
Mn	10	Influence on the nervous system
Cu	5	Harmful, but removable
	Σ = 100	

TABLE III. Preference flows for case scenario

Location	Φ^+	Φ^-	Φ
1	0.2575	0.1338	0.1237
2	0.2794	0.4138	–0.1344
3	0.2910	0.1295	0.1615
4	0.0225	0.8536	–0.8310
5	0.3445	0.1025	0.2421
6	0.3222	0.0862	0.2360
7	0.3203	0.0889	0.2314
8	0.0516	0.8402	–0.7886
9	0.3692	0.0510	0.3183
10	0.3813	0.1475	0.2338
11	0.2382	0.3131	–0.0749
12	0.3387	0.0565	0.2822

The PROMETHEE II method provided a complete ranking spanning from the best to the worst location, based on the heavy metal content in the soil (Fig. 4), where the “best” locations were those with the lowest concentrations of heavy metals and the “worst” were those with the highest concentrations. The obtained results showed that the most polluted locations were: Hospital (Location 4) and city location “Šumska sekcija – Forest Section” (Location 8), and the least pol-

luted locations were found on the territory of the village Krivelj (Location 9) and the sampling location "Iza planira" (Location 12).

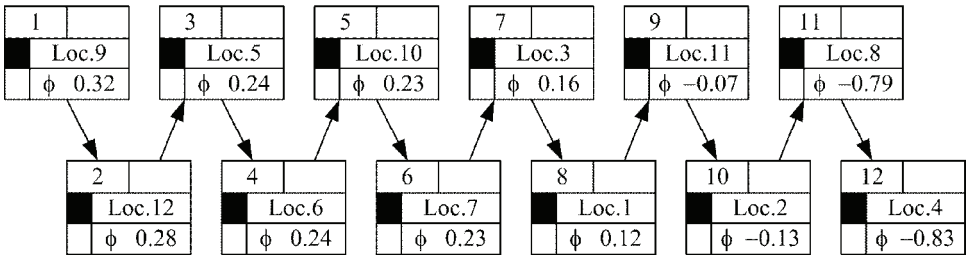

Fig. 4. PROMETHEE II Ranking of locations (sampling locations were ranked from left to right, which is from the best to the worst location).

Advantages of Decision Lab software package can be found within implementation of geometrical analysis for interactive assistance (GAIA). Considering that the value of the delta parameter (Δ) was rather large (85.15 %), the validity of this tool should be taken into account. This means that only 14.85 % of the total information is lost in the projection. In real world applications, the value of Δ should always be larger than 60 % and in most cases larger than 80 %. This means that even when the number of criteria is large, the GAIA plane still provides reliable information.[42]

Based on the position of the criterion in GAIA plan (squares), Fig. 5, conformity or conflict between individual criterions can be determined. Thus, one conformable group of criterions consists of Hg, Pb, As and Cu, a second conformable group consists of Ni and Cd, while Mn does not concur with any of the given criterions. Likewise, the positions of the alternatives (triangles) determine the strength and weakness with respect to the criteria. Alternatives present the investigated locations from which the soil samples were taken. The closer it is to the orientation of the individual criterion axis, the better the individual alternative is, judging by that criterion. Thus, the contamination level of specific location is lower if it is closer to a particular heavy metal in the GAIA plane.

Within Cluster A, locations Hospital (Location 4) and "Šumska sekcija – Forest Section" (Location 8) can be found, having the largest percentage of heavy metals in the soil, apparently not being ranked as good by any criterion and as such being orientated in an opposite direction with respect to the decision axis (*pi*), which defines a compromising solution in accordance with the given weight criteria. As opposed to them, the location group B (Cluster B) represents a better solution by a greater number of criteria, among which Location 12 sets itself apart as the closest to the decision axis (*pi*), as well as location Village of Krivelj (Location 9), which was judged the best in terms of the content of Ni and Cd. These ranking results were also determined with PROMETHEE II complete ranking.

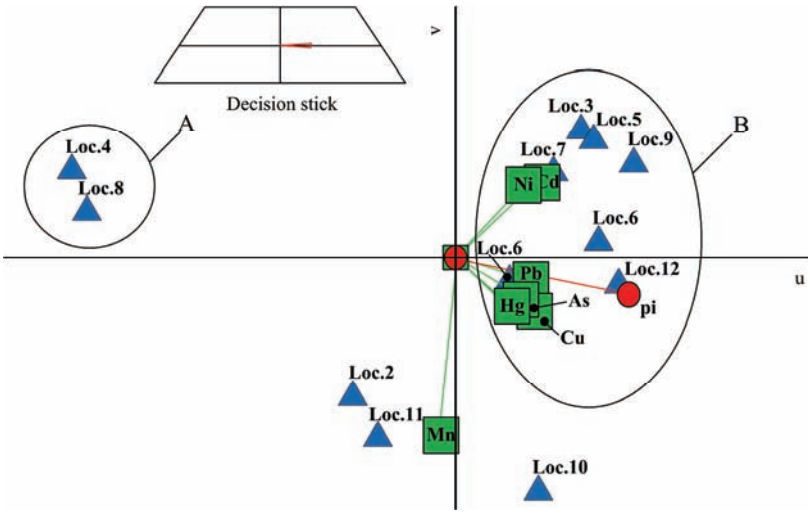

Fig. 5. GAIA plane analysis for the defined model of heavy metal soil contamination.

The ranking results in this study indicate certain correlation with the results of a similar model used for air pollution in same area.[20] The reason for such coincidence is the fact that the soil pollution is caused by the temporal atmospheric distribution and fallout of heavy metal emissions from the Copper Smelting Plant in Bor, as well as meteorological and geographical conditions and the distance from the point sources. This means that the employed multi-criteria model represents a reliable way for analyzing and solving ecological problems, because it is possible to determine the distribution and impact of all pollutants simultaneously around the emission source, and to define the relations among them regarding the locations.

CONCLUSIONS

The determined contents of heavy metals in the layer of soil down to 30 cm in depth do not originate from ore mineralization in this region because the heavy metals exist at much deeper levels – on the contrary they are the consequence of precipitation of airborne particles and aero-sediments from the air over many years, which originated from the oxidation roasting and smelting of the copper concentrate containing heavy metals. This was proved after analyzing the soil samples obtained at greater distances from the smelting plant.

Through ranking of obtained results with the PROMETHEE/GAIA method, the most polluted zones are on the locations Hospital (Location 4) and the city location “Šumska sekcija – Forest Section” (Location 8), which have vital functions for the town, therefore representing a risk for human health. The determined heavy metal contents (Cu, Pb, Ni, Mn, As and Hg) in the soil in the studied area of the Bor region indicate a large degree of soil degradation, with the potential

danger of heavy metals entering the animal and human food chains with the associated severe consequences.[17]

Some of these consequences were already reported.[22] The contents of As and heavy metals in food supplies from four villages around Bor were determined. The results revealed that the Cu and As contents in the food supplies from the village Krivelj (Location 9 in Fig. 2) were much higher than in the other 3 villages (Oštrelj, Zlot and Šarbanovac), which are more distant from the Copper Smelter Plant and do not lie in the path of the prevailing wind direction. As discussed above, this location was ranked the best compared to other urban areas in Bor; nevertheless, it is more polluted compared to other more distant villages. Higher than allowed concentrations of As and heavy metals were found in fruits, grapes, vegetables and eggs.

Research has also been conducted on lead and As content in blood and urine of children in Bor and village Zlot (outside metallurgical smoke range). This research showed that children from Bor have considerably higher contents of these metals. This means that there is a continued risk of lead and As input into the organisms of children from Bor, especially if they spend their whole life in polluted surroundings. By studying the impact of pollution on health, growth and development of children in Bor and Sokobanja (unpolluted region 100 km from Bor), it was found that the hemoglobin content was 1.1 % lower and number of red blood cells in general was 400,000 lower for the children from Bor than the children from Sokobanja. The same study showed that children from Bor are more liable to diseases of the respiratory organs: blocked nose, enlarged tonsils, swollen pharynx and swollen gland secretion in bronchi. For these reasons, children in Bor are more liable to allergy diseases, particularly to bronchial asthma.[22]

The shortage of food supplies caused by soil contamination has resulted in the need for people to obtain food from elsewhere, which results in higher prices and a further reduction in living standards. Consequently, the people in Bor buy cheap but not varied food, which affects child growth and development and human health in general. Due to the existing situation, village farmers are unwilling to invest in agricultural development, with some choosing instead to go to the town to search for employment. This, in turn, leads to neglect of their farms and consequentially a further decrease in agricultural production.

After obtaining the very alarming results presented in this paper, the authors believe that the further strategy for the environmental protection of this region should include a wider methodological approach, such as the Ecological Risk Assessment (ERA) methodology.[57,58] This kind of methodology enables a detailed identification of situations dangerous for humans under conditions of this kind.

In addition, the facts described in this paper imply the necessity for urgent intervention at the source of the emissions of sulfur dioxide, As and heavy metals airborne particles, and for the modernization and reconstruction of the Copper

Smelting Plant in Bor, as well as urgent restoration of the already degraded soil. Continued operation of the smelting plant under the existing conditions will increase the heavy metal content in the soil resulting from their precipitation from the air.

Acknowledgements. The presented paper is a result of work on the Project No. TP 21009, which is financially supported by the Ministry of Science and Technological Development of the Republic of Serbia. The authors are grateful to the company Visual Decision Inc. Montreal, Canada for providing, free of charge, the software package Decision Lab 2000 for the PROMETHEE/GAIA method.

И З В О Д

ВИШЕКРИТЕРИЈУМСКА АНАЛИЗА ЗАГАЂЕНОСТИ ЗЕМЉИШТА ТЕШКИМ МЕТАЛИМА У ШИРОЈ ОКОЛИНИ ТОПИОНИЦЕ БАКРА У БОРУ

ЂОРЂЕ НИКОЛИЋ[1], НОВИЦА МИЛОШЕВИЋ[2], ЖИВАН ЖИВКОВИЋ[1], ИВАН МИХАЈЛОВИЋ[1], РЕНАТА КОВАЧЕВИЋ[2] и НЕВЕНКА ПЕТРОВИЋ[2]

[1]*Универзитет у Београду, Технички факултет у Бору, Војске Југославије 12, 19210 Бор и* [2]*Институт за рударство и металургију Бор, Зелени булевар 35, 19210 Бор*

У овом раду предочене су последице стогодишње производње у топионици бакра у Бору на загађење земљишта. У ту сврху, извршено је површинско узорковање земљишта на дванаест различитих мерних локација. Све мерне локације се налазе у пречнику од 20 километара од извора загађења, у урбаним и руралним деловима града Бора. Узорак земљишта је узиман сондом на тај начин да је вађено језгро земљишта пречника 5 цм и дубине 30 цм. Након тога, извршена је анализа pH вредности узорка и саржаја тешких метала (Cu, Pb, As, Cd, Mn, Ni и Hg) коришћењем различитих метода спектрофотометрије. Резултати анализе садржаја тешких метала у узорцима земљишта показали су високе вредности: 2,540 mg kg^{-1} Cu; 230 mg kg^{-1} Pb; 6 mg kg^{-1} Cd; 530 mg kg^{-1} Ni; 1,300 mg kg^{-1} Mn; 260 mg kg^{-1} As и 0,3 mg kg^{-1} Hg. За идентификовање и рангирање критичних зона загађеног земљишта на основу пристуства тешких метала у њима, у овом раду је коришћена PROMETHEE/GAIA метода, која се често користи у хемометријским студијама. Резултати рангирања јасно указују да се најзагађеније зоне налазе на виталним локацијама у самом центру града. Због тога, услед повећане биодоступности тешких метала и њихових комплексних реакција са органским врстама у земљишту, последице по људско здравље се могу драстично увећати уколико ови тешки метали доспеју у ланце исхране.

(Примљено 28. марта, ревидирано 23. септембра 2010)

REFERENCES

1. K. Nikolaou, *J. Environ. Prot. Ecol.* **4** (2003) 477
2. T. Gotschi, J. Hazenkap-Von Arx, R. Heinrich, P. Bono, B. Burney, D. Forsberg, J. Jarvis, D. Maldonado, W. B. Norback, J. Stern, K. Sunyer, G. Toren, S. Verlato, N. Villani, N. Kunzil, *Atmos. Environ*. **39** (2005) 5947
3. M. C. Periera, R. C. Santos, M. C. M. Alvim-Ferraz, *J. Toxicol. Environ. Health A* **70** (2007) 347
4. J. C. M. Pires, S. I. V. Sousa, M. C. Pereira, M. C. M. Alvim-Ferraz, F. G. Martind, *Atmos. Environ*. **42** (2008) 1249

5. F. Beavington, *Aust. J. Soil Res*. **11** (1973) 27
6. L. Faitondjiev, L. Stanislavova, H. Tchuldjian, S. K. Gupta, R. Schulin, *Soil Sci Agrochem. Ecol.* **35** (2000) 3
7. F. Beavington, P. A. Cawse, A. Wakenshaw, *Sci. Total Environ.* **322** (2004) 39
8. E. Martley, B. L. Gulson, H. R. Pfeifer, *Sci. Total Environ.* **325** (2004) 113
9. K. Sichorova, P. Thustos, J. Szakova, K. Korinek, J. Balik, *Plant Soil Environ.* **50** (2004) 525
10. M. V. Kozlov, *Environ. Pollut.* **135** (2005) 91
11. O. Parceval, Y. Couillard, B. Pinel-Alloul, E. Bonneris, P. G. C. Campbell, *Sci. Total Environ.* **369** (2006) 403
12. R. Schulin, F. Curchod, M. Mondeshka, A. Daskalova, A. Krller, *Geoderma* **140** (2007) 52
13. A. M. Shanchez de la Campa, J. D. De la Rosa, D. Sanchez-Rodos, V. Oliveira, A. Alastuey, X. Querol, J. L. Gomez Ariza, *Atmos. Environ*. **42** (2008) 6487
14. W. G. Franzin, G. A. McFarlane, A. Lutz, *Environ. Sci. Technol*. **13** (1979) 1513
15. M. K. Jamali, T. G. Kazi, M. B. Arain, H. I. Arfidi, N. Jalbani, A. R. Memon, A. Shah, *Environ. Chem. Lett*. **5** (2007) 209
16. J. C. Aznar, M. Richer-Lafleche, D. Cluis, *Environ. Pollut*. **156** (2008) 76
17. P. Babula, V. Adam, R. Opartilova, J. Zehnalek, L. Havel, R. Kizek, *Environ. Chem. Lett.* **6** (2008) 189
18. Y. Yang, F. S. Zhang, H. F. Li, R. F. Jaing, *J. Environ. Manage*. **90** (2009) 1117
19. *Encyclopedia Britannica***,** *Bor Resource document*, *Encyclopedia Britannica Online*, http://www.britannica.com/EBchecked/topic/73768/Bor (27 August, 2009)
20. Dj. Nikolić, N. Milošević, I. Mihajlović, Ž. Živković, V. Tasić, R. Kovačević, N. Petrović, *Water Air Soil Pollut*. **206** (2010) 369
21. I. Mihajlović, Dj. Nikolić, N. Štrbac, Ž. Živković, *Serb. J. Manage*. **5** (2010) 39
22. *(LEAP)*-Local *Environmental Action Plan Bor. Resource document*, Municipality, Bor, http://enrin.grida.no/htmls/yugo/bor/leap_ENG.pdf (25 January 2009)
23. J. Parnel, *Serb. J. Manage*. **1** (2006) 21
24. S. Yorgun, *Serb. J. Manage*. **2** (2007) 247
25. M. Dimitrijević, A. Kostov, V. Tasić, N. Milosević, *J. Hazard. Mater*. **164** (2009) 892
26. W. G. Devenport, M. King, M. Schlesinger, A. K. Biswas, *Extractive Metallurgy of Copper*, 4th ed., Pergamon Press, Elsevier Science, Amsterdam, Netherlands, 2002, p. 14
27. F. Habashi, *J. Mining Metall*. **45B** (2009) 1
28. S. Magaeva, G. Patronov, A. Lenchev, I. Granchorov, *J. Mining Metall.* **36B** (2000) 77
29. V. M. Zhukovsky, *J. Mining Metall.* **36B** (2000) 93
30. *1999/30/CE, Council Directive relating to limit values for sulphur dioxide, nitrogen dioxide and oxide of nitrogen, particulate matter and lead in ambient air*, http://eur--lex.europa.eu/LexUriServ/LexUriServ.do?uri=OJ:L:1999:163:0041:0060:EN:PDF (20 January 2010)
31. *2004/107/CE, Council Directive relating to arsenic, cadmium, mercury, nickel and polycyclic aromatic hydrocarbons in ambient air*, http://eur-lex.europa.eu/LexUriServ/ /LexUriServ.do?uri=OJ:L:2005:023:0003:0016:EN:PDF, (20. January 2010)
32. D. Živković, Ž. Živković, *Serb. J. Manage*. **2** (2007) 57
33. H. Bradl, C. Kim, U. Kramar, D. Stüben, in *Heavy Metals in the Environment: Origin, Interaction and Remediation*, H. Bradl, Ed., Elsevier, Amsterdam, Netherlands, 2005, p. 28
34. Ž. Živkovic, N. Mitevska, I. Mihajlovic, Đ. Nikolic, *J. Mining Metall*. **45B** (2009) 23

35. Ž. Živkovic, I. Mihajlovic, Dj. Nikolic, *Serb. J. Manage*. **4** (2009) 137
36. K. Rousis, K. Moustakas, S. Malamis, A. Papadopoulos, M. Loizidou, *Waste Manage*. **28** (2008) 1941
37. D. Al-Rashdan, B. Al-Kloub, A. Dean, T. Al-Shemmeri, *Eur. J. Operational Res.* **118** (1999) 30
38. W. Al-Shiekh Khalil, A. Goonetilleke, S. Kokot, S. Carroll, *Anal. Chim. Acta* **506** (2004) 41
39. M. C. H. Lim, G. A. Ayoko, L. Morawska, *Atmos. Environ*. **39** (2005) 463
40. M. C. H. Lim, G. A. Ayoko, L. Morawska, Z. D. Ristovski, E. R. Jayaratne, S. Kokot, *Atmos. Environ*. **40** (2006) 3111
41. Visual Decision Inc. *Why to use PROMETHEE/GAIA instead AHP? Resource document*, Montreal, Quebec, Canada, http://www.visualdecision.com/promethee_vs_ahp.htm (25 November 2008)
42. J. P. Brans, B. Mareschal, *Decision Support Systems* **12** (1994) 297
43. C. Macharis, J. Springael, K. De Brucker, A. Verbeke, *Eur. J. Operational Res.* **153** (2004) 307
44. *Visual Decision Inc.*, *Getting Started Guide*, *Decision Lab 2000 – Executive Edition*, Montreal, Quebec, Canada, 2007, p. 16
45. G. Vego, S. Kučar-Dragičević, N. Koprivanac, *Waste Manage*. **28** (2008) 2192
46. J. P. Brans, in *L'aide à la décision: Nature, Instruments et Perspectives d'Avenir*, R. Nadeau, M. Landry, Eds., Presses de l'Université Laval, Québec, Canada, 1982, p. 183
47. J. P. Brans, B. Mareschal, Ph. Vincke, in *Operational Research '84*, J. P. Brans, Ed., North-Holland, Amsterdam, Netherlands, 1984, p. 477
48. J. P. Brans, Ph. Vincke, *Manage. Sci.* **31** (1985) 647
49. L. Herngren, A. Goonetilleke, G. A. Ayoko, *Anal. Chim. Acta* **571** (2006) 270
50. A. Albadvi, S. K. Chaharsooghi, A. Esfahanipour, *Eur. J. Operational Res.* **177** (2007) 673
51. G. Anand, R. Kodali, *J. Modell. Manage*. **3** (2008) 40
52. Ministry of Housing, *Spatial Planning and Environment Directorate-General for Environmental Protection, Circular on target values and intervention values for soil remediation*, Netherlands Government Gazette, 2000, p. 39.
53. *Regulations about allowed quantities of dangerous and harmful matters in soil and irrigating waters and methods about their analysis*, Official Herald of the Republic of Serbia, No. 23/94 (1994) (in Serbian)
54. V. Doichinova, M. Sokolovska, E. Velizarova, *Environ. Chem. Lett.* **2** (2006) 101
55. D. Salvagio Manta, M. Angelone, A. Bellanca, R. Neri, M. Sprovieri, *Sci. Total Environ*. **300** (2002) 229
56. J. Bech, P. Tume, L. Longan, F. Reverter, J. Bech, L. Tume, M. Tempio, *Environ. Monit. Assess*. **145** (2008) 257
57. EPA (U.S. Environmental Protection Agency), *Guidelines for Ecological Risk Assessment*, *Resource document*, Washington, DC, USA, http://cfpub.epa.gov/ncea/CFM/ /recordisplay.cfm?deid=12460 (30 August 2009)
58. S.M. Bartell, in *Encyclopedia of Ecology*, S. E. Jorgensen, B. Fath, Eds., Elsevier, Amsterdam, Netherlands, 2008, p. 1097.

Journal of the Serbian Chemical Society
JSCS@tmf.bg.ac.rs • www.shd.org.rs/JSCS
J. Serb. Chem. Soc. *76* (4) 643–646 (2010)
UDC 543+061.3(4)
EuCheMS news

DIVISION OF ANALYTICAL CHEMISTRY
EUROPEAN ASSOCIATION FOR CHEMICAL AND MOLECULAR SCIENCES

EUCHEMS NEWS

European Analytical Column No. 39
Analytical chemistry and bioanalytical chemistry – an unshaped social relationship

(January 2010)

GEORGE HORVAI[1], PAUL WORSFOLD[2], BO KARLBERG[3] and JENS E. T. ANDERSEN[4]*

[1]*Department of Inorganic and Analytical Chemistry, Budapest University of Technology and Economics, Gellert ter 4, H-1111 Budapest, Hungary,* [2]*School of Geography, Earth and Environmental Sciences, University of Plymouth, Plymouth PL4 8AA, UK,* [3]*Department of Analytical Chemistry, Stockholm University, 10691 Stockholm, Sweden and* [4]*Department of Chemistry, Technical University of Denmark, Building 207, 2800 Lyngby, Denmark*

Keywords: analytical chemistry; bioanalysis; EuCheMS-DAC.

The title Analytical and Bioanalytical Chemistry (ABC) represents a trend that has been observed in several important analytical chemistry journals: more and more papers on research in bioanalytical chemistry are being published in traditional analytical chemistry journals. For an outsider this might be seen as evidence of the attraction of more and more analytical chemists to bioanalytical topics. However, a more thorough investigation does not fully support this observation. Many authors of bioanalytical papers in the traditional analytical journals come from outside of the traditional analytical chemistry community. This has led the Division of Analytical Chemistry (DAC) within the European Association for Chemical and Molecular Sciences (EuCheMS) to set up a study group to investigate the reasons for this phenomenon.

The first thing to clarify is a broad definition of bioanalytical chemistry. This is far from easy because the term has been used for a variety of fields. Analytical chemists tend to think that bioanalytical chemistry is a science devoted partly to the chemical analysis of biological systems/analytes and partly to the application of tools derived from biology to other branches of analytical chemistry. A different, much narrower definition has been used for some time in the pharmaceutical industry, where bioanalysis is the name for the biological testing of pharmaceuticals, *e.g.*, in bioequivalence studies. Then there is a huge field, clinical chemistry, which might be considered as a subdivision of bioanalytical chemistry, but has developed in its own way and remains a distinct field.

* Corresponding author. E-mail: jeta@dac-euchems.org; jeta@kemi.dtu.dk

The uncertainty surrounding the definition of bioanalytical chemistry is reflected in the social aspects of this science, which appears to be very fragmented and geographically unevenly distributed. A survey of some prominent bioanalytical chemists showed that researchers in this area are not so well organised socially as analytical chemists have traditionally been. They have societies and meetings devoted to sub-fields of bioanalysis, *e.g.*, proteomics analysis or, specifically, mass spectrometry in proteomics, but a broader community does not seem to have formed. The geographical distribution of authors of bioanalytical papers published in analytical chemistry journals appears to be biased towards a few countries. For example, in two recent issues of the Analyst (10 and 11 in 2010), twenty-two bioanalytical papers were published (this number having been established by a somewhat subjective classification) and only two of them were authored from Europe. While this is a single example, the impression has been obtained that there is a preponderance of US compared with European contributors in this field. A good service to the community has been, *e.g.*, to profile many European authors in recent bioanalytical thematic issues of ABC 391(5) and 398(6).

Who are the scientists doing bioanalytical research? When browsing the affiliations the authors of bioanalytical papers published in analytical journals, familiar sounding names of departments and industries that have been strongholds of analytical chemistry are rarely found. There are naturally many authors coming from institutions devoted to biology and biochemistry, and pharmaceutical chemists appear to play an important role. This might be due to their training, which is a suitable mix of biology and chemistry.

The observations made above quite naturally raise the question: should the two, apparently only slightly overlapping communities of analytical and bioanalytical chemists, who are now sharing the pages of many analytical journals, be brought closer together in a more personal way? Can these communities understand each other and offer something that is mutually beneficial? At this moment, the answers are unknown. The DAC of EuCheMS has been promoting the social mixing of these scientists by encouraging the organizers of its meetings, particularly traditional Euroanalysis meetings, to organize bioanalytical sessions. The last Euroanalysis meeting in Innsbruck, Austria,[1] attracted many bioanalytical presentations and it is hoped this will also be the case in Belgrade, Serbia, in 2011.[2]

What can the two communities offer each other? Biology has undergone a revolution in the last two decades. It has been transformed from a phenomena-descriptive science to a much more measurement result-based science. Biological studies have enriched science with many new ideas, which are potentially very useful within the analytical chemistry community. It should not be forgotten that some of the most important tools of analytical chemistry of today came from

biological laboratories, *e.g.*, chromatography, immunoassays and enzymatic methods. Analytical chemists can offer from their side basic concepts and approaches for qualitative and quantitative analysis, including vast experience in metrology and quality assurance. These include the establishment of more universal and sustainable reference systems, approaches to calibration and estimation of measurement uncertainty. In this respect, one should mention the important role of metrological institutes (such as NIST in the US, LGC in the UK, and IRMM for the EU) that have also embraced with great enthusiasm the issue of quality assurance in bioanalytical assays. It is useful to note here that the science of analytical chemistry developed into a distinct discipline within chemistry when – following the explosive development of chemistry at the turn of the 19th and the 20th century – many chemists devoted their research efforts to the realisation of precise and reliable chemical quantification. A similar development may be needed in the wake of the biological revolution.

If the two communities are to meet for their mutual benefit, there is a clear obstacle to be overcome: analytical chemists need to be better trained in biology and biochemistry while those already in the profession should pay more attention to the rapid progress of biological sciences. In some sub-fields of analytical chemistry, this was not a problem, *e.g.*, in food analysis, where such an education has always been a necessity. The education of biochemists would also certainly benefit from courses given by traditional analytical chemists.

When underlining the importance of bringing analytical chemists and biochemists closer together, it should not be forgotten that bioanalysis is not restricted to these two communities. Physicists are making important contributions, *e.g.*, by providing novel optical tools for biosensors. Engineers and medical doctors play a crucial role in, *e.g.*, developing point of care devices. Fellow chemists should also be mentioned, *e.g.*, for the creation of various nanoparticles and biomimetic systems. The long experience of analytical chemists as team players will help us to integrate the efforts of all these groups of scientists.

The annual reports of the Bioanalytics study group of the EuCheMS-DAC can be found at the DAC website.[3] The 2010 report includes a non-exhaustive list of bioanalytical scientists from Europe to help with the identification of this community. Comments about this list and the DAC reports are welcome and should be addressed to George Horvai (george.horvai@mail.bme.hu).

Information from the EuCheMS Division of Analytical Chemistry

Euroanalysis 16 is the main DAC event of 2011. Slavica Ražić is the Chairman of Euroanalysis 16,[2] to be held in Belgrade, Serbia, 11–15 September 2011. The international year of chemistry will be celebrated at Euroanalysis 16, thus promoting chemistry to young students.

Euroanalysis 17 is planned for Warsaw, Poland, in 2013.

The Robert Kellner Lecture (RKL), generously sponsored by Springer Publishers, was awarded to Jonas Bergquist of Uppsala University who will give his lecture at Euroanalysis 16.

The Chairman of the DAC retired from office at the end of 2010 and Paul Worsfold was elected as the new Chairman by the Delegates at the Annual Meeting in Nuremberg on Sunday, August 29, 2010. The EuCheMS-DAC congratulates Paul Worsfold and supports his plans for inviting Delegates to participate in making the DAC more visible by contributing to newsletters, supporting Study Groups and Task Forces, establishing scientific and social networks and maintaining Euroanalysis as the number one DAC event. Bo Karlberg and George Horvai retired from the Steering Committee (StC) but will continue to participate as Delegates. Jiri Barek and Slavica Ražić were appointed as new Members of the StC. The Members Wolfgang Buchberger, Paul Worsfold (Chairman) and Jens Andersen (Secretary) complete the StC for 2011.

The DAC has appointed liaison persons to other EuCheMS Divisions: Education (Reiner Salzer), Food (Bo Karlberg), Environment (Gemma Rauret), Electrochemistry (Luigia Sabbatini), Computational Chemistry (Maria Filomena Camoes and Bo Karlberg) and Life Sciences (George Horvai), while Jan Labuda is the liaison person to the IUPAC. Nominations for liaison representatives at other EuCheMS Divisions are welcome.

The Delegates of the DAC are also organized in Task Forces and Study Groups. A single Task Force entitled “Opportunities for Analytical Chemistry” is currently initiated while other matters of importance to the DAC remain in the custody of the five Study Groups Education, History, Quality Assurance, Bioanalytics and European Analytical Chemistry on the Web.

The Study Group on Quality Assurance also considers the development of Metrology where Hendrik Emons reported that a large EU programme in Metrology has commenced, with a budget of 400 M Euros over 7 years.

Additional matters arising: the journal Analytical and Bioanalytical Chemistry is considering publishing a special issue on GMO analysis. It was proposed a separate list be prepared with the names of potential conferences in the field of Bioanalysis.

The DAC is looking forward to seeing you in Belgrade!

Acknowledgements. The authors are indebted to the other members of the Bioanalysis study group of EuCheMS-DAC (H. Emons, G. Gauglitz, J. Labuda, J. M. Pingarron and K. van Staden) for their contributions.

REFERENCES

1. www.euroanalysis2009.at/
2. www.euroanalysis2011.rs/
3. www.dac-euchems.org/reports/bioanalytics